ABSTRACT

ROBALINO, PABLO JOSÉ. Shear Performance of Reinforced Lightweight Concrete Square Columns in Seismic Regions. (Under the direction of Dr. Mervyn J. Kowalsky.)

Considering the importance of shear capacity under seismic demands, clarifying existing differences between analytical models and existing experimental data, further experimental research on shear performance of reinforced lightweight concrete (RLWC) square columns signifies a current necessity for the civil engineering community. Responding to that necessity and in contrast to the majority of past research that considered monotonic loading, this research evaluated the performance of eight normal strength RLWC large scale square columns, under reversed cyclic loading, simulating earthquake demands, and considering shear failure mechanisms. The variables consisted of different types of aggregate for the concrete mixtures and two sets of specimens with different amount of transverse reinforcement. Moreover, one normal weight and three lightweight structural aggregates such as expanded shale, clay, and slate were considered in order to represent the production in the United States. Two sets of four specimens were designed to develop brittle and ductile shear failures at low and high levels of deformation respectively.

A comparative analysis between normal, lightweight concrete, experimental, and analytical data was performed focusing on the shear resistance mechanism and behavior under simulated seismic demands. Shear resistance and deformation components were obtained to determine the difference between lightweight and normal weight concrete shear strengths and behavior at different levels of deformation. In general, results consistently revealed that, at

low levels of deformation, the concrete shear strength component was lower in the case of lightweight concrete compared to normal weight concrete. Consequently, a shear strength reduction is recommended for normal strength RLWC square columns compared to capacity assessment models for normal weight concrete. Strength degradation, at low levels of deformation, occurred earlier in the case of RLWC compared to normal weight concrete and recommendations are presented also in this regard. Compared to normal weight concrete, lightweight concrete specimens behaved in a slightly less ductile manner, but they were capable to develop large inelastic deformation. In fact, there were no significant differences in terms of energy dissipation between normal and lightweight specimens.

SHEAR PERFORMANCE OF REINFORCED LIGHTWEIGHT CONCRETE SQUARE COLUMNS IN SEISMIC REGIONS

by
PABLO JOSÉ ROBALINO

A thesis submitted to the Graduate Faculty of
North Carolina State University
in partial fulfillment of the
requirements for the Degree of
Master of Science

CIVIL ENGINEERING

Raleigh

August, 2006

APPROVED BY:

Dr. Paul Zia	Dr. James M. Nau

Dr. Mervyn J. Kowalsky
Chair of Advisory Committee

To God, my wife Monica, and my daughter Irene

for whom I breathe, and whose support

gives me the strength along the way

BIOGRAPHY

Pablo José Robalino began his study of civil engineering in 1993 at Pontificia Universidad Católica del Ecuador in Quito. With concentration in structural engineering and construction, he obtained his Bachelor's of Science in 1999 with the third highest point average of that year and as the first in class graduated as Civil Engineer. Pablo joined the engineering consulting and construction industry, and as a registered professional engineer in Quito, he conducted various structural studies and construction projects from 1999 to 2004. Pablo was also a professor of structural engineering at Pontificia Universidad Católica del Ecuador, school of architecture, from 2000 to 2004. As a Fulbright scholar, Pablo continued his graduate studies at North Carolina State University, and participated in research projects related to the field of structural and earthquake engineering under the advice of Dr. Mervyn J. Kowalsky from 2004 to 2006. In August, 2006, he obtained his Master of Science degree in civil engineering with concentration in structural and earthquake engineering.

ACKNOWLEDGMENTS

The accomplishment of this experimental research would not have been possible without the generous contribution of numerous people during all the stages of the project. I would like to sincerely express my gratitude to my advisor Dr. Mervyn J. Kowalsky for his patience and guidance. It was a great honor for me to work with him and being enriched by his knowledge in the field. In the same manner, I extend my gratitude to Dr. Paul Zia, Dr. James Nau, and Dr. Tasnim Hassan for the valuable advice as part of my committee. In addition, I am grateful for the valuable support provided by the Expanded Shale, Clay and Slate Institute ESCSI. In a special manner, I would like to thank Michael Robinson who was always available and willing to support the research project in various aspects.

The support provided by the administrative and technical staff at the Constructed Facilities Laboratory as well as in Mann Hall is sincerely appreciated and was decisive for the completion of the research. In a special manner, I would like to thank William Dunleavy, Greg Lucier, Jerry Atkinson, Lee Nelson, and Amy Yonai. I extend my gratitude to all the students and friends that participated in different stages and whose help was crucial to accomplish the objectives of the research. Among others, I would like to thank Hazim Dwairi, Katrina Walters, Luis Montejo, Aidcer Vidot, Benjamin Possiel, Serena Hendrix, Mike Roselli, Chip DeVoto, Omid Abdi, and all the students that supported me during any specific stage of the project.

Finally, I would like to express my gratitude for the financial support provided by the University and the Fulbright Program to accomplish my graduate studies. In the same manner, I am thankful for the support provided by all the staff at the Fulbright Commission in Ecuador. Lastly, I appreciate all the valuable support of my family and friends that were always present no matter the distance, the language, or the culture.

TABLE OF CONTENTS

LIST OF TABLES

LIST OF FIGURES

SHEAR PERFORMANCE OF REINFORCED LIGHTWEIGHT CONCRETE SQUARE COLUMNS IN SEISMIC REGIONS

by
PABLO JOSÉ ROBALINO

Under the Advice of
DR. MERVYN J. KOWALSKY

Chapter 1: INTRODUCTION

Structural lightweight concrete represents an alternative for designers to reduce mass of structural members if compared to normal weight concrete. As a result of using lightweight concrete, dead loads and seismic demands that are a function of mass and acceleration can be significantly reduced. The unit weight of structural lightweight concrete is typically between 90 to 120 lbs/ft^3 compared to 150 lbs/ft^3 for normal weight concrete. Consequently, size of structural members such as columns and footings may be reduced producing a positive effect in the cost and efficiency of the structure. Moreover, a significant reduction of the mass in structures such as tall buildings and long span bridges, located in high risk seismic regions, will result in reduced seismic forces. For instance, in the case of columns located in the first story of a building, where the base shear is a function of cumulative lateral forces induced by the earthquake at each mass location, a reduction of 30% in the weight of the entire structure represents a significant reduction in the seismic demands compared to normal weight concrete structures.

On the other hand, past performance of lightweight concrete structures under earthquake demands has indicated potential problems, particularly with regards to shear behavior. For instance, lightweight concrete structures of the Olive View Hospital constructed between 1964 and 1970 were considerably damaged during the 1971 San Fernando earthquake as reported by Jennings (1971). For example, a lightweight concrete single storey assembly hall that consisted of eight lightweight concrete columns supporting a grid roof developed large

residual displacements due to insufficient shear strength as reported by Jennings (1971). Moreover, the Psychiatric Day-Care Center, also part of the Olive View Hospital complex, collapsed due to a brittle shear failure of the first storey columns that lost axial load capacity as the second story fell down over the first. Considering code provisions at that time and as discussed by Kowalsky and Dwairi (2003), a lack of shear and confinement reinforcement was the possible cause of the collapse rather than the concrete properties.

Jennings (1971) also mentioned in his report that a free-standing lightweight concrete canopy failed at the connection of the cantilever beams due to torsional demands.

As a result, considering past performance as well as monotonic tests data on shear critical lightweight concrete beams, there is a general agreement that the shear capacity of lightweight concrete is somewhat lower than that of normal weight concrete of equivalent compressive strength as discussed in chapter 2. The mechanism behind this reduction in shear has often been attributed to reduced aggregate interlock. Lightweight concrete aggregates are typically weaker than the surrounding cement matrix. As a result, cracks tend to form through the aggregate resulting in smother crack boundaries compared to normal weight concrete. In the case of seismic loading, where cracks form and widen with increasing ductility, any loss of aggregate interlock could be substantial with regard to the overall shear resisting mechanism. Consider Figure 1.1 and Figure 1.2 which show cracked surfaces of lightweight and normal weight concrete. Note the smother surface in the case of lightweight concrete.

Figure 1.1. Lightweight Concrete Fractures

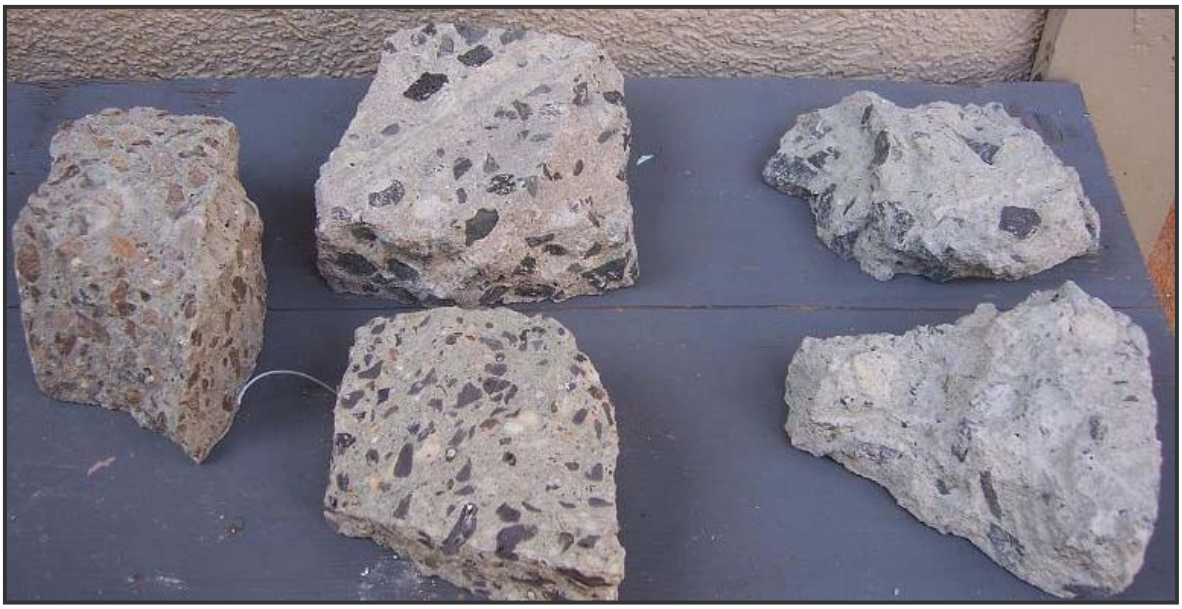

Figure 1.2. Lightweight concrete cracked surfaces (Left) - Normal weight concrete (Right)

While reduction factors for lightweight concrete shear capacity have been in place for some time, the database of tests that have justified this reduction are comparatively small. Furthermore, they are almost exclusively monotonic beam tests. Such tests, while important, do not give any indication of the performance of reinforced lightweight concrete under seismic load conditions. In order to understand the effect of seismic loading on lightweight concrete shear performance, it is essential to conduct large scale experiments utilizing representative load histories, which in the case of earthquake engineering typically consists of reversed cyclic loading. Unfortunately, there are very few reversed cyclic shear critical lightweight concrete tests.

Code provisions do not consider the shear performance of the composite material taking into account the effect of the transverse steel in the behavior of the structural member under cyclic critical shear. For instance, concrete shear strength is determined in relation to the diagonal tension strength (ACI 318-05, 2005). In order to avoid overly conservative code provisions, and to acquire a better understanding of the shear resistance mechanism of reinforced lightweight concrete columns under seismic demands, further research is necessary taking into account the composite material under reversed cyclic or dynamic loading. The motivation of this research is based on the above mentioned necessity to study the shear performance of reinforced lightweight concrete square columns under seismic demands. Experimental studies such as those presented in this thesis may lead to more efficient and economic designs in the future.

1.1 Objective

Given the apparent lack of experimental data on the reversed cyclic shear performance of shear critical lightweight concrete members, a comprehensive study was needed where the effect of the aggregate type, compressive concrete strength, and steel reinforcement details are investigated.

The research described in this thesis is focused on the shear performance of reinforced lightweight concrete square columns under reversed cyclic shear loading. The objective of the research is to evaluate the behavior of lightweight concrete square columns under seismic shear demands, to determine the shear strength and deformation components under low and high levels of deformation, and to compare the results to similar columns made of normal weight concrete and to analytical models to predict shear strength and deformation components. Moreover, the research takes into account normal strength structural lightweight concrete mixtures made with the most representative lightweight aggregates produced in the United States such as expanded shale, clay, and slate.

In order to pursue the objective, a comparative analysis of the experimental and analytical results was conducted to determine the effect of lightweight concrete on shear performance of reinforced square columns with low and high levels of deformation capacities. A total of eight reinforced concrete square columns have been tested considering various lightweight aggregates produced with raw material from different quarries located in the United Sates.

Moreover, to cover most of the spectra, the most representative types of lightweight aggregate were used such as expanded slate from the southeast, expanded shale from the Midwest and north, and expanded clay from the west coast. In addition, two normal weight concrete specimens were tested as reference and control specimens. Finally, there were two sets of specimens with different confinement levels and shear reinforcement ratios in order to analyze brittle shear failure mechanisms at low levels of deformation, and ductile shear failure mechanisms at high levels of deformation.

1.2 Scope of the Research

The different stages of the research included the literature review described in chapter 2, design and construction of the specimens and test setup as described in chapters 3 and 4, eight reversed cyclic shear critical tests of single bending columns with two failure mechanisms (brittle and ductile shear failure) as presented in chapters 5 and 6, and the analysis of experimental and analytical data as well as recommendations and conclusions are included in chapters 7 and 8.

Among the main aspects of the research, analysis of the experimental data included actual values of the shear strength component provided by lightweight concrete specimens and those values were compared to strength values in the case of normal weight concrete specimens and to predicted values. In addition, actual displacements due to shear and flexural deformation are also presented and compared between the experimental results of all normal and lightweight concrete columns as well as to predicted analytical values. Finally,

seismic performance of reinforced lightweight concrete subjected to hysteretic cyclic shear is evaluated considering aspects such as strength degradation, ductility capacity, energy dissipation, and damping.

1.3 Structural Lightweight Concrete

There were three types of structural lightweight aggregate used for the concrete mixtures in addition to normal weight aggregate. In fact, most common and representative lightweight aggregates produced in different regions of the United States such as expanded shale, clay, and slate were considered for the research. For the production of the aggregate, raw material (slate, shale, or clay) is subjected to high temperatures (2000 F) in a rotary kiln to acquire a porous structure while maintaining good mechanical properties such as toughness. Lightweight aggregates are significantly lighter than normal weight aggregates. In the case of this research, lightweight aggregates used for six specimens were approximately 42% lighter than the normal weight aggregate used for two normal weight concrete specimens as it can be observed in Table 1.1 and Table 1.2. Finally, lightweight concrete mixtures are 20% to 35% lighter than normal weight concrete mixtures. In the case of the specimens of this research, lightweight concrete mixtures were approximately 21% lighter than the normal weight concrete mixture as it can be observed in Table 1.1 and Table 1.2.

Table 1.1. Concrete Mixture Proportions – Expanded Slate and Expanded Shale Aggregates

Concrete Mixture - Expanded Slate Lighweight Aggregate

Material	Normalized Weight (Proportions)	Normalized Volume (Proportions)	Ratio: Weight / Volume	Unit Weight (Kg/m^3)	Unit Weight (lbs/ft^3)
Water	**1.00**	**1.00**	**1.00**	**1,000.00**	**62.30**
Cement	2.23	0.71	3.15	3,150.00	196.24
Exp. Slate - Stalite 1/2"	**2.99**	**1.95**	**1.53**	**1,530.00**	**95.31**
Sand	4.41	1.68	2.63	2,630.62	163.88
Air		0.27			

Concrete Mixture	**10.63**	**5.61**	**1.89**	**1,894.93**	**118.05**
Estimated Equilibrium Unit Weight				1,780.02	111.11

Concrete Mixture - Expanded Shale Lighweight Aggregate

Material	Normalized Weight (Proportions)	Normalized Volume (Proportions)	Ratio: Weight / Volume	Unit Weight (Kg/m^3)	Unit Weight (lbs/ft^3)
Water	**1.00**	**1.00**	**1.00**	**1,000.00**	**62.30**
Cement	2.13	0.68	3.15	3,150.00	196.24
Exp. Shale - Buildex 1/2"	**3.06**	**2.00**	**1.53**	**1,530.00**	**95.31**
Sand	4.51	1.71	2.63	2,631.16	163.91
Air		0.36			

Concrete Mixture	**10.70**	**5.75**	**1.86**	**1,862.14**	**116.01**
Estimated Equilibrium Unit Weight				1,789.55	111.71

Table 1.2. Concrete Mixture Proportions – Expanded Clay and Normal Weight Aggregates

Concrete Mixture - Expanded Clay Lighweight Aggregate

Material	Normalized Weight (Proportions)	Normalized Volume (Proportions)	Ratio: Weight / Volume	Unit Weight (Kg/m^3)	Unit Weight (lbs/ft^3)
Water	**1.00**	**1.00**	**1.00**	**1,000.00**	**62.30**
Cement	2.17	0.69	3.15	3,150.00	196.24
Exp. Clay - TXI Fraiser Park 1/2"	**3.09**	**2.02**	**1.53**	**1,530.00**	**95.31**
Sand	4.53	1.74	2.61	2,606.53	162.38
Air		0.28			
Concrete Mixture	**10.78**	**5.72**	**1.88**	**1,884.75**	**117.41**
Estimated Equilibrium Unit Weight				1,759.07	109.80

Concrete Mixture - Normal Weight Aggregate

Material	Normalized Weight (Proportions)	Normalized Volume (Proportions)	Ratio: Weight / Volume	Unit Weight (Kg/m^3)	Unit Weight (lbs/ft^3)
Water	**1.00**	**1.00**	**1.00**	**1,000.00**	**62.30**
Cement	2.13	0.67	3.15	3,150.00	196.24
Normal Weight #67	**6.29**	**2.39**	**2.63**	**2,630.00**	**163.84**
Sand	4.38	1.67	2.63	2,628.54	163.75
Air		0.39			
Concrete Mixture	**13.80**	**6.12**	**2.25**	**2,254.40**	**140.44**

Chapter 2: LITERATURE REVIEW

In order to provide the reader an overall perspective of the current necessities in terms of research focusing on the behavior of lightweight concrete structural elements under seismic demands, this section presents relevant aspects of previous experimental studies on lightweight concrete shear performance. Experimental tests of structural lightweight concrete members such as beams and columns have been considered in this section in order to cover relevant previous research. It is important to mention that, as discussed by Kowalsky and Dwairi (2003), the majority of previous experimental studies on lightweight concrete shear performance considered only monotonic loading. For that reason, there is a current necessity of evaluating the performance of reinforced lightweight concrete columns simulating earthquake demands, taking into account the shear resistance mechanism, including transverse reinforcement steel, and considering different shear span depth ratios and cross section configurations.

2.1 Shear Performance of Lightweight Concrete Beams

2.1.1 J. A. Hanson, 1958 (USA)

In 1958, twenty-one beams of the same size, made of eight different structural lightweight aggregates, and considering four different concrete strengths, were tested by Hanson (1958). The same type of loading, at third points, was applied in all the tests. Moreover, the specimens were tested under monotonic loading, and all the beams were built without including shear reinforcement. In fact, for all lightweight concrete mixtures, the

experimental research determined values of nominal shear strengths considering the load level that produced diagonal tension cracking.

It is important to mention that, as observed during the tests (Hanson, 1958) most beams resisted a higher load level after diagonal cracking. The higher ultimate shear resistance was attributed to be related to the location of the diagonal shear crack that was observed to appear randomly within certain boundaries. Consequently, the ultimate shear strength was assumed to not have a dependable variable. Finally, even though the shear strength of the lightweight concrete beams was lower than that of normal weight concrete beams, the shear strength was still higher than the allowable stress stipulated by (ACI 318-56) with safety factors between two and four.

The obtained shear strength values were similar and consistent for all the beams. Compressive concrete strengths of the tested specimens ranged from 3000 to 9000 psi. Moreover, no seismic demands were simulated since the specimens were tested monotonically. In addition, the specimens did not include shear reinforcement, so aspects such as the truss mechanism as well as the effect of confinement in the concrete strength (Mander et al., 1988) were not considered at that time. However, it is important to mention that current code provisions require designers to include shear reinforcement in structural members. This is especially important for columns and for structural members in seismic regions.

Higher shear strength values were obtained for some of the short beam specimens compared to those obtained when diagonal tension cracking occurred. However, it was concluded that the ultimate strength was dependent on shear diagonal crack location, that the location appeared randomly within a range, and that it was not a dependent variable.

2.1.2 Don L. Ivey and Eugene Buth, 1967 (USA)

Results of twenty-six simple supported lightweight concrete beams were analyzed to study the shear strength of structural lightweight concrete (Ivey and Buth, 1967). In this case, variables such as the shear span, the cross section, and the longitudinal steel ratio were included. Moreover, expanded slate and shale structural lightweight aggregates were used for concrete mixtures with compressive strengths that ranged from 3000 to 4500 psi. In addition, the specimens did not include shear reinforcement and were tested under monotonic loading. The authors (Ivey and Buth, 1967) observed that the shear strength at tension diagonal cracking was influenced by the ratio between the shear span and the depth of the section, and by the longitudinal reinforcement steel ratio. Results obtained by Hanson (1958) were validated due to the consistency between predicted values (Hanson, 1958) and experimental results (Ivey and Buth, 1967) even though the shear strengths were approximately 14% lower that the predicted values.

Finally, ACI standard building code provisions for lightweight concrete beams (ACI 318-63) were evaluated by the authors (Ivey and Buth, 1967). In fact, experimental results were compared to values obtained by the above mentioned code provisions (Eq. 2-1) and (Eq.

2-2), and to modified equations proposed by the authors as shown in equations (Eq. 2-3), (Eq. 2-4), and (Eq. 2-5). As a conclusion, results showed that equations (Eq. 2-3) and (Eq. 2-4), were the most conservative of the three methods (60% including ϕ), that the least conservative was equation (Eq. 2-5) considering the splitting tensile strength as the strength factor (26% including ϕ), and that ACI provision, (Eq. 2-2), had intermediate values (21 to 42 % including ϕ).

(ACI 318-63):

Normal weight concrete:

$$\upsilon_c = \phi \cdot \left(1.90 \cdot \sqrt{f'_c} + 2500 \cdot \frac{\rho \cdot V \cdot d}{M} \right) \quad \textbf{(Eq. 2-1)}$$

Lightweight concrete:

$$\upsilon_c = \phi \cdot \left(0.28 \cdot F_{sp} \sqrt{f'_c} + 2500 \cdot \frac{\rho \cdot V \cdot d}{M} \right) \quad \textbf{(Eq. 2-2)}$$

F_{sp} = Ratio of splitting strength to the square root of (f'_c)

Proposed (0.75 – 0.85) method:

All lightweight concrete:

$$\upsilon_c = 0.75 \cdot \phi \cdot \left(1.90 \cdot \sqrt{f'_c} + 2500 \cdot \frac{\rho \cdot V \cdot d}{M} \right) \quad \textbf{(Eq. 2-3)}$$

Sand lightweight concrete:

$$\upsilon_c = 0.85 \cdot \phi \cdot \left(1.90 \cdot \sqrt{f'_c} + 2500 \cdot \frac{\rho \cdot V \cdot d}{M} \right) \quad \textbf{(Eq. 2-4)}$$

Proposed alternative equation:

Lightweight concrete:

$$\upsilon_c = \phi \cdot \left(0.28 \cdot f'_{sp} + 2500 \cdot \frac{\rho \cdot V \cdot d}{M} \right) \quad \textbf{(Eq. 2-5)}$$

f'_{sp} = *Splitting tensile strength of concrete*

2.1.3 Y. D. Hamadi and P.E. Regan, 1980 (UK)

Five pairs of T beams were tested under shear critical monotonic loading by Hamadi and Regan (1980) in the United Kingdom. Moreover, the specimens included shear reinforcement, and different structural aggregates. In general, the concrete mixtures included normal weight aggregate and expanded clay structural lightweight aggregate. It is important to mention that the authors (Hamadi and Regan, 1980) considered the truss mechanism of shear resistance, and the influence of the fracture surface roughness in the shear aggregate interlock mechanism. Finally, it was observed by the authors (Hamadi and Regan, 1980) that ultimate shear strengths depended principally on the type of aggregate as well as on normal stresses.

It was observed that for normal weight concrete, the shear resistance factor due to aggregate interlock was higher since the fracture did not cross the aggregate as it was observed in lightweight concrete specimens where the cracks passed through the aggregate according to the authors (Hamadi and Regan, 1980). The fracture surface was rougher in the case of normal weight compared to lightweight concrete.

Another important observation was the difference in the behavior and strength between normal and lightweight concrete specimens related to the angle of the truss analogy compression strut. The authors (Hamadi and Regan, 1980) observed that the angle was less inclined for normal than for lightweight concrete. Moreover, for lightweight concrete specimens, stresses in transverse steel were higher that in normal weight specimens. Finally, there was a good agreement between tests results and predicted values, and equations for transverse steel shear contribution were proposed by the authors.

2.1.4 J. L. Clarke, 1987 (UK)

Having the purpose of evaluating code provisions (BS 8110) related to shear strength of lightweight concrete that included a reduction factor of eighty percent of the normal weight concrete shear strength, a paper presented by Clarke (1987) discusses about experimental data obtained by Berge (1981) and Lambert (1982). In fact, various tests results of lightweight concrete beams, with and without shear reinforcement, and tested by Berge (1981) under monotonic loading were analyzed. The conclusion made by the author (Clarke, 1987) for beams with stirrups was that the code provisions were overly conservative, that the reduction factor of 80% was necessary, and that proposed equations for code provisions (BS 8110 -1985) might be included. For lightweight concrete without stirrups the proposed reduction factor was 90%. The analysis was based on tests that included various lightweight concrete mixtures with different strength, density, and type of aggregate (Lytag, Pellite and Pumice).

2.1.5 Miguel A. Salandra and Shuaib H. Ahmad, 1989

Sixteen high strength lightweight concrete beams, with and without shear reinforcement, were tested by Salandra and Ahmad (1989). Expanded slate structural lightweight aggregate was used for the concrete mixtures. The purpose of the research was to acquire information about ultimate and diagonal cracking shear strengths. Compressive strengths of the lightweight concrete ranged between 7,800 to 10,500 psi. Moreover, other variables such as the amount of shear reinforcement and the ratio between the shear span and the depth of the cross section were included. In addition, larger shear strengths after diagonal tension cracking were observed and considered for the analysis observing the positive fact that concrete continued to contribute to the shear strength mechanism after having reached a maximum value.

2.1.6 S. H. Ahmad, Y. Xie & T. Yu, 1995

Ahmad et al. (1995) tested fifteen normal and high strength reinforced lightweight concrete beams, with and without shear reinforcement, and taking into account shear critical failure mechanisms. Moreover, the amount of shear reinforcement (from 0 to 0.784%), the shear span depth ratio (a/d from 1 to 4), and the concrete compressive strength that ranged between (4,430 to 12,950 psi) were the variables for the research. Furthermore, relevant to seismic shear performance, it is important to note that the authors (Ahmad et al., 1995) related shear ductility to shear concrete strength, and also shear strength to shear reinforcement ratios. It was observed that greater shear reinforcement ratios improve the shear capacity, energy dissipation capacity, and the behavior after reaching the maximum shear strength.

2.1.7 J.A. Ramirez, 2003

In order to compare experimental results and code provisions related to minimum shear reinforcement required for lightweight concrete beams, Ramirez (2003) presented experimental results of four prestressed concrete beam shear critical tests as well as predicted values considering code provisions (ACI 318-02). Moreover, Haydite particles were used as the structural lightweight aggregate. Furthermore, the shear reinforcement was close to the minimum required by (ACI 318-02), equation (11-13) and is a function of the compressive strength of the concrete as changes were made for the code provision. Moreover, the concrete compressive strengths were the variable to compare predicted increments in the shear strength. Ramirez (2003) observed that all the actual shear capacities were greater that the predicted values. The author suggested that the respective code provisions for minimum reinforcement of lightweight concrete should be revised since the experimental results were not consistent. The code provision aims to provide less shear reinforcement for higher strength lightweight concrete compared to normal weight concrete minimum requirements.

2.2 Shear Performance of Lightweight Concrete Columns

2.2.1 Mervyn J. Kowalsky, M. J. Nigel Priestley, and Frieder Seible, 1999 (USA)

In 1999, Kowalsky et al. presented a research work related to shear behavior of lightweight concrete bridge columns under seismic demands. In fact, two lightweight concrete circular columns were subjected to double bending cyclic hysteretic loading simulating earthquake demands. The specimens had concrete compressive strengths of 48 and 51 Mpa at the days

of tests. The columns were designed and consistently failed with brittle and ductile shear failure mechanism respectively. The columns that developed a ductile shear failure had significant more transverse steel than the other one, and failed presenting transverse steel fracture at ductility six. The authors (Kowalsky et al., 1999) observed that, for lightweight concrete, a reduction in shear and flexural strength was appropriate. It was also observed that displacement and energy absorption capacities were not significantly lower for lightweight concrete circular columns. Finally, the three component shear resistance mechanism proposed by Priestley et al. (1994) was modified by Kowalsky et al. (1999), and a further revision was presented for lightweight concrete (Kowalsky et al., 2000 b). The proposed formulation recommended reductions in the shear strength concrete component of 15% and 30% for low and high levels of deformation respectively.

The authors (Kowalsky et al., 1999) concluded that, even in seismic regions, reinforced lightweight concrete can be used for structural elements such as bridge columns considering its capacity to develop significant inelastic deformation. However, it was observed that service limit states should be considered at lower levels in terms of the demand because crushing of the concrete occurred at lower concrete strain values (0.0025) compared to normal weight concrete. The authors also suggested, in agreement with ACI code provisions, that a reduction in the lightweight concrete elastic modulus might be appropriate.

2.2.2 Mervyn J. Kowalsky, M. J. Nigel Priestley, and Frieder Seible, 2000 (USA)

In order to evaluate the dynamic behavior of lightweight concrete under simulated seismic events, and to supporting research described in section 2.2.1 that considered cyclic hysteretic lateral loading of lightweight concrete columns, Kowalsky et al. (2000 b) presented a study that included three dynamic shake-table tests of reduced scale lightweight concrete bents with two columns. Moreover, according to the authors, previous research (Kowalsky et al., 1999) was validated in terms of ductility, energy dissipation, and general behavior of reinforced lightweight concrete columns under seismic demands. In fact, proposed design procedures lead to system with sufficient shear strength, and that develop a ductile response as desired under such seismic demands. It is important to mention that the authors presented a modified set of equations for the stress-strain relationship of confined lightweight concrete based on the model developed by Mander, Priestley, and Park (1988) for confined normal weight concrete.

2.3 Current Research Necessities

A detailed discussion on aspects related to seismic behavior of structural lightweight concrete systems was presented by Kowalsky and Dwairi (2003). In addition, focusing on the shear performance under seismic demands, the authors discussed about aspects related to previous research studies on lightweight concrete, code provisions from various countries, and finally future research needs to acquire a better understanding in the field. In fact, one of the conclusions presented by Kowalsky and Dwairi (2003) constituted a motivation for the

research project presented in this document to study the shear performance of lightweight concrete columns in seismic regions.

> *"A case can be made that much of the past research on shear capacity of lightweight concrete members does not apply to structures in seismic regions. This is largely due to the fact that in many cases, only monotonic loading was considered. Furthermore, many of the tests used to develop code provisions consisted of beams without transverse reinforcement…" (Kowalsky and Dwairi, 2003, p. 42)*

In addition, the very few researches that considered cyclic or dynamic loading of lightweight concrete structural columns considered circular cross-sections. In fact, it appears to be that there are not relevant studies for shear performance of square reinforced lightweight concrete columns under reversed loading at the moment. This was also considered a strong motivation for designing the specimens presented in this document as shown in chapter 3, to test them under simulated seismic demands, and to considering shear reinforcement typically used for square columns in seismic and non-seismic regions.

2.4 Shear Transfer Mechanism

The three shear strength component model proposed by Priestley et al. (1994), modified for lightweight concrete (Kowalsky et al., 1999), revised by Kowalsky and Priestley (2000 a) for normal weight concrete, and then revised for lightweight concrete by Kowalsky et al. (2000 b) is based on experimental tests of large scale concrete columns under reversed loading and was used to predict the shear capacity envelope of the specimens of this research. The above mentioned shear transfer mechanism was developed to predict the nominal shear strength of reinforced concrete columns considering the lower bound of various experimental results to asses the shear capacity envelope at various levels of deformation. The same criterion was considered when analyzing the results of this research as well as to revise the shear capacity envelope model for reinforced lightweight concrete square columns as discussed in chapter 7.

Based on large scale reversed loading tests, the shear transfer mechanism (STM) has three components of shear strength to asses the shear capacity envelope of lightweight concrete columns (Kowalsky et al., 2000 b). One component due to the strength of the concrete shear resisting mechanism, another component based on a truss mechanism provided by transverse reinforcement to resist shear, and the last one due to the shear strength enhancement provided by a compressive axial load. Equations from (Eq. 2-6) to (Eq. 2-14) summarize the STM analytical model used in this research to predict the shear strength of the specimens at different levels of deformation. This model was developed based on experimental tests that considered circular columns, but was assumed to estimate the shear capacity of the test

specimens (square columns). Finally, with the experimental results of this research, the specific objective was to review and improve the shear capacity envelope formulation to be applied for lightweight concrete square columns.

Among the components, as described in (Eq. 2-6), the model takes into account an axial load shear strength component contribution (*Vp*) as a mechanism that considers the enhancement of shear strength provided by the axial load due to arch effect. The effect of the axial load in the shear resistance mechanism was explained by Priestley at al. (1994) where (*Vp*) is the horizontal component of a compressive axial load that is transferred through an inclined compressive strut along a structural member under single or double bending as described in Figure 2.1. In the case of this research, a constant axial load of 96 kips (5% of axial load capacity) was applied to all the specimens.

Moreover, equations (Eq. 2-10) and (Eq. 2-11) consider elements subjected either to single or double bending. In the case of this research equation (Eq. 2-10) applies for all the specimens because it considers cantilever columns. In this research, the shear strength contribution due to the axial load was calculated at different levels of deformation using actual data of each specimen. In the equation (P) is the axial load, (L) is the clear length of the column, (D) is the depth of the section that was the same for all the specimens (21 inches), and (c) is the neutral axis depth from the extreme fiber under compression where the maximum moment was located (at the column base).

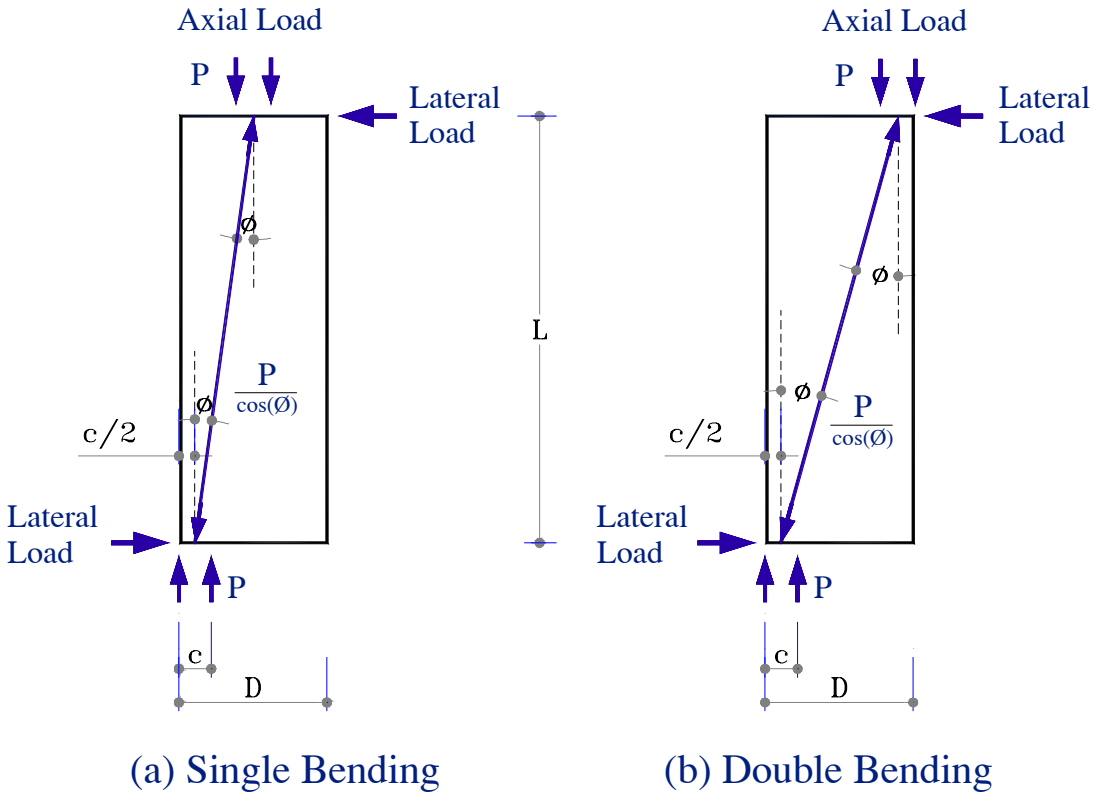

Figure 2.1. Shear Strength Contribution due to Compressive Axial Load - Priestley et al. (1994)

The shear transfer mechanism also considers the shear strength contribution provided by the transverse steel reinforcement through the truss mechanism. The model considers rectangular and circular cross sections as shown in equations (Eq. 2-8) and (Eq. 2-9) respectively. In the case of this research, this component was calculated using actual data obtained in each test for different levels of deformation and using equation (Eq. 2-8) for rectangular columns. For design purposes, (*Vs*) is calculated considering an angle of the compression strut (θ) of 45^{o} degrees, and the stress of the transverse reinforcement (*fsh*) is considered to be the yielding stress (*fy*).

For the case of this research (*Vs*) was calculated taking into account the actual angle of the compression strut (θ) as measured during each test by visual inspection of the cracks, and the actual stress of the transverse reinforcement (*fsh*) at specific levels of deformation. The actual angle of the compression strut (θ) was measured from the vertical axis as illustrated by Figure 2.2 and it was defined by the average slope of the principal shear cracks on faces (E & W). The stress of the transverse steel was estimated as a function of the strain profile of the transverse reinforcement obtained by internal instruments (strain gages) at different levels of deformation as shown in chapters 5 and 6 for each set of specimens. The maximum tensile strain in the transverse steel was considered to estimate the actual stress in the stirrups (*fsh*). Moreover, the spacing between stirrups (*s*), and the area of the transverse steel (*Ash*) was assigned for each specimen as they were built, and the transverse steel ratio was different for brittle and ductile shear failure specimens. The concrete cover (*cov*) was the same for all the specimens.

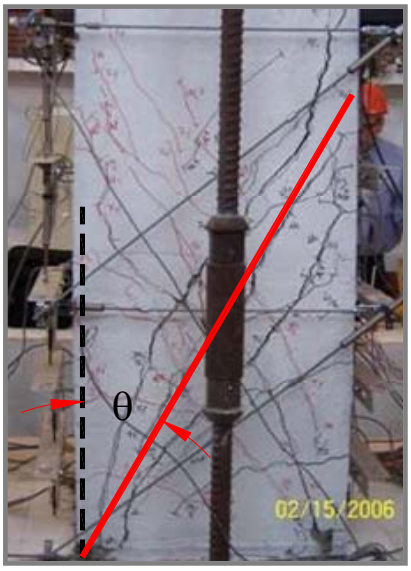

Figure 2.2. Example of angle measurement of the compression strut (θ)

The shear strength component provided by the concrete (*Vc*) is estimated by the STM model taking into account the material properties, the shear span depth ratio, the longitudinal steel ratio, and different levels of deformation or displacement ductility as described in equations (Eq. 2-7), (Eq. 2-12), (Eq. 2-13), and (Eq. 2-14). In the case of this research, coefficients (α) and (β) in equations (Eq. 2-12) and (Eq. 2-13) were constant values for all the specimens because they relate shear span depth ratio and longitudinal steel ratio respectively to the shear strength component of the concrete (*Vc*), and these values were the same for all the specimens.

$$V_n = V_c + V_p + V_s \qquad \textbf{(Eq. 2-6)}$$

$$V_c = \alpha\beta\gamma\sqrt{f'c}\left(0.8A_g\right) \qquad \textit{(Mpa)} \qquad \textbf{(Eq. 2-7)}$$

$$V_s = A_{sh} \cdot f_{sh} \cdot \frac{D - c - \text{cov}}{s} \cdot \cot(\theta) \qquad \textit{(Rectangular Section)} \qquad \textbf{(Eq. 2-8)}$$

$$V_s = \frac{\pi}{2} A_{sp} \cdot f_{sp} \cdot \frac{D - c - \text{cov}}{s} \cdot \cot(\theta) \qquad \textit{(Circular Section)} \qquad \textbf{(Eq. 2-9)}$$

$$V_p = \frac{P(D - c)}{2L} \qquad \textit{(Single Bending)} \qquad \textbf{(Eq. 2-10)}$$

$$V_p = \frac{P(D-c)}{L} \qquad \textit{(Double Bending)} \qquad \textbf{(Eq. 2-11)}$$

Coefficients for Shear Strength of Concrete Component (Vc) – (Mpa) units:

$$\alpha = 3 - \frac{M}{V \cdot D} = 3 - \frac{L_{clear}}{D} \qquad \textbf{(Eq. 2-12)}$$

$$(1 \le \alpha \le 1.50)$$

$$\beta = (0.50 + 20\rho) \le 1 \qquad \textbf{(Eq. 2-13)}$$

$$0.035 \le \gamma = 0.25 - 0.0358 \cdot (\mu_\Delta - 2) \le 0.25 \qquad \textbf{(Eq. 2-14)}$$

Notation for the shear transfer mechanism described in this section is presented in section 9.14 of the appendix. It is important to notice that the value ($0.8A_g$) represents an approximated value of the confined concrete core area of the cross section. In addition, Figure 2.3 and Figure 2.4 show the original and revised models for normal and lightweight concrete pertaining to the (γ) coefficient that defines the concrete shear strength degradation at different levels of deformation or displacement ductility based on experimental data that has revealed a reduction of shear strength with increasing levels of deformation due to progressive widen of cracks and loss of aggregate interlock.

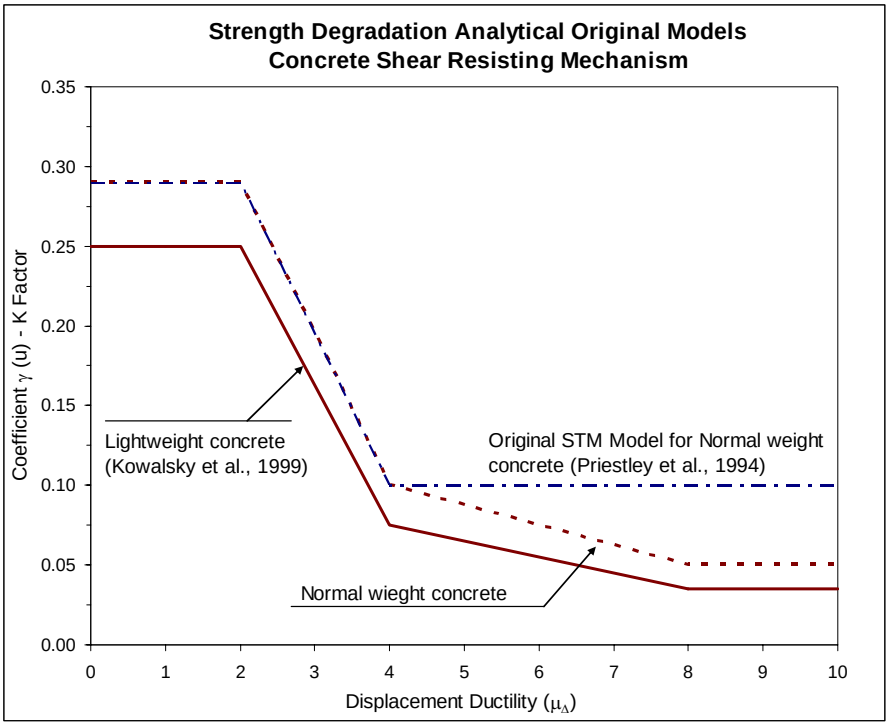

Figure 2.3. Original Models - (γ) coefficient of Shear Transfer Mechanism

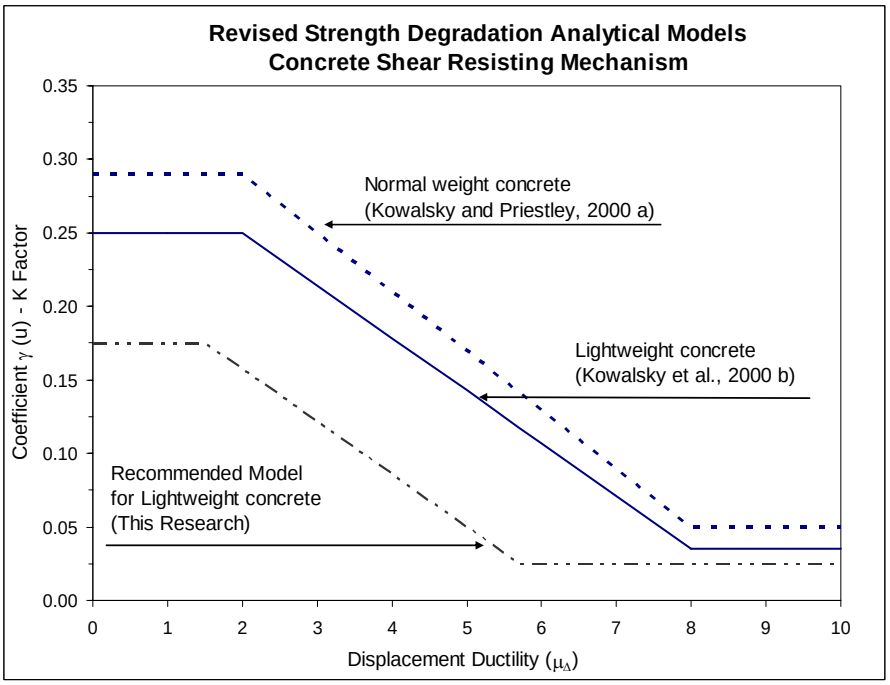

Figure 2.4. Revised Models - (γ) coefficient of Shear Transfer Mechanism

Chapter 3: TEST DESIGN AND CONSTRUCTION

3.1 Analytical Models

In order to capture the strength of the concrete shear resisting mechanism, both ductile and brittle shear failure modes were desired for a single bending reinforced lightweight concrete column with a square cross section. The cross section configurations were obtained considering the equipment and limitations at the laboratory and the desired failure modes for both specimens of the same shape. Limitations such as the height of the column, the size of the footing, the capacity of the actuator, and the square shape of the column cross section narrowed the spectra of possibilities. In brief, it was imperative for the research to ensure the shear failure of the specimens, a brittle and a ductile shear failure at low and high levels of deformation respectively. That was critical for the ductile shear failure model where the probability of reaching that type of failure was very low compared to a brittle shear failure mode.

Given the height of the column, the capacity of the actuator, a normal concrete compressive strength, and commercial reinforcement steel, various square columns with different shear span ratios and cross section configurations were analyzed. Moment versus curvature analysis was performed taking into account the effect of confinement in the concrete strength, the effect of the axial load in the response, and the reinforcement steel strain hardening as proposed by Mander et al. (1988). In addition, considering single bending of

the specimens subjected to a lateral load, a force deformation response graph was obtained and compared to the shear capacity envelope of the respective cross section. Indeed, the shear capacity envelope was obtained by a three component shear transfer mechanism initially proposed by Priestley et al. (1994), modified by Kowalsky and Priestley (2000 a), and revised for lightweight concrete by Kowalsky et al. (2000 b) as described in section 2.4. In brief, three components of shear strength were determined for the shear capacity envelope. One component due to the strength of the concrete shear resisting mechanism, another component based on a truss mechanism provided by transverse reinforcement to resist shear, and the last one due to the shear strength enhancement provided by a compressive axial load as explained in section 2.4. Details regarding the above mentioned shear transfer mechanism are discussed in detail in chapter 2. The above mentioned shear capacity envelope (Kowalsky et al., 2000 b) is based on shear critical lightweight concrete column tests under cyclic loading taking into account circular cross sections only. In any case, considering the purpose of the research as that of revising the model for square lightweight concrete columns, it was assumed to be a good estimate of the shear capacity envelope of square sections for the analytical models.

Finally, the failure mechanism was determined by both curves, shear capacity envelope and force displacement response. For instance, a brittle shear failure was obtained if the lateral force deformation response of the model crossed the shear capacity envelope in the location where the shear strength components of the column, including the shear strength provided by the concrete, have not developed any degradation as shown in Figure 3.2. That is the first

plateau of the shear capacity envelope curve. The ductile shear failure mode, Figure 3.3, may be developed when the lateral force deformation response curve crosses the shear capacity envelope curve in the lower plateau where the shear strength of the element has lost most of the concrete component shear strength. In fact, most of the shear resistance is provided by the transverse steel and axial load components considering that shear resistance provided by aggregate interlock may not be significant since cracks may be developed crossing through the aggregate as discussed in chapter 1.

After analyzing several options, the cross sections specified in Table 3.1 and Figure 3.1 were selected. The amount of transverse reinforcement was a variable as well as the concrete mixture: Four different types of normal strength concrete mixtures were selected. Except for the area of transverse reinforcement and the concrete mixture, the configuration of each specimen remained the same. All the specimens had a square cross section with two axes of symmetry, the same longitudinal reinforcement steel ratio, the same shear span ratio, geometry, and approximately the same concrete strength. Figure 3.1 and Table 3.1 show the specifications for both cross sections.

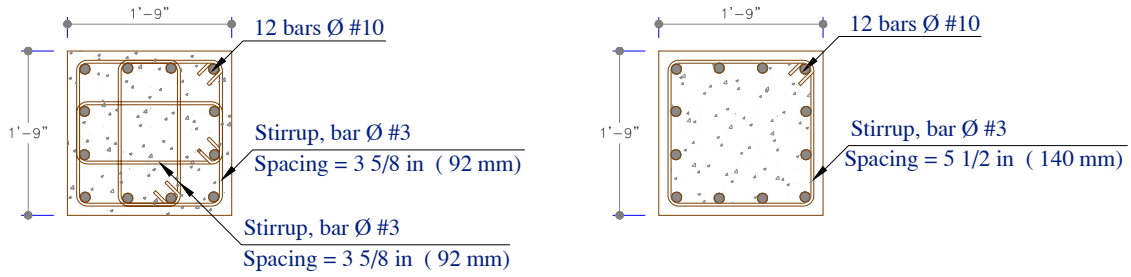

(a) DUCTILE SHEAR FAILURE SPECIMEN (b) BRITTLE SHEAR FAILURE SPECIMEN

Figure 3.1: Column cross-sections, a) Ductile shear failure specimen b) Brittle shear failure specimen

Table 3.1 Specimen specifications

CROSS-SECTION SPECIFICATIONS	DUCTILE SHEAR FAILURE MODEL				BRITTLE SHEAR FAILURE MODEL			
NUMBER OF LONG. BARS	12	u			12	u		
NUMBER OF BARS IN EACH SIDE	4	u			4	u		
STEEL RATIO	3.46%	%			3.46%	%		
AXIAL FORCE %	5.00%	%			5.00%	%		
WIDTH OF SECTION	21	(in)	533	(mm)	21	(in)	533	(mm)
DEPTH OF SECTION	21	(in)	533	(mm)	21	(in)	533	(mm)
COVER TO MAIN STEEL	1 2/8	(in)	30	(mm)	1 2/8	(in)	30	(mm)
fy =	65,000	(psi)	448	(MPa)	65,000	(psi)	448	(MPa)
Es =	29,007,548	(psi)	200,000	(MPa)	29,007,548	(psi)	200,000	(MPa)
f'c =	4,351	(psi)	30	(MPa)	4,351	(psi)	30	(MPa)
Ec =	3,759,897	(psi)	25,924	(MPa)	3,759,897	(psi)	25,924	(MPa)
APPLIED AXIAL LOAD (P)	96	(kip)	427	(kN)	96	(kip)	427	(kN)
MAIN BAR DIAMETER	10.00	#	32	(mm)	10.00	#	32	(mm)
DISTANCE BETWEEN LONG. BARS	5 1/2	(in)	141	(mm)	5 1/2	(in)	141	(mm)
TENSION STEEL AREA	5	(in^2)	3,281	(sq mm)	5	(in^2)	3,281	(sq mm)
COMPRESSION STEEL AREA	5	(in^2)	3,281	(sq mm)	5	(in^2)	3,281	(sq mm)
SIDE STEEL AREA	5	(in^2)	3,281	(sq mm)	5	(in^2)	3,281	(sq mm)
NUMBER OF TIE LEGS	4.00	(u)	4	u	2.00	(u)	2	u
TIE DIAMETER	3.00	#	9.51	(mm)	3.00	#	9.51	(mm)
TIE SPACING	3 5/8	(in)	92	(mm)	5 1/2	(in)	140	(mm)
TIE STRENGTH	65,000	(psi)	448	(MPa)	65,000	(psi)	448	(MPa)

3.1.2 Brittle Shear Failure Column - Analytical Model

As part of the experimental program, one of the objectives was to test a specimen with a specific amount of transverse reinforcement to develop a brittle shear failure mode. Four identical specimens with the only difference being the aggregate type, one with normal weight and three with lightweight aggregate, were tested under constant axial and cyclic lateral loading. Expanded shale, clay, and slate were used for the lightweight concrete mixtures. In brief, the purpose was to asses the shear resistance of lightweight concrete when developing a brittle shear failure mechanism. Indeed, that would occur if the shear demand exceeds the shear strength of the element in a region where all the components of shear

resistance, including the concrete component (*Vc)*, contribute to the total shear resistance of the specimen.

In the analytical model, the force versus displacement response curve crosses the shear capacity envelope in the location of the desired brittle shear failure which is the upper plateau where the level of deformation is low. The brittle shear failure specimen had less shear reinforcement and consequently less displacement ductility capacity than the ductile shear failure specimen. In fact, it has the amount of transverse steel that permits a failure when the concrete shear resistance component has not developed a significant degradation just before the failure. Hence, the specimen develops its maximum concrete shear capacity at failure. Finally, the predicted force displacement response and shear capacity envelope for the brittle shear failure mode specimen are shown in Figure 3.2.

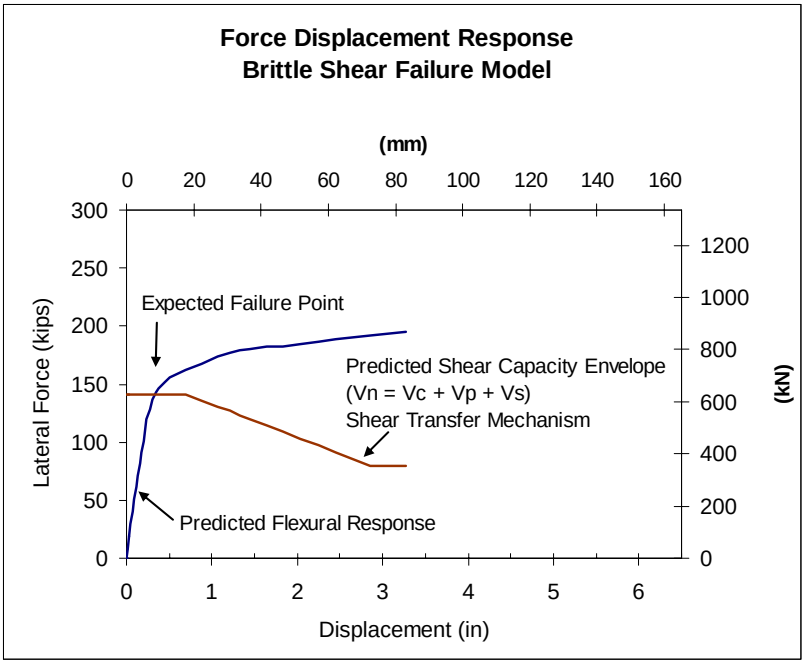

Figure 3.2: Lateral Force Displacement Response (Brittle Shear Failure Specimen)

3.1.3 Ductile Shear Failure Column – Analytical Model

Experimental data related to failures at low and high levels of ductility was important to obtain in the research to asses the shear performance of lightweight concrete, and to obtain a representative data of the shear capacity envelope of the concrete. For the above reason, a ductile shear failure was part of the program, and four identical specimens, with the only difference being the aggregate type, were tested under constant axial and cyclic lateral loading. One specimen was made of normal weight concrete and three with lightweight concrete. In brief, the purpose was to asses the shear resistance of lightweight concrete when developing a ductile shear failure mechanism.

The predicted force versus displacement response curve crosses the shear capacity envelope at the lower plateau where the level of deformation is significant. The ductile shear failure specimen had a larger shear reinforcement ratio and displacement ductility capacity compared to the brittle shear failure specimen. The failure was intended to occur beyond the linear range and when a significant portion of the response of the system was in the non linear range. Moreover, high levels of ductility, and significant degradation of the concrete component shear strength were expected at failure. Finally, the predicted force displacement response and shear capacity envelope for the ductile shear failure model are shown in Figure 3.3.

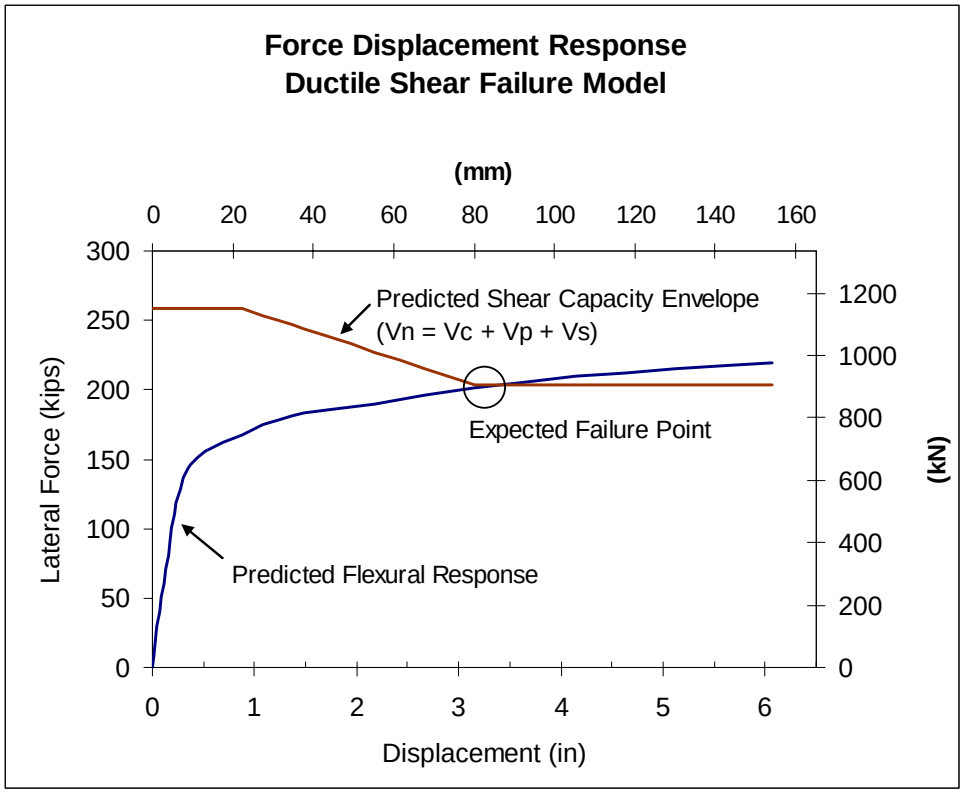

Figure 3.3. Lateral Force Displacement Response (Ductile Shear Failure Model)

3.2 Test Setup and Specimen Design

The test setup for both brittle and ductile shear failure specimens is illustrated in Figure 3.4. The specimens were designed to fail under a cyclic lateral force provided by either a 220 kips or a 440 kips actuator that was horizontally connected to a reaction wall on one side, and to the column on the other. Additionally, the actuator had pinned connections at both tips releasing any moment transfer, and making sure the columns were under single bending. Furthermore, the specimen was located where the actuator had enough stroke to apply forces and displacements in both directions, pushing and pulling. Moreover, the axial load was

constant and it was applied concentrically by two 60 ton jacks located symmetrically over a cross beam located on top of the column. The axial load was applied through two 1 3/8 inches Dwyidag bars under tension, located at both sides of the column, and connected to the cross beam on top of the column and to the laboratory floor at the bottom. In addition, to avoid any lifting of the footing, it was anchored to the floor by four 1 3/8 inches Dwyidag bars that were prestressed with a force of 100 kips in each location.

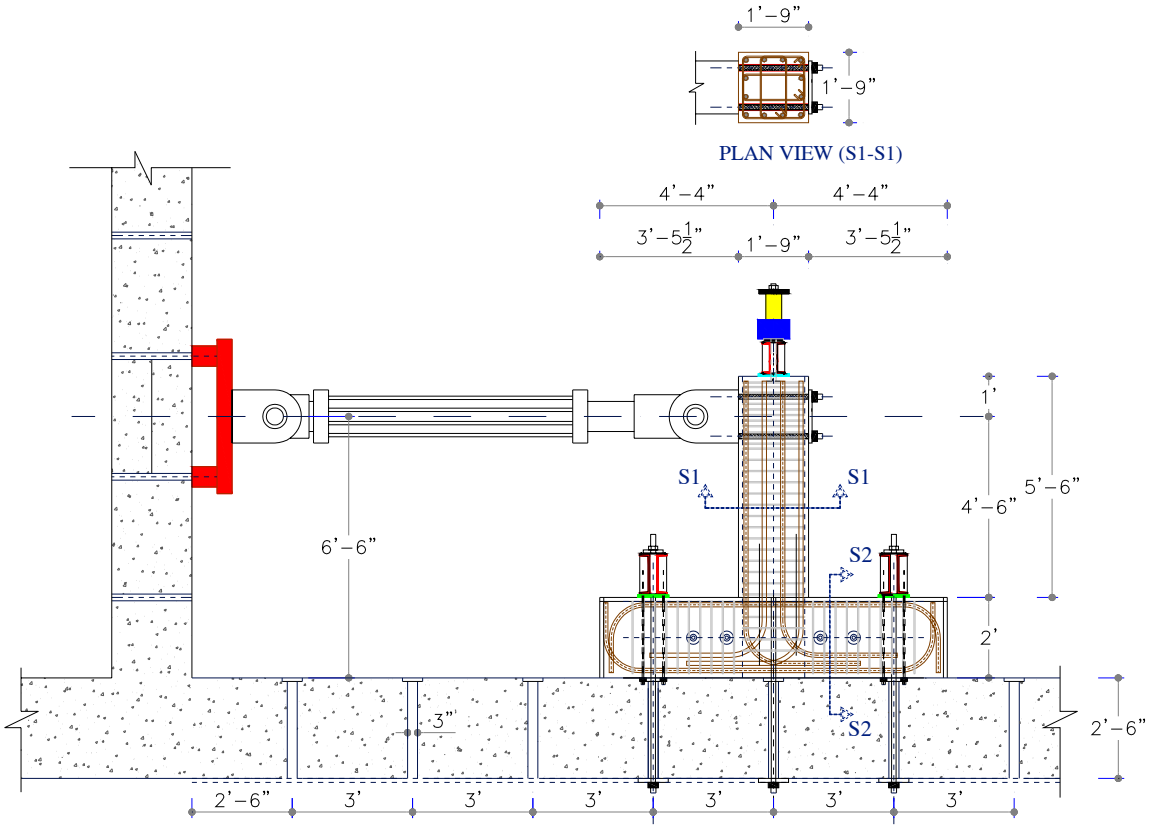

Figure 3.4. Lateral View of Column Shear Test Setup

3.2.1 Form Design

To obtain a good footing-column connection and the same concrete properties in both elements, the footing and column were cast at the same time as one element. As shown in Figure 3.5, a casting bed (8x16 ft^2) was designed to cast two specimens at each time. Both specimen types, brittle and ductile shear failure, were made of exactly the same concrete mixture and cast at the same time in pairs. Finally, the same forms were used four times to obtain eight specimens.

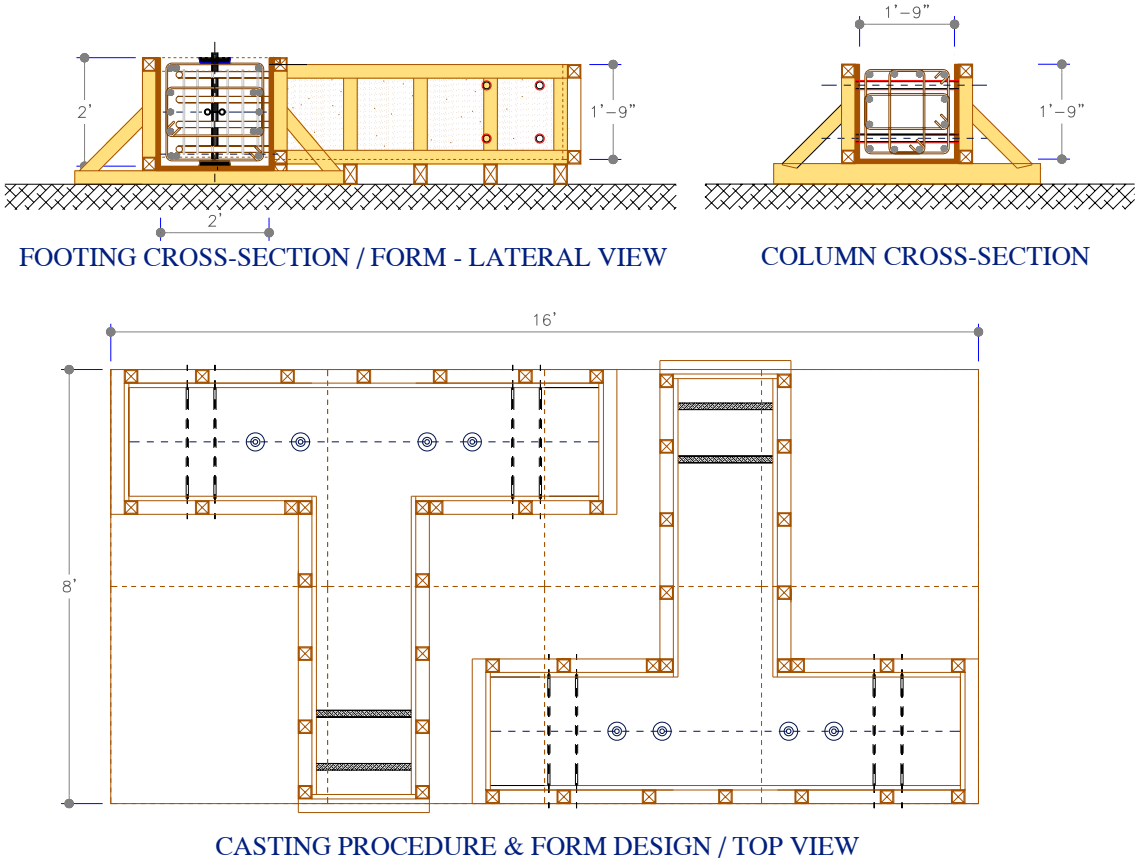

Figure 3.5. Casting Bed and Forms Design

3.2.2 Column and Footing Design

The reinforcement steel details for both column cross sections are shown in Figure 3.1. The rest of the elements such as the reinforced concrete footing sections, steel cross beams, and prestressing bars were designed to remain elastic, and to not develop any significant damage during the tests.

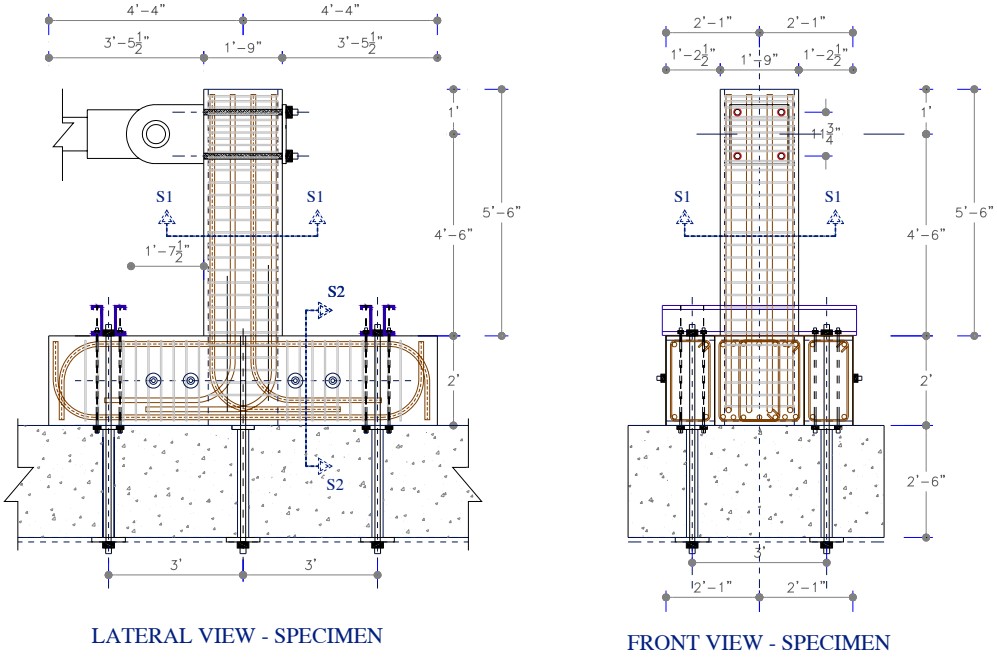

Figure 3.6. Specimen Reinforcement Details - Column and Footing

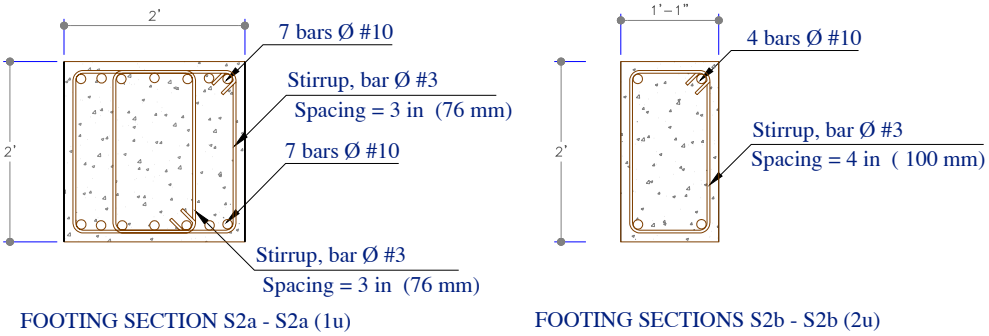

Figure 3.7. Footing Reinforcement Details – Cross Sections

In addition, the footing was designed using three reinforced concrete members as shown in Figure 3.6 and Figure 3.7. The element in the middle was cast at the same time with the column as one member while the two side beams were cast separately, using a normal weight concrete mixture, higher strength of the concrete, and were used in every test. The side footing beams and the footing beam of the specimen were prestressed together with a horizontal compression force of 100 kips. The footing members were also designed to resist vertical prestressing forces of 100 kips in four locations where the specimen was anchored to the floor to avoid any lifting.

3.3 Specimens Construction

Some details of the construction process are discussed in this section. Before the construction of the specimens, reinforcement steel design was detailed for the members and connections. For instance, more stirrups were placed on the top region of the column where the actuator was connected, and where otherwise, some stress concentration could have caused some damage (see Figure 3.8). Furthermore, the transverse reinforcement of the column was placed along the entire element including the depth of the footing-column connection. Similarly, the connection was confined in both directions since footing stirrups were also placed along the entire footing length as shown in Figure 3.9.

The cages were tied and the specimens cast either inside or near the laboratory where high quality control was possible. During the construction, the spacing between stirrups and longitudinal bars was carefully controlled to follow the design as close as possible. In the

same manner, the forms were carefully built making sure the shape of the specimen matched the design as accurately as possible. Furthermore, while casting the specimens, and after that, all the recommendations to acquire good quality concrete were followed. For instance, Figure 3.13 shows the specimens being cured.

Figure 3.8. Reinforcement Steel - Ductile Shear Failure Specimen (Top), Brittle Shear Failure (Bottom)

Figure 3.9. Reinforcement Steel – Column - Footing Connection

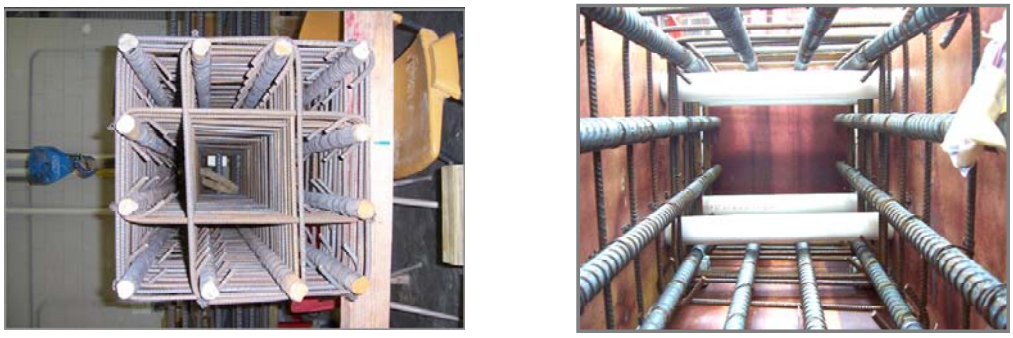

Figure 3.10. Steel Column Cross Sections – Ductile Shear Failure (Left), Brittle Shear Failure (Right)

Figure 3.11. Forms, Reinforcement Steel, and Ducts - Two Specimens

Figure 3.11 shows a pair of specimens, ductile and brittle shear failure over the casting bed before being cast. Ducts were placed for the actuator-column connection, for the prestressing bars to connect the footing elements, for the prestressing bars to anchor the specimen to the floor, and for the strain gages cables.

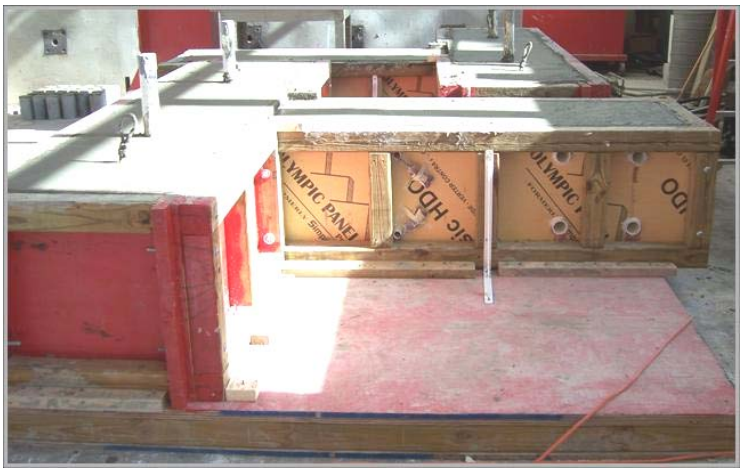

Figure 3.12. Two Specimens after Being Cast

Figure 3.13. Curing of the Specimens

Figure 3.14. Specimens after Being Cured

Representative samples of the each concrete mixture were obtained while casting the specimens. The material tests were performed to estimate the strength of the concrete at the 7^{th}, 14^{th}, 21^{st}, and 28^{th} days, and also at the day of the test. Information such as air content and unit weight was also obtained. Material tension tests of the longitudinal reinforcement steel of the columns were also performed. As a result, it was possible to obtain the actual stress versus strain curve of the steel including the strain hardening portion of the curve. Consequently, the force deformation response of each column was recreated more accurately using real data such as the actual concrete compressive strength as well as the longitudinal steel strength.

3.4 Material Tests and Results

Four concrete mixtures were used for eight specimens. Each concrete mixture was used for both specimen types, brittle and ductile shear failure. Moreover, normal strength and normal weight concrete was used for the first two specimens. In addition, expanded shale, clay, and slate structural lightweight aggregates were used for six specimens as summarized in Table 3.2. The specifications for each concrete mixture are also specified in Table 3.3.

Concrete cylinders were cast and set beside the specimens under the same environmental conditions to obtain consistent results. For each pair of specimens cast at the same time, twenty-one four by eight inches cylinders were cast and tested following ASTM procedures to estimate the strength at 7, 14, 21, 28, and at the day of the test. A total of 84 cylinders were tested. The results are shown in Table 3.4.

Table 3.2. Tests Program

Project Test Program			
STRENGTH	**FAILURE MECHANISM**	**AGGREGATE**	**TEST NAME**
Normal Strength (4 ksi)	Brittle Shear Failure	Normal Weight	(NW-NS-BSF)
		Lightweight (1)	(LW1-NS-BSF)
		Lightweight (2)	(LW2-NS-BSF)
		Lightweight (3)	(LW3-NS-BSF)
	Ductile Shear Failure	Normal Weight	(NW-NS-DSF)
		Lightweight (1)	(LW1-NS-DSF)
		Lightweight (2)	(LW2-NS-DSF)
		Lightweight (3)	(LW3-NS-DSF)

Table 3.3. Specimens Concrete Mixture Specifications

Concrete Mixture Specifications				
Concrete Type	**Aggregate Type**	**Aggregate Location in the U.S.**	**Unit Weight (lbs/ft^3)**	**Air Content (%)**
Normal Weight	Normal Weight	-	143.08	6.50%
Lightweight (1)	Expanded Slate	Southeast	119.00	4.75%
Lightweight (2)	Expanded Shale	Midwest and North	116.64	5.00%
Lightweight (3)	Expanded Clay	West Coast	122.45	5.00%

Table 3.4. Average Concrete Strength Results

Average Concrete Strength (psi)				
Days after Casting Date	**Normal Weight Concrete Specimens**	**Lightweight Concrete (1) Specimens**	**Lightweight Concrete (2) Specimens**	**Lightweight Concrete (3) Specimens**
7	3,116	5,249	-	4,125
14	3,204	6,060	4,277	4,660
21	2,959	6,421	4,236	5,006
28	3,580	6,409	4,842	4,931
Test	3,946	7,315	5,164	4,969

Regarding the material tests for the reinforcement steel, six samples were taken from different column stirrups and longitudinal column bars. It is important to observe that all the steel for the columns was acquired at once, and form the same supplier. Accordingly, the steel came from the same production batch, and had the same properties in all the specimens. Finally, stress-strain curves were obtained to improve the moment curvature analysis and force deformation response analytical models with the actual material properties of each test.

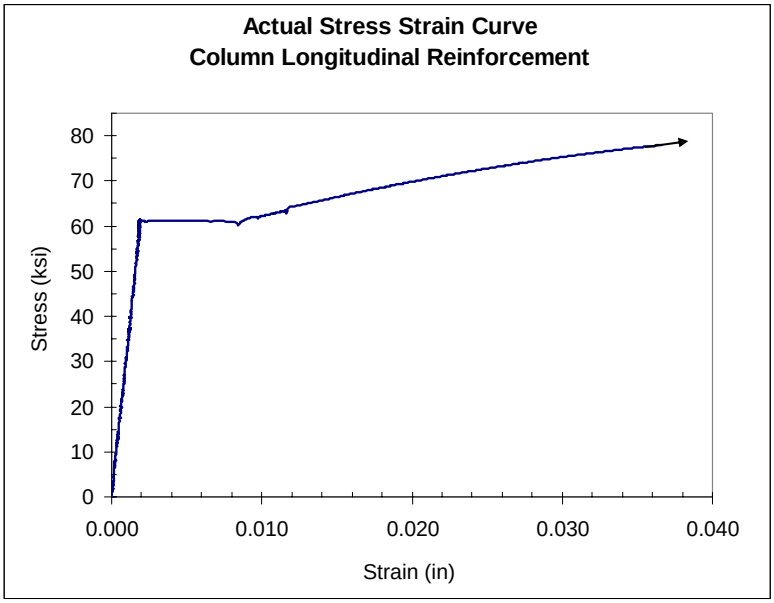

Figure 3.15. Stress Strain Curve – Longitudinal Column Bar - Tension Test Result

Table 3.5. Stress Strain Curve –Column Stirrup - Tension Test Result

Average Reinforcement Steel Strengths (ksi)			
Description	**Diameter (in)**	**Actual Yielding Strength (ksi)**	**Estimated Ultimate Strength (ksi)**
Longitudinal Column Reinforcement	1 2/8	62.35	90.00

Chapter 4: TEST SETUP

4.1 Test Setup Details

Figure 4.1 illustrates all the elements involved in the test setup. Among others, the design of the setup considered factors such as the necessity of applying a cyclic lateral load and a constant axial load, the importance of avoiding lifting or sliding of the footing, as well as avoiding any damage in any element other than the column.

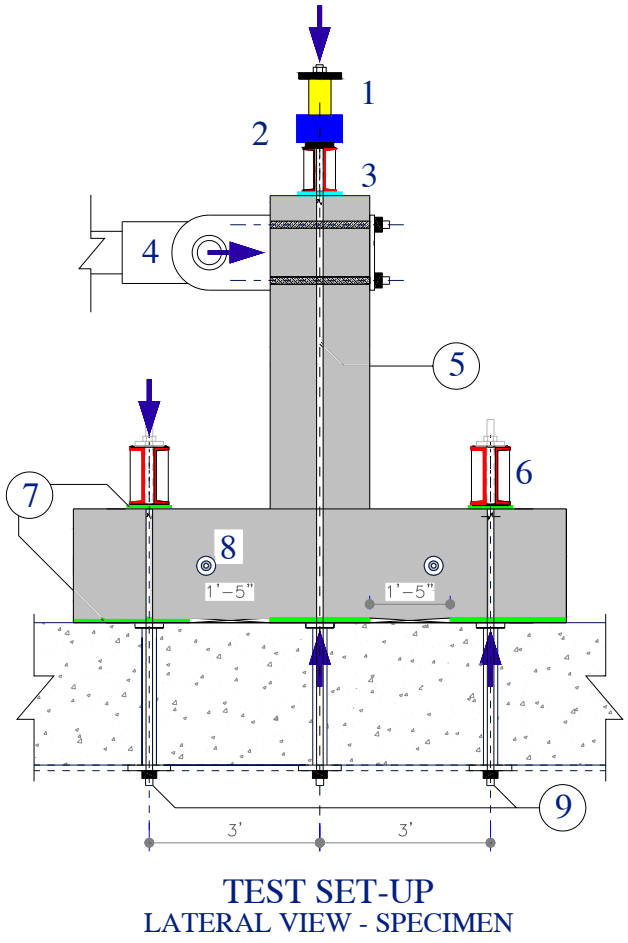

1.- 60 ton jack

2.- Two 200 kips load cells – Axial load

3.- Cross beam - Axial load

4.- 220 or 440 kips actuator – Lateral load

5.- Two 1 3/8" Dwyidag bars
50 kips each, axial Load

6.- Cross Beam – Tie-downs

7.- Hydro-stone – Supports

8.- Two 1 3/8" Dwyidag bars – 50 kips each footing beam side location

9.- Four 1 3/8" Dwyidag bars – 110 kips each support

Figure 4.1. Test Setup Lateral View

4.1.1 Footing and Supports Setup

A compressible material was placed on specific areas between the footing and the floor of the laboratory leaving a gap in the remaining areas. Figure 4.2 shows the areas where the compressible material was placed on. The gap between the footing and the floor of the laboratory was filled with hydro-stone to guarantee a uniform distribution of the reaction forces at the supports. Moreover, the specimen was leveled before pouring the hydro-stone making sure it was vertical and aligned with the actuator. Figure 4.3 shows the specimen over the insulating boards before the hydro-stone was poured to fill the gap.

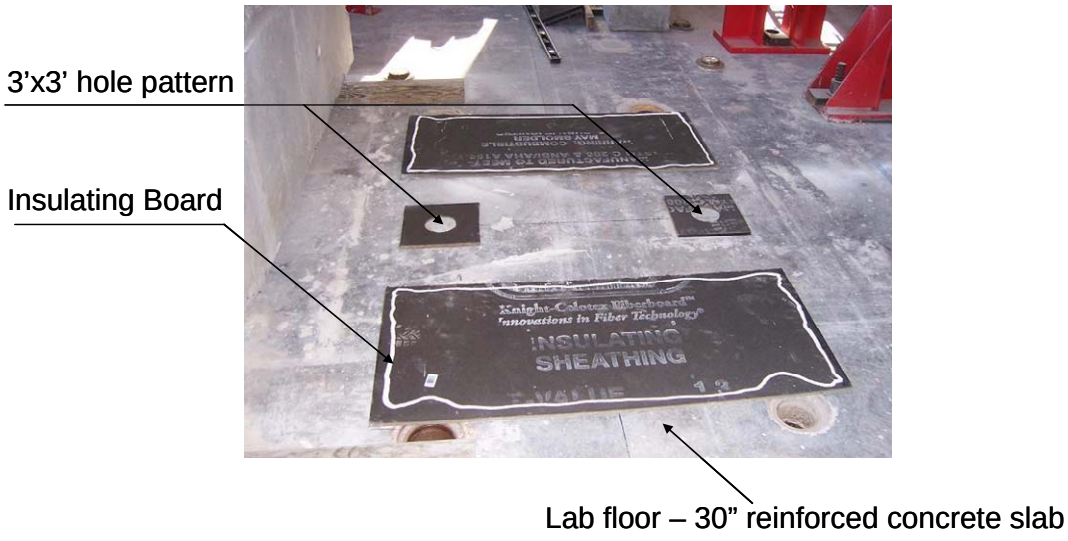

Figure 4.2. Supports Design and Details

The presence of the compressible material is part of the supports design. The purpose was to force the reaction loads to remain in the same location defined by the area filled with hydro-stone. Figure 4.1 and Figure 4.3 show the location of the voids and hydro-stone illustrating the purpose of the design.

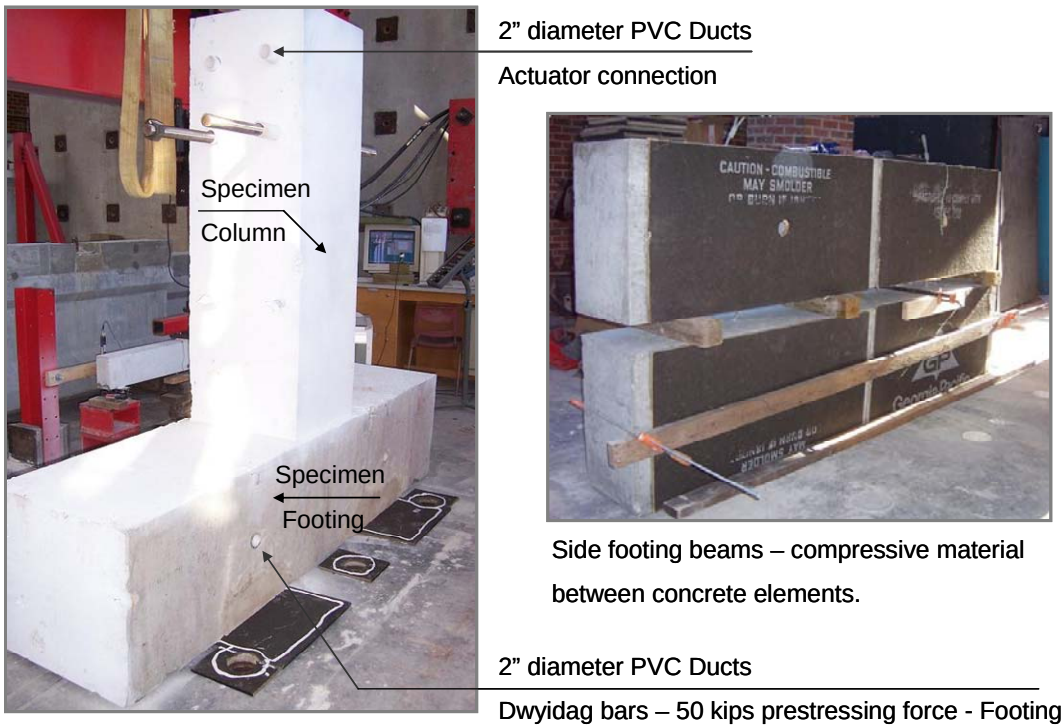

Figure 4.3. Test Setup Support Details (Left), Footing Side Beams (Right)

As analyzed using a finite element model of the specimen, the design of the supports reduced the rocking effect induced by the lateral load applied on top of the column because it prevents a portion of the footing to make contact with the floor. The moment at the base of the column is transferred to the footing elements, and it is critical in the sections closer to the column. As a result, curvature of the footing elements is higher in the sections closer to the column also. Finally, the proposed design with gaps under the sections of the footing closer to the column, allows the footing to develop curvature without re-distributing the reaction force towards the column. Otherwise, when significant level of deformation exists, the resultant force of the reaction located on the side of the footing in contact with the floor, moves towards the column and loses lever arm. As a result, the deformed shape of the

footing is modified inducing absolute rotation of the connection and possibly some lifting of the footing on its opposite side. In brief, since this design reduced the possibility of footing lifting, the risk of additional increments in the axial load was reduced. Finally, lifting of the footing would have caused stretching of the bars that transferred axial load, and that was prevented by implementing the above mentioned design.

A compressible material was also used between footing elements as shown in Figure 4.3. The purpose was to distribute the prestressing force of 100 kips that was applied to compress the three elements against each other. In general, avoiding stress concentration in small areas was important since no damage should occur in the footing elements.

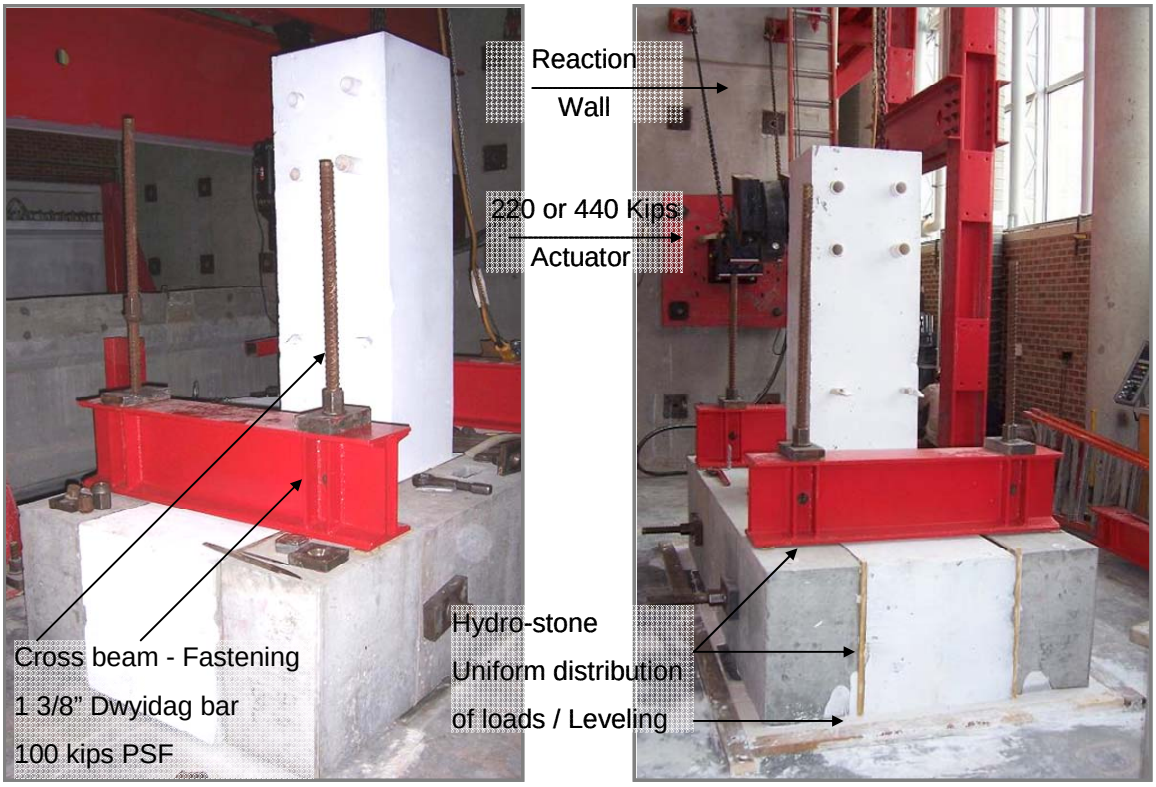

Figure 4.4. Cross Beams to Anchor the Footing (Left) Hydro-stone (Right)

As shown in Figure 4.4, hydro-stone was also placed under the two cross beams that were used to anchorage the footing to the floor. In the same manner, the purpose was to uniformly distribute the forces between the steel beams and the top of the footing. In fact, a total of 200 kips were distributed to the area in contact.

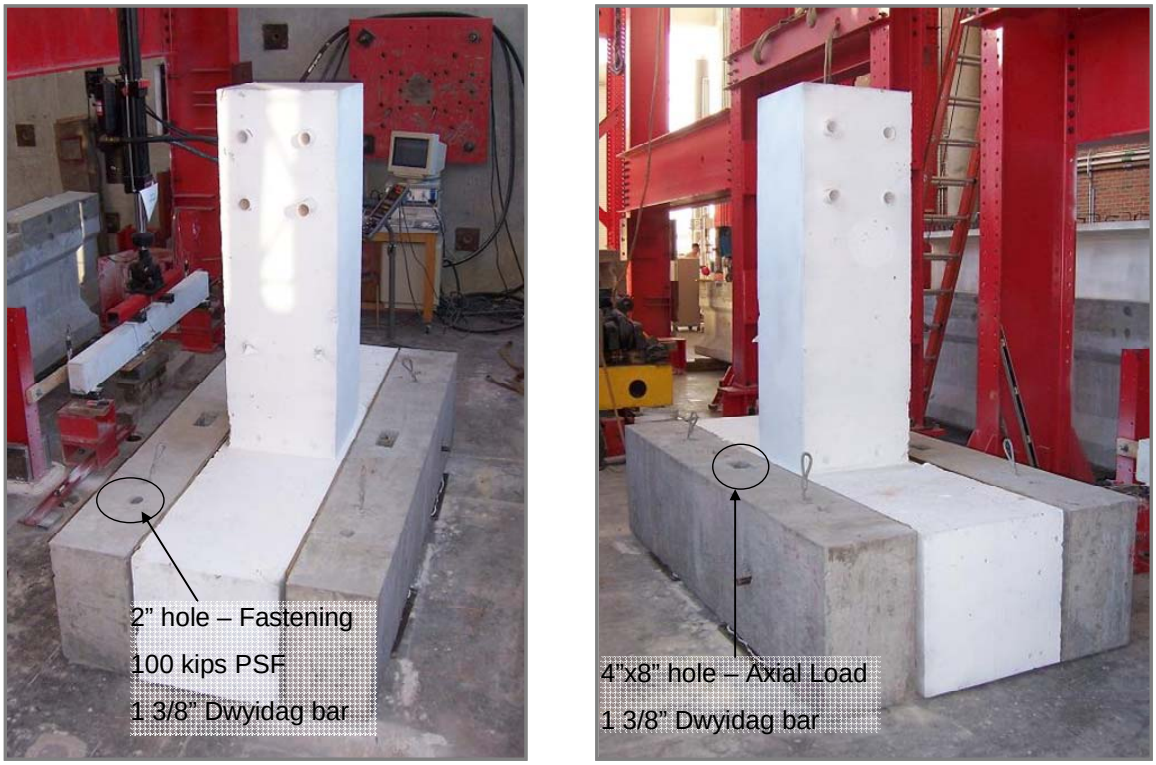

Figure 4.5. Fastening Ducts Locations

As Figure 4.5 illustrates, the design included several ducts that allowed 1 3/8 inches diameter Dwyidag bars to fasten the footing to the floor, and to apply the axial load with bars that crossed the footing.

4.1.2 Axial and Lateral Loads Setup

The axial load was applied through a cross beam located on top of the column, and in the center of the column cross section. Moreover, a neoprene bearing pad was placed between the steel beam and the top of the column to uniformly distribute the load. In addition, parallel to the column, Two 1 3/8 inches diameter Dwyidag bars connected the tips of the cross beam to the floor of the laboratory as shown in Figure 4.6. Furthermore, two 60 ton capacity jacks were used to apply the axial load through the bars while two 200 kips load cells were used to measure and control the level of axial load. In order to guarantee symmetry, only one pump was connected to both jacks to distribute the same pressure. Consequently, the same load was applied at both tips of the cross beam.

Figure 4.6. Axial Load Setup

During the first four tests, the cyclic lateral load was applied using an actuator with a capacity of 220 kips in the pushing direction, and 150 kips in the pulling direction. An actuator with a capacity of 440 kips in the pushing direction, and 300 kips in the pulling direction was used for the last four tests. The actuator was horizontally connected to the reaction wall on one side and to the column on the other side. Four threaded rods connected the actuator to the specimen through ducts located on top of the column as shown in Figure 4.7. It is important to notice that the specimen was designed to match the height of both connections at the tips of the actuator to make sure it was horizontal and aligned with the column axis.

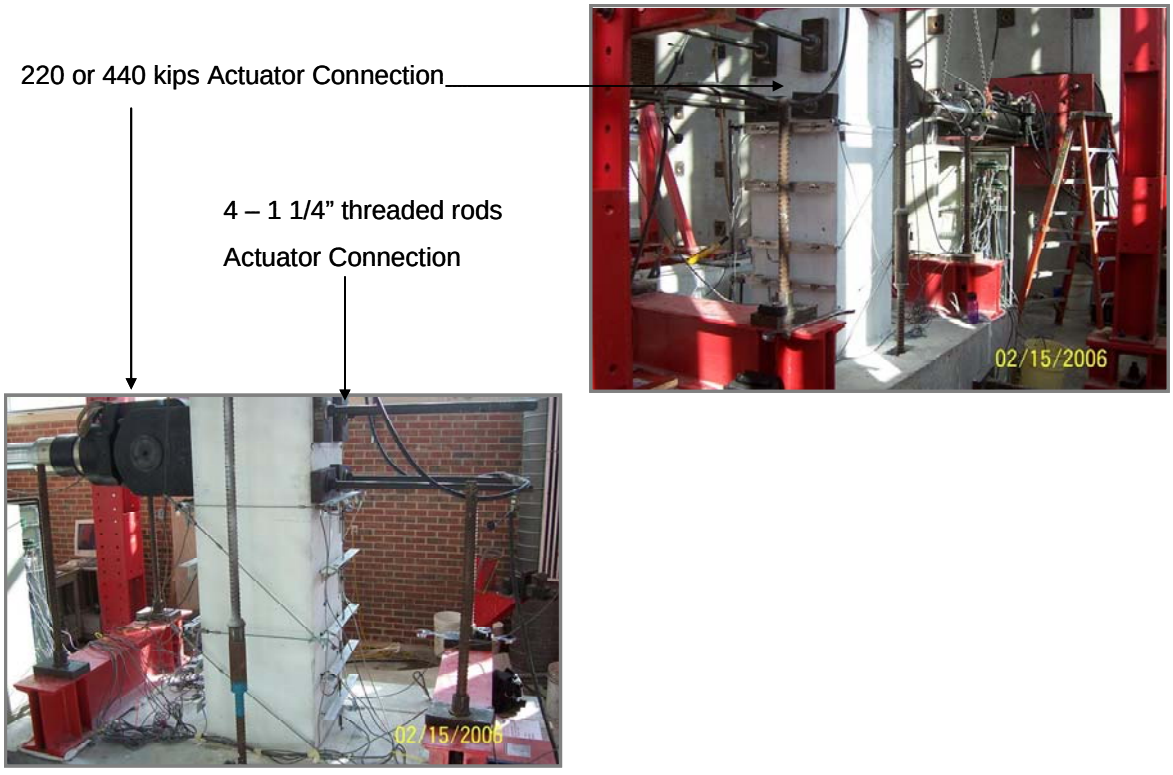

Figure 4.7. Lateral Load Setup

4.2 Instrumentation

For all the tests, the location of the specimen and instruments followed the same adopted sign and direction convention, and it was related to the loading directions and to the relative instrumentation measurements. The direction of the lateral load defined the north and south directions. As a result, from the center of the column cross section, south was the direction defined by the pushing action of the actuator away from the reaction wall, and north by the pulling action of the actuator towards the reaction wall. East and west directions were perpendicular to the north - south line, in the same horizontal plane, and following the same order as geographic coordinates. Faces north and south of the specimen were the planes of the column perpendicular to the lateral load while east and west faces of the specimen were the planes of the column parallel to the lateral load. Finally, all the instruments were placed and labeled considering this convention, and all the observations, notes, and data of all tests followed the same rules.

In terms of relative measurement, the instruments measured values with a positive sign when extending or elongating, and negative signs when getting shorter. In addition, regarding the location of the instruments in the vertical direction, along the longitudinal axis of the column, they were labeled in ascending order from bottom (at the base of the column) to top (at the connection between actuator and column). For instance, a linear potentiometer located in the first cell at the bottom of the north face of the column was labeled as P1N. The letter P was used for linear potentiometers, letters SP for linear string potentiometers, letters SG for strain

gages, and letters LC for load cells. Finally, the first letter of the direction word was used to represent the respective direction.

In brief, the instrumentation consisted of strain gages, linear potentiometers, string potentiometers, and load cells. Moreover, the same procedure was followed for all the instruments in terms of calibration and location in the specimen. In the same manner, the data acquisition system was the same for all the tests. Minutes before each test, notes about the actual location of external instruments were taken, and the data was processed with this information.

4.2.1 Strain Gauges

Internal instruments located on the outside of the stirrups and at the middle of the east and west faces of the column were used to measure deformation of the transverse reinforcement steel at different heights of the column. Strain gages obtained from the same supplier and batch were used in all the specimens. Among other specifications, a C2A strain gage produced by Vishay Micro-Measurements with a two percent strain limit, 120 Ohms resistance, and a 2.075 gage factor were used in all tests. Finally, they were placed following the recommended procedure as described in the following paragraphs.

In order to have a flat clean surface of the reinforcement steel, an electric grinder was used as shown in Figure 4.8. Moreover, the surface of the stirrup was sanded carefully to not reduce the cross section of the stirrup. Due to the small diameter of the bar (#3), the sanded surface

was located between one long rib and half of the distance to the next one (1/4 of the circle). In that way, most of the material taken off from the bar was part of the ribs. However, considering the diameter of the bar and the width of the strain gage (2.5 to 3 mm approximately) the cross section of the bar was barely reduced, but the reduction is assumed to be insignificant.

Figure 4.8. Strain Gages Setup – Materials Used (Left), Grinder (Right)

After getting a flat, smooth, and clean surface of the steel, plastic zip ties were used to hook the wires of the strain gage matching the position in which the strain gages could be placed over the smoothest surface of the steel. Moreover, the surface was cleaned using Methyl Ethyl Ketone M.E.K. Afterwards, the plastic protection of the strain gage was taken off without touching the strain gage, and type was stuck to the top of the strain gage. Then, Catalyst was spread over the strain gage surface, and after 60 seconds; one drop of glue was placed close to the location of the wires at one edge of the strain gage. The glue was spread and squeezed gradually from the wire to the end of the strain gage until all the strain gage surface was in contact with the steel. In addition, pressure was applied for at least one minute. After that, the type was removed carefully from the end of the strain gage to the

location of the wires. In order to not lift the strain gage, the type was removed in a parallel direction relative to the stirrup. Finally, the wires were lifted from the bar making sure that they were not in contact with any steel element.

Figure 4.9. Strain Gage without Coating

In addition, the resistance signal was checked to be 120 Ohms as specified by the supplier. Thereafter, a coating material was used to isolate the wires and to prevent any damage in the strain gage and contiguous wires before and during the test, and then, additional protection was provided over the strain gage as shown in Figure 4.10.

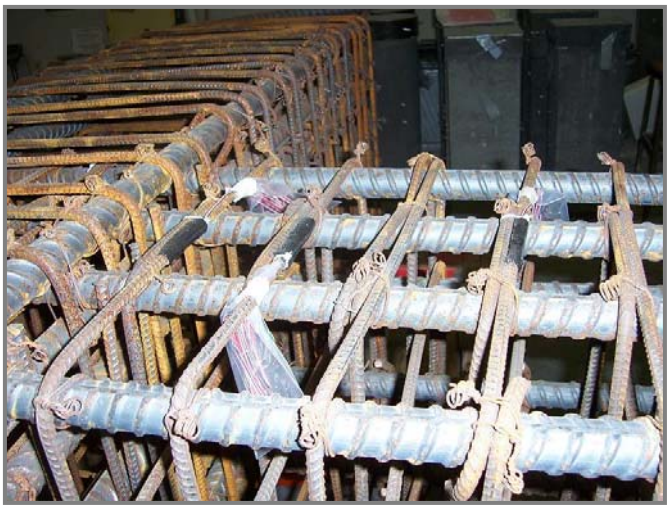

Figure 4.10. Protected Strain Gages

Finally, small plastic ties were used to carry the wires through the rebar to a specific location in the column and then outside. Moreover, there were two holes in the forms for the wires to come out. In addition, notes were taken about the location of the strain gages. Specifically, side and distance from the footing beam were used to label the wires. In general, the location of the strain gages followed the configuration shown in Figure 4.11 in all the specimens.

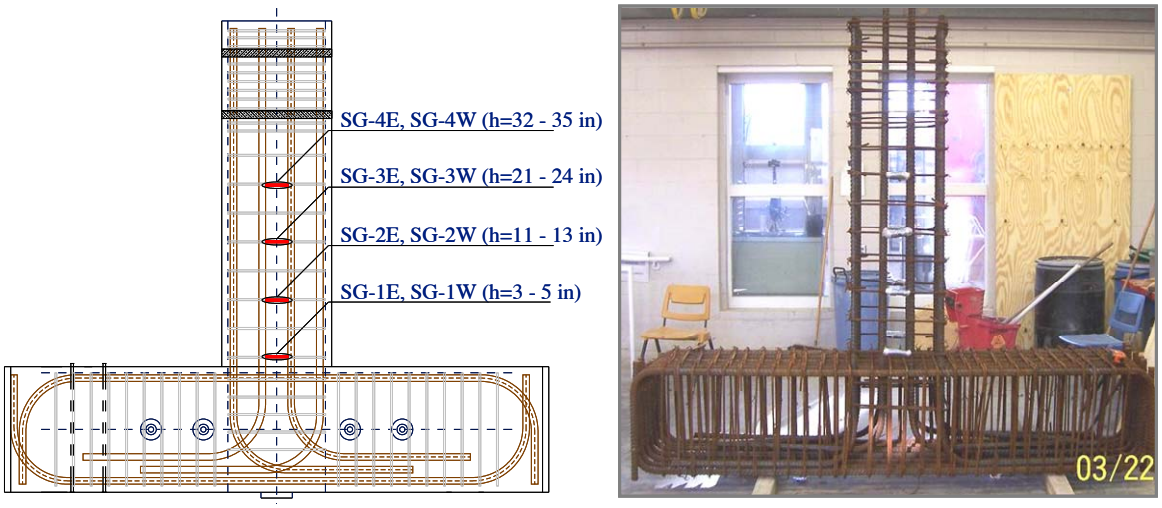

Figure 4.11. Strain Gages - Location

4.2.2 Linear Potentiometers

Linear potentiometers were externally used to measure displacements due to flexural and shear deformation. To measure displacements parallel to the column face caused by flexural deformation of the specimen, five linear potentiometers were placed besides the north and south planes of the column. Additionally, the potentiometers were located vertically in the middle of north and south faces to measure displacements over each cell length proportional to those at the column faces. The potentiometers were placed between aluminum angles

anchored to the column, and were labeled from bottom to top gages defined by the aluminum angles. In fact, from the data obtained by these instruments, curvature and flexural deformation was determined and analyzed. In addition, the same configuration was followed for all the tests, and Figure 4.12 illustrates the location of the potentiometers located in north and south faces. Finally, the exact location and distances for each specimen were measured and written down some minutes before each tests.

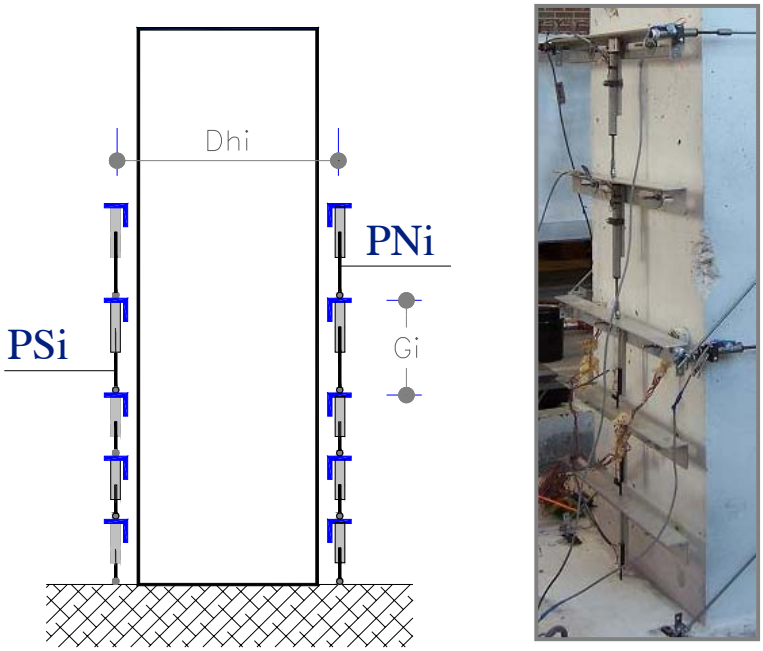

Figure 4.12. Linear Potentiometers for Flexural Analysis

$$\theta_i = \frac{PNi - PSi}{Dhi} \qquad \textbf{(4–1)}$$

$$\phi_i = \frac{\theta_i}{Gi} \qquad \textbf{(4–2)}$$

$$\Delta_{flex} = \iint \phi \qquad \textbf{(4–3)}$$

Having the displacements measured by the potentiometers located on faces north and south, the relative angle of rotation at each gage cell was calculated using equation (4–1). It is important to notice that the sign convention described in section 4.2 was followed, and that the calculations are valid only if that is the case. Moreover, it is also important to notice that no absolute values were used in equation (4–1) to not introduce errors considering the elongation of the column due to cracking of the concrete in the non linear range. Otherwise, even when there was no actual rotation, an angle of rotation would have been calculated as a result of positive readings of both potentiometers located in north and south sides. Furthermore, the rotation calculated using equation (4–1) has a sign for each direction according to the sign convention. For instance, the relative rotation will be positive for push direction and negative for pull direction when the specimen is in the linear range. Beyond the linear range, residual deformation may appear even without applying any lateral force. Continuing with the calculations, curvature was obtained using equation (4–2) where the rotation at each gage cell is divided by the vertical length of the respective cell. Finally, the displacement component due to flexural deformation of the specimen was obtained by a double integration of the actual curvature along the desired length of the column.

In addition, linear potentiometers were also externally used to measure displacements due to shear deformation. Four linear potentiometers were placed on east and west faces of the column to measure displacements parallel to the column face due to shear. In addition, two diagonal and two horizontal elements were placed as shown in Figure 4.13. The potentiometers were labeled from bottom to top. Therefore, the diagonal elements had

numbers 1 and 3, and the horizontal elements had numbers 2 and 4. Furthermore, contiguous elements were connected to the same joints making sure they were aligned with the joint. Finally, shear deformation and shear displacement components were derived and analyzed from the data obtained by these instruments. Indeed, the same configuration was followed for all the tests in terms of the location of the instruments as shown in Figure 4.13. Certainly, the exact location and distances for each specimen were measured and written down some minutes before each tests.

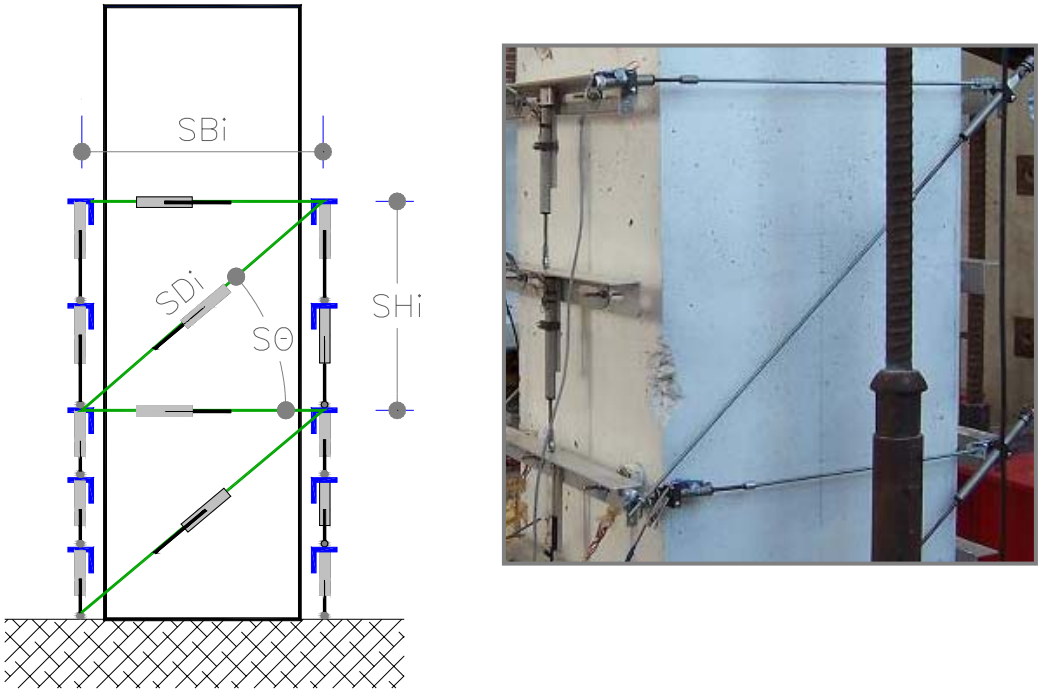

Figure 4.13. Linear Potentiometers for Shear Deformation Analysis

$$S\theta_i = \sin^{-1}\left(\frac{SH_i}{SD_i}\right) \qquad \textbf{(4–4)}$$

$$S\theta_i^{\Delta} = \sin^{-1}\left(\frac{SH_i^{\Delta}}{SD_i^{\Delta}}\right) \qquad \textbf{(4–5)}$$

$$\Delta si = \cos(S\theta_i^{\Delta}) \cdot SD_i^{\Delta} - SB_i^{\Delta} \quad \textbf{(4–6)}$$

$$\varepsilon s_i = \frac{\Delta si}{(SH_i^{\Delta})} \quad \textbf{(4–7)}$$

$$\Delta_{Shear} = \sum \varepsilon_{si} SH_i^{\Delta} \quad \textbf{(4–8)}$$

Similarly, displacements measured by potentiometers located on faces east and west allowed the calculation of shear strains and column displacements due to shear deformation. Indeed, equation (4–4) defines the initial angle between the diagonal and horizontal elements considering joint to joint distances. In addition, using equation (4–5) the new angle was calculated as a function of the new diagonal and vertical distances considering length changes read by the potentiometers. Furthermore, the same sign convention described in section 4.2 was used for these equations. The relative shear displacement of the specific gage was calculated using equation (4–6) having the new angle, and diagonal and horizontal distances. Moreover, average shear strain for a specific gage was also determined using equation (4–7). Finally, the column displacement component due to shear deformation was calculated using equation (4–8).

In conclusion, the purpose of obtaining column displacement components due to flexural and shear deformation was to compare those values to total top displacement values measured

separately by string linear potentiometers. Moreover, as conceptually shown in Figure 4.14, flexural and shear displacement components were compared at different displacement ductility levels. Finally, it is important to notice that this analysis shows the differences between deformation components along the whole response of the specimen.

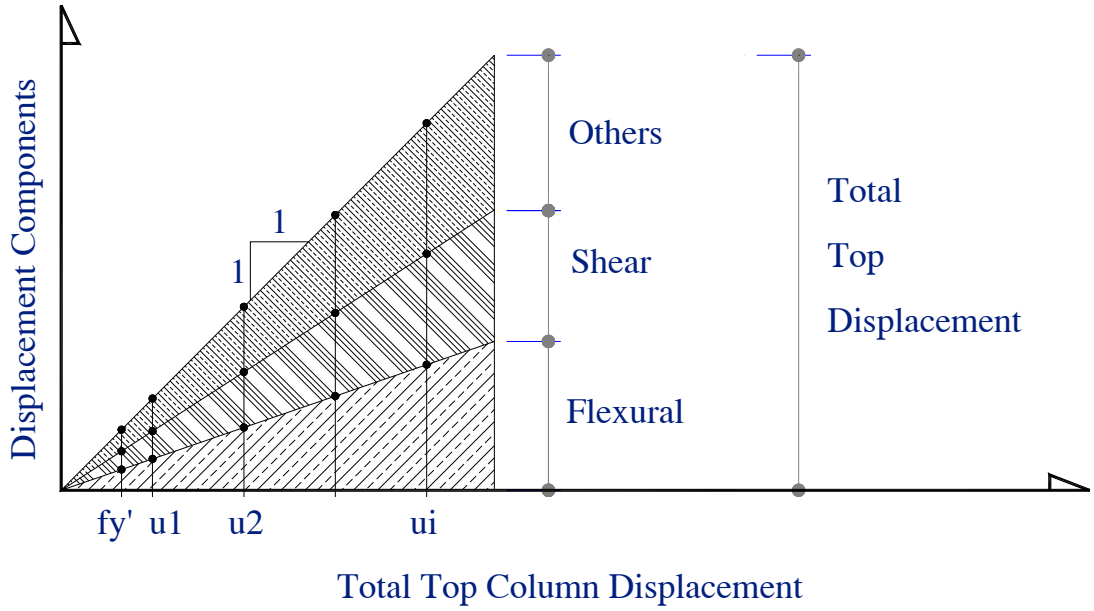

Figure 4.14. Displacement Components versus Total Top Displacement Graph - Conceptual

4.2.3 String Linear Potentiometers

String linear potentiometers where used to measure total displacements at the top the column. Two string potentiometers were anchored to a separate steel element that was connected to the laboratory floor with no contact or interference with the specimen. Moreover, as shown in Figure 4.15, the string potentiometers measured horizontal displacements at the location of

the lateral load (center of the actuator). In brief, the strings were horizontal, parallel to each other, parallel to the lateral force vector, and located on the south face (10 1/8 inches towards east and west directions from the center of the column).

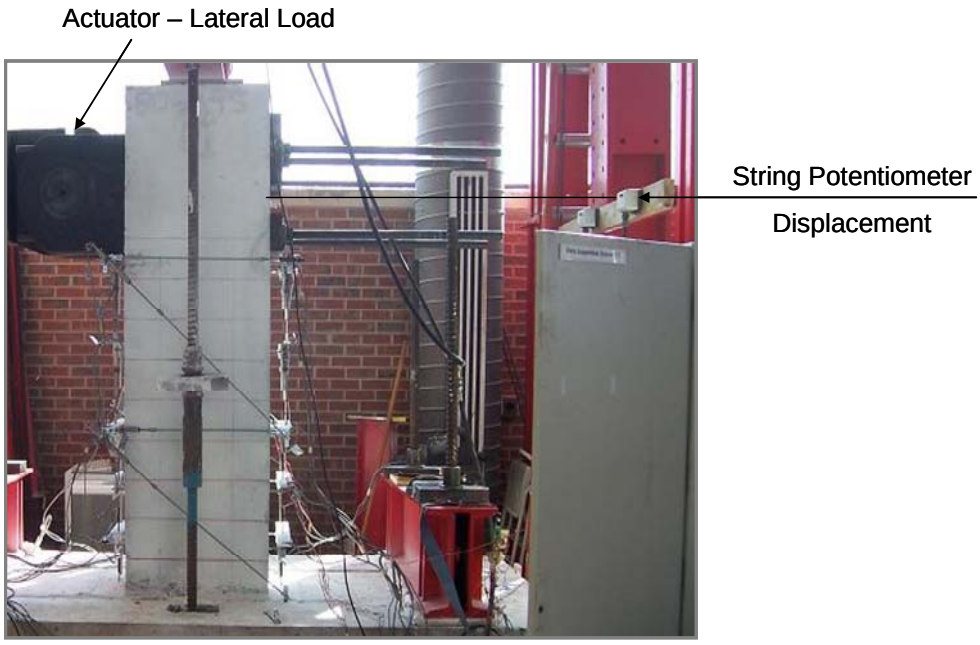

Figure 4.15. String Linear Potentiometers – Location

4.2.4 Load Cells Specifications

Two load cells were used to measure and control the magnitude of the axial load. In fact, the load cells, model 1240BTN-200k-B, had a capacity of 200 kips, and were placed over the cross beam located on top of the column. Specifically, between steel plates and the jacks that applied the axial load.

4.2.5 Actuator Specifications

The first four specimens, two made of normal weigh and two made of lightweight concrete type one, were tested using a 243.60T actuator model with maximum force capacities of 220 kips and 150 kips in the pushing and pulling direction respectively. Whereas, the remaining four specimens, made of light weigh concrete types 2 and 3, were tested using an actuator model 243.80T, with maximum force capacities of 440 kips in the pushing direction, and 300 kips in the pulling direction. Both actuators had the same stroke capacity of 40 inches.

4.2.6 Data Acquisition System Specifications

An Optim - Megadac data acquisition system was used to read all the data. Moreover, a TCS program was used to configure all the channels using the same sign convention described in section 4.2. For instance, the wires of the instruments were labeled at the end that was connected to the data acquisition, and the channels were assigned to the respective instrument in the file created to record the data of each test. In addition, all the instruments were calibrated and checked before being used, as well as the signal range, and the linearity of the signal as a function of the displacements read by the instruments. Finally, data points were taken every five seconds, and a lateral force versus displacement graph was plotted simultaneously using an (x-y) recorder connected to the data acquisition card.

4.2.7 Tests Loading Protocol

Having the analytical model as a reference, two procedures were followed in terms of loading protocol during the test. First, a force controlled cyclic loading from zero to the first

yielding point, and then a displacement controlled cyclic loading beyond the first yielding point. Moreover, a lateral load of 127 kips was estimated as the required load to reach the first yielding point, or the point at which the longitudinal reinforcement steel of the column reaches the yielding strength. Furthermore, for the force controlled procedure, the cyclic lateral load was applied from zero to the first yielding point in increments of a quarter of the first yielding force. In fact, only one cycle was applied during force controlled loading. Subsequently, three cycles for each displacement ductility level were applied during the displacement controlled procedure up to failure. Finally, Figure 4.16 shows an example of the loading protocol.

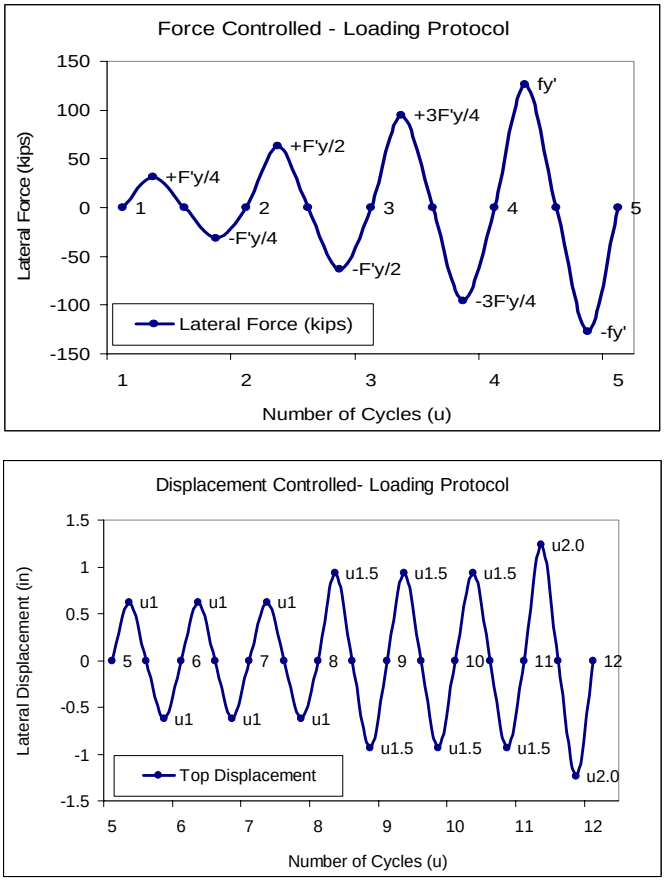

Figure 4.16. Lateral Loading Protocol

Chapter 5: TEST SPECIMENS – BRITTLE SHEAR FAILURE MODE

Facets of all four brittle shear failure tests are discussed in this chapter. It is important to notice that, except for the concrete mixture, all the specimens were built using the same materials and according to the same design. Moreover, the same procedures were applied for all the specimens in relation to the test setup and the actual test. Tests observations are presented in this chapter for one normal weight concrete specimen, and for three lightweight concrete specimens as described in Table 5.1. Finally, following the same order for each specimen, sections such as loading history, test observations, and test results are presented in this chapter.

Table 5.1. Brittle Shear Failure Tests Specifications

Project Test Program - Brittle Shear Failure Specimens							
ACTUAL CONCRETE STRENGTH (psi)	DESIRED FAILURE MECHANISM	AGGREGATE TYPE	AGGREGATE MATERIAL DESCRIPTION	AGGREGATE QUARRY LOCATION IN THE U.S.A.	PREDICTED LWC SHEAR CAPACITY (kips) [a]	MAXIMUM RECORDED SHEAR FORCE (kips)	TEST NAME
3,946	Brittle Shear Failure	Normal Weight	-	-	**143**	144	(NW-NS-BSF)
7,315		Lightweight (1)	Expanded Slate	Southeast		129	(LW1-NS-BSF)
5,164		Lightweight (2)	Expanded Shale	Midwest and North		140	(LW2-NS-BSF)
4,969		Lightweight (3)	Expanded Clay	West Coast		127	(LW3-NS-BSF)

[a] Based on shear transfer mechanism developed by Priestley et al. (1994) and modified for lightweight concrete (Kowalsky et al., 1999 b) as described in section 7.2.

5.1. Normal Weight Concrete – Brittle Shear Failure Test (NW-NS-BSF)

A normal weight concrete, normal strength, and brittle shear failure (NW-NS-BSF) column was tested as a control and reference specimen. The analytical model was used to determine the force controlled loading history, and test data of specimen (NW-NS-BSF) confirmed the consistency between the analytical model and the response of the specimen. Consequently, the remaining specimens were tested using the same loading protocol. In brief, the specimen test discussed in this section was made of normal weight aggregate and normal strength concrete mixture.

5.1.1 Loading History

Loading of the specimen consisted of two procedures to apply a constant axial and a cyclic lateral load during the course of the test. An axial load of 96 kips was applied before applying the force controlled lateral loading as shown in Figure 5.1. One cycle was applied at each level of lateral load for the respective stage. Moreover, force controlled loading continued from a force of zero to the force where the longitudinal reinforcement of the column was assumed to reach the yielding strain in tension, typically referred to as the yielding point (Fy'). Moment versus curvature analysis was used to determine the maximum moment at the base of the column required to reach first yield as some predicted values are shown in Table 5.1. The respective lateral force was calculated as a function of the lever arm of the column under single bending demands. Afterwards, in order to capture the entire force displacement response of the system, a displacement controlled cyclic lateral loading was

applied during the second stage of the test from the equivalent yielding point up to failure. As a result, data was captured even when the strength decreased towards failure. In brief, various cycles were applied to identify stiffness degradation and ductility capacity of the system.

Table 5.2. Predicted Values for a Brittle Shear Failure Test

PREDICTED VALUES	First Yield (εs = 0.002)				Predicted Failure				Theoretical Point Beyond Failure to Determine Bi-linear Aproximation (Mn & Fi at εc = 0.004)			
		Units		Units		Units		Units		Units		Units
Curvature	0.00017	(1/in)	0.00674	(1/m)	0.00020	(1/in)	0.00801	(1/m)	0.00079	(1/in)	0.03119	(1/m)
Moment	571.20	(kip-ft)	774.45	(kN-m)	641.68	(kip-ft)	870.00	(kN-m)	796.49	(kip-ft)	1079.90	(kN-m)
Concrete Strain	0.0013	(u)	0.0013	(u)	0.0015	(u)	0.0015	(u)	0.0040	(u)	0.0040	(u)
Neutral Axis Depth	7.51	(in)	190.67	(mm)	7.38	(in)	187.33	(mm)	5.05	(in)	128.24	(mm)
Steel strain	0.0020	(u)	0.0020	(u)	0.0024	(u)	0.0024	(u)	0.0112	(u)	0.0112	(u)
Shear Demand	127.08	(kips)	565.29	(kN)	142.76	(kips)	635.04	(kN)	177.21	(kips)	788.25	(kN)
Top Displacement [a]	0.27		6.80	(mm)	0.34	(in)	8.70	(mm)	1.21	(in)	30.70	(mm)
Shear capacity	141.32	(kips)	628.64	(kN)	141.32	(kips)	628.64	(kN)	126.69	(kips)	563.55	(kN)
Ductility	0.72	(u)	0.72	(u)	0.92	(u)	0.92	(u)	3.24	(u)	3.24	(u)

Delta y = (Fi/F'y)*Δ'y	0.37	(in)	9.48	(mm)

[a] The predicted top displacements were estimated without considering the displacement component due to shear deformation.

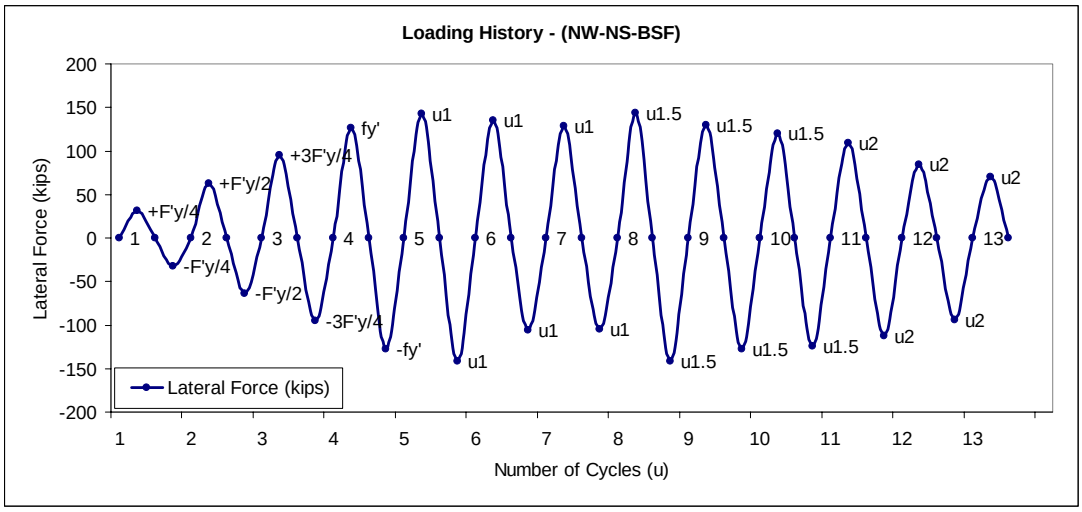

Figure 5.1. Load History (NW-NS-BSF) Specimen

Having the actual lateral force and displacement at the first yielding point (Fy'), and the nominal capacity from the analytical model, an equivalent yielding displacement was calculated according to (Eq. 5-1). The equivalent yielding point was determined by extrapolating the actual displacement at (Fy') in proportion to the nominal force divided by the first yielding force obtained from the analytical model. As a result, displacement ductility one was defined by the above mentioned equivalent yielding point (Fy), and was the reference to calculate different levels of ductility. During displacement controlled loading history, three cycles at each level of deformation were applied starting from displacement ductility one to failure. For instance, displacement ductility two was twice the value of displacement ductility one. The displacement history of test (NW-NS-BSF) is shown in Figure 5.2. It is important to notice the strength degradation of the specimen that occurred in subsequent cycles at each ductility level as shown in Figure 5.1.

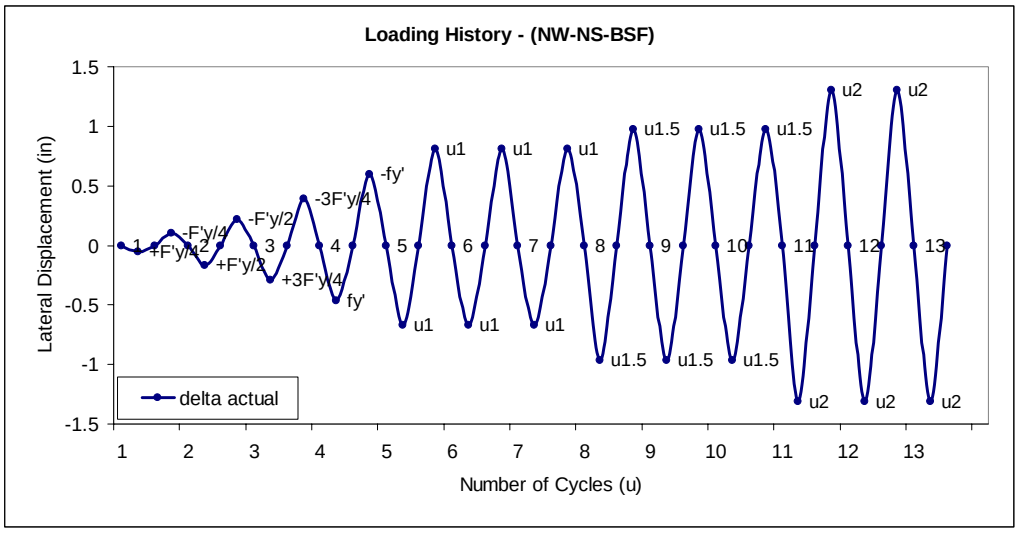

Figure 5.2. Displacement History (NW-NS-BSF) Specimen

5.1.2 Relevant Observations

Relevant test observations are presented in this section. It is important to mention that the same format has been used for all the specimens. Matrices are presented with information obtained during the test such as lateral force, displacement, crack location, orientation, width, crushing of the concrete, spalling, exposure of the reinforcement, and buckling of longitudinal reinforcement. The information contained in the matrices considers various levels of lateral force and displacement, and has been divided into force and displacement controlled loading procedures.

5.1.2.1 Force Controlled

Before test (NW-NS-BSF) was officially initiated, the specimen was accidentally loaded in the pushing direction with a lateral force of 100 kips, equivalent to 80% of the lateral force required to reach the first yielding point. As a result, cracks corresponding to the pushing direction appeared suddenly at this level of shear without being gradually traced as desired. However, the effect for the pulling direction was not significant, and the cracks were traced in each cycle during force controlled loading for the pulling direction. After the accidental load was applied, the specimen was unloaded, the test was initiated from the beginning, and the regular procedure was followed up to failure as shown in Figure 5.1 and Figure 5.2.

During force controlled cycles at lateral forces (Fy'/4 & Fy'/2), horizontal flexural cracks appeared on the tension sides of the column as described in Table 5.3. On the north (N) face when pushing, and on the south (S) face when pulling the specimen. Moreover, at low levels

of lateral load, flexural cracks started to propagate from the face in tension to faces east and west (E & W). The orientation of the cracks was horizontal close to faces (N & S) as Figure 5.4. (a & b) shows. For higher levels of lateral load (3Fy'/4 & Fy'), cracks on faces (E & W) propagated significantly to the middle of the face developing an angle between 30 to 35 degrees, from the vertical axis, that revealed some initial shear deformation of the specimen. Finally, cracks covered 80% of (E & W) faces at the end of the force controlled stage when the lateral force was approximately 127 kips at (Fy').

The predicted lateral displacement at (Fy') was 0.47 inches. The spacing between cracks on faces (E & W) was between 5 to 7 inches, and the crack width was 0.016 inches. Shear only cracks appeared on faces (E & W) at (Fy'). Moreover, in addition to the horizontal flexural cracks, vertical cracks appeared on faces (N & S) also at (Fy'). In fact, these cracks coincided with the location of the longitudinal reinforcement of the column with less confinement, and were located in the middle of faces (N & S) as shown in Figure 5.3. Consequently, vertical splitting of the concrete cover along the length of the column was observed. This observation was evident in the cases of all brittle shear failure tests where the columns had a low level of confinement compared to all ductile shear failure specimens. In addition, it is suggested in this document that vertical splitting was caused by the lateral expansion of the column cross section in the direction of the reversed lateral loading (N & S) while widen of shear cracks in faces (E & W) was observed, and when the transverse reinforcement was yielding as measured by internal strain gages. Figure 5.3 illustrates the observation as well as the suggested cause of vertical splitting cracks. A longitudinal

fracture due to bond interaction over the longitudinal reinforcement, where relative displacements between the rebar and concrete are developed during various cycles of reversed loading with repetitive tensile and compressive strains in the steel, may represent another factor that contributed to the splitting of the concrete cover. Finally, no significant damage of the column was observed during force controlled loading.

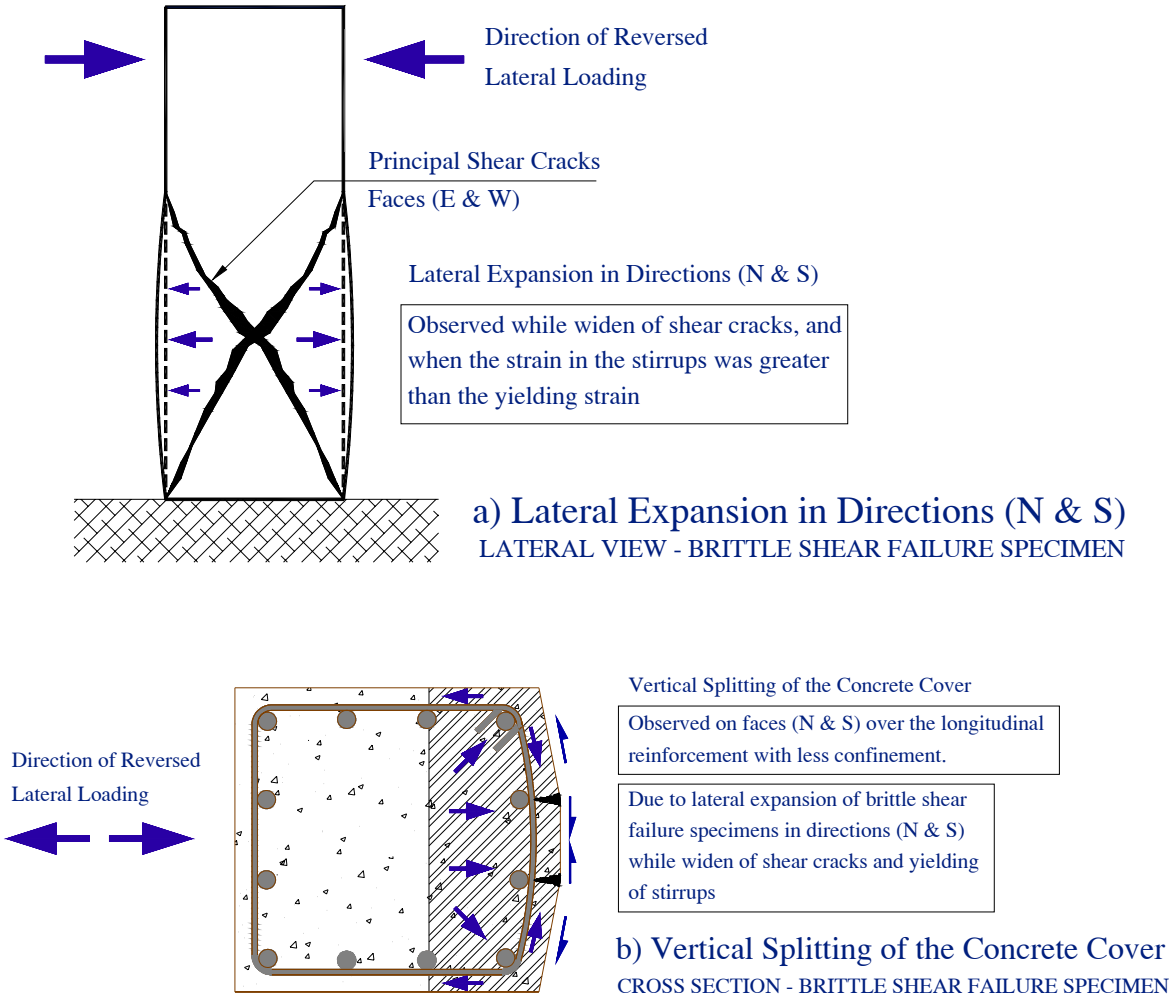

Figure 5.3. Vertical Splitting of the Concrete Cover in Brittle Shear Failure Specimens

5.1.2.2 Displacement Controlled

The test continued with the displacement controlled cyclic lateral loading. The recorded top displacement at first yielding was (0.47 in) resulting in an equivalent yielding displacement of (0.66 in) that was calculated using (Eq. 5-1). Afterwards, three cycles were applied at different levels of deformation considering the calculated yielding displacement as a reference value of displacement ductility one ($\mu_\Delta 1$). As a result, the applied top displacements used for displacement controlled loading were 0.66 inches for ($\mu_\Delta 1$), 0.98 inches for ($\mu_\Delta 1.5$), and 1.31 inches for ($\mu_\Delta 2$). As expected, the specimen failed at a low level of deformation equal to twice the displacement of the equivalent yielding point (1.31 inches).

$$\Delta y = \Delta y' \cdot \frac{Fi}{Fy'} \qquad \textbf{(Eq. 5-1)}$$

The maximum actual shear capacity of the specimen was approximately 144 kips for displacement ductility ($\mu_\Delta 1$ & 1.5) as described in Table 5.4. According to the analytical model, the predicted shear capacity should have been 143 kips which was consistent with the actual data. The variation of the axial load within plus or minus ten percent was not considered to be significant. In addition, spacing between flexural cracks in (N & S) faces was between 4 to 6 inches during displacement controlled loading. Vertical splitting in (N & S) faces became more evident at levels of displacement ductility ($\mu_\Delta 1.5$ & 2). Furthermore, spacing between shear cracks on the middle of (E & W) faces had values of between 3 to 4

inches at displacement ductility (μ_Δ1.5 & 2). Finally a well defined 2 mm crack on (E & W) faces crossed the entire column section from north to south at displacement ductility (μ_Δ1.5). The angle defined by the crack from the vertical axis was 32.5 degrees. The width of shear cracks continued increasing from 0.035 inches at (μ_Δ1) to 0.10 inches at (μ_Δ1.5), and to 0.25 inches at (μ_Δ2). No significant increment in the number of flexural cracks in (N & S) faces was observed for levels of deformation beyond the equivalent yielding point. However, new shear only cracks were observed during displacement ductility (μ_Δ1 & 1.5).

Regarding damage of the specimen, spalling of the concrete cover started during displacement ductility (μ_Δ1), and it was located at the bottom of faces (N & S) of the column. In addition, some crushing of the concrete was also observed at the bottom of faces (N & S) at a displacement ductility of (μ_Δ1). Thereafter, spalling of the concrete cover was also observed on faces (E & W) as the reinforcement steel was exposed at a displacement ductility of (μ_Δ2) as described in Table 5.4. Finally, it is important to notice that the intersection between the principal shear cracks on faces (E & W) was approximately located at a height of 27 inches from the base of the column as shown in Figure 5.5. (c & d).

Table 5.3. Force Controlled Test Observation Matrix (NW-NS-BSF)

	Force Controlled - Test Observation Matrix – (NW-NS-BSF)			
Test Observation	**Fy'/4**	**Fy'/2**	**3Fy'/4**	**fy'**
Maximum lateral force (kips)	32.06	63.81	95.54	126.67
Axial load (kips)	93.42	98.55	101.88	103.14
Lateral displacement (in)	0.07	0.19	0.33	0.47
(N & S) Cracks location (Ih/Fh/s(s1-s2)) (in) [a]	0/24/6	0/28/6	0/39/6	0/45/6
(N & S) Cracks orientation (Horizontal (H)/Vertical (V)/Both (B))	H	H	H	B
(E & W) Cracks location (Ih/Fh/s(s1-s2)) (in) [a]	0/24/6	0/28/6	0/39/6	0/45/5-7
(E & W) Average crack slope and location (Slope/L(%)) [b]	90/10	85/30	45/50	35/50
(E & W) Face crack propagation (Total-P(%)/Rel.-Length(r1-r2)) [c]	10/3	30/3-4	65/7-10	80/6-8
New flexural cracks (Yes/No)	Yes	Yes	Yes	No
New shear cracks only (L(%)/Length/Height) [d]	No	No	(25/5/35) (50/8/20)	(50/7/28) (25/7/42) (70/4/10)
(N & S) Crack width (in/mm)	<(0.005/0.15)	-	-	(0.016/0.40)
(E & W) Crack width (in/mm)	<(0.005/0.15)	<(0.005/0.15)		(0.016/0.40)
Spalling of concrete cover (Location-Face/Damaged Height (in))	-	-	-	-
Crushing of concrete (Location-Face/Damaged Depth(in))	-	-	-	-
Exposure of reinforcement steel (Location-Face/Height (in))	-	-	-	-
Buckling of longitudinal reinforcement (Location)	-	-	-	-

[a] (Initial height from the column base (in) /Final height form the column base (in) / Average values of spacing between cracks (in))
[b] (Crack slope from vertical line / Location in east or west faces from tension face north or south, e.g., 50% as the middle of east or west faces)
[c] (Maximum total crack propagation percentage in east or west faces from tension face north or south, e.g., 50% as half of east or west faces covered with cracks / Values of relative crack length propagation (in))
[d] (Location in east or west faces from tension face north or south, e.g., 50% as the middle of east or west faces / Shear only crack length (in) / Height at the middle of the crack in east or west planes (in))

Table 5.4. Displacement Controlled Test Observation Matrix (NW-NS-BSF)

	Displacement Controlled - Test Observation Matrix – (NW-NS-BSF)		
Test Observation	**Displacement Ductiliy (1)**	**Displacement Ductiliy (1.5)**	**Displacement Ductiliy (2)**
Maximum lateral force (kips)	143.21	144.02	112.39
Axial load (kips)	103.85	104.58	94.30
Lateral displacement (in)	0.66	0.98	1.31
(N & S) Cracks location (Ih/Fh/s(s1-s2)) (in) [a]	0/45/4-6	0/45/4-6	0/45/4-6
(N & S) Cracks orientation (Horizontal (H)/Vertical (V)/Both (B))	B	B	B
(E & W) Cracks location (Ih/Fh/s(s1-s2)) (in) [a]	0/50/4-6	0/50/3-4	0/50/3-4
(E & W) Average crack slope and location (Slope/L(%)) [b]	(70/10-30) (35/30-70) (20/70-90)	32.5/50	32.5/50
(E & W) Face crack propagation (Total-P(%)/Rel.-Length(r1-r2)) [c]	95/4-6	100/3-5	100/3-5
New flexural cracks (Yes/No)	Yes	No	No
New shear cracks only (L(%)/Length/Height) [d]	(25/8/40) (70/4/18)	(50/5/34)	No
(N & S) Crack width (in/mm)	0.05/1.25	-	-
(E & W) Crack width (in/mm)	0.035/0.90	0.10/2.50	0.25/6.00
Spalling of concrete cover (Location-Face/Damaged Height (in))	Base-(N&S)/3	(Base-(N&S)/5) (Center-(E&W)/-) (Top-S/-)	(Base-(N&S)/5) (Center-(E&W)/0-34) (Top-S/-)
Crushing of concrete (Location-Face/Damaged Depth(in))	Base-(N&S)/1	Base-(N&S)/3	Base-(N&S)/-
Exposure of reinforcement steel (Location-Face/Height (in))	-	-	(Center-(E&W)/0-34)
Buckling of longitudinal reinforcement (Location)	-	-	-

[a] (Initial height from the column base (in) /Final height form the column base (in) / Average values of spacing between cracks (in))
[b] (Crack slope from vertical line / Location in east or west faces from tension face north or south, e.g., 50% as the middle of east or west faces)
[c] (Maximum total crack propagation percentage in east or west faces from tension face north or south, e.g., 50% as half of east or west faces covered with cracks / Values of relative crack length propagation (in))
[d] (Location in east or west faces from tension face north or south, e.g., 50% as the middle of east or west faces / Shear only crack length (in) / Height at the middle of the crack in east or west planes (in))

Force Controlled - Test Pictures – (NW-NS-BSF)

Force:	Fy'/4	Face (South - East)

a)

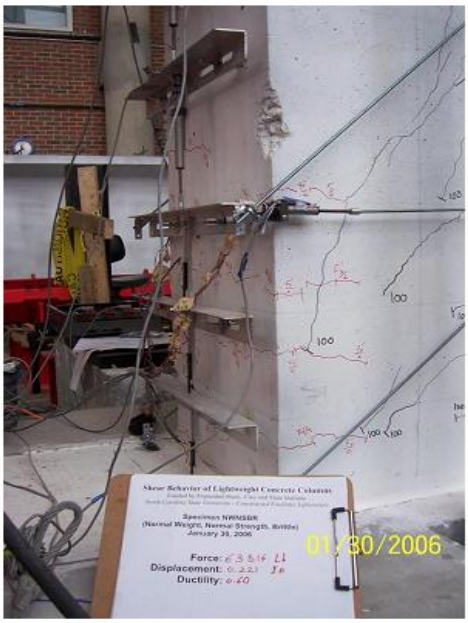

Force:	Fy'/2	Face (South - East)

b)

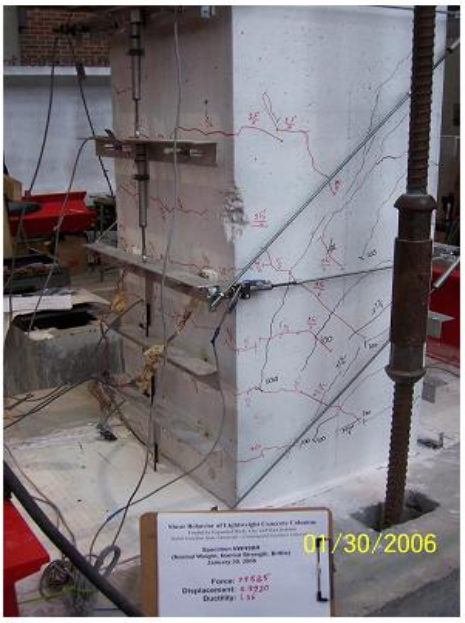

Force:	3Fy'/4	Face (South - East)

c)

Force:	Fy'	Face (North - East)

d)

Figure 5.4. Force Controlled Loading – (NW-NS-BSF)

Displacement Controlled - Test Pictures – (NW-NS-BSF)

Disp. Ductiliy (1)	Face (East)

a)

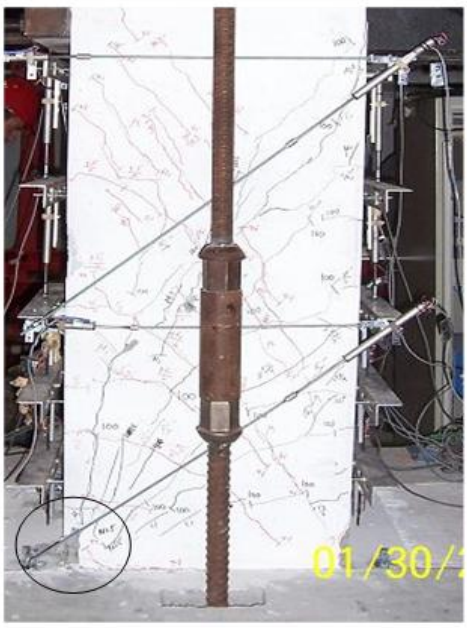

Disp. Ductiliy (1.5)	Face (East)

b)

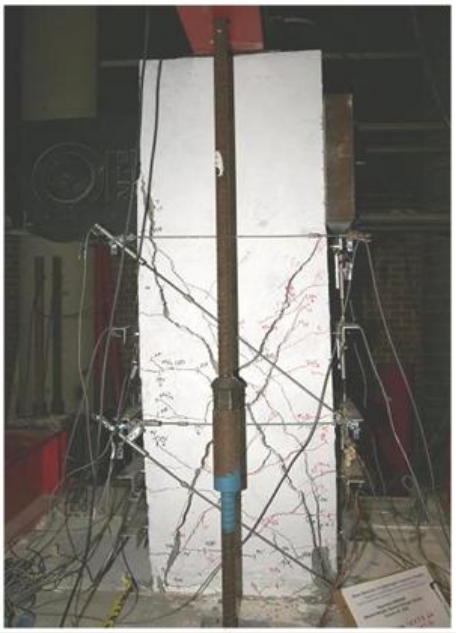

Disp. Ductiliy (2)	Face (West)

c)

Disp. Ductiliy (2/c3)	Face (West)

d)

Figure 5.5. Displacement Controlled Loading – (NW-NS-BSF)

5.2. Lightweight Concrete Type One - Brittle Shear Failure Test (LW1-NS-BSF)

In order to be consistent with the control specimen, (LW1-NS-BSF) specimen was tested following the same procedure as described in section 5.1. In brief, the same test setup, loading, equipment, and instrumentation used in test (NW-NS-BSF) were used in all brittle shear failure tests.

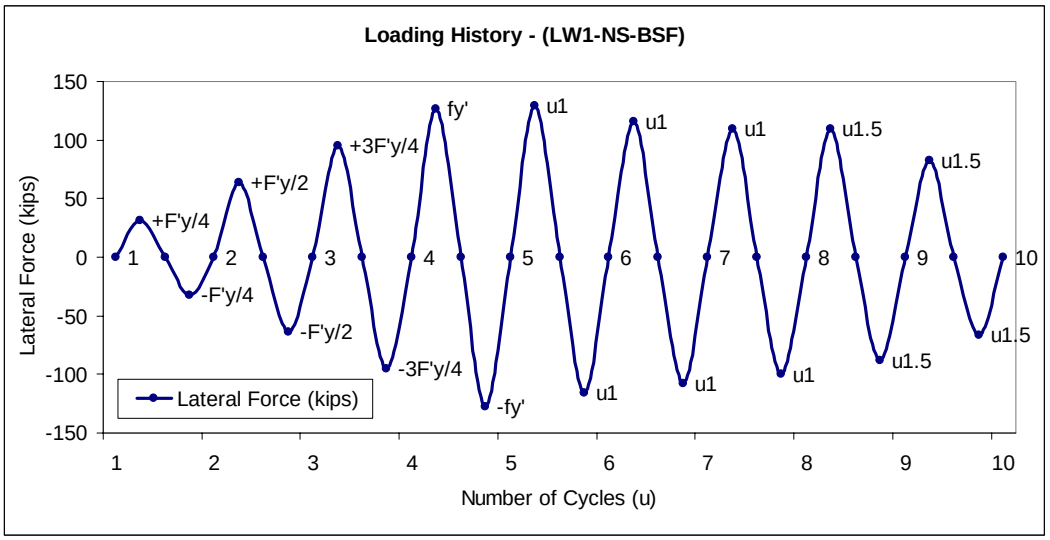

Figure 5.6. Load History (LW1-NS-BSF) Specimen

5.2.1 Loading History

During the course of the test, force controlled lateral loading was used for the first four cycles as shown in Figure 5.6 and Figure 5.7. One cycle was applied at each level of lateral load during force controlled. Furthermore, displacement controlled cyclic lateral loading was applied during the second stage of the test from cycle five to nine as shown in Figure 5.6 and Figure 5.7, and as described in section 5.1.1. Finally, data was captured even when the

strength decreased. Shear strength degradation was observed in subsequent cycles at the same level of deformation (see Figure 5.6).

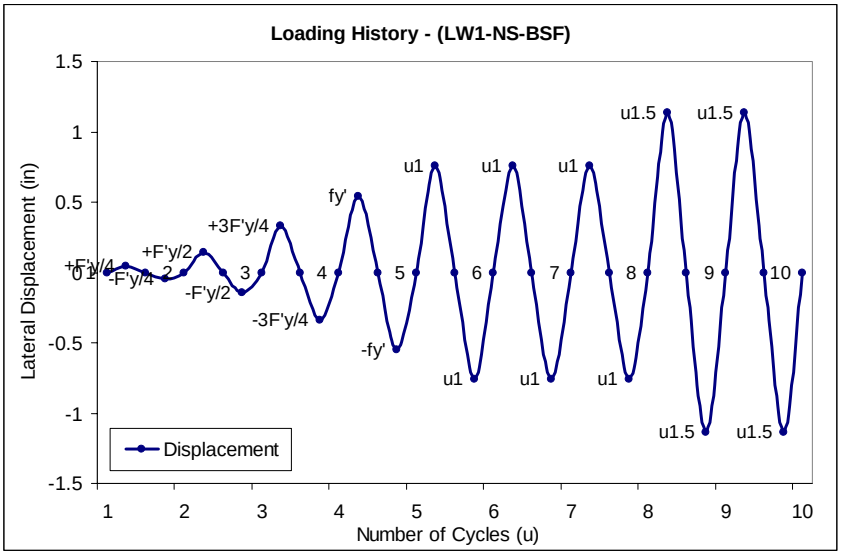

Figure 5.7. Displacement History (LW1-NS-BSF) Specimen

5.2.2 Relevant Observations

Test observations are presented in this section using the same format as in section 5.1. Matrices are provided with concise information obtained during the test such as lateral force, displacement, crack location, slope, crack width, and more. Furthermore, the information contained in the matrices considers various levels of lateral force and displacement.

5.2.2.1 Force Controlled

During the force controlled loading and except for some differences, the behavior of (LW1-NS-BSF) specimen was consistent and similar to the behavior of (NW-NS-BSF). In fact, at low levels of lateral load (Fy'/4 & Fy'/2), horizontal flexural cracks appeared on the tension sides of the column (N & S) as described in Table 5.5. Moreover, the flexural cracks started

to propagate from the face in tension to faces (E & W). The spacing between flexural cracks at (Fy') was approximately 6 to 7 inches compared to 6 inches in test (NW-NS-BSF). The orientation of the cracks was initially horizontal close to faces (N & S) as shown in Figure 5.8 (a & b). Then, for higher levels of lateral load (Fy') the cracks on faces (E & W) propagated significantly covering 80% of (E & W) faces as in test (NW-NS-BSF). A better distribution of shear cracks on faces (E & W) was observed as the spacing between cracks was reduced to values between 3 to 5 inches at (Fy') compared to a value between 5 to 7 in test (NW-NS-BSF). It is also important to mention that shear only cracks appeared earlier at (Fy'/2) compared to test (NW-NS-BSF) where shear only cracks were observed at (3Fy'/4). Finally, specimen (LW1-NS-BSF) failed at a lower level of deformation ($\mu_\Delta 1.5$) reaching a top displacement of 1.13 inches while tests (NW-NS-BSF) failed with a top displacement of 1.31 inches at a displacement ductility of ($\mu_\Delta 2$).

The actual top displacement at (Fy') was 0.58 inches compared to 0.47 inches in test (NW-NS-BSF). In addition, vertical cracks appeared on (N & S) faces at (Fy') as it happened with test (NW-NS-BSF). In fact, these cracks coincided with the location of the longitudinal reinforcement of the column revealing vertical splitting of the concrete along the length of the column. Finally, as in test (NW-NS-BSF), no significant damage of the column was observed during force controlled loading.

5.2.2.2 Displacement Controlled

The same procedure described in section 5.1.2.2 was followed for the displacement controlled loading. In fact, the equivalent yielding displacement was calculated using (Eq. 5-1) as a function of the actual top displacement at first yielding (0.58 in). In addition, three cycles were applied at different levels of deformation considering top displacements of 0.76 inches for ($\mu_\Delta 1$), and 1.13 inches for ($\mu_\Delta 1.5$). As expected, the specimen failed at a low level of deformation equal to fifty percent more than the displacement of the equivalent yielding point (1.13 inches).

As described in Table 5.6, the maximum actual shear capacity of the specimen was 129 kips developed at a displacement ductility of ($\mu_\Delta 1$). Shear capacity was approximately 10% lower than the actual capacity developed by specimen (NW-NS-BSF), and also lower than the predicted by the analytical model. The variation of the axial load during the test was in a range of plus or minus ten percent that was not considered to be significant. Moreover, spacing between flexural cracks in (N & S) faces had values between 6 to 7 inches during displacement controlled loading. Furthermore, spacing between shear cracks on the middle of (E & W) faces continued getting shorter with values between 1 to 2 inches at displacement ductility ($\mu_\Delta 1.5$). A better distribution of shear cracks on faces (E & W) was observed, and there was not one big well defined crack at failure, but three as shown in Figure 5.9.(c). The angle defined by the failure cracks from the vertical axis was approximately 30 degrees. Moreover, as observed in test (NW-NS-BSF), the width of shear cracks continued increasing

up to 0.25 inches at (μ_Δ1.5). No significant increment in the number of flexural cracks in (N & S) faces was observed for levels of deformation beyond the equivalent yielding point as in test (NW-NS-BSF). On the contrary, new shear only cracks were observed during displacement ductility (μ_Δ1 & 1.5).

Consistent with test (NW-NS-BSF), spalling of the concrete cover started during displacement ductility (μ_Δ1), and it was located at the bottom of faces (N & S) of the column. Some crushing of the concrete was also observed at the bottom of faces (N & S) at a displacement ductility of (μ_Δ1). In the same manner, spalling of the concrete cover was also observed on faces (E & W), and the reinforcement steel was exposed at a displacement ductility of (μ_Δ1.5) as described in Table 5.6. Finally, it is also important to mention that the location of the intersection between the principal shear cracks on faces (E & W) was consisted with what was expected from geometry, considering the depth of the section, shear cracks starting near the support at each corner of the column base, and going to the opposite sides (N & S) with an angle defined by the compression strut. The location of the intersection between principal shear cracks was slightly lower than the one of test (NW-NS-BSF). In fact, as shown in Figure 5.9 (b, c & d), it was approximately located at a height of 23 inches from the base of the column compared to 27 inches in test (NW-NS-BSF).

Table 5.5. Force Controlled Test Observation Matrix (LW1-NS-BSF)

	Force Controlled - Test Observation Matrix – (LW1-NS-BSF)			
Test Observation	**Fy'/4**	**Fy'/2**	**3Fy'/4**	**fy'**
Maximum lateral force (kips)	31.93	63.77	95.38	127.31
Axial load (kips)	91.33	92.56	99.64	102.07
Lateral displacement (in)	0.05	0.14	0.34	0.58
(N & S) Cracks location (Ih/Fh/s(s1-s2)) (in) [a]	0/41/10-11	0/41/6-7	0/41/6-7	0/50/6-7
(N & S) Cracks orientation (Horizontal (H)/Vertical (V)/Both (B))	H	H	H	B
(E & W) Cracks location (Ih/Fh/s(s1-s2)) (in) [a]	0/34/10	0/34/6-7	0/40/4-6	0/50/3-5
(E & W) Average crack slope and location (Slope/L(%)/Hcs) [b]	90/10/-	65/40/-	45/50/-	(35/50/36) (45/50/14) (60/50/7)
(E & W) Face crack propagation (Total-P(%)/Rel.-Length(r1-r2)) [c]	10/1.50	55/5-10	70/2-15	80/2-8
New flexural cracks (Yes/No)	Yes	Yes	Yes	No
New shear cracks only (L(%)/Length/Height location) [d]	-	(25/4/24) (25/3/7)	(50/4/20) (50/4/17)	(50/7/30) (30/22/32)
(N & S) Crack width (in/mm)	-	-	0.035/0.90	0.035/0.90
(E & W) Crack width (in/mm)	-	<(0.005/0.15)	0.013/0.33	0.025/0.60
Spalling of concrete cover (Location-Face/Damaged Height (in))	-	-	-	-
Crushing of concrete (Location-Face/Damaged Depth(in))	-	-	-	-
Exposure of reinforcement steel (Location-Face/Height (in))	-	-	-	-
Buckling of longitudinal reinforcement (Location)	-	-	-	-

[a] (Initial height from the column base (in) /Final height form the column base (in) / Average values of spacing between cracks (in))
[b] (Crack slope from vertical line / Location in east or west faces from tension face north or south, e.g., 50% as the middle of east or west faces)
[c] (Maximum total crack propagation percentage in east or west faces from tension face north or south, e.g., 50% as half of east or west faces covered with cracks / Values of relative crack length propagation (in))
[d] (Location in east or west faces from tension face north or south, e.g., 50% as the middle of east or west faces / Shear only crack length (in) / Height at the middle of the crack in east or west planes (in))

Table 5.6. Displacement Controlled Test Observation Matrix (LW1-NS-BSF)

	Displacement Controlled - Test Observation Matrix – (LW1-NS-BSF)		
Test Observation	**Displacement Ductiliy (1)**	**Displacement Ductiliy (1.5)**	**Displacement Ductiliy (2)**
Maximum lateral force (kips)	129.15	109.51	
Axial load (kips)	96.71	86.83	
Lateral displacement (in)	0.76	1.13	
(N & S) Cracks location (Ih/Fh/s(s1-s2)) (in) [a]	0/50/6-7	0/50/6-7	
(N & S) Cracks orientation (Horizontal (H)/Vertical (V)/Both (B))	B	B	
(E & W) Cracks location (Ih/Fh/s(s1-s2)) (in) [a]	0/50/1-3	0/50/1-2	
(E & W) Average crack slope and location (Slope/L(%)/Hcs) [b]	(35/50/36) (45/50/14) (60/50/7)	30/50/-	
(E & W) Face crack propagation (Total-P(%)/Rel.-Length(r1-r2)) [c]	95/3-14	100/-	
New flexural cracks (Yes/No)	No	No	
New shear cracks only (L(%)/Length/Height location) [d]	50/5/36	50/6/42	
(N & S) Crack width (in/mm)	0.08/2.00	-	
(E & W) Crack width (in/mm)	0.04/1.00	0.25/5.00	
Spalling of concrete cover (Location-Face/Damaged Height (in))	Base-(N&S)/3	(Base-(N&S)/7) (Center-(E&W)/0-30)	
Crushing of concrete (Location-Face/Damaged Depth(in))	Base-(N&S)/1	Base-(N&S)/2	
Exposure of reinforcement steel (Location-Face/Height (in))	-	(Center-(E&W)/0-30)	
Buckling of longitudinal reinforcement (Location)	-	-	

[a] (Initial height from the column base (in) /Final height form the column base (in) / Average values of spacing between cracks (in))
[b] (Crack slope from vertical line / Location in east or west faces from tension face north or south, e.g., 50% as the middle of east or west faces)
[c] (Maximum total crack propagation percentage in east or west faces from tension face north or south, e.g., 50% as half of east or west faces covered with cracks / Values of relative crack length propagation (in))
[d] (Location in east or west faces from tension face north or south, e.g., 50% as the middle of east or west faces / Shear only crack length (in) / Height at the middle of the crack in east or west planes (in))

Force Controlled - Test Pictures – (LW1-NS-BSF)

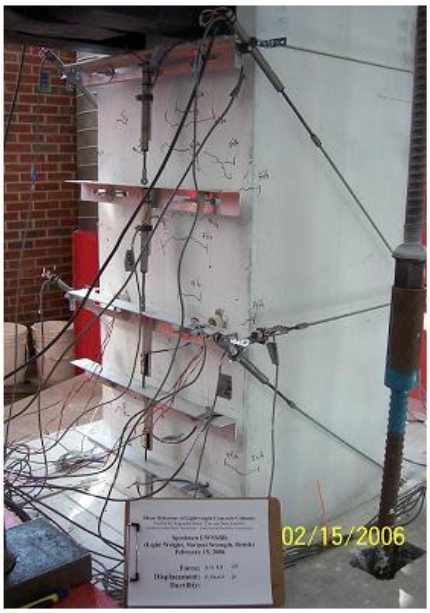

Force:	Fy'/4	Face (North - West)

a)

Force:	Fy'/2	Face (North - West)

b)

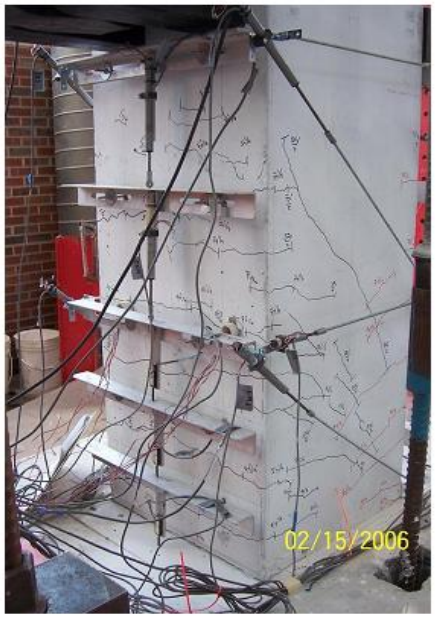

Force:	3Fy'/4	Face (North - West)

c)

Force:	Fy'	Face (North - East)

d)

Figure 5.8. Force Controlled Loading – (LW1-NS-BSF)

Displacement Controlled - Test Pictures – (LW1-NS-BSF)

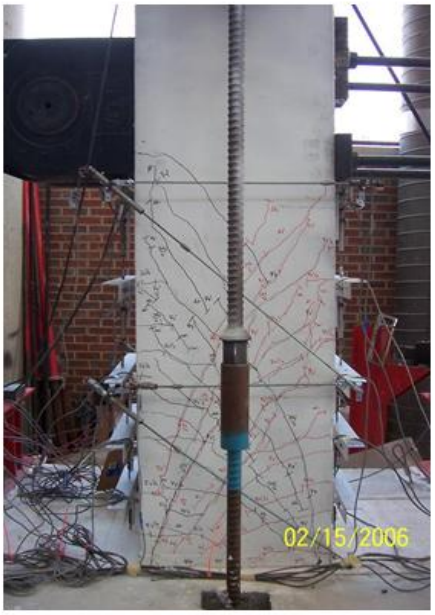

Disp. Ductiliy (1)	Face (West)

a)

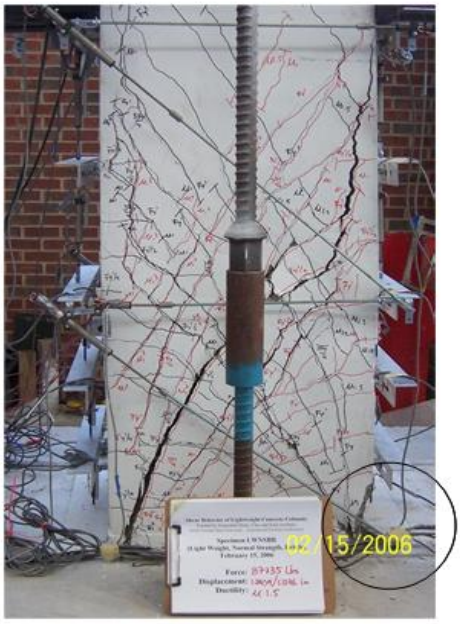

Disp. Ductiliy (1.5)	Face (West)

b)

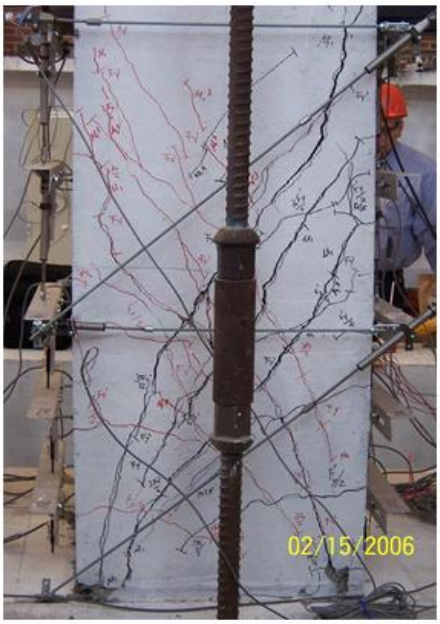

Disp. Ductiliy (1.5)	Face (East)

c)

Disp. Ductiliy (1.5/c2)	Face (South - West)

d)

Figure 5.9. Displacement Controlled Loading – (LW1-NS-BSF)

5.3. Lightweight Concrete Type Two - Brittle Shear Failure Test (LW2-NS-BSF)

A brittle shear failure specimen made of lightweight concrete (LW2-NS-BSF) was tested under the same criteria applied to specimens (NW-NS-BSF) and (LW1-NS-BSF). The procedure followed was the same as section 5.1 describes. In the same manner, the same test setup, loading, equipment, and instrumentation were used for test (LW2-NS-BSF).

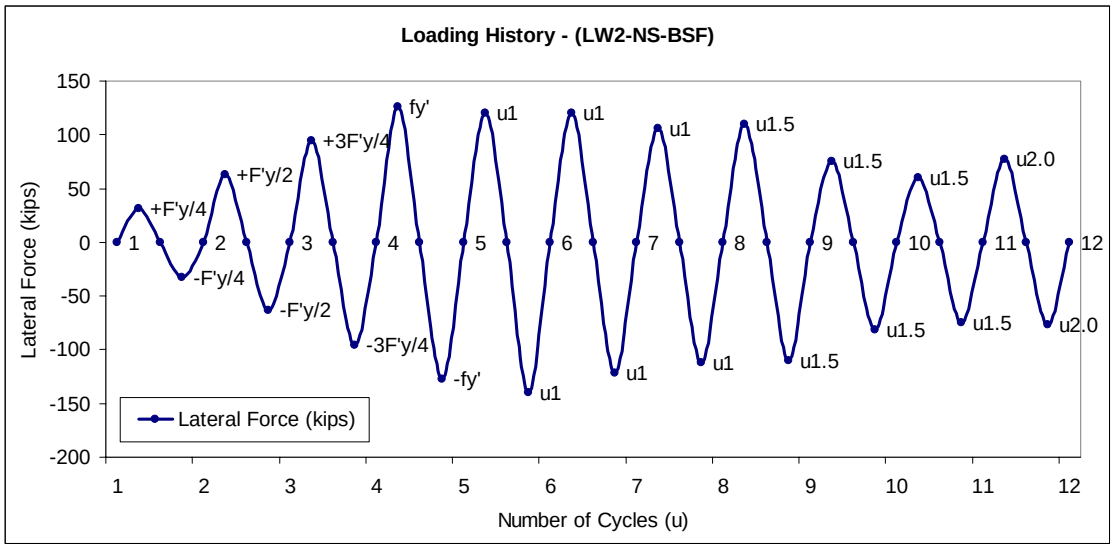

Figure 5.10. Load History (LW2-NS-BSF) Specimen

5.3.1 Loading History

Force controlled lateral loading was used in the initial stage of the test. The first four cycles in Figure 5.10 and Figure 5.11 illustrate the force controlled procedure. One cycle was applied at each level of lateral load during force controlled loading.

Displacement controlled cyclic lateral loading was applied during the second stage of the test from cycle five to eleven as shown in Figure 5.10 and Figure 5.11. Finally, shear strength degradation at same levels of deformation was observed during subsequent cycles of force controlled loading as illustrated in Figure 5.10.

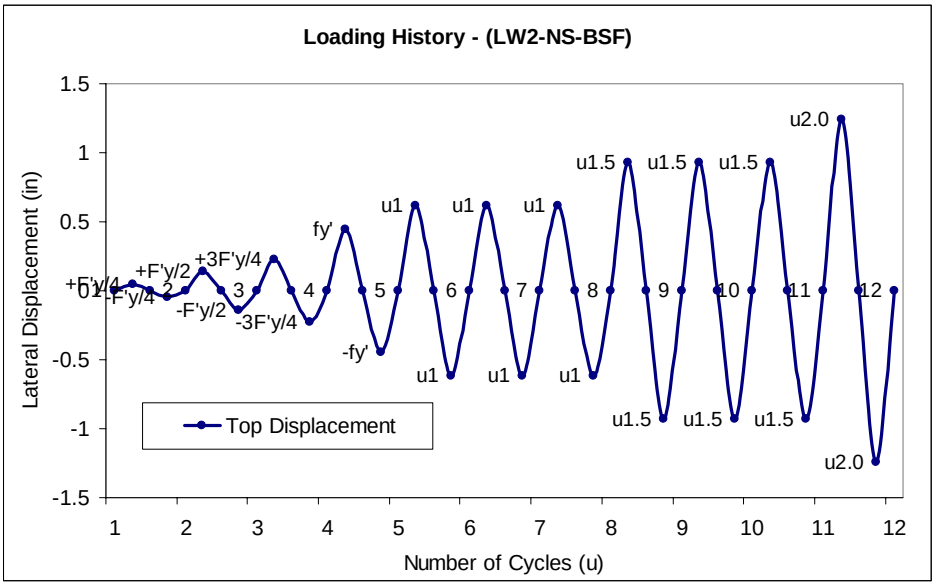

Figure 5.11. Displacement History (LW2-NS-BSF) Specimen

5.3.2 Relevant Observations

Test observations are also presented in this section using the same format as in sections 5.1 and 5.2. Matrices are provided with concise information obtained during the test such as lateral force, displacement, crack location, slope, crack width, and more. Furthermore, the information contained in the matrices considers various levels of lateral force and displacement.

5.3.2.1 Force Controlled

As observed in specimens tests (NW-NS-BSF) and (LW1-NS-BSF), at low levels of lateral load (Fy'/4 & Fy'/2), horizontal flexural cracks appeared on the tension sides of the column (N & S) as described in Table 5.7. In the same manner, the flexural cracks started to propagate from the face in tension to faces (E & W). Similar to specimens (NW-NS-BSF) and (LW1-NS-BSF), the spacing between flexural cracks at (Fy') was approximately between 5 to 7 inches. The orientation of the cracks was also initially horizontal close to faces (N & S) as shown in Figure 5.12 (a & b). Afterwards, when the lateral load was equal to (Fy'), the cracks on faces (E & W) propagated significantly covering 95% of (E & W) faces compared to 80% in test (NW-NS-BSF).

Similar to test (LW1-NS-BSF), a better distribution of shear cracks on faces (E & W) was observed considering a spacing of 2 to 3 inches between shear cracks that was shorter than in test (NW-NS-BSF) at (Fy'). In addition, shear only cracks started to appear at a lateral load level of (3Fy'/4) as it happened with test (NW-NS-BSF). The actual top displacement at (Fy') was 0.45 inches compared to 0.47 inches obtained in test (NW-NS-BSF). Similarly, vertical cracks appeared on (N & S) faces at (Fy') revealing vertical splitting of the concrete along the length of the column as it happened with test (NW-NS-BSF). Finally, as in test (NW-NS-BSF), no significant damage of the column was observed during force controlled loading. Finally, consistent with test (NW-NS-BSF), that failed when reaching a top

displacement of 1.31 inches at displacement ductility ($\mu_\Delta 2$), specimen (LW2-NS-BSF) failed when reaching a top displacement of 1.24 inches and at the same level of deformation.

5.3.2.2 Displacement Controlled

As described in section 5.1.2.2, the same procedure was followed for the displacement controlled loading, and the equivalent yielding displacement was calculated using (Eq. 5-1) as a function of the actual top displacement at first yielding (0.45 in). The cyclic lateral loading was applied considering levels of deformation with top displacements of 0.62 inches for ($\mu_\Delta 1$), 0.93 inches for ($\mu_\Delta 1.5$), and 1.24 inches for ($\mu_\Delta 2$). In brief, the specimen failed at a low level of deformation as expected ($\mu_\Delta 2$).

Furthermore, the maximum actual shear capacity of the specimen was 140 kips developed at a displacement ductility of ($\mu_\Delta 1$) as described in Table 5.8. The shear capacity was similar to the actual capacity of test (NW-NS-BSF) equals to 144 kips, and was also consistent with the analytical model. Moreover, the axial load had variations during the test that ranged between plus or minus fifteen percent. Furthermore, during displacement controlled loading, spacing between flexural cracks in (N & S) faces had values between 5 to 7 inches, similar to those of tests (NW-NS-BSF) and (LW1-NS-BSF). In addition, similar to test (NW-NS-BSF), there was a well defined shear crack at a displacement ductility ($\mu_\Delta 1.5$) as shown in Figure 5.13.(b). The angle defined by the failure cracks from the vertical axis was approximately 30 degrees, and it was similar to those observed in tests (NW-NS-BSF) and (LW1-NS-BSF).

Additionally, as observed in test (NW-NS-BSF), the width of the shear cracks continued increasing up to 0.40 inches at ($\mu_\Delta 2$). Consistent with test (NW-NS-BSF), no significant increment in the number of flexural cracks in (N & S) faces was observed for levels of deformation beyond the equivalent yielding point. However, new shear only cracks were observed during displacement ductility ($\mu_\Delta 1$ & 1.5) in faces (E & W).

Damage in the specimen was related to the level of deformation. In fact, as observed in tests (NW-NS-BSF) and (LW1-NS-BSF), spalling of the concrete cover started during displacement ductility ($\mu_\Delta 1$), and it was located at the bottom of faces (N & S) of the column. Some crushing of the concrete was also observed at the bottom of faces (N & S) at displacement ductility ($\mu_\Delta 1$). In the same manner, spalling of the concrete cover was also observed on faces (E & W), and the reinforcement steel was exposed at a displacement ductility of ($\mu_\Delta 1.5$ & 2) as described in Table 5.8. Finally, similar to test (LW1-NS-BSF), the location of the intersection between the principal shear cracks on faces (E & W) was located at approximately 23 inches from the base of the column as shown in Figure 5.13 (b & c).

Table 5.7. Force Controlled Test Observation Matrix (LW2-NS-BSF)

	Force Controlled - Test Observation Matrix – (LW2-NS-BSF)			
Test Observation	**Fy'/4**	**Fy'/2**	**3Fy'/4**	**fy'**
Maximum lateral force (kips)	32.19	63.34	95.75	127.41
Axial load (kips)	90.17	86.48	92.33	95.65
Lateral displacement (in)	0.07	0.13	0.25	0.45
(N & S) Cracks location (Ih/Fh/s(s1-s2)) (in) [a]	0/14/7	0/37/5-7	0/43/5-7	0/43/5-7
(N & S) Cracks orientation (Horizontal (H)/Vertical (V)/Both (B))	H	H	H	B
(E & W) Cracks location (Ih/Fh/s(s1-s2)) (in) [a]	0/13/6.5	0/37/5-7	0/43/4-5	0/43/2-3
(E & W) Average crack slope and location (Slope/L(%)/Hcs) [b]	85/15/-	55/45/-	(45/60/12) (30/50/36)	30/50/22-45
(E & W) Face crack propagation (Total-P(%)/Rel.-Length(r1-r2)) [c]	15/3	55/4-10	80/5-12	95/5-10
New flexural cracks (Yes/No)	Yes	Yes	Yes	No
New shear cracks only (L(%)/Length/Height location) [d]	-	-	30/5/25	40/8/38
(N & S) Crack width (in/mm)	-	-	0.020/0.50	0.025/0.60
(E & W) Crack width (in/mm)	-	-	0.016/0.40	0.025/0.60
Spalling of concrete cover (Location-Face/Damaged Height (in))	-	-	-	-
Crushing of concrete (Location-Face/Damaged Depth(in))	-	-	-	-
Exposure of reinforcement steel (Location-Face/Height (in))	-	-	-	-
Buckling of longitudinal reinforcement (Location)	-	-	-	-

[a] (Initial height from the column base (in) /Final height form the column base (in) / Average values of spacing between cracks (in))
[b] (Crack slope from vertical line / Location in east or west faces from tension face north or south, e.g., 50% as the middle of east or west faces)
[c] (Maximum total crack propagation percentage in east or west faces from tension face north or south, e.g., 50% as half of east or west faces covered with cracks / Values of relative crack length propagation (in))
[d] (Location in east or west faces from tension face north or south, e.g., 50% as the middle of east or west faces / Shear only crack length (in) / Height at the middle of the crack in east or west planes (in))

Table 5.8. Displacement Controlled Test Observation Matrix (LW2-NS-BSF)

	Displacement Controlled - Test Observation Matrix – (LW2-NS-BSF)		
Test Observation	**Displacement Ductiliy (1)**	**Displacement Ductiliy (1.5)**	**Displacement Ductiliy (2)**
Maximum lateral force (kips)	140.00	110.00	77.00
Axial load (kips)	89.15	85.80	87.07
Lateral displacement (in)	0.62	0.93	1.24
(N & S) Cracks location (Ih/Fh/s(s1-s2)) (in) [a]	0/45/5-7	0/50/5-7	0/50/5-7
(N & S) Cracks orientation (Horizontal (H)/Vertical (V)/Both (B))	B	B	B
(E & W) Cracks location (Ih/Fh/s(s1-s2)) (in) [a]	0/45/1.5-4	0/50/1.5-4	0/50/1.5-4
(E & W) Average crack slope and location (Slope/L(%)/Hcs) [b]	30/50/24	30/50/24	30/50/24
(E & W) Face crack propagation (Total-P(%)/Rel.-Length(r1-r2)) [c]	95/2-3	100/2-4	100/-
New flexural cracks (Yes/No)	No	No	No
New shear cracks only (L(%)/Length/Height location) [d]	(25/8/40) (75/8/23) (75/4/10)	(75/7/40) (75/7/45)	-
(N & S) Crack width (in/mm)	-	-	-
(E & W) Crack width (in/mm)	0.05/1.25	0.16/4.00	0.40/10.00
Spalling of concrete cover (Location-Face/Damaged Height (in))	Base-(S)/4	(Base-(N&S)/-) (Corners-(E&W)/-) (Left-(E)/0-18)	(Base-(N&S)/-) (Corners-(E&W)/-) (Center-(E&W)/0-30)
Crushing of concrete (Location-Face/Damaged Depth(in))	Base-(S)/1	Base-(N&S)/2.5	Base-(N&S)/-
Exposure of reinforcement steel (Location-Face/Height (in))	-	(Left-(E)/0-18) Cycle #3	(Center-(E&W)/0-30)
Buckling of longitudinal reinforcement (Location)	-	-	-

[a] (Initial height from the column base (in) /Final height form the column base (in) / Average values of spacing between cracks (in))
[b] (Crack slope from vertical line / Location in east or west faces from tension face north or south, e.g., 50% as the middle of east or west faces)
[c] (Maximum total crack propagation percentage in east or west faces from tension face north or south, e.g., 50% as half of east or west faces covered with cracks / Values of relative crack length propagation (in))
[d] (Location in east or west faces from tension face north or south, e.g., 50% as the middle of east or west faces / Shear only crack length (in) / Height at the middle of the crack in east or west planes (in))

Force Controlled - Test Pictures – (LW2-NS-BSF)

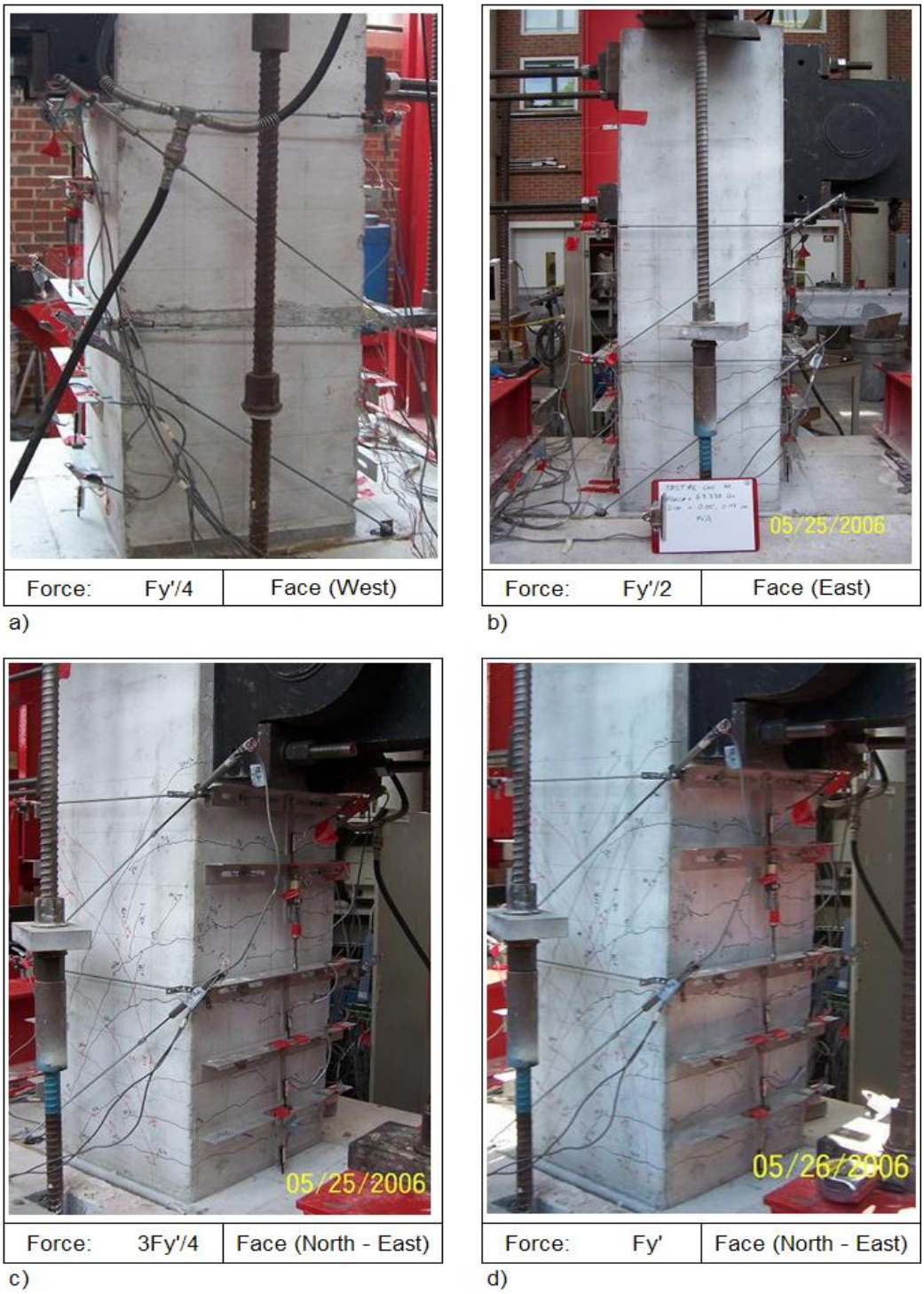

Figure 5.12. Force Controlled Loading – (LW2-NS-BSF)

Displacement Controlled - Test Pictures – (LW2-NS-BSF)

Disp. Ductiliy (1)	Face (West)

a)

Disp. Ductiliy (1.5)	Face (East)

b)

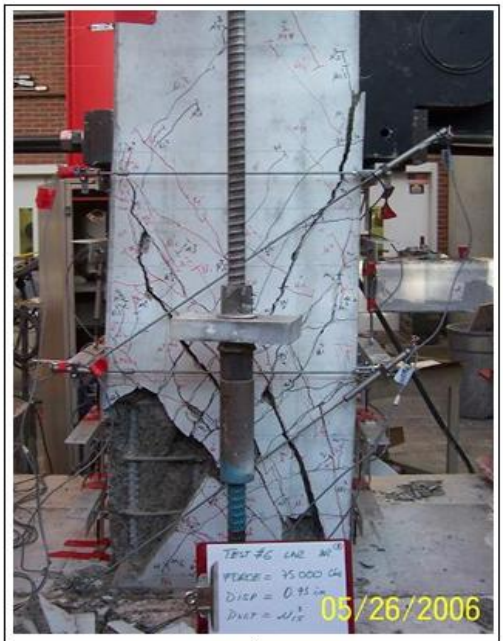

Disp. Ductiliy (2/c1)	Face (East)

c)

Disp. Ductiliy (2/c1)	Face (West)

d)

Figure 5.13. Displacement Controlled Loading – (LW2-NS-BSF)

5.4. Lightweight Concrete Type Three - Brittle Shear Failure Test (LW3-NS-BSF)

Completing the set of brittle shear failure tests, lightweight concrete specimen (LW3-NS-BSF) was tested following the same procedure described in section 5.1 regarding force controlled loading. In the same manner, the test setup, equipment, and instrumentation were also the same as in all previous brittle shear failure tests. The specimen failed with a brittle shear failure mode when attempting to change from force controlled to displacement controlled loading, and at a lower level of lateral load than the expected one. Despite the early brittle shear failure of the specimen, valuable information was acquired during the test.

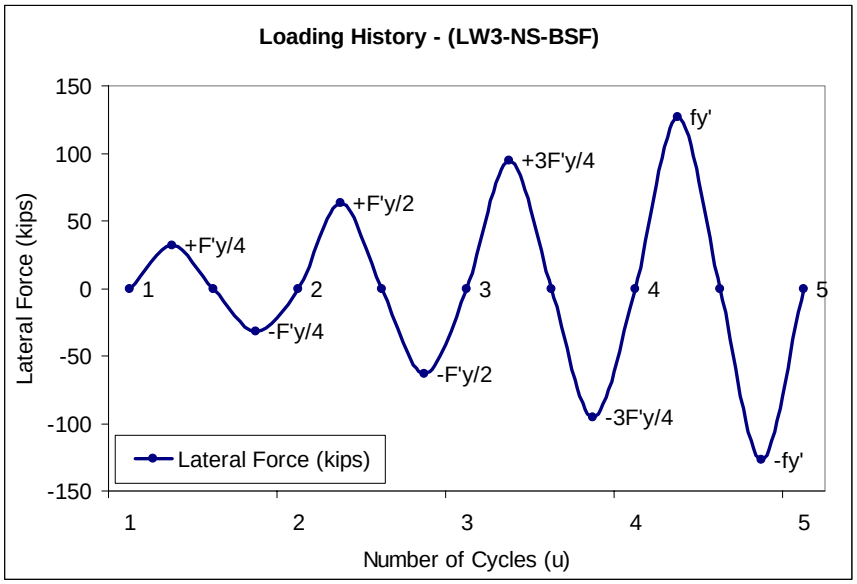

Figure 5.14. Load History (LW3-NS-BSF) Specimen

5.4.1 Loading History

Force controlled lateral loading was applied for the first four cycles as shown in Figure 5.14 and Figure 5.15. One cycle was applied at each level of lateral load during force controlled. Afterwards, when attempting to change to displacement controlled loading, the specimen failed at (Fy') after sustaining the lateral load of 127 kips for some minutes. Finally, the specimen failed with a monotonic response in the pushing direction as it was recorded by the instruments.

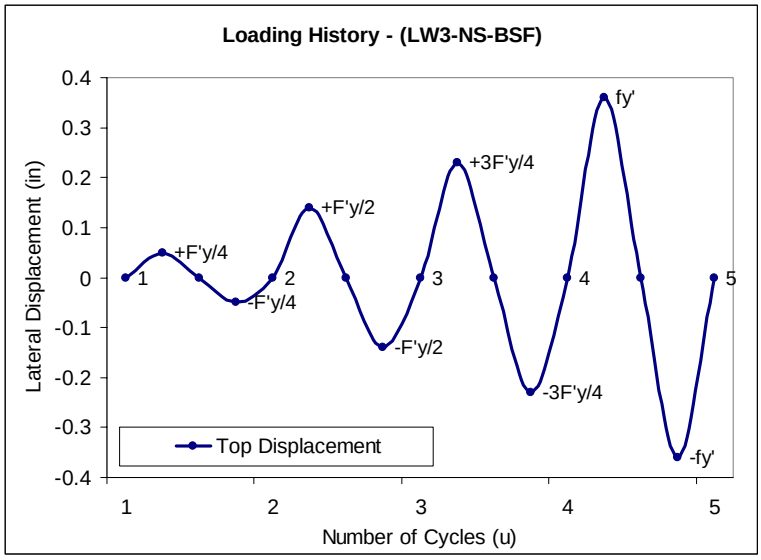

Figure 5.15. Displacement History (LW3-NS-BSF) Specimen

5.4.2 Relevant Observations

Test observations are presented in this section using the same format as in section 5.1. Matrices are provided with concise information obtained during the test such as lateral force, displacement, crack location, slope, crack width, and more. Furthermore, the information contained in the matrices considers various levels of lateral force and displacement.

5.4.2.1 Force Controlled

At low levels of lateral load (Fy'/4 & Fy'/2), horizontal flexural cracks appeared on the tension sides of the column (N & S) as described in Table 5.9, and as observed in all brittle shear failure tests. However, propagation from tension faces (N & S) to (E & W) faces was larger than in previous tests during force controlled loading, and cracks covered the entire surface earlier. In fact, cracks covered 100% of faces (E & W) at first yielding (Fy') while the same happened at displacement ductility (μ_Δ1.5) in all previous brittle shear failure tests (NW-NS-BSF), (LW1-NS-BSF), and (LW2-NS-BSF).

Similar to what was observed in all brittle shear failure tests, the spacing between flexural cracks at (Fy') had values between 6 to 8 inches. In the same manner, the cracks were initially horizontal close to faces (N & S), but in the middle of faces (E & W) the angle measured from a vertical line was approximately 30 degrees as shown in Figure 5.16. It is also important to mention that shear only cracks appeared earlier than in test (NW-NS-BSF) where shear only cracks were observed at (3Fy'/4).

In addition, vertical cracks also appeared earlier on (N & S) faces at (Fy'/2) while that happened at (Fy') in test (NW-NS-BSF). As a result, it was observed that vertical splitting of the concrete along the length of the column happened earlier than in all the previous brittle shear failure tests. Finally, damage of the column was also observed earlier during force controlled loading (Fy').

Lastly, the maximum actual shear capacity of the specimen was 127 kips, and it was approximately 11% lower than the actual capacity developed by specimen (NW-NS-BSF). The variation of the axial load during the test was in a range of plus or minus ten percent. Finally, the angle defined by the failure crack from the vertical axis was approximately 30 degrees.

Specimen (LW3-NS-BSF) failed when attempting to change from force controlled to displacement controlled loading. A brittle shear failure mode occurred at a level of lateral load (127 kips), 12% lower than the predicted (143 kips). For that reason, the test did not continued with the displacement controlled loading as in all other brittle shear failure tests. However, data pertaining to the monotonic response beyond first yield was recorded and analyzed.

Table 5.9. Force Controlled Test Observation Matrix (LW3-NS-BSF)

	Force Controlled - Test Observation Matrix – (LW3-NS-BSF)			
Test Observation	**Fy'/4**	**Fy'/2**	**3Fy'/4**	**fy'**
Maximum lateral force (kips)	31.89	63.61	95.43	127.00
Axial load (kips)	92.22	95.55	96.58	94.67
Lateral displacement (in)	0.06	0.14	0.27	-
(N & S) Cracks location (Ih/Fh/s(s1-s2)) (in) [a]	0/23/8-13	0/28/8-13	(0/23/6-8) (23/40/10)	(0/45/6-8)
(N & S) Cracks orientation (Horizontal (H)/Vertical (V)/Both (B))	H	H	B	B
(E & W) Cracks location (Ih/Fh/s(s1-s2)) (in) [a]	0/23/10-13	0/28/7-13	0/40/5-7	0/45/3-4
(E & W) Average crack slope and location (Slope/L(%)/Hcs) [b]	90/20/-	60/35/-	35/50/24	30/50/24
(E & W) Face crack propagation (Total-P(%)/Rel.-Length(r1-r2)) [c]	20/4	55/8	80/10-15	100/5-15
New flexural cracks (Yes/No)	Yes	Yes	Yes	No
New shear cracks only (L(%)/Length/Height location) [d]	-	(35/12/13) (20/3/41)	30/4/34	(25/4/40) (50/8/45)
(N & S) Crack width (in/mm)	-	-	-	-
(E & W) Crack width (in/mm)	-	0.005/0.15	0.013/0.33	0.06/1.50
Spalling of concrete cover (Location-Face/Damaged Height (in))	-	-	-	Base-(N&S)/5
Crushing of concrete (Location-Face/Damaged Depth(in))	-	-	-	Base-(N&S)/<1
Exposure of reinforcement steel (Location-Face/Height (in))	-	-	-	-
Buckling of longitudinal reinforcement (Location)	-	-	-	-

[a] (Initial height from the column base (in) /Final height form the column base (in) / Average values of spacing between cracks (in))
[b] (Crack slope from vertical line / Location in east or west faces from tension face north or south, e.g., 50% as the middle of east or west faces)
[c] (Maximum total crack propagation percentage in east or west faces from tension face north or south, e.g., 50% as half of east or west faces covered with cracks / Values of relative crack length propagation (in))
[d] (Location in east or west faces from tension face north or south, e.g., 50% as the middle of east or west faces / Shear only crack length (in) / Height at the middle of the crack in east or west planes (in))

Table 5.10. Displacement Controlled Test Observation Matrix (LW3-NS-BSF)

	Displacement Controlled - Test Observation Matrix – (LW3-NS-BSF)		
Test Observation	**Displacement Ductiliy (1)**	**Displacement Ductiliy (1.5)**	**Displacement Ductiliy (2)**
Maximum lateral force (kips)	124.02	55.15	35.56
Axial load (kips)	112.69	111.27	55.49
Lateral displacement (in)	-	-	-
(N & S) Cracks location (Ih/Fh/s(s1-s2)) (in) [a]	0/45/6-8	0/45/6-8	0/45/6-8
(N & S) Cracks orientation (Horizontal (H)/Vertical (V)/Both (B))	B	B	B
(E & W) Cracks location (Ih/Fh/s(s1-s2)) (in) [a]	-	-	-
(E & W) Average crack slope and location (Slope/L(%)/Hcs) [b]	30/50/24	30/50/24	30/50/24
(E & W) Face crack propagation (Total-P(%)/Rel.-Length(r1-r2)) [c]	100/-	100/-	100/-
New flexural cracks (Yes/No)	-	-	-
New shear cracks only (L(%)/Length/Height location) [d]	-	-	-
(N & S) Crack width (in/mm)	-	-	-
(E & W) Crack width (in/mm)	-	-	-
Spalling of concrete cover (Location-Face/Damaged Height (in))	(N&S) / (E&W)	(N&S) / (E&W)	(N&S) / (E&W)
Crushing of concrete (Location-Face/Damaged Depth(in))	Base-(S)	Base-(S)	Base-(S)
Exposure of reinforcement steel (Location-Face/Height (in))	(N&S) / (E&W)	(N&S) / (E&W)	(N&S) / (E&W)
Buckling of longitudinal reinforcement (Location)	-	-	-

[a] (Initial height from the column base (in) /Final height form the column base (in) / Average values of spacing between cracks (in))
[b] (Crack slope from vertical line / Location in east or west faces from tension face north or south, e.g., 50% as the middle of east or west faces)
[c] (Maximum total crack propagation percentage in east or west faces from tension face north or south, e.g., 50% as half of east or west faces covered with cracks / Values of relative crack length propagation (in))
[d] (Location in east or west faces from tension face north or south, e.g., 50% as the middle of east or west faces / Shear only crack length (in) / Height at the middle of the crack in east or west planes (in))

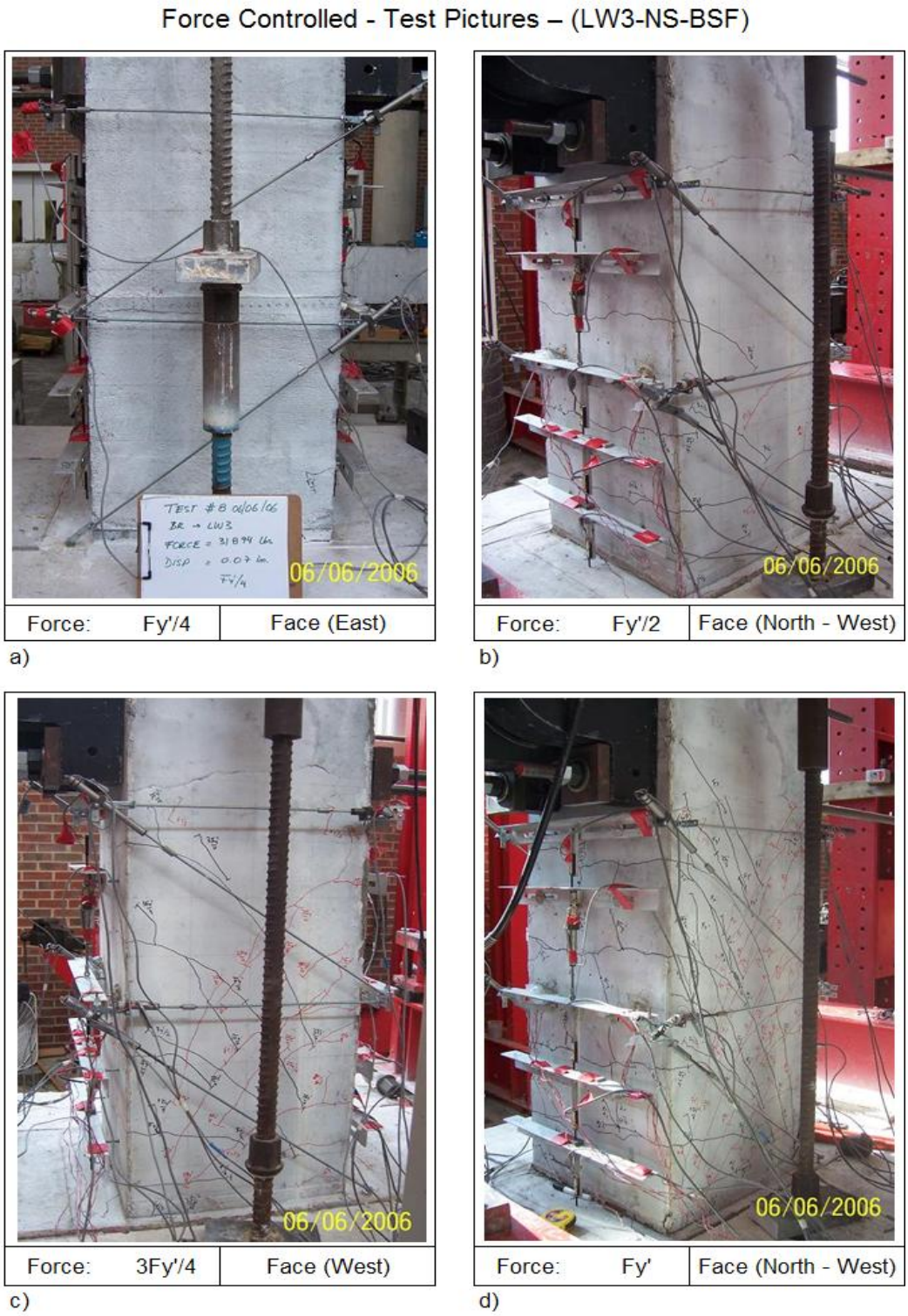

Figure 5.16. Force Controlled Loading – (LW3-NS-BSF)

Displacement Controlled - Test Pictures – (LW3-NS-BSF)

Disp. Ductiliy (<1)	Face (North - West)

a)

Disp. Ductiliy (<1)	Face (West)

b)

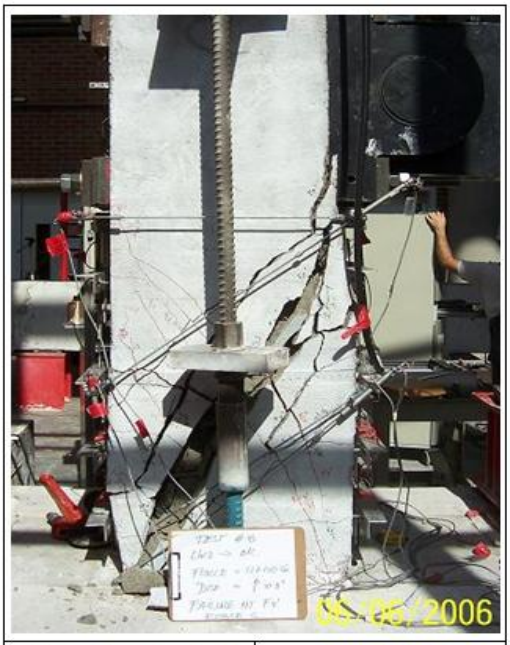

Disp. Ductiliy (<1)	Face (East)

c)

Disp. Ductiliy (<1)	Face (East)

d)

Figure 5.17. Displacement Controlled Loading – (LW3-NS-BSF)

5.5 Tests Results

Most relevant results of all brittle shear failure tests are presented and discussed in this section. However, a comparative analysis of all test results is presented in chapter seven. More specifically, aspects related to the shear performance of the specimens such as shear strength, strength degradation, displacement capacity, flexural and shear deformation, and others are discussed in this section. It is important to mention that while in this section results are presented, it is in chapter seven where the analysis of the data is discussed in depth.

5.5.1 Hysteretic Responses and Peak Cycle Envelopes

Complete force versus displacement histories are presented in Figure 5.18 (a, b, c, & d) corresponding to specimen tests (NW-NS-BSF), (LW1-NS-BSF), (LW2-NS-BSF), and (LW3-NS-BSF). In all these tests, the hysteretic loops defined by the lateral force versus the lateral top displacement have a well defined pinched shape that is not desired for reinforced concrete elements under seismic demands. The above mentioned shape was particularly clear in the case of test (LW2-NS-BSF). Moreover, the pinched shape of the hysteretic loops is associated with reinforced concrete elements under significant shear demands. That effect was desired for the experimental tests in order to study the shear performance of reinforced lightweight concrete. Moreover, as shown in Figure 5.20, the same pinched shape was observed in all the moment versus base curvature hysteretic responses, being more obvious in the case of test (LW2-NS-BSF).

Between the four brittle shear failure tests, the normal weight concrete specimen (NW-NS-BSF) was the one that reached the maximum lateral displacement, and the one that resisted more hysteretic cycles. In addition, force versus displacement and moment versus curvature hysteretic loops of test (NW-NS-BSF) have less abrupt losses of strength, less imperfections or kinks, and the shape is slightly more rounded and smoother. Consequently, specimens made of lightweight concrete types one, two, and three were slightly less ductile and behaved in a slightly more brittle manner. Another reason to support this argument is that the strength degradation was more significant and occurred earlier in all lightweight concrete specimens compared to specimen (NW-NS-BSF). On the other hand, the normal weight concrete specimen continued providing more strength after yielding up to displacement ductility ($\mu_{\Delta}1.5$), Figure 5.18 (a) and Figure 5.19 (a). Finally, between all brittle shear failure specimens, the maximum shear strength was provided by specimen (NW-NS-BSF). It is also important to notice that specimen (LW1-NS-BSF) was the one that behaved more similar to specimen (NW-NS-BSF) considering the shape of the hysteretic loops, and the maximum shear strength.

Furthermore, as it can be observed in Figure 5.18, Figure 5.19, and Figure 5.20, all brittle shear failure specimens developed negative stiffness after the yielding point, and this was more evident for lightweight concrete specimens (LW1, 2 &3-NS-BSF). As a commentary, negative stiffness after yielding is not desired for reinforced concrete elements under seismic

demands. The reason is that after yielding it is more difficult for the system to return to the original position since the system tends to continue yielding. Once again, the above mentioned behavior is common in brittle shear failure elements with low ductility capacity levels. In fact, lack of ductility is indirectly shown by force displacement responses considering the significant strength deterioration when comparing peak forces of all cycles at the same level of deformation (see Figure 5.19).

5.5.2 Average Curvature and Transverse Reinforcement Steel Strain Profiles

Average curvature profiles were used to calculate top displacements due to flexural deformation. As shown in Figure 5.22, average curvature profiles of brittle shear failure specimens are relatively similar and consistent with expected results. Indeed, the maximum curvature is located at the base of the column in all cases. It is important to mention that it was calculated considering a strain penetration length of the longitudinal reinforcement steel in the footing member. In fact, the calculated curvature at the bottom gage, in the non-linear range, represents the average value of the maximum curvature considered to be constant along a distance (*Lp*) at the base of the column. In the same manner, curvature profiles are relatively similar between each specimen. Finally in all cases, the first yielding curvature was reached when first yielding (Fy') of the column cross section was reached.

Regarding the transverse reinforcement steel strain profiles shown in Figure 5.21, all the strain profiles of all the brittle shear failure specimens show that yielding in the stirrups occurred close to the moment when the column reached the first yielding point (Fy'), and

before reaching the equivalent yielding displacement at ductility one. As a result, this explains the formation of shear only cracks during force controlled loading at (Fy'/2 and 3Fy'/4) as described in the test observation matrices presented in this chapter.

Moreover, maximum transverse reinforcement steel strains tended to occur at a height over two feet from the column base as it can be observed in Figure 5.21. In fact, this observation is confirmed by visual observation of the area of more shear activity and deformation, or at the intersection of principal shear cracks on the middle of faces (E & W).

In order to check maximum values of strain profiles with physical measurements obtained during the tests, transverse steel strains were estimated and calculated as a function of the shear crack width, the spacing between shear cracks, and the orientation of the cracks from the vertical axis. For instance, considering a maximum strain in the stirrups greater than 0.002 at first yielding (Fy') as it was observed in all brittle shear failure tests, the value of the strain can be correlated to the shear deformation using (Eq. 5-2). In fact, for test (NW-NS-BSF), the stirrup strain was estimated to be approximately 0.0023 if we consider physical measurements obtained during the test such as the shear crack width (SCw) of 0.016 inches at (Fy'), the average shear crack spacing (SCs) of 6.00 inches at (Fy'), and the angle of the crack measured from the vertical axis of the column (θ) of approximately 30 degrees. Finally, the same thing can be done for different levels of deformation.

$$\varepsilon s = \frac{SCw}{SCs} \cdot \cos(\theta) \qquad \textbf{(Eq. 5-2)}$$

5.5.3 Displacement Components

Displacement components due to Flexural and shear deformation were calculated separately using the data obtained during the test by linear potentiometers. In fact, the displacement components were compared to the total top displacement of the specimen separately measured by string linear potentiometers. As a result, Figure 5.23 (a – d) shows the graphs that relate top column displacements versus displacement components of each brittle shear failure specimen.

In general, it can be observed that the flexural displacement component increases rapidly during the initial stage of all tests when force controlled loading is applied, and before the specimens have reached the yielding point (see Figure 5.23). In addition, in most cases the rate of increment in the flexural displacement component tends to decrease after reaching the yielding point. Furthermore, before failure, flexural displacement components do not increase significantly during the last levels of deformation (see Figure 5.23). On the contrary, shear displacement components increase slowly during force controlled loading, but increase more and more as the level of deformation increases. Indeed, the shear displacement component increases more rapidly after reaching a displacement close to yielding of the specimen as can be observed in Figure 5.23 (a – d).

The above mentioned behavior of the displacement components has been confirmed by visual observations during the tests. In fact, as described in all test observation matrices

presented in this chapter, flexural cracks appeared mainly during the force controlled loading. After having reached the yielding point, almost no new flexural cracks appeared. In fact, flexural cracks remained stable. On the contrary, shear only cracks did not appear at low levels of lateral load, but most of them started to appear towards reaching the first yielding point and beyond that level of deformation. Significant activity in terms of shear deformation and damage was observed on faces (E & W) in the non-linear range

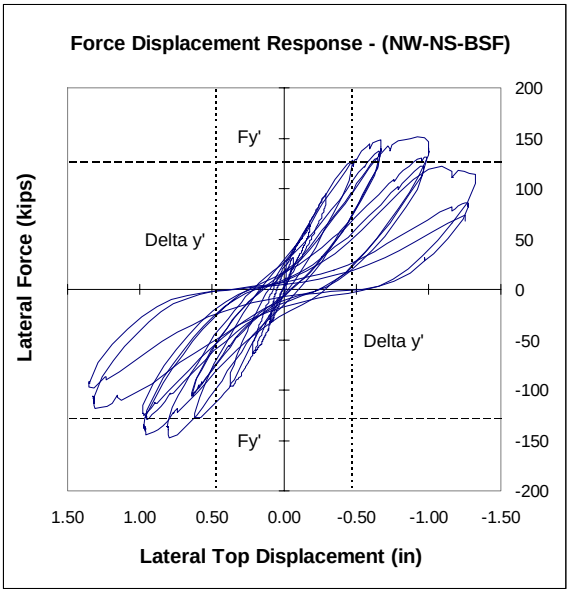

a) Specimen (NW-NS-BSF)

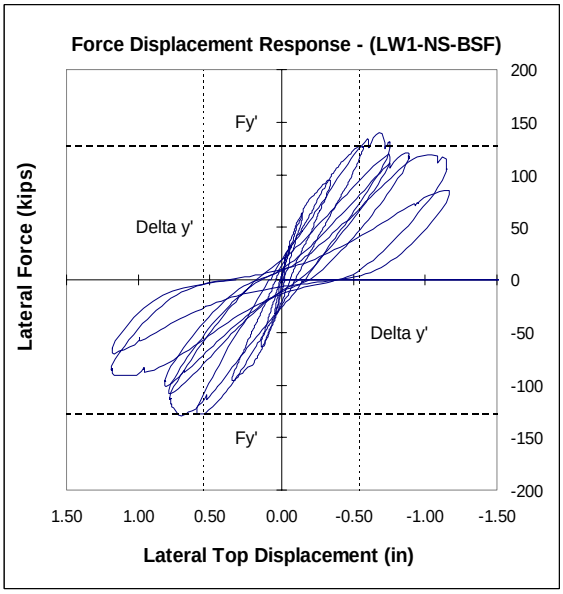

b) Specimen (LW1-NS-BSF)

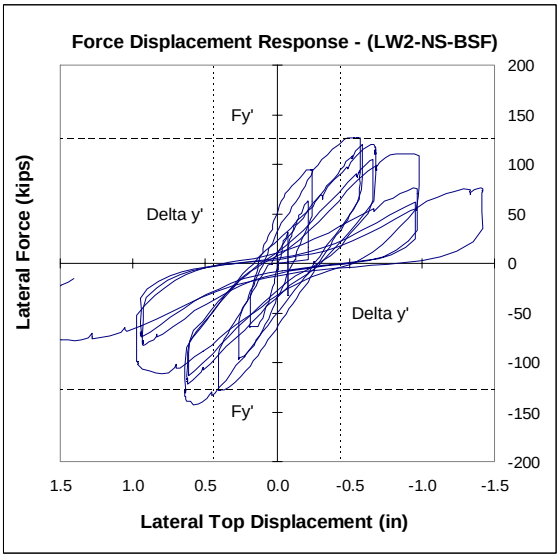

c) Specimen (LW2-NS-BSF)

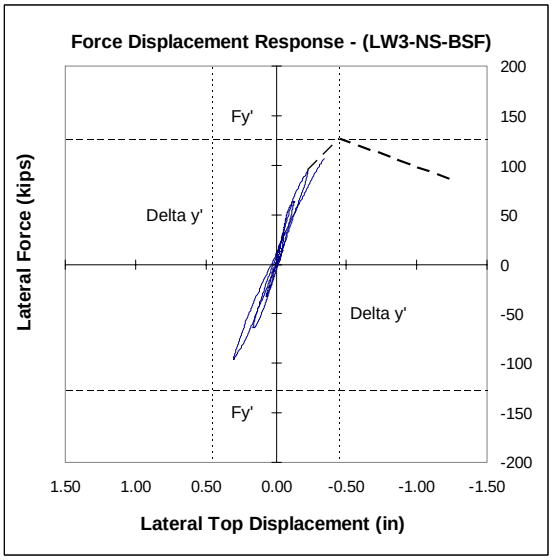

d) Specimen (LW3-NS-BSF)

Figure 5.18. Force versus Lateral Top Displacement Histories – Brittle Shear Failure Specimens

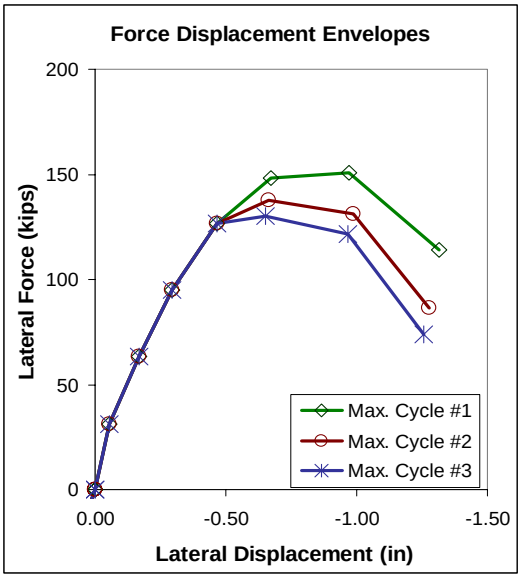

a) Specimen (NW-NS-BSF)

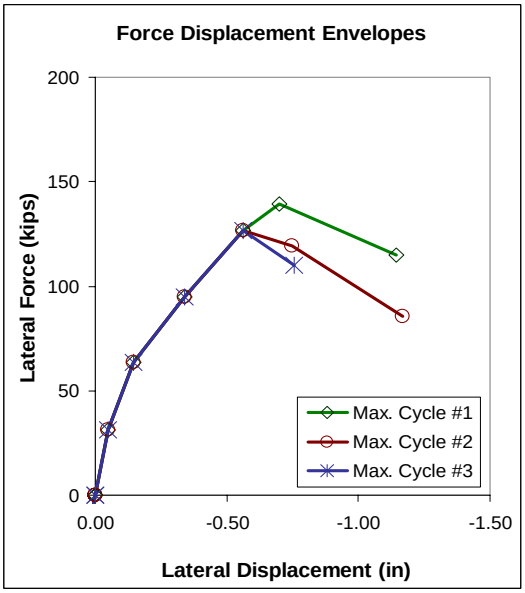

b) Specimen (LW1-NS-BSF)

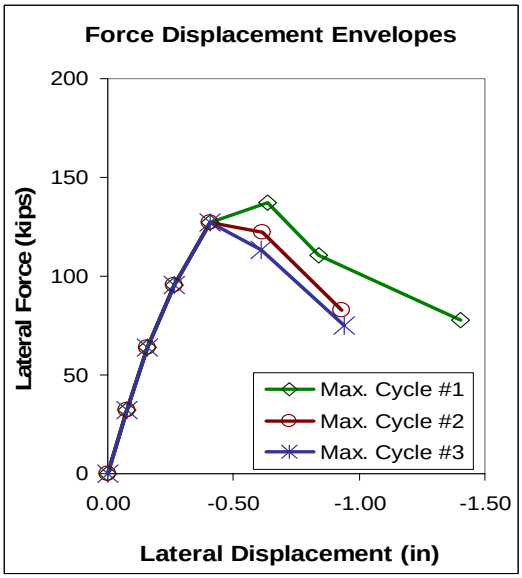

c) Specimen (LW2-NS-BSF)

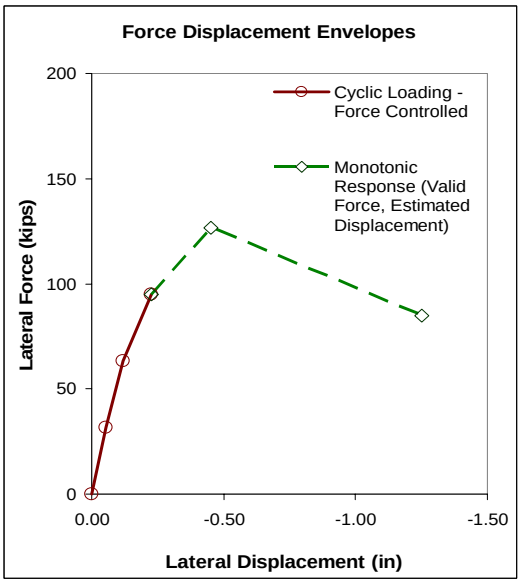

d) Specimen (LW3-NS-BSF)

Figure 5.19. Force Displacement Envelopes – Brittle Shear Failure Specimens

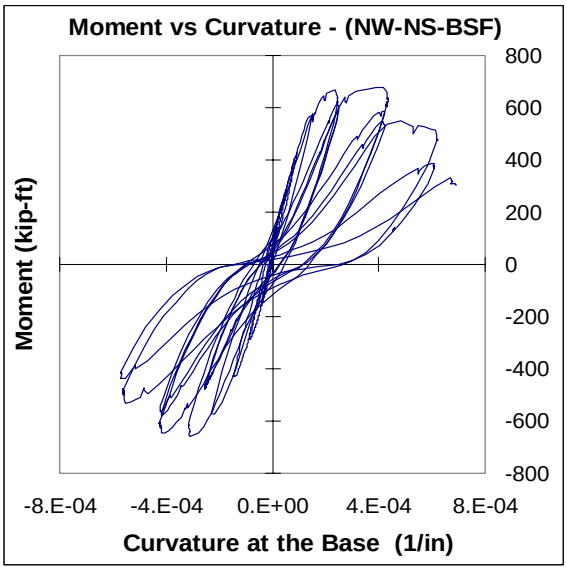

a) Specimen (NW-NS-BSF)

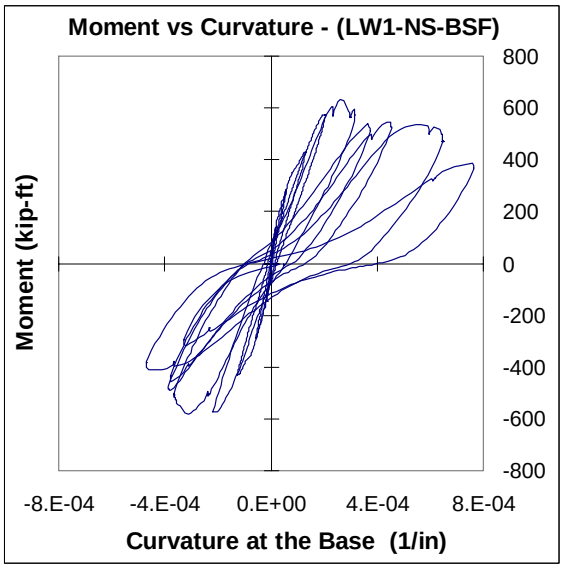

b) Specimen (LW1-NS-BSF)

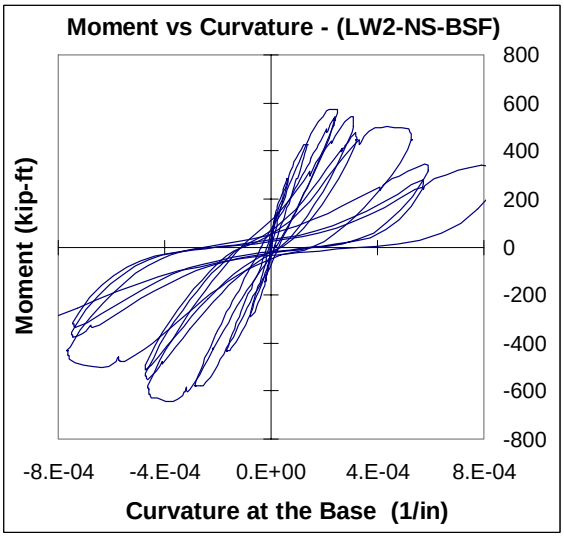

c) Specimen (LW2-NS-BSF)

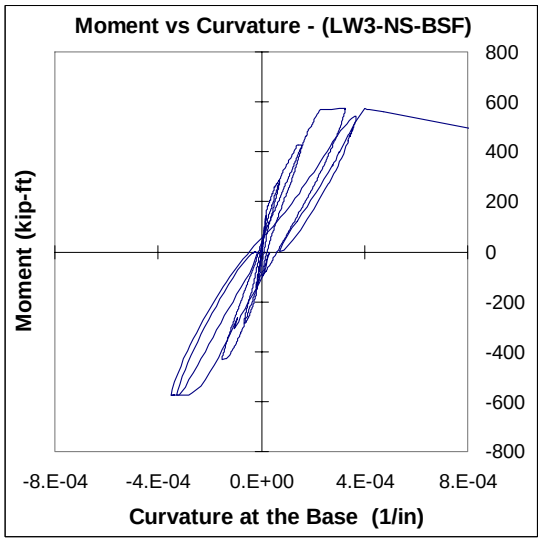

d) Specimen (LW3-NS-BSF)

Figure 5.20. Moment versus Curvature Histories – Brittle Shear Failure Specimens

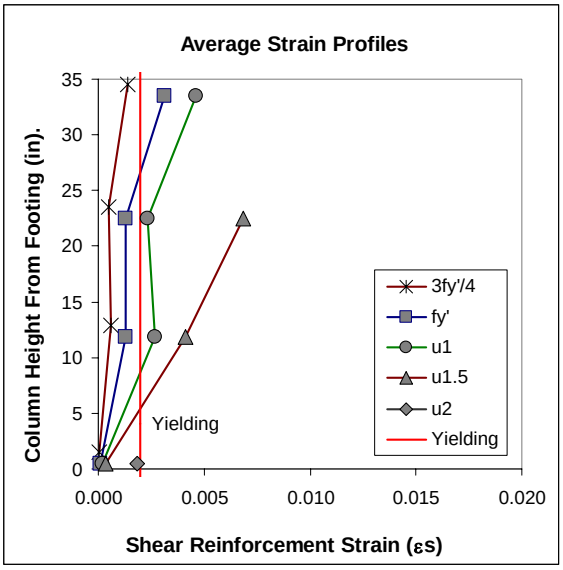

a) Specimen (NW-NS-BSF)

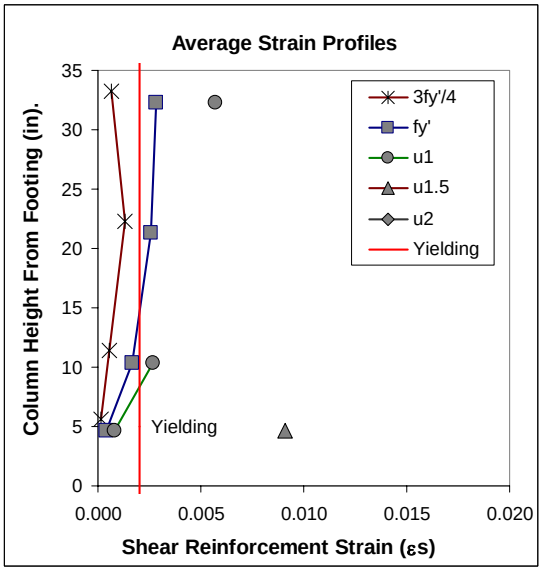

b) Specimen (LW1-NS-BSF)

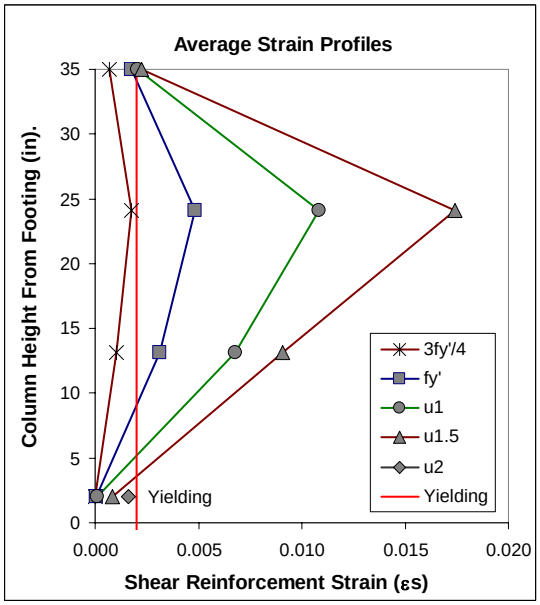

c) Specimen (LW2-NS-BSF)

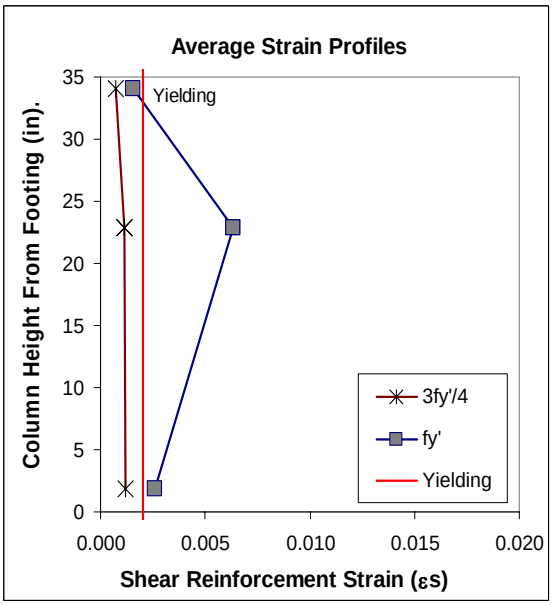

d) Specimen (LW3-NS-BSF)

Figure 5.21. Transverse Reinforcement Steel Strain Profiles – Brittle Shear Failure Specimens

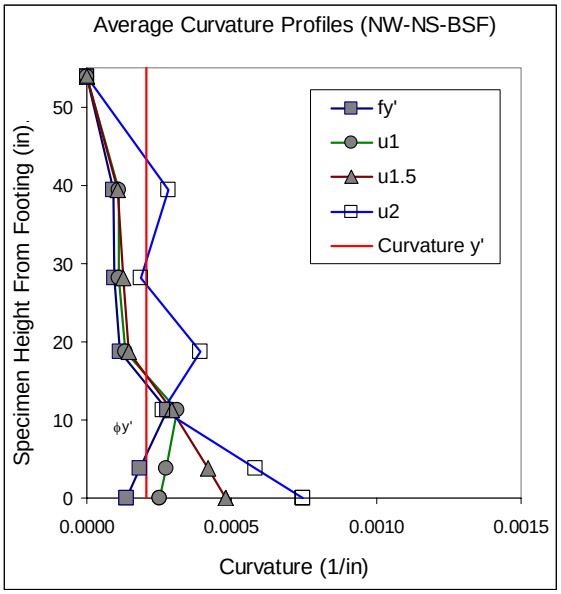

a) Specimen (NW-NS-BSF)

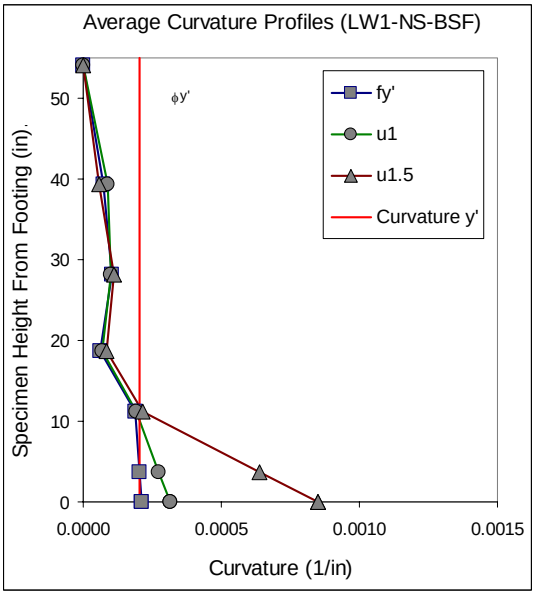

b) Specimen (LW1-NS-BSF)

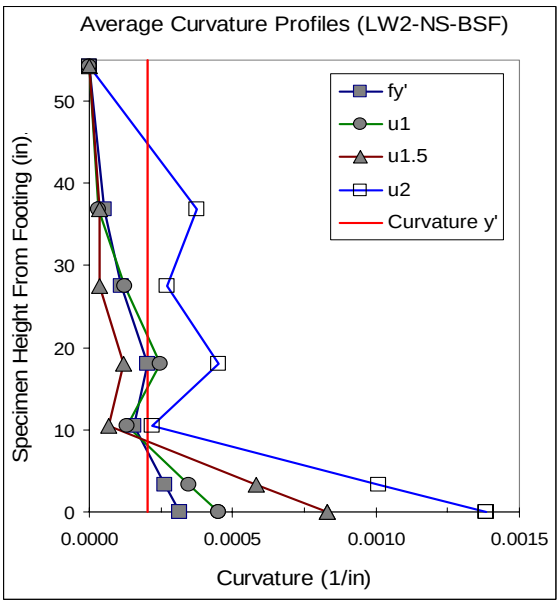

c) Specimen (LW2-NS-BSF)

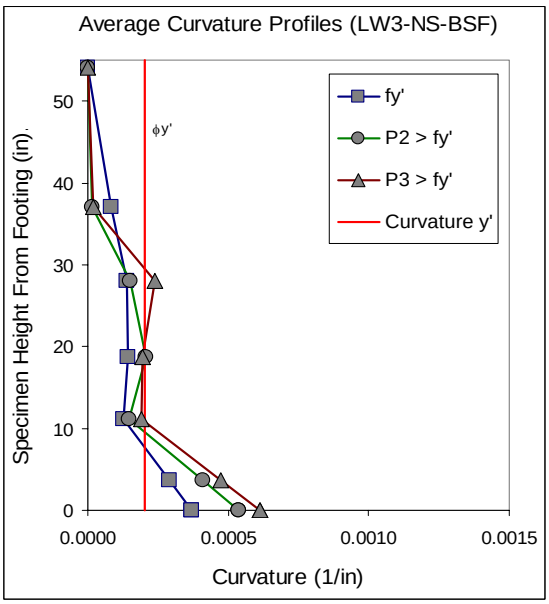

d) Specimen (LW3-NS-BSF)

Figure 5.22. Curvature Profile – Brittle Shear Failure Specimens

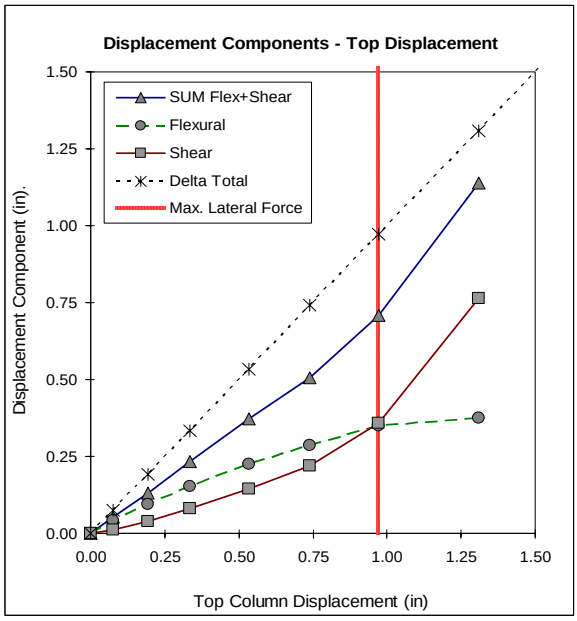

a) Specimen (NW-NS-BSF)

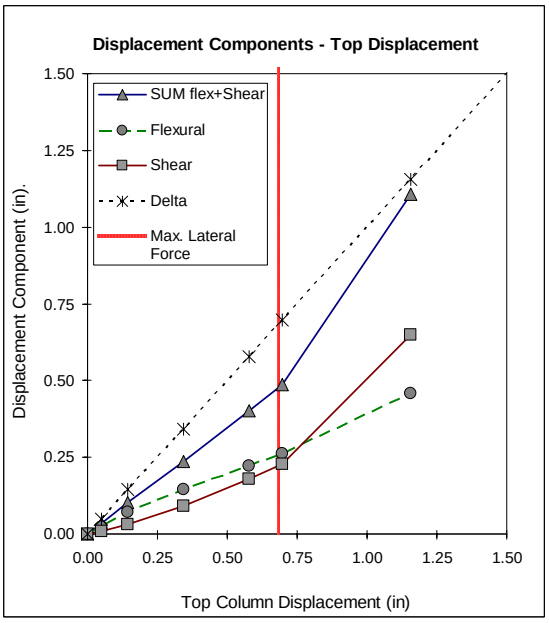

b) Specimen (LW1-NS-BSF)

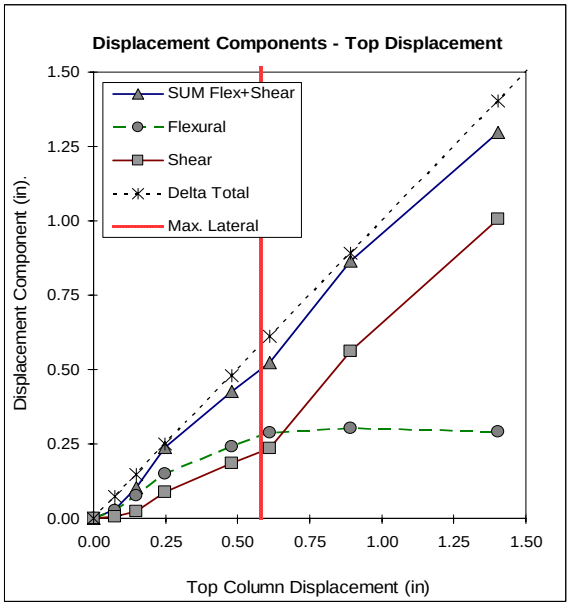

c) Specimen (LW2-NS-BSF)

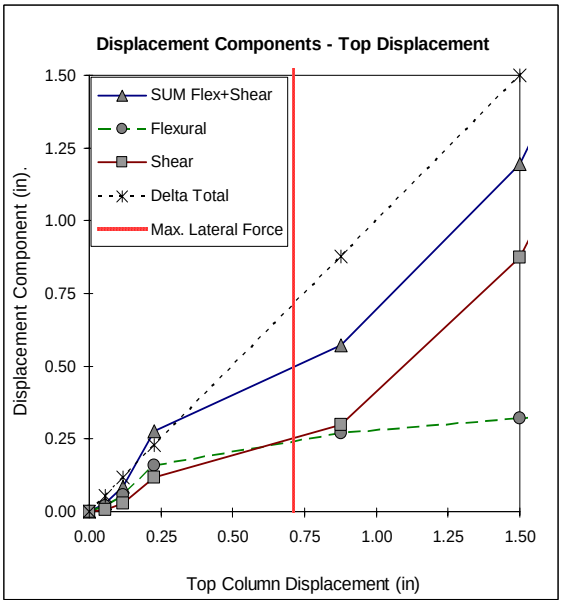

d) Specimen (LW3-NS-BSF)

Figure 5.23. Displacement Components – Brittle Shear Failure Specimens

Chapter 6: TEST SPECIMENS – DUCTILE SHEAR FAILURE MODE

Facets of all four ductile shear failure tests are discussed in this chapter. It is important to notice that, except for the concrete mixture, all the specimens were built using the same materials and according to the same design. Similarly, the specimens were tested following the same procedures. In addition, tests observations are presented in this chapter for one normal weight concrete and three lightweight concrete specimens as described in Table 5.1. Furthermore, for each test, sections such as loading history, test observations, and test results are presented following the same order for each specimen.

Table 6.1. Ductile Shear Failure Tests Specifications

Project Test Program - Ductile Shear Failure Specimens							
ACTUAL CONCRETE STRENGTH (psi)	DESIRED FAILURE MECHANISM	AGGREGATE TYPE	AGGREGATE MATERIAL DESCRIPTION	AGGREGATE QUARRY LOCATION IN THE U.S.A.	PREDICTED LWC SHEAR CAPACITY (kips) [a]	MAXIMUM RECORDED LATERAL FORCE (kips)	TEST NAME
3,946	Ductile Shear Failure	Normal Weight	-	-	201	175	(NW-NS-DSF)
7,315		Lightweight (1)	Expanded Slate	Southeast		173	(LW1-NS-DSF)
5,164		Lightweight (2)	Expanded Shale	Midwest and North		172	(LW2-NS-DSF)
4,969		Lightweight (3)	Expanded Clay	West Coast		176	(LW3-NS-DSF)

[a] Based on shear transfer mechanism developed by Priestley et al. (1994) and modified for lightweight concrete (Kowalsky et al., 1999 b) as described in section 7.2.

6.1. Normal Weight – Normal Strength - Ductile Shear Failure Test (NW-NS-DSF)

For the ductile shear failure specimens set, a normal weight concrete, normal strength, and ductile shear failure column (NW-NS-DSF) was tested as a control and reference specimen as it was done for the brittle shear failure set. Moreover, the specimen was made of the same concrete mixture of specimen (NW-NS-BSF). In a similar manner, even though the analytical model was used to determine the force controlled loading history, test (NW-NS-DSF) was used to confirm the loading protocol as it was observed to be consistent. Finally, the remaining specimens were tested using the same procedure. In brief, the specimen test discussed in this section was made of normal weight aggregate and normal strength concrete mixture.

6.1.1 Loading History

Loading of the specimen consisted of two procedures to apply a constant axial and a cyclic lateral load during the course of the test. First, a force controlled lateral loading was used as the initial procedure as shown in the first four cycles of Figure 6.1. In this case, one cycle was applied at each level of lateral load. The lateral load was increased from zero to a point in which the longitudinal reinforcement of the column in the tension side was assumed to have reached the yielding strain (Fy'). For that purpose, moment versus curvature analysis was used to determine the maximum moment at the base of the column required for reaching (Fy'), and the respective lateral force was obtained as a function of the lever arm of the column under single bending as some predicted values are shown in Table 6.2. Second, in

order to capture the entire force displacement response of the system through the non-linear range, a displacement controlled cyclic lateral loading was applied. As a result, data was acquired even if there was a negative stiffness of the specimen beyond yielding. In brief, various cycles at the same level of deformation were applied as a way of observing any stiffness degradation and ductility capacity of the system.

Table 6.2. Predicted Response Values – Ductile Shear Failure Specimens

PREDICTED VALUES	First Yield (εs = 0.002)				Predicted Failure				Point Beyond Yield for Bi-linear Aproximation (Mn & Fi at εc = 0.004)			
		Units		Units		Units		Units		Units		Units
Curvature	0.00017	(1/in)	0.00676	(1/m)	0.00220	(1/in)	0.08672	(1/m)	0.00081	(1/in)	0.03177	(1/m)
Moment	571.25	(kip-ft)	774.51	(kN-m)	904.62	(kip-ft)	1226.50	(kN-m)	802.03	(kip-ft)	1087.40	(kN-m)
Concrete Strain	0.0013	(u)	0.0013	(u)	0.0120	(u)	0.0120	(u)	0.0040	(u)	0.0040	(u)
Neutral Axis Depth	7.53	(in)	191.14	(mm)	5.45	(in)	138.38	(mm)	4.96	(in)	125.92	(mm)
Steel strain	0.0020	(u)	0.0020	(u)	0.0303	(u)	0.0303	(u)	0.0115	(u)	0.0115	(u)
Shear Demand	127.09	(kips)	565.34	(kN)	201.26	(kips)	895.26	(kN)	178.44	(kips)	793.72	(kN)
Top Displacement [a]	0.27		6.82	(mm)	3.16	(in)	80.30	(mm)	1.23	(in)	31.20	(mm)
Shear capacity	258.67	(kips)	1150.60	(kN)	203.21	(kips)	903.92	(kN)	250.27	(kips)	1113.28	(kN)
Ductility	0.71	(u)	0.71	(u)	8.39	(u)	8.39	(u)	3.26	(u)	3.26	(u)
Delta y = (Fi/F'y)*Δ'y	0.38	(in)	9.58	(mm)								

[a] The predicted top displacements were estimated without considering the displacement component due to shear deformation.

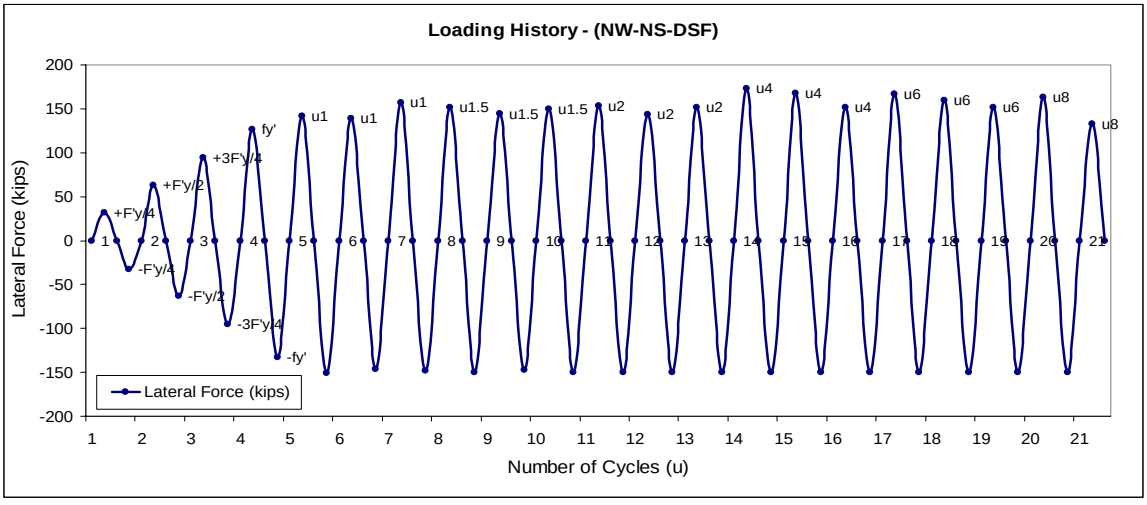

Figure 6.1. Load History (NW-NS-DSF) Specimen

Having the actual force and displacement at the first yielding point (Fy'), and the nominal capacity from the analytical model, an equivalent yielding displacement was calculated. The equivalent yielding point was determined by extrapolating the actual displacement at (Fy') in proportion to the nominal force divided by the fist yielding force obtained from the analytical model. As a result, displacement ductility one, defined by the equivalent yielding point, was the reference to calculate different levels of deformation. Finally, during displacement controlled loading history, three cycles at each level of deformation were applied starting from displacement ductility one to failure. The displacement history of test is shown in Figure 6.2. It is important to notice that due to the limitation in the maximum capacity of the actuator in the pulling direction (150 kips), the displacement controlled loading was only successfully applied in the pushing direction as it can be observed in Figure 6.2.

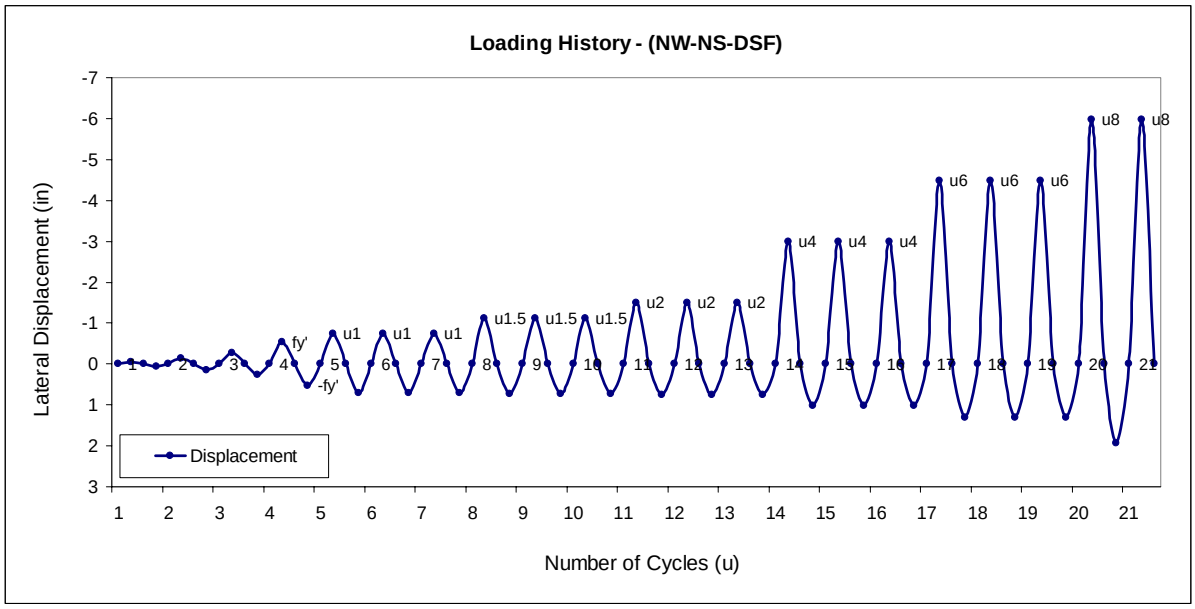

Figure 6.2. Displacement History (NW-NS-DSF) Specimen

6.1.2 Relevant Observations

Relevant test observations are presented in this section with the same format used for all the specimens. Matrices with information obtained during the tests such as lateral force, displacement, cracks location, slope, crack width, and more are presented in this section. Furthermore, the information contained in the matrices considers various levels of lateral force and displacement. Regarding specimens (NW-NS-DSF), test observations during displacement controlled loading refer to the pushing direction only.

6.1.2.1 Force Controlled

During force controlled loading, at low levels of lateral load (Fy'/4 & Fy'/2), horizontal flexural cracks appeared on the tension sides of the column (N & S) as described in Table 6.3. Moreover, the flexural cracks started to propagate from tension faces to (E & W) faces, and the spacing between flexural cracks at (Fy') was approximately 6 inches. Similar spacing was observed during brittle shear failure tests at the same level of lateral load. The orientation of the cracks was initially horizontal close to faces (N & S) as shown in Figure 6.3 (a & b). For higher levels of lateral load (Fy'), cracks on faces (E & W) propagated significantly covering 75% of (E & W) faces similar to what was observed in the brittle shear failure tests. In addition, the spacing between cracks in faces (E & W) was reduced between 4 to 6 inches at (Fy'). It is also important to mention that a few shear only cracks started to appear early at lateral loads of (Fy'/2) as described in Table 6.3.

In addition, the actual top displacement at (Fy') was 0.53 inches, 13% greater than the top displacement of test (NW-NS-BSF). In addition, no vertical splitting of the concrete along the longitudinal reinforcement of the column was observed in this test as it was observed during all brittle shear failure tests at force controlled loading. Vertical splitting was not observed thanks to the significant additional amount of transverse steel and the better confinement provided to all ductile shear failure specimens. Finally, no significant damage of the column was observed during force controlled loading.

6.1.2.2 Displacement Controlled

During displacement controlled loading, the same procedure described in section 5.1.2.2 was followed. In addition, three cycles were applied at different levels of deformation considering top displacements of 0.75 inches for ($\mu_\Delta 1$), 1.12 inches for ($\mu_\Delta 1.5$), 1.50 inches for ($\mu_\Delta 2$), 2.99 inches for ($\mu_\Delta 4$), 4.49 inches for ($\mu_\Delta 6$), and 5.98 inches for ($\mu_\Delta 8$). As expected, the specimen failed at a high level of deformation when reaching a top displacement eight times greater than the equivalent yielding displacement.

The maximum actual shear capacity of the specimen was 175 kips reached at a displacement ductility of ($\mu_\Delta 6$) as shown in Table 6.5. Moreover, the specimen continued resisting the shear force with a positive stiffness beyond the yielding point and up to ($\mu_\Delta 6$). In addition, the shear capacity was approximately 13% lower than the predicted by the analytical model. The maximum variation of the axial load during the test was in the range of plus or minus twenty to thirty percent. Moreover, during displacement controlled loading the average

spacing between flexural cracks in (N & S) faces was between 3 to 4 inches along the first two feet from the base of the column, and between 5 to 7 inches along the next two feet. Furthermore, spacing between shear cracks on the middle of (E & W) faces continued getting shorter with values between 3 to 4 inches at displacement ductility levels of (μ_Δ6 & 8). A well defined shear crack on (E & W) faces was observed at ductility (μ_Δ8), and the angle from the vertical axis was 34.31 degrees as shown in Figure 6.5 (c). Moreover, the width of shear cracks continued increasing up to 0.24 inches at (μ_Δ8). No significant increment in the number of flexural cracks in (N & S) faces was observed for levels of deformation beyond the equivalent yielding point. However, several new shear only cracks were observed during displacement controlled loading.

In terms of damage, minor spalling of the concrete cover started at the bottom of faces (N & S) during displacement ductility (μ_Δ1). Moreover, beyond (μ_Δ1) spalling on faces (N & S) became more severe, and at (μ_Δ6) spalling of the concrete cover was observed on faces (E & W) as some of the reinforcement steel was exposed. Furthermore, some crushing of the concrete was also observed at the bottom of faces (N & S) at displacement ductility (μ_Δ1.5). In the same manner, crushing of the concrete became more evident towards (μ_Δ8) as described in Table 6.5. Finally, it is important to mention that most of the activity in terms of deformation and damage was concentrated towards the base of the column while in all brittle shear failures tests it was located significantly higher. This revealed the tendency of all ductile shear failure specimens to develop a plastic hinge close to the column base and to the

location of maximum moment. Most of the activity in terms of deformation and damage in faces (E & W) was located approximately at 10 to 15 inches from the column base. This distance over the column base was located between the observed in all brittle shear failure specimens (governed by shear) of approximately 23 inches and the plastic hinge length over the base of a column primarily governed by a flexural failure of approximately 4 inches (8% of the clear length) as proposed by Priestley et al. (1996) using the plastic hinge method. This fact reveals the nature of the failure of all ductile shear failure specimens that was considered of a flexural or flexural-shear type as discussed in depth in chapter 7.

Table 6.3. Force Controlled Test Observation Matrix (NW-NS-DSF)

	Force Controlled - Test Observation Matrix – (NW-NS-DSF)			
Test Observation	**Fy'/4**	**Fy'/2**	**3Fy'/4**	**fy'**
Maximum lateral force (kips)	32.48	63.46	95.38	132.76
Axial load (kips)	90.79	92.46	96.56	103.83
Lateral displacement (in)	0.05	0.14	0.27	0.53
(N & S) Cracks location (Ih/Fh/s(s1-s2)) (in) [a]	0/39/-	0/39/6-9	0/40/4-8	0/42/6
(N & S) Cracks orientation (Horizontal (H)/Vertical (V)/Both (B))	H	H	H	H
(E & W) Cracks location (Ih/Fh/s(s1-s2)) (in) [a]	0/39/6-9	0/39/6-9	0/40/4-6	0/48/4-6
(E & W) Average crack slope and location (Slope/L(%)/Hcs) [b]	90/10	60/35/12	45/50/18	(45/50/-)
(E & W) Face crack propagation (Total-P(%)/Rel.-Length(r1-r2)) [c]	7/1-2	50/5-10	55/4	75/2-6
New flexural cracks (Yes/No)	Yes	Yes	Yes	No
New shear cracks only (L(%)/Length/Height location) [d]	-	25/5/18	30/9/37	(25/9/45) (50/6/40)
(N & S) Crack width (in/mm)	-	-	-	0.02/0.50
(E & W) Crack width (in/mm)	-	-	-	0.016/0.40
Spalling of concrete cover (Location-Face/Damaged Height (in))	-	-	-	-
Crushing of concrete (Location-Face/Damaged Depth(in))	-	-	-	-
Exposure of reinforcement steel (Location-Face/Height (in))	-	-	-	-
Buckling of longitudinal reinforcement (Location)	-	-	-	-

[a] (Initial height from the column base (in) /Final height form the column base (in) / Average values of spacing between cracks (in))
[b] (Crack slope from vertical line / Location in east or west faces from tension face north or south, e.g., 50% as the middle of east or west faces / Height of the crack slope (in))
[c] (Maximum total crack propagation percentage in east or west faces from tension face north or south, e.g., 50% as half of east or west faces covered with cracks / Values of relative crack length propagation (in))
[d] (Location in east or west faces from tension face north or south, e.g., 50% as the middle of east or west faces / Shear only crack length (in) / Height at the middle of the crack in east or west planes (in))

Table 6.4. Displacement Controlled Test Observation Matrix (NW-NS-DSF) – Ductility One to Two

	Displacement Controlled - Test Observation Matrix – (NW-NS-DSF)		
Test Observation	**Displacement Ductiliy (1)**	**Displacement Ductiliy (1.5)**	**Displacement Ductiliy (2)**
Maximum lateral force (kips)	150.87	155.93	162.02
Axial load (kips)	114.00	121.14	120.57
Lateral displacement (in)	0.75	1.12	1.50
(N & S) Cracks location (Ih/Fh/s(s1-s2)) (in) [a]	0/48/6	0/48/6	(0/8/3-5) (8/48/6)
(N & S) Cracks orientation (Horizontal (H)/Vertical (V)/Both (B))	H	H	H
(E & W) Cracks location (Ih/Fh/s(s1-s2)) (in) [a]	0/48/3-5	0/48/3-5	0/48/3-5
(E & W) Average crack slope and location (Slope/L(%)/Hcs) [b]	(45/50/36) (60/50/10)	(45/50/36) (60/50/10)	(45/50/36) (60/50/8)
(E & W) Face crack propagation (Total-P(%)/Rel.-Length(r1-r2)) [c]	75/1-2	80/2-4	95/2-4
New flexural cracks (Yes/No)	No	No	Yes
New shear cracks only (L(%)/Length/Height location) [d]	(40/4/38) (25/8/42)	-	(30/4/4)
(N & S) Crack width (in/mm)	0.02/0.50	0.06/1.50	-
(E & W) Crack width (in/mm)	0.016/0.40	0.016/0.40	-
Spalling of concrete cover (Location-Face/Damaged Height (in))	Base-(N&S)/-	Base-(N&S)/3	Base-(N&S)/4
Crushing of concrete (Location-Face/Damaged Depth(in))	-	Base-(N&S)/2	Base-(N&S)/2
Exposure of reinforcement steel (Location-Face/Height (in))	-	-	-
Buckling of longitudinal reinforcement (Location)	-	-	-

[a] (Initial height from the column base (in) /Final height form the column base (in) / Average values of spacing between cracks (in))
[b] (Crack slope from vertical line / Location in east or west faces from tension face north or south, e.g., 50% as the middle of east or west faces / Height of the crack slope (in))
[c] (Maximum total crack propagation percentage in east or west faces from tension face north or south, e.g., 50% as half of east or west faces covered with cracks / Values of relative crack length propagation (in))
[d] (Location in east or west faces from tension face north or south, e.g., 50% as the middle of east or west faces / Shear only crack length (in) / Height at the middle of the crack in east or west planes (in))

Table 6.5. Displacement Controlled Test Observation Matrix (NW-NS-DSF) – Ductility Four to Failure

	Displacement Controlled - Test Observation Matrix – (NW-NS-DSF)		
Test Observation	**Displacement Ductiliy (4)**	**Displacement Ductiliy (6)**	**Displacement Ductiliy (8)**
Maximum lateral force (kips)	173.41	174.63	161.20
Axial load (kips)	124.14	121.33	106.90
Lateral displacement (in)	2.99	4.49	5.98
(N & S) Cracks location (Ih/Fh/s(s1-s2)) (in) [a]	(0/24/3-5) (24/48/6)	(0/24/3-5) (24/48/6)	(0/24/3-5) (24/48/6)
(N & S) Cracks orientation (Horizontal (H)/Vertical (V)/Both (B))	H	B	B
(E & W) Cracks location (Ih/Fh/s(s1-s2)) (in) [a]	(0/24/3-5) (24/48/5-6)	0/24/2-4	0/24/2-4
(E & W) Average crack slope and location (Slope/L(%)/Hcs) [b]	(45/50/15) (60/50/5)	(45/50/15) (60/50/5)	34.31/50/15
(E & W) Face crack propagation (Total-P(%)/Rel.-Length(r1-r2)) [c]	95/2-3	100/1	100/-
New flexural cracks (Yes/No)	No	No	No
New shear cracks only (L(%)/Length/Height location) [d]	20/3/19	-	-
(N & S) Crack width (in/mm)	-	-	-
(E & W) Crack width (in/mm)	0.08/2.00	0.18/4.50	0.24/6.00
Spalling of concrete cover (Location-Face/Damaged Height (in))	Base-(N&S)/5	(Base-(N&S)/5) (Center-(E&W)/-)	(Base-(N&S)/5) (Center-(E&W)/0-15)
Crushing of concrete (Location-Face/Damaged Depth(in))	Base-(N&S)/2.5	Base-(N&S)/2.5	Base-(N&S)/-
Exposure of reinforcement steel (Location-Face/Height (in))	-	-	Center-(E&W)/0-15
Buckling of longitudinal reinforcement (Location)	-	-	Base-(N&S)

[a] (Initial height from the column base (in) /Final height form the column base (in) / Average values of spacing between cracks (in))
[b] (Crack slope from vertical line / Location in east or west faces from tension face north or south, e.g., 50% as the middle of east or west faces / Height of the crack slope (in))
[c] (Maximum total crack propagation percentage in east or west faces from tension face north or south, e.g., 50% as half of east or west faces covered with cracks / Values of relative crack length propagation (in))
[d] (Location in east or west faces from tension face north or south, e.g., 50% as the middle of east or west faces / Shear only crack length (in) / Height at the middle of the crack in east or west planes (in))

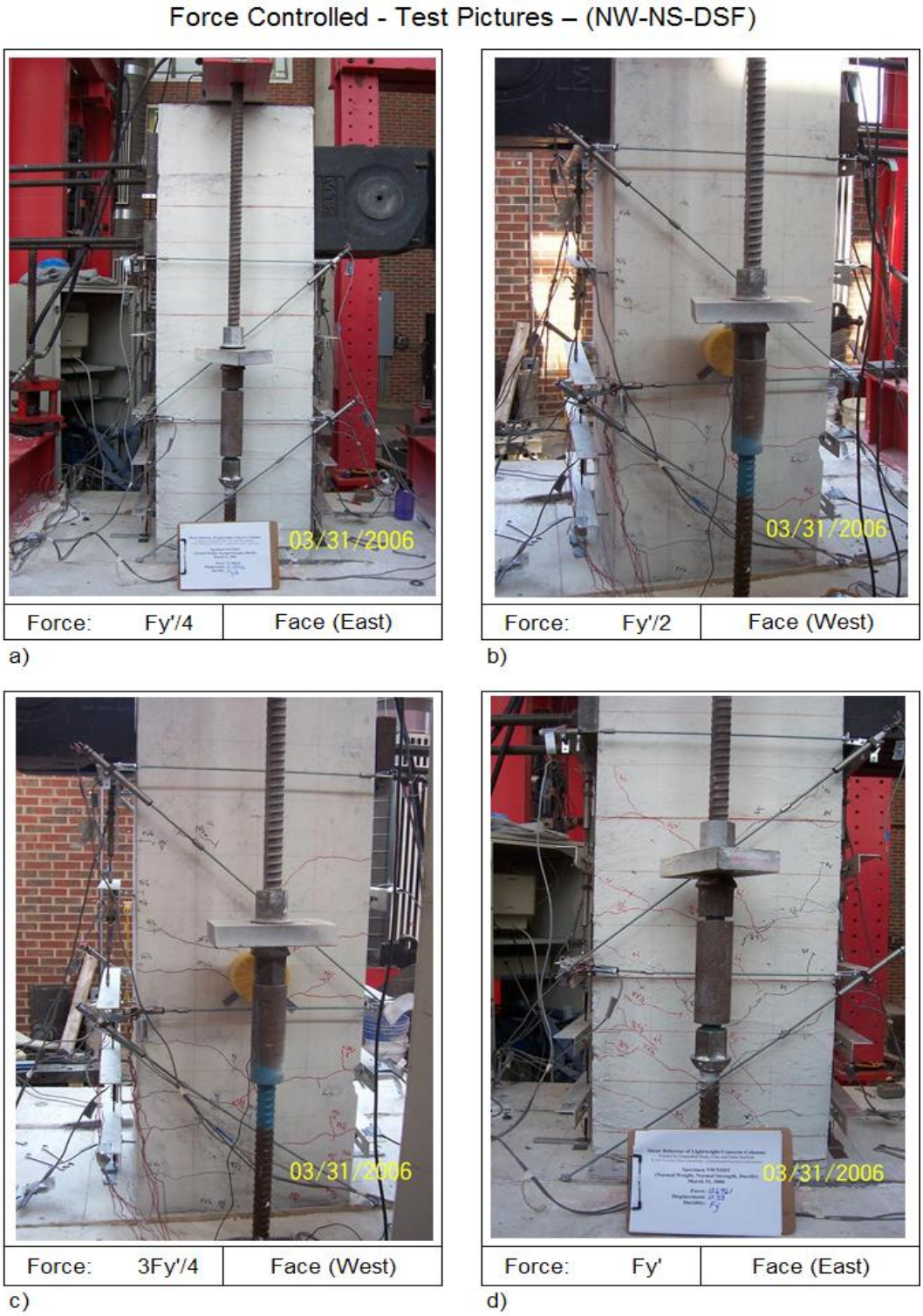

Figure 6.3. Force Controlled Loading – (NW-NS-DSF)

Displacement Controlled - Test Pictures – (NW-NS-DSF)

Disp. Ductiliy (1/c3)	Face (East)

a)

Disp. Ductiliy (1.5)	Face (East)

b)

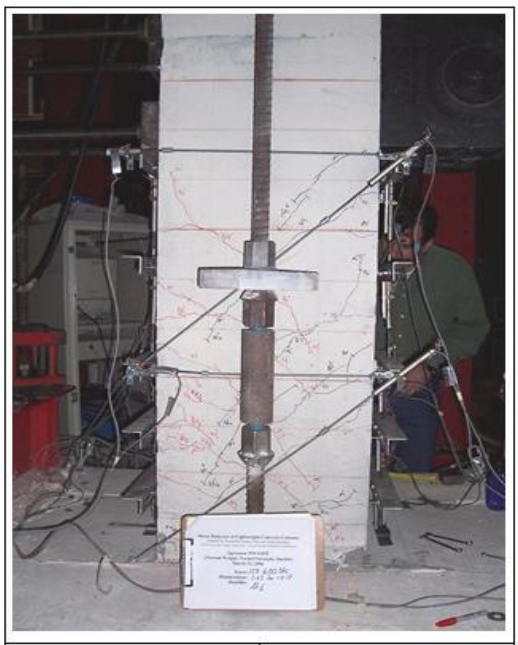

Disp. Ductiliy (2)	Face (East)

c)

Disp. Ductiliy (4/c3)	Face (South - East)

d)

Figure 6.4. Displacement Controlled Loading – (NW-NS-DSF) – Ductility One to Four

Displacement Controlled - Test Pictures – (NW-NS-DSF)

Disp. Ductiliy (6)	Face (North - East)

a)

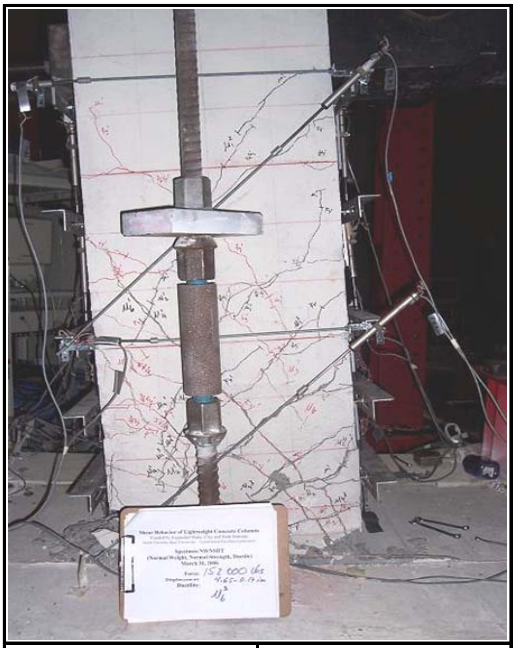

Disp. Ductiliy (6/c3)	Face (East)

b)

Disp. Ductiliy (8)	Face (North - East)

c)

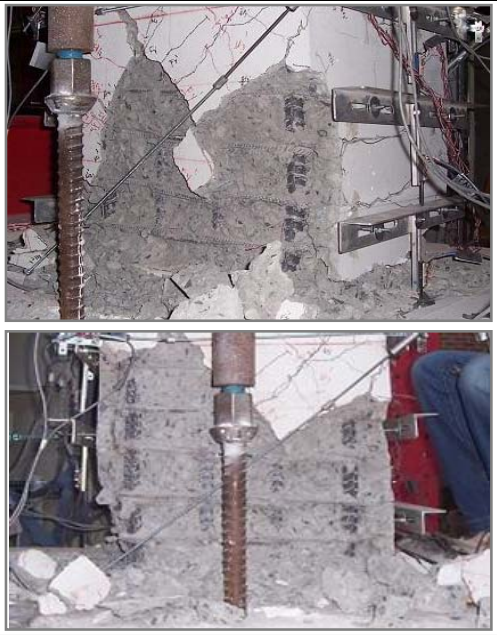

Disp. Ductiliy (8/c3)	Face (East)

d)

Figure 6.5. Displacement Controlled Loading – (NW-NS-DSF) – Ductility Six to Failure

6.2. Lightweight Concrete Type One – Normal Strength - Ductile Shear Failure Test (LW1-NS-DSF)

A ductile shear failure specimen made of lightweight concrete (LW1-NS-DSF) was tested under the same criteria applied for specimen (NW-NS-DSF). The procedure was the same as described in section 5.1. Similarly, the test setup was also the same as well as the loading procedure, the equipment, and instrumentation used for test (NW-NS-DSF). In brief, the specimen test discussed in this section was made of the same lightweight aggregate and normal strength concrete mixture as specimen (LW1-NS-BSF).

6.2.1 Loading History

Loading of the specimen consisted of two procedures to apply a constant axial and a cyclic lateral load, force controlled and displacement controlled loading. Figure 6.6 shows the force controlled loading history that corresponds to the initial four cycles. In fact, one cycle was applied at each level of lateral load from zero to first yielding. Afterwards, during displacement controlled loading, three cycles were applied at each level of deformation. Indeed, applying various cycles at the same level of deformation, stiffness degradation was observed (see Figure 6.6). Finally, Figure 6.7 shows the displacement controlled loading history of the test.

In addition, it is important to notice that due to the limitation in the maximum capacity of the actuator in the pulling direction (150 kips), the displacement controlled loading was

successfully applied in the pushing direction only (see Figure 6.7). This applies for tests (LW1-NS-DSF) and (NW-NS-DSF).

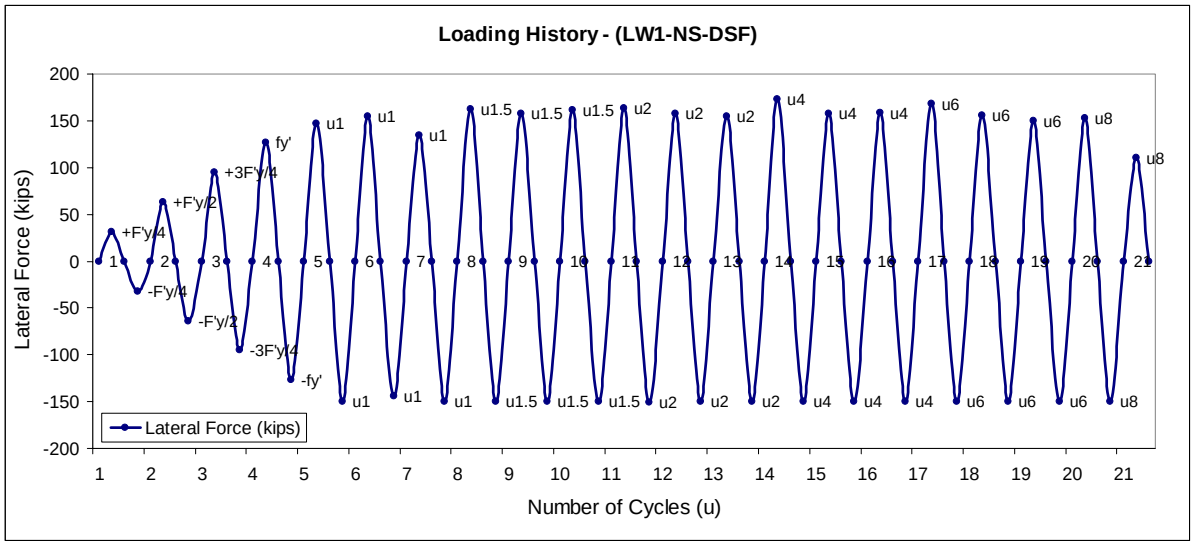

Figure 6.6. Load History (LW1-NS-DSF) Specimen

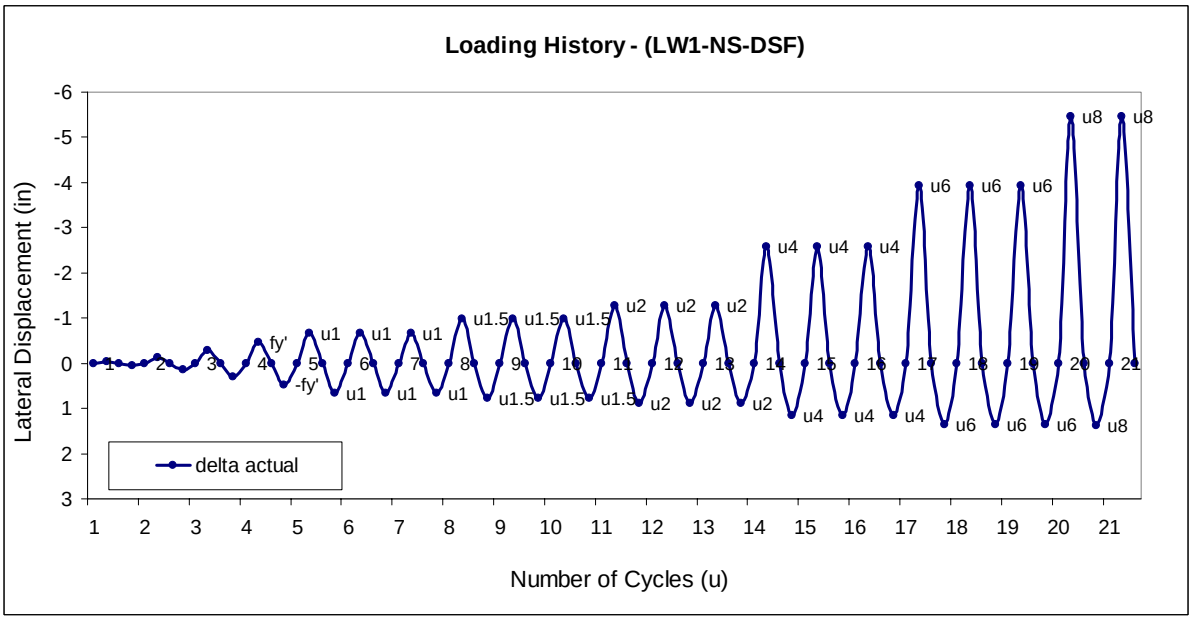

Figure 6.7. Displacement History (LW1-NS-DSF) Specimen

6.2.2 Relevant Observations

Relevant observations of test (LW1-NS-DSF) are presented in this section following the same format used for all tests. Data focusing on shear and displacement capacity, level of damage, cracks location, orientation, spacing, and width, are presented in this section. Furthermore, there is information contained matrices considering various levels of lateral force and displacement. Observations about test (LW1-NS-DSF) regarding displacement controlled loading, apply only for the pushing direction.

6.2.2.1 Force Controlled

Horizontal flexural cracks were observed on the tension sides (N & S) at low levels of lateral load (Fy'/4 & Fy'/2) as described in Table 6.6. With the increasing lateral load, the above mentioned flexural cracks started to propagate to faces (E & W). Moreover, the spacing between flexural cracks at (Fy') was between 3 to 4 inches along the first two feet from the column base, and between 5 to 7 inches along the next two feet. The orientation of the cracks was initially horizontal close to faces (N & S) as shown in Figure 6.8 (a & b) for lateral load levels (Fy'/4 & Fy'/2). Afterwards, cracks on faces (E & W) propagated significantly covering 75% of the face at (Fy') lateral force. Similar propagation values were observed in test (NW-NS-DSF) and also in all brittle shear failure tests. The spacing between cracks in faces (E & W) was not uniformly distributed and varied from 3 to 6 inches at (3Fy'/4 & Fy'). As also observed during test (NW-NS-DSF), a few new shear only cracks started to appear early at a lateral load level of (Fy'/2) as described in Table 6.6.

The actual top displacement at (Fy') was 0.47 inches, 12% lower than the top displacement of test (NW-NS-DSF). In the same manner, no vertical splitting of the concrete along the longitudinal reinforcement of the column was observed in this test during force controlled loading. Finally, no significant damage of the column was observed during force controlled loading.

6.2.2.2 Displacement Controlled

The same procedure described in section 5.1.2.2 was followed during displacement controlled loading from displacement ductility ($\mu_\Delta 1$) up to ($\mu_\Delta 8$). In the same manner, three cycles were applied at different levels of deformation considering top displacements of 0.66 inches for ($\mu_\Delta 1$), 0.98 inches for ($\mu_\Delta 1.5$), 1.32 inches for ($\mu_\Delta 2$), 2.63 inches for ($\mu_\Delta 4$), 3.95 inches for ($\mu_\Delta 6$), and 5.26 inches for ($\mu_\Delta 8$). As expected, the specimen failed at a high level of deformation when reaching a top displacement eight times greater than the equivalent yielding displacement.

The maximum actual shear capacity of the specimen was 173 kips reached at a displacement ductility of ($\mu_\Delta 4$) as shown in Table 6.8. In fact, the specimen continued resisting the shear force with a positive stiffness beyond the yielding point up to ($\mu_\Delta 4$) compared to ($\mu_\Delta 6$) observed in test (NW-NS-DSF). In brief, shear capacity of tests (LW1-NS-DSF) was very similar and consistent with that of test (NW-NS-DSF). The maximum variation of the axial load during the test was in the range of plus or minus twenty five percent. Furthermore, during displacement controlled loading the average spacing between flexural cracks in (N &

S) faces was between 2 to 3 inches along the first two feet from the column base, and between 5 to 6 inches along the next two feet. Furthermore, spacing between shear cracks on the middle of (E & W) faces continued getting shorter with values between 1 to 2 inches along the first two feet from the column base, and between 2 to 4 inches along the next two feet.

Additionally, a well defined shear crack on west (W) face was observed during the second cycle of displacement ductility ($\mu_\Delta 6$), and the angle from the vertical axis was approximately 36.00 degrees as shown in Figure 6.10 (b). In contrast to what was observed in test (NW-NS-DSF) during displacement controlled loading, some new flexural cracks were observed at the bottom of faces (N & S) for levels of deformation ($\mu_\Delta 1$ & 2). New shear only cracks were also observed during displacement controlled loading.

Regarding damage of the specimen during the test, minor spalling of the concrete cover started during displacement ductility ($\mu_\Delta 1.5$) at the bottom of faces (N & S). Also, at displacement ductility ($\mu_\Delta 6$), spalling of the concrete cover was observed in faces (E & W), and some reinforcement steel was exposed. Some crushing of the concrete was also observed at the bottom of faces (N & S) at a displacement ductility of ($\mu_\Delta 2$). In the same manner, crushing of the concrete became more evident towards ($\mu_\Delta 8$) as described in Table 6.8. Finally, it is also important to mention that most of the activity, in terms of deformation and damage, was concentrated towards the base of the column while in all brittle shear

failure tests it was located significantly higher. The intersection between the principal cracks on faces (E & W) was located approximately at 10 inches from the column base, and in a similar location as in test (NW-NS-DSF).

Table 6.6. Force Controlled Test Observation Matrix (LW1-NS-DSF)

	Force Controlled - Test Observation Matrix – (LW1-NS-DSF)			
Test Observation	**Fy'/4**	**Fy'/2**	**3Fy'/4**	**fy'**
Maximum lateral force (kips)	32.03	63.66	95.42	127.22
Axial load (kips)	94.21	95.81	100.99	106.57
Lateral displacement (in)	0.05	0.14	0.30	0.47
(N & S) Cracks location (Ih/Fh/s(s1-s2)) (in) [a]	0/22/7-8	(0/24/3-5) (24/45/57)	(0/24/3-5) (24/45/57)	(0/24/3-4) (24/45/57)
(N & S) Cracks orientation (Horizontal (H)/Vertical (V)/Both (B))	H	H	H	H
(E & W) Cracks location (Ih/Fh/s(s1-s2)) (in) [a]	0/40/6-8	0/42/4-6	0/42/3-6	0/48/2-4
(E & W) Average crack slope and location (Slope/L(%)/Hcs) [b]	90/10	70/35/14	40-60/50/24	40-60/50/24
(E & W) Face crack propagation (Total-P(%)/Rel.-Length(r1-r2)) [c]	10/2	50/5-10	70/5-8	75/3-5
New flexural cracks (Yes/No)	Yes	Yes	Yes	Yes
New shear cracks only (L(%)/Length/Height location) [d]	-	25/2/23	(35/8/27) (20/3/38)	(35/6/34) (35/8/43)
(N & S) Crack width (in/mm)	-	0.005/0.15	-	-
(E & W) Crack width (in/mm)	-	0.005/0.15	-	0.007/0.20
Spalling of concrete cover (Location-Face/Damaged Height (in))	-	-	-	-
Crushing of concrete (Location-Face/Damaged Depth(in))	-	-	-	-
Exposure of reinforcement steel (Location-Face/Height (in))	-	-	-	-
Buckling of longitudinal reinforcement (Location)	-	-	-	-

[a] (Initial height from the column base (in) /Final height form the column base (in) / Average values of spacing between cracks (in))
[b] (Crack slope from vertical line / Location in east or west faces from tension face north or south, e.g., 50% as the middle of east or west faces / Height of the crack slope (in))
[c] (Maximum total crack propagation percentage in east or west faces from tension face north or south, e.g., 50% as half of east or west faces covered with cracks / Values of relative crack length propagation (in))
[d] (Location in east or west faces from tension face north or south, e.g., 50% as the middle of east or west faces / Shear only crack length (in) / Height at the middle of the crack in east or west planes (in))

Table 6.7. Displacement Controlled Test Observation Matrix (LW1-NS-DSF) – Ductility One to Two

	Displacement Controlled - Test Observation Matrix – (LW1-NS-DSF)		
Test Observation	**Displacement Ductiliy (1)**	**Displacement Ductiliy (1.5)**	**Displacement Ductiliy (2)**
Maximum lateral force (kips)	150.43	167.39	170.71
Axial load (kips)	114.70	115.31	125.63
Lateral displacement (in)	0.66	0.99	1.32
(N & S) Cracks location (Ih/Fh/s(s1-s2)) (in) [a]	(0/24/3-4) (24/45/5-7)	(0/24/3-4) (24/45/5-7)	(0/24/2-4) (24/45/5)
(N & S) Cracks orientation (Horizontal (H)/Vertical (V)/Both (B))	H	H	H
(E & W) Cracks location (Ih/Fh/s(s1-s2)) (in) [a]	(0/48/3-4)	(0/48/3-4)	(0/48/2-4)
(E & W) Average crack slope and location (Slope/L(%)/Hcs) [b]	40-60/50/24	40-60/50/24	(60/50/5) (45/50/22) (35/50/34)
(E & W) Face crack propagation (Total-P(%)/Rel.-Length(r1-r2)) [c]	80/3-10	85/1.5-2	88/2-3
New flexural cracks (Yes/No)	Yes	No	Yes
New shear cracks only (L(%)/Length/Height location) [d]	(75/5/12) (40/3/8) (35/8/40)	(30/4/15)	(20/3/50)
(N & S) Crack width (in/mm)	-	0.035/0.90	0.06/1.50
(E & W) Crack width (in/mm)	0.009/0.25	0.025/0.60	0.04/1.00
Spalling of concrete cover (Location-Face/Damaged Height (in))	-	Base-(N&S)/-	Base-(N&S)/0-8
Crushing of concrete (Location-Face/Damaged Depth(in))	-	-	Base-(N&S)/<1
Exposure of reinforcement steel (Location-Face/Height (in))	-	-	-
Buckling of longitudinal reinforcement (Location)	-	-	-

[a] (Initial height from the column base (in) /Final height form the column base (in) / Average values of spacing between cracks (in))
[b] (Crack slope from vertical line / Location in east or west faces from tension face north or south, e.g., 50% as the middle of east or west faces / Height of the crack slope (in))
[c] (Maximum total crack propagation percentage in east or west faces from tension face north or south, e.g., 50% as half of east or west faces covered with cracks / Values of relative crack length propagation (in))
[d] (Location in east or west faces from tension face north or south, e.g., 50% as the middle of east or west faces / Shear only crack length (in) / Height at the middle of the crack in east or west planes (in))

Table 6.8. Displacement Controlled Test Observation Matrix (LW1-NS-DSF) – Ductility Four to Failure

	Displacement Controlled - Test Observation Matrix – (LW1-NS-DSF)		
Test Observation	**Displacement Ductiliy (4)**	**Displacement Ductiliy (6)**	**Displacement Ductiliy (8)**
Maximum lateral force (kips)	173.22	166.27	157.62
Axial load (kips)	116.96	108.39	103.88
Lateral displacement (in)	2.63	3.95	5.26
(N & S) Cracks location (Ih/Fh/s(s1-s2)) (in) [a]	(0/24/2.75) (24/45/5-6)	(0/24/2.75) (24/45/5-6)	(0/24/2.75) (24/45/5-6)
(N & S) Cracks orientation (Horizontal (H)/Vertical (V)/Both (B))	B	B	B
(E & W) Cracks location (Ih/Fh/s(s1-s2)) (in) [a]	0/50/1-2.5	(0/24/1-2) (24-48/2-4)	(0/24/1-2) (24-48/2-4)
(E & W) Average crack slope and location (Slope/L(%)/Hcs) [b]	(60/50/5) (45/50/22) (35/50/34)	36/50/10	36/50/10
(E & W) Face crack propagation (Total-P(%)/Rel.-Length(r1-r2)) [c]	90/1	100/<1	100/-
New flexural cracks (Yes/No)	Yes	No	No
New shear cracks only (L(%)/Length/Height location) [d]	-	-	-
(N & S) Crack width (in/mm)	0.08/2.00	-	-
(E & W) Crack width (in/mm)	0.06/1.50	0.16/4.00	-
Spalling of concrete cover (Location-Face/Damaged Height (in))	Base-(N&S)/0-10	(Base-(N&S)/12)	(Base-(N&S)/15) (Center-(E&W)/0-24)
Crushing of concrete (Location-Face/Damaged Depth(in))	Base-(N&S)/2.5	Base-(N&S)/-	Base-(N&S)/-
Exposure of reinforcement steel (Location-Face/Height (in))	-	-	Center-(E&W)/0-24
Buckling of longitudinal reinforcement (Location)	-	-	Base-(N&S)

[a] (Initial height from the column base (in) /Final height form the column base (in) / Average values of spacing between cracks (in))
[b] (Crack slope from vertical line / Location in east or west faces from tension face north or south, e.g., 50% as the middle of east or west faces / Height of the crack slope (in))
[c] (Maximum total crack propagation percentage in east or west faces from tension face north or south, e.g., 50% as half of east or west faces covered with cracks / Values of relative crack length propagation (in))
[d] (Location in east or west faces from tension face north or south, e.g., 50% as the middle of east or west faces / Shear only crack length (in) / Height at the middle of the crack in east or west planes (in))

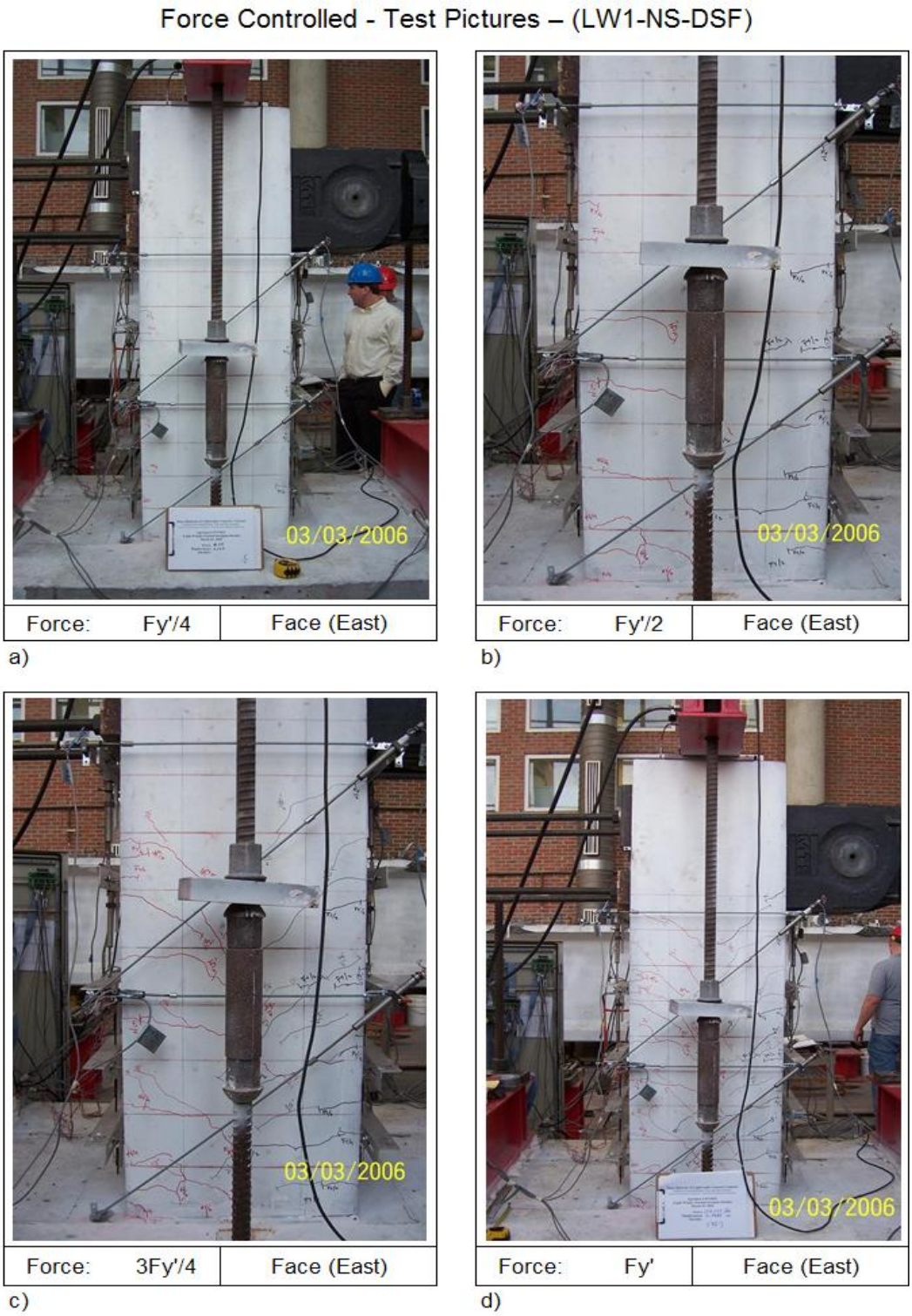

Figure 6.8. Force Controlled Loading – (LW1-NS-DSF)

Figure 6.9. Displacement Controlled Loading – (LW1-NS-DSF) – Ductility One to Four

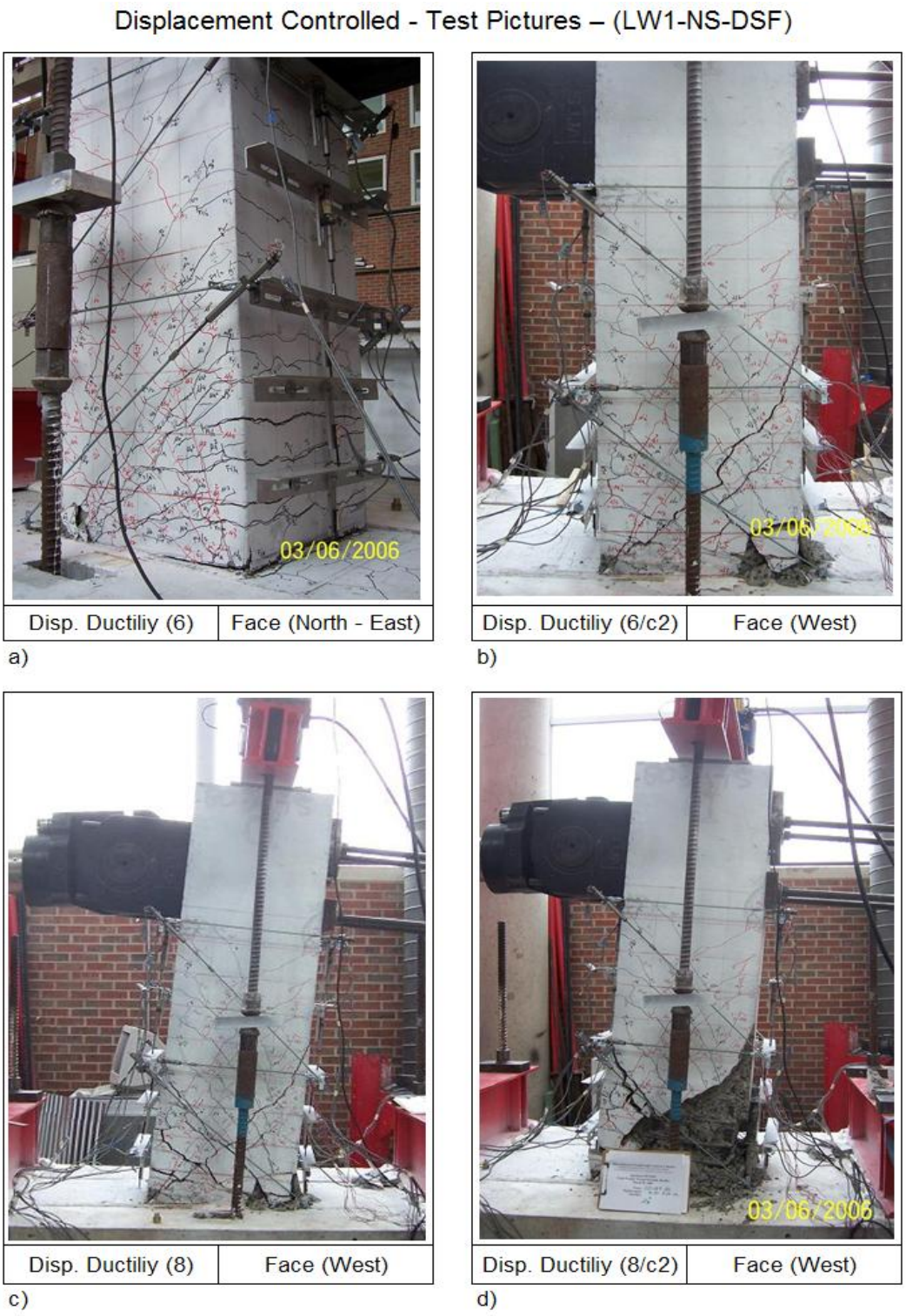

Figure 6.10. Displacement Controlled Loading – (LW1-NS-DSF) – Ductility Six to Failure

6.3. Lightweight Concrete Type Two – Normal Strength - Ductile Shear Failure Test (LW2-NS-DSF)

A ductile shear failure specimen made of lightweight concrete type two (LW2-NS-DSF) was tested under the same criteria described in section 5.1. Similarly, the test setup was also the same as well as the loading procedure, the equipment, and instrumentation used for all ductile and brittle shear failure tests. The only difference between test (LW2-NS-DSF) and tests (NW-NS-DSF) and (LW1-NS-DSF) was the capacity of the actuator. In fact, the actuator was changed with one of higher capacity in the pulling direction (300 kips) in order to apply the cyclic lateral load in both directions during displacement controlled loading. In brief, the specimen test discussed in this section was made of the same lightweight aggregate and normal strength concrete mixture as specimen (LW2-NS-BSF).

6.3.1 Loading History

As for all tests, loading of the specimen consisted of force controlled and displacement controlled loading. Figure 6.11, shows the load history of the entire test. In fact, force controlled loading corresponds to the initial four cycles, and displacement controlled loading to the remaining cycles. Indeed, one cycle was applied at each level of lateral load from zero to first yielding during force controlled loading while for displacement controlled loading, three cycles were applied at each level of deformation. Stiffness degradation was observed during displacement controlled loading as a way to determine how ductile the behavior of the specimen was. Figure 6.12 shows the displacement history of the test. Finally, it is

important to notice that after changing the actuator for one with higher capacity in the pulling direction (300 kips), the displacement controlled loading was successfully applied in the pushing and pulling directions as shown in Figure 6.12. This applies for tests (LW2-NS-DSF) and (LW3-NS-DSF).

It is important to mention that in this particular test, during displacement controlled loading, and specifically during displacement ductility ($\mu_\Delta 1$ & 1.5), the footing of the specimen slid about one inch. Apparently, the problem was caused by losses in the prestressed bars at the supports where the footing was anchored to the floor. Apparently, the layer of hydro-stone in this specific case was thicker than in all previous tests, and because of that, it took more time for the material to reach the necessary strength before applying the prestressing force at the supports. The hydro-stone might have been compressed during the test releasing some prestressing force. Despite the above mentioned undesired event, the problem was solved immediately before continuing. Measurements and notes were taken, the supports were prestressed once again, and the test continued without presenting the same problem again. However, it is important to notice that the reduction in the lateral force during displacement ductility ($\mu_\Delta 1$ & 1.5) as shown in Figure 6.11, was not caused by any strength degradation, but due to the above mentioned particular situation.

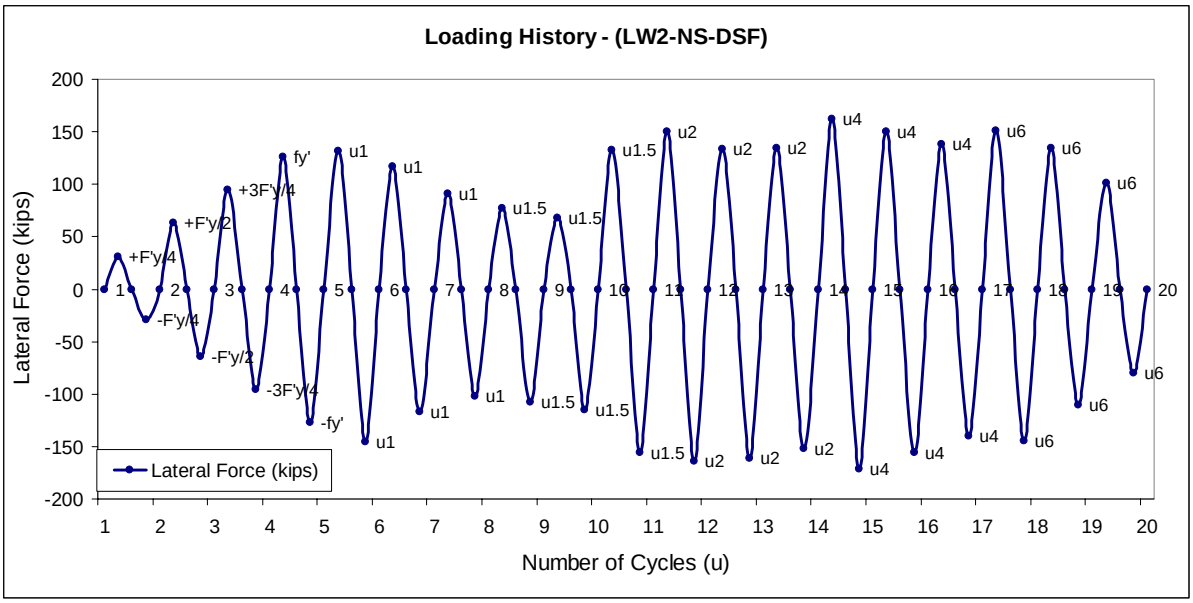

Figure 6.11. Load History (LW2-NS-DSF) Specimen

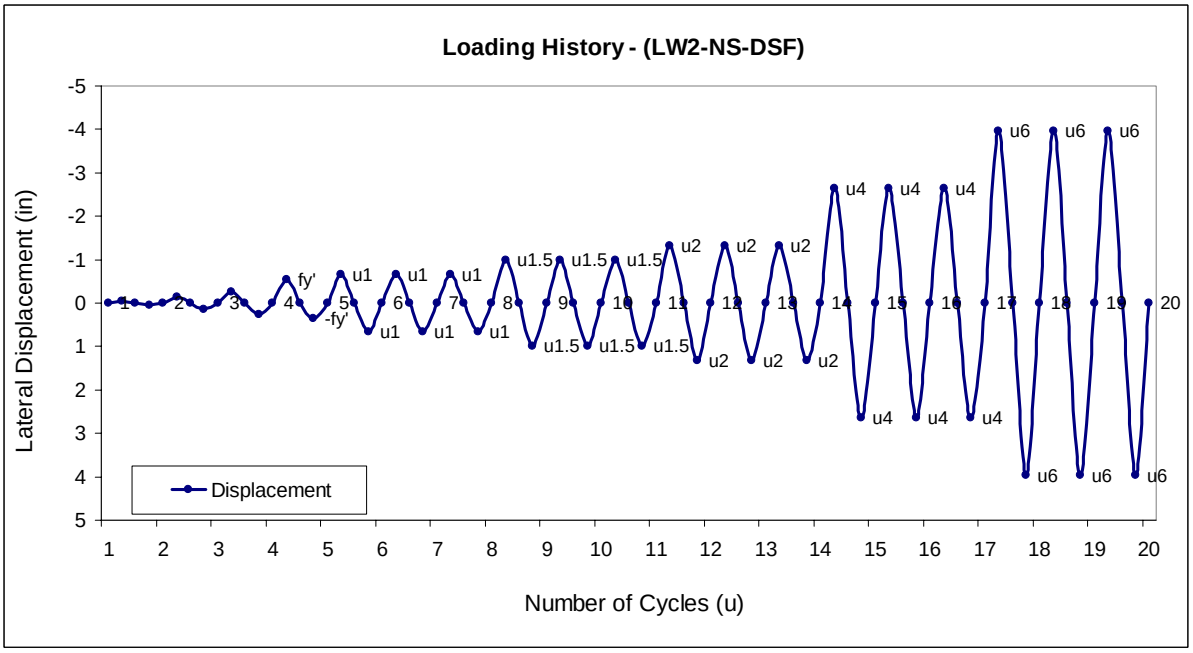

Figure 6.12. Displacement History (LW2-NS-DSF) Specimen

6.3.2 Relevant Observations

Relevant observations of test (LW2-NS-DSF) are presented in this section following the same format used for all tests. Comments on aspects related to shear and displacement capacity, level of damage, cracks location, orientation, spacing, and width, and other relevant test observations are presented in this section. Furthermore, there is information contained in matrices related to various levels of lateral force and displacement.

6.3.2.1 Force Controlled

The initial cracks appeared when the specimen was subjected to low levels of lateral load (Fy'/4 & Fy'/2). Flexural cracks were observed on the tension sides (N & S) of the column as described in Table 6.9. The above mentioned flexural cracks gradually propagated to faces (E & W) as the lateral load was increased. Furthermore, between 6 to 7 inches was the spacing between flexural cracks at (Fy'). For lateral load levels (Fy'/4 & Fy'/2), the orientation of the cracks was close to be horizontal when closer to faces (N & S) as shown in Figure 6.13 (a & b). For subsequent cycles, cracks on faces (E & W) propagated significantly covering 75% of the face surface at (Fy') lateral load. Similar propagation values were observed in tests (NW-NS-DSF) and (LW1-NS-DSF). The spacing between cracks in faces (E & W) varied from 3 to 6 inches at (Fy'). Finally, shear only cracks started to appear at a lateral load level of (3Fy'/4) as described in Table 6.9.

The actual top displacement at (Fy') was 0.47 inches, 12% lower than the top displacement of test (NW-NS-DSF), and very similar to that of test (LW1-NS-DSF). In the same manner,

no vertical splitting of the concrete along the longitudinal reinforcement of the column in faces (N & S) was observed during force controlled loading. Finally, no significant damage of the column was observed during force controlled loading.

6.3.2.2 Displacement Controlled

The same procedure described in section 5.1.2.2 was followed during displacement controlled loading from displacement ductility ($\mu_\Delta 1$) up to ($\mu_\Delta 6$). In the same manner, three cycles were applied at different levels of deformation considering top displacements of 0.66 inches for ($\mu_\Delta 1$), 1.00 inches for ($\mu_\Delta 1.5$), 1.32 inches for ($\mu_\Delta 2$), 2.64 inches for ($\mu_\Delta 4$), and 3.96 inches for ($\mu_\Delta 6$). As expected, the specimen failed at a high level of deformation corresponding to displacement ductility ($\mu_\Delta 6$).

The maximum actual shear capacity of the specimen was 172 kips reached at displacement ductility levels of ($\mu_\Delta 2$ & 4) as shown in Table 6.10 and Table 6.11. The response of the specimen did not develop a positive stiffness beyond displacement ductility ($\mu_\Delta 2$) compared to specimens (NW-NS-DSF) and (LW1-NS-DSF) where positive stiffness beyond yielding were observed up to ($\mu_\Delta 8$) and ($\mu_\Delta 6$) respectively. In any case, the maximum shear capacity of specimen (LW2-NS-DSF) was very similar to that of specimens (NW-NS-DSF) and (LW1-NS-DSF). The maximum variation of the axial load during the test was in the range of plus or minus thirty percent. In addition, between 4 to 7 inches was the average spacing between flexural cracks in (N & S) faces during displacement controlled loading.

Furthermore, spacing between shear cracks on the middle of (E & W) faces continued getting shorter with values between 1.5 to 3 inches along the first two feet from the column base, and between 2.5 to 5 inches along the next two feet. Finally, as observed during test (NW-NS-DSF) during displacement controlled loading, almost no new flexural cracks were observed on faces (N & S). However, new shear only cracks were observed during displacement controlled loading.

In relation to damage of the specimen observed during the test, minor spalling of the concrete cover started during displacement ductility ($\mu_\Delta 1.5$) at the bottom of faces (N & S). Moreover, at displacement ductility ($\mu_\Delta 6$) spalling of the concrete cover was observed in faces (E & W), and some reinforcement steel bars were exposed. Some minor crushing of the concrete was also observed at the bottom of faces (N & S) at a displacement ductility of ($\mu_\Delta 1.5$). In the same manner, crushing of the concrete became more evident towards ($\mu_\Delta 6$) as described in Table 6.11. Finally, it is also important to mention that the location of most of the activity in terms of deformation and damage was concentrated close to the base of the column while it was located significantly higher in all brittle shear failure tests. The intersection between the principal cracks on faces (E & W) was located approximately at 10 inches from the column base, and in a similar location as in tests (NW-NS-DSF) and (LW1-NS-DSF). Finally, after the test, shear cracks were also observed in the connection between the column and the principal footing beam revealing the effect of considerable shear deformation as well as strain penetration of the longitudinal column reinforcement in the

footing. The same effect was observed in all ductile shear failure tests as shown in Figure 6.15 (d).

Table 6.9. Force Controlled Test Observation Matrix (LW2-NS-DSF)

	Force Controlled - Test Observation Matrix – (LW2-NS-DSF)			
Test Observation	**Fy'/4**	**Fy'/2**	**3Fy'/4**	**fy'**
Maximum lateral force (kips)	30.85	64.03	95.63	127.32
Axial load (kips)	89.97	88.46	86.34	90.99
Lateral displacement (in)	0.05	0.13	0.24	0.47
(N & S) Cracks location (Ih/Fh/s(s1-s2)) (in) [a]	0/22/8	0/35/7-8	0/35/7	0/45/6-7
(N & S) Cracks orientation (Horizontal (H)/Vertical (V)/Both (B))	H	H	H	B
(E & W) Cracks location (Ih/Fh/s(s1-s2)) (in) [a]	0/22/7-10	0/35/7	0/40/5-9	0/45/3-6
(E & W) Average crack slope and location (Slope/L(%)/Hcs) [b]	90/25/-	40-50/50/-	(40-50/50/-)	(30/50/36) (60/50/11)
(E & W) Face crack propagation (Total-P(%)/Rel.-Length(r1-r2)) [c]	25/5	60/7-10	70/5-7	75/3-7
New flexural cracks (Yes/No)	Yes	Yes	Yes	Yes
New shear cracks only (L(%)/Length/Height location) [d]	-	-	(15/6/3) (50/7/24)	(62/4/4) (25/15/45)
(N & S) Crack width (in/mm)	-	0.005/0.15	0.016/0.40	0.02/0.50
(E & W) Crack width (in/mm)	-	-	0.005/0.15	0.009/0.25
Spalling of concrete cover (Location-Face/Damaged Height (in))	-	-	-	-
Crushing of concrete (Location-Face/Damaged Depth(in))	-	-	-	-
Exposure of reinforcement steel (Location-Face/Height (in))	-	-	-	-
Buckling of longitudinal reinforcement (Location)	-	-	-	-

[a] (Initial height from the column base (in) /Final height form the column base (in) / Average values of spacing between cracks (in))
[b] (Crack slope from vertical line / Location in east or west faces from tension face north or south, e.g., 50% as the middle of east or west faces / Height of the crack slope (in))
[c] (Maximum total crack propagation percentage in east or west faces from tension face north or south, e.g., 50% as half of east or west faces covered with cracks / Values of relative crack length propagation (in))
[d] (Location in east or west faces from tension face north or south, e.g., 50% as the middle of east or west faces / Shear only crack length (in) / Height at the middle of the crack in east or west planes (in))

Table 6.10. Displacement Controlled Test Observation Matrix (LW2-NS-DSF) – Ductility One to Two

	Displacement Controlled - Test Observation Matrix – (LW2-NS-DSF)		
Test Observation	**Displacement Ductiliy (1)**	**Displacement Ductiliy (1.5)**	**Displacement Ductiliy (2)**
Maximum lateral force (kips)	151.06	157.49	172.48
Axial load (kips)	87.57	102.41	108.10
Lateral displacement (in)	0.66	1.00	1.32
(N & S) Cracks location (Ih/Fh/s(s1-s2)) (in) [a]	0/45/6-7	0/45/6-7	0/45/4-7
(N & S) Cracks orientation (Horizontal (H)/Vertical (V)/Both (B))	H	B	B
(E & W) Cracks location (Ih/Fh/s(s1-s2)) (in) [a]	0/45/3-5	0/45/3-5	(0/24/2-3) (24/48/3-5)
(E & W) Average crack slope and location (Slope/L(%)/Hcs) [b]	(30/50/36) (60/50/11)	(30/50/36) (60/50/11)	(35/50/14)
(E & W) Face crack propagation (Total-P(%)/Rel.-Length(r1-r2)) [c]	78/1.5-2	85/-	100/2-4
New flexural cracks (Yes/No)	No	No	Yes
New shear cracks only (L(%)/Length/Height location) [d]	(70/4/28) (20/2/42)	-	25/7/7.5
(N & S) Crack width (in/mm)	0.02/0.50	0.025/0.60	0.05/1.25
(E & W) Crack width (in/mm)	0.009/0.25	0.010/0.30	0.020/0.50
Spalling of concrete cover (Location-Face/Damaged Height (in))	-	Base-(N&S)/3	Base-(N&S)/0-5
Crushing of concrete (Location-Face/Damaged Depth(in))	-	Base-(N&S)/<1	Base-(N&S)/2
Exposure of reinforcement steel (Location-Face/Height (in))	-	-	-
Buckling of longitudinal reinforcement (Location)	-	-	-

[a] (Initial height from the column base (in) /Final height form the column base (in) / Average values of spacing between cracks (in))
[b] (Crack slope from vertical line / Location in east or west faces from tension face north or south, e.g., 50% as the middle of east or west faces / Height of the crack slope (in))
[c] (Maximum total crack propagation percentage in east or west faces from tension face north or south, e.g., 50% as half of east or west faces covered with cracks / Values of relative crack length propagation (in))
[d] (Location in east or west faces from tension face north or south, e.g., 50% as the middle of east or west faces / Shear only crack length (in) / Height at the middle of the crack in east or west planes (in))

Table 6.11. Displacement Controlled Test Observation Matrix (LW2-NS-DSF) – Ductility Four to Failure

	Displacement Controlled - Test Observation Matrix – (LW2-NS-DSF)		
Test Observation	**Displacement Ductiliy (4)**	**Displacement Ductiliy (6)**	**Displacement Ductiliy (8)**
Maximum lateral force (kips)	172.13	152.10	
Axial load (kips)	126.51	112.62	
Lateral displacement (in)	2.64	3.96	
(N & S) Cracks location (Ih/Fh/s(s1-s2)) (in) [a]	0/45/4-7	0/45/4-7	
(N & S) Cracks orientation (Horizontal (H)/Vertical (V)/Both (B))	B	B	
(E & W) Cracks location (Ih/Fh/s(s1-s2)) (in) [a]	(0/24/1.5-3) (24/48/2.5-5)	(0/24/1.5-3) (24/48/2.5-5)	
(E & W) Average crack slope and location (Slope/L(%)/Hcs) [b]	35/50/14	35/50/14	
(E & W) Face crack propagation (Total-P(%)/Rel.-Length(r1-r2)) [c]	100/2-5	100/<1	
New flexural cracks (Yes/No)	No	No	
New shear cracks only (L(%)/Length/Height location) [d]	50/3/9.5	-	
(N & S) Crack width (in/mm)	0.16/4.00	-	
(E & W) Crack width (in/mm)	0.06/1.5	0.16/4.00	
Spalling of concrete cover (Location-Face/Damaged Height (in))	Base-(N&S)/5-10	(Base-(N&S)/5-10) (Center-(E&W)/0-20)	
Crushing of concrete (Location-Face/Damaged Depth(in))	Base-(N&S)/3	Base-(N&S)/-	
Exposure of reinforcement steel (Location-Face/Height (in))	-	(Center-(E&W)/0-20) (Base-(E&W)/5-10)	
Buckling of longitudinal reinforcement (Location)	-	-	

[a] (Initial height from the column base (in) /Final height form the column base (in) / Average values of spacing between cracks (in))
[b] (Crack slope from vertical line / Location in east or west faces from tension face north or south, e.g., 50% as the middle of east or west faces / Height of the crack slope (in))
[c] (Maximum total crack propagation percentage in east or west faces from tension face north or south, e.g., 50% as half of east or west faces covered with cracks / Values of relative crack length propagation (in))
[d] (Location in east or west faces from tension face north or south, e.g., 50% as the middle of east or west faces / Shear only crack length (in) / Height at the middle of the crack in east or west planes (in))

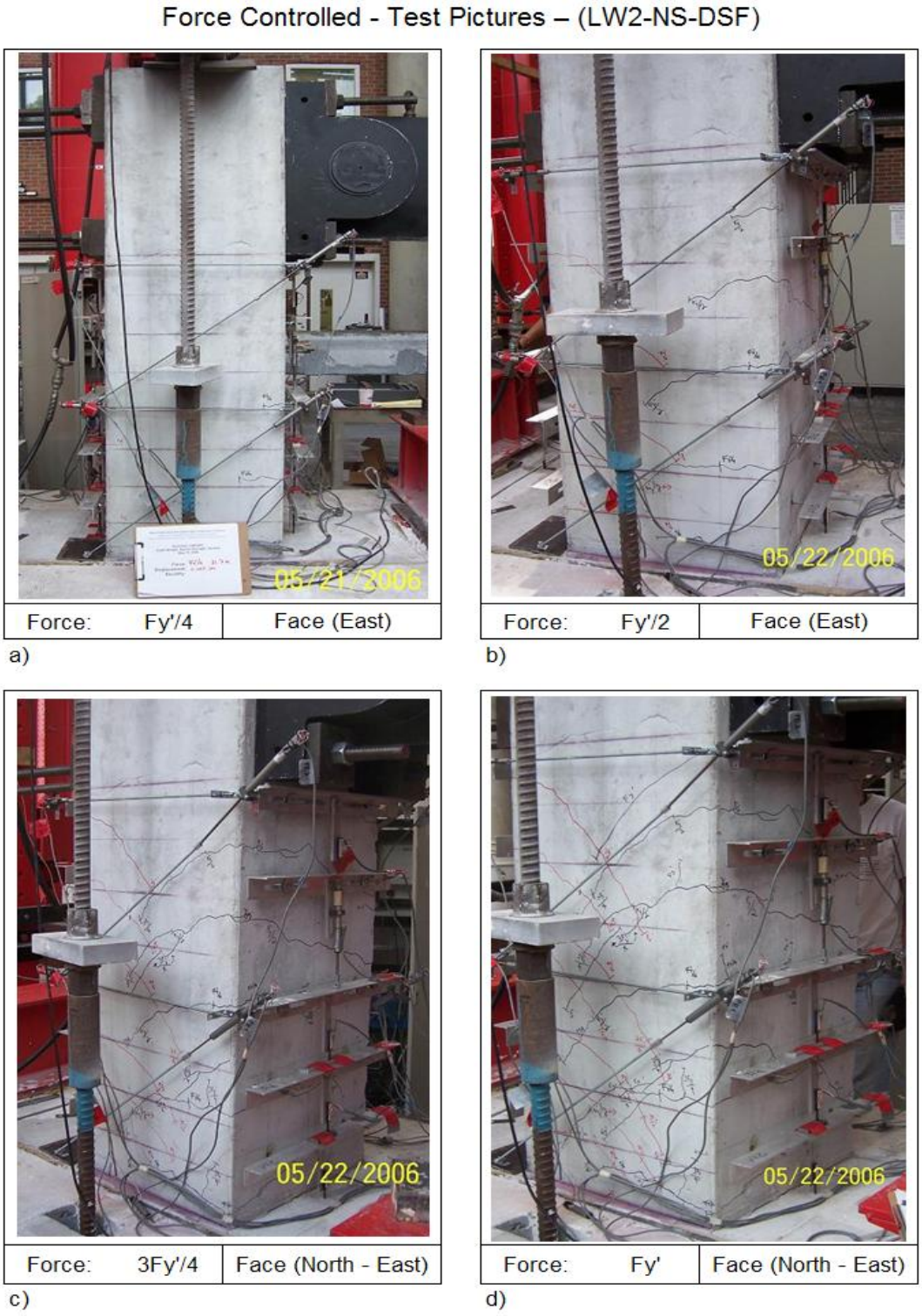

Figure 6.13. Force Controlled Loading – (LW2-NS-DSF)

Displacement Controlled - Test Pictures – (LW2-NS-DSF)

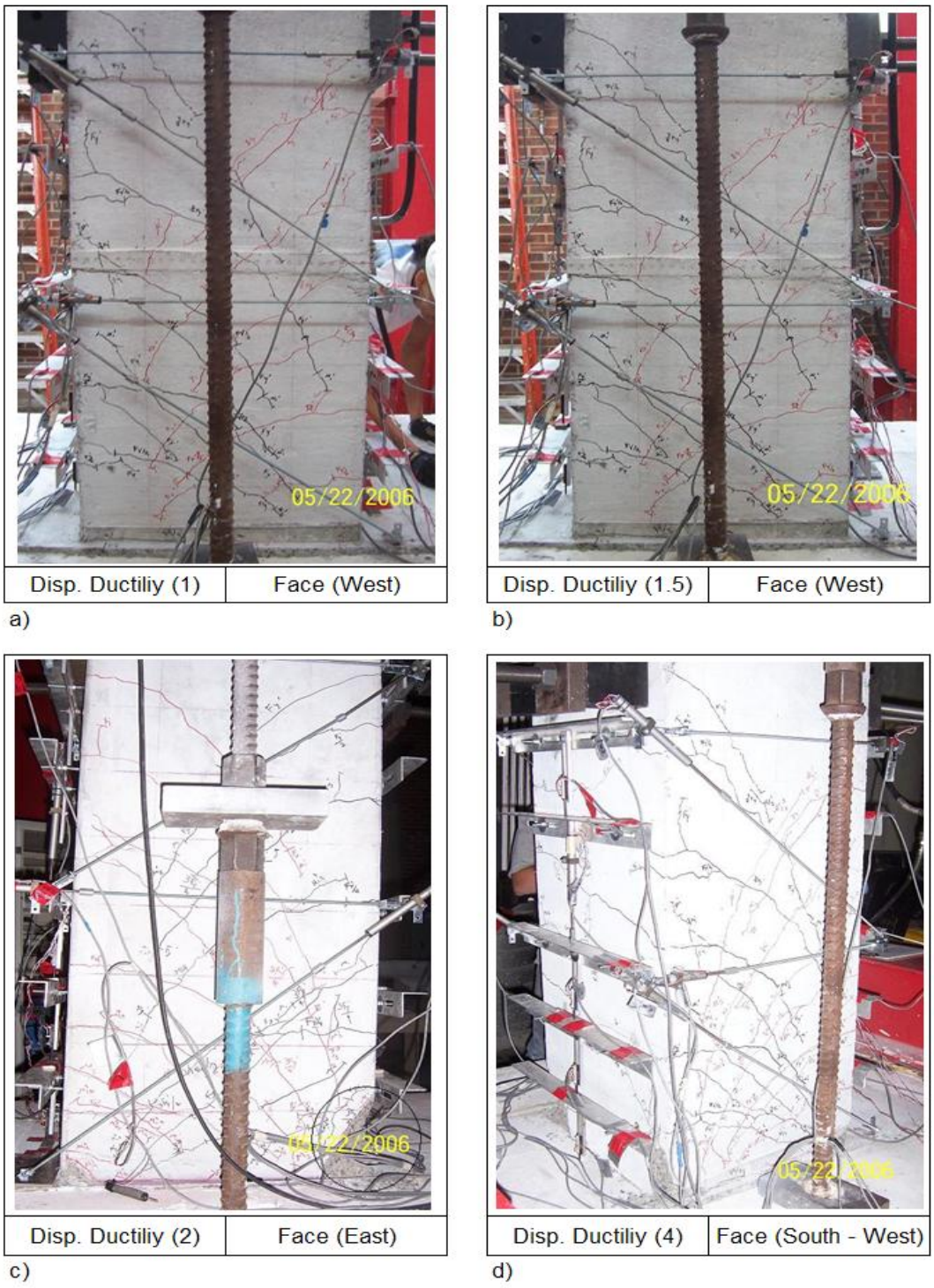

Figure 6.14. Displacement Controlled Loading – (LW2-NS-DSF) – Ductility One to Four

Figure 6.15. Displacement Controlled Loading – (LW2-NS-DSF) – Ductility Six to Failure

6.4. Lightweight Concrete Type Three – Normal Strength - Ductile Shear Failure Test (LW3-NS-DSF)

A ductile shear failure specimen made of lightweight concrete (LW3-NS-DSF) was tested under the same criteria described in section 5.1. Similarly, test setup, loading procedure, equipment, and instrumentation used were the same as that of all ductile and brittle shear failure tests. During displacement controlled loading, the cyclic lateral load was applied in both directions as in test (LW2-NS-DSF). In brief, the specimen test discussed in this section was made of the same lightweight aggregate and normal strength concrete mixture as specimen (LW3-NS-BSF).

6.4.1 Loading History

Loading of the specimen consisted of two procedures, force controlled and displacement controlled loading. Figure 6.16, shows the load history of the entire test. In fact, force controlled loading corresponds to the initial four cycles, and displacement controlled loading to the remaining cycles. Indeed, one cycle was applied at each level of lateral load from zero to first yielding during force controlled loading. For displacement controlled loading, three cycles were applied at each level of deformation. Stiffness degradation was observed during displacement controlled loading (see Figure 6.16). Finally, Figure 6.17 shows the entire displacement history of the test.

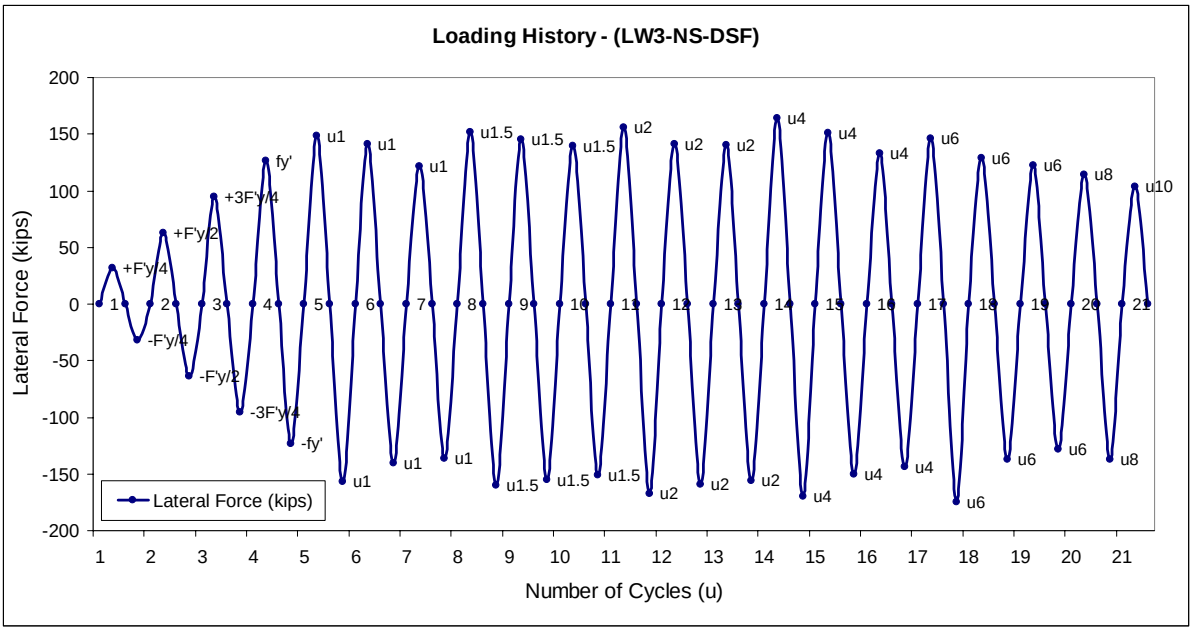

Figure 6.16. Load History (LW3-NS-DSF) Specimen

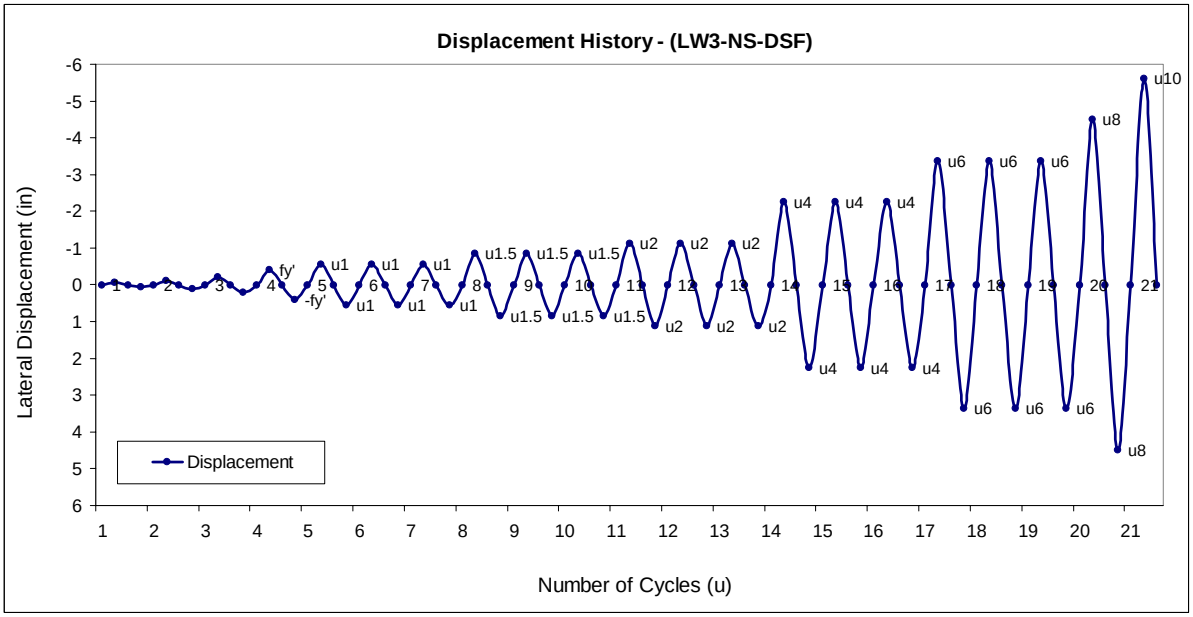

Figure 6.17. Displacement History (LW3-NS-DSF) Specimen

6.4.2 Relevant Observations

Following the same format as in all the tests, relevant observations of test (LW3-NS-DSF) are presented in this section. Aspects related to shear and displacement capacity, level of damage, cracks location, orientation, spacing, and width, and other relevant aspects are discussed this section. Furthermore, the information contained in the matrices considers various levels of lateral force and displacement.

6.4.2.1 Force Controlled

Initially, flexural cracks appeared when the specimen was subjected to low levels of lateral load (Fy'/4 & Fy'/2) on tension sides (N & S) as described in Table 6.12. In addition, Flexural cracks gradually propagated to faces (E & W) as the lateral load was increased as observed in all ductile shear failure tests. Moreover, between 6 to 7 inches was the spacing between flexural cracks at (Fy'). Similar values were observed in all ductile shear failure tests. Furthermore, for lateral load levels (Fy'/4 & Fy'/2), the orientation of the cracks was close to be horizontal when closer to faces (N & S) as shown in Figure 6.18 (a & b). For subsequent cycles, cracks on faces (E & W) propagated significantly covering 75% of the face surface at a lateral load of (Fy'). Similar propagation values were observed in all ductile shear failure tests. The spacing between cracks in faces (E & W) varied from 3 to 6 inches at (Fy').

The actual top displacement at (Fy') was 0.40 inches, 25% lower than the top displacement of test (NW-NS-DSF), and 15% lower than that of tests (LW1-NS-DSF) and (LW2-NS-

DSF). In the same manner, no vertical splitting of the concrete along the longitudinal reinforcement of the column was observed during force controlled loading. Finally, no significant damage of the column was observed during force controlled loading.

6.4.2.2 Displacement Controlled

The same procedure described in section 5.1.2.2 was followed during displacement controlled loading from displacement ductility ($\mu_\Delta 1$) to ($\mu_\Delta 6$). In the same manner, three cycles were applied at different levels of deformation considering top displacements of 0.56 inches for ($\mu_\Delta 1$), 0.84 inches for ($\mu_\Delta 1.5$), 1.12 inches for ($\mu_\Delta 2$), 2.24 inches for ($\mu_\Delta 4$), 3.37 inches for ($\mu_\Delta 6$), and 4.49 inches for ($\mu_\Delta 8$). As expected, the specimen failed at a high level of deformation corresponding to displacement ductility ($\mu_\Delta 8$).

The maximum shear capacity between all ductile shear failure specimens was very similar and consistent. In fact, the maximum actual shear capacity of specimen (LW3-NS-DSF) was 176 kips reached at a displacement ductility level of ($\mu_\Delta 6$) as shown in Table 6.14. The shear strength of the specimen continued increasing after yielding. Consequently, there was a positive stiffness beyond yielding up to displacement ductility ($\mu_\Delta 6$), and similar to specimens (NW-NS-DSF) and (LW1-NS-DSF) where positive stiffness beyond yielding were observed up to ($\mu_\Delta 8$) and ($\mu_\Delta 6$) respectively. The maximum variation of the axial load during the test was in the range of plus or minus twenty six percent. In addition, between 4 to 7 inches was the average spacing between flexural cracks in (N & S) faces during

displacement controlled loading. Furthermore, spacing between shear cracks on the middle of (E & W) faces continued getting shorter with values between 1 to 3 inches along the first two feet from the column base, and between 3 to 4 inches along the next two feet. Finally, as observed during tests (NW-NS-DSF) and (LW2-NS-DSF), almost no new flexural cracks were observed on faces (N & S) during displacement controlled loading. On the other hand, some new shear only cracks were observed during displacement controlled loading.

Damage of the specimen was observed during displacement controlled loading. First, minor spalling of the concrete cover started during displacement ductility (μ_Δ1.5) at the bottom of faces (N & S). Moreover, at displacement ductility (μ_Δ6), spalling of the concrete cover was observed in face (E), and some reinforcement steel bars were exposed. It is important to mention that some torsion of the column was observed at high levels of deformation. For that reason, more damage was observed in face east than west as shown in Figure 6.20 (b, c, & d). Crushing of the concrete was also observed at the bottom of faces (N & S), and started at a displacement ductility of (μ_Δ4) being more evident at (μ_Δ6 & 8) as described in Table 6.14. Finally, it is also important to mention that the location of most activity in terms of deformation and damage was concentrated close to the base of the column while it was located significantly higher in all brittle shear failure tests. The intersection between the principal cracks on faces (E & W) was located approximately between 10 to 15 inches from the column base, in a similar location as in tests (NW-NS-DSF), (LW1-NS-DSF), and (LW2-NS-DSF).

Table 6.12. Force Controlled Test Observation Matrix (LW3-NS-DSF)

	Force Controlled - Test Observation Matrix – (LW3-NS-DSF)			
Test Observation	**Fy'/4**	**Fy'/2**	**3Fy'/4**	**fy'**
Maximum lateral force (kips)	31.96	63.69	95.74	127.35
Axial load (kips)	91.06	95.61	96.53	97.53
Lateral displacement (in)	0.05	0.13	0.23	0.40
(N & S) Cracks location (Ih/Fh/s(s1-s2)) (in) [a]	0/7/7	0/31/7	0/31/6-7	0/40/6-7
(N & S) Cracks orientation (Horizontal (H)/Vertical (V)/Both (B))	H	H	H	B
(E & W) Cracks location (Ih/Fh/s(s1-s2)) (in) [a]	0/14/5-9	0/30/7	0/50/7	0/55/3-6
(E & W) Average crack slope and location (Slope/L(%)/Hcs) [b]	90/10/-	70/50/14	45/65/8	(30/50/25) (45/50/15)
(E & W) Face crack propagation (Total-P(%)/Rel.-Length(r1-r2)) [c]	10/2.5	50/8	70/3-5	75/2-5
New flexural cracks (Yes/No)	Yes	Yes	Yes	Yes
New shear cracks only (L(%)/Length/Height location) [d]	-	-	(10/3/33) (40/3/22)	-
(N & S) Crack width (in/mm)	-	-	-	-
(E & W) Crack width (in/mm)	-	-	0.01/0.30	0.016/0.40
Spalling of concrete cover (Location-Face/Damaged Height (in))	-	-	-	-
Crushing of concrete (Location-Face/Damaged Depth(in))	-	-	-	-
Exposure of reinforcement steel (Location-Face/Height (in))	-	-	-	-
Buckling of longitudinal reinforcement (Location)	-	-	-	-

[a] (Initial height from the column base (in) /Final height form the column base (in) / Average values of spacing between cracks (in))
[b] (Crack slope from vertical line / Location in east or west faces from tension face north or south, e.g., 50% as the middle of east or west faces / Height of the crack slope (in))
[c] (Maximum total crack propagation percentage in east or west faces from tension face north or south, e.g., 50% as half of east or west faces covered with cracks / Values of relative crack length propagation (in))
[d] (Location in east or west faces from tension face north or south, e.g., 50% as the middle of east or west faces / Shear only crack length (in) / Height at the middle of the crack in east or west planes (in))

Table 6.13. Displacement Controlled Test Observation Matrix (LW3-NS-DSF) – Ductility One to Two

	Displacement Controlled - Test Observation Matrix – (LW3-NS-DSF)		
Test Observation	**Displacement Ductiliy (1)**	**Displacement Ductiliy (1.5)**	**Displacement Ductiliy (2)**
Maximum lateral force (kips)	158.15	163.03	169.06
Axial load (kips)	102.90	105.83	114.43
Lateral displacement (in)	0.56	0.84	1.12
(N & S) Cracks location (Ih/Fh/s(s1-s2)) (in) [a]	0/40/6-7	0/40/6-7	0/40/5-7
(N & S) Cracks orientation (Horizontal (H)/Vertical (V)/Both (B))	B	B	B
(E & W) Cracks location (Ih/Fh/s(s1-s2)) (in) [a]	0/55/3-6	(0/55/1-4)W (0/45/3-5)E	(0/55/1-4)W (0/45/3-5)E
(E & W) Average crack slope and location (Slope/L(%)/Hcs) [b]	30-45/50/15-25	(30/50/-)W (45/50-)E	(30/50/-)W (45/50-)E
(E & W) Face crack propagation (Total-P(%)/Rel.-Length(r1-r2)) [c]	80/1-3	90/-	95/1
New flexural cracks (Yes/No)	No	No	Yes
New shear cracks only (L(%)/Length/Height location) [d]	10/2.5/38	-	-
(N & S) Crack width (in/mm)	-	0.04/1.00	0.08/2.00
(E & W) Crack width (in/mm)	0.025/0.60	0.025/0.60	-
Spalling of concrete cover (Location-Face/Damaged Height (in))	-	Base-(N&S)/3	Base-(N&S)/3
Crushing of concrete (Location-Face/Damaged Depth(in))	-	-	-
Exposure of reinforcement steel (Location-Face/Height (in))	-	-	-
Buckling of longitudinal reinforcement (Location)	-	-	-

[a] (Initial height from the column base (in) /Final height form the column base (in) / Average values of spacing between cracks (in))
[b] (Crack slope from vertical line / Location in east or west faces from tension face north or south, e.g., 50% as the middle of east or west faces / Height of the crack slope (in))
[c] (Maximum total crack propagation percentage in east or west faces from tension face north or south, e.g., 50% as half of east or west faces covered with cracks / Values of relative crack length propagation (in))
[d] (Location in east or west faces from tension face north or south, e.g., 50% as the middle of east or west faces / Shear only crack length (in) / Height at the middle of the crack in east or west planes (in))

Table 6.14. Displacement Controlled Test Observation Matrix (LW3-NS-DSF) – Ductility Four to Failure

	Displacement Controlled - Test Observation Matrix – (LW3-NS-DSF)		
Test Observation	**Displacement Ductiliy (4)**	**Displacement Ductiliy (6)**	**Displacement Ductiliy (8)**
Maximum lateral force (kips)	170.90	176.08	117.07 / 142.64
Axial load (kips)	116.76	121.43	103.30
Lateral displacement (in)	2.24	3.37	4.49
(N & S) Cracks location (Ih/Fh/s(s1-s2)) (in) [a]	(0/14/4-6) (14/40/5-7)	(0/14/4-6) (14/40/5-7)	(0/14/4-6) (14/40/5-7)
(N & S) Cracks orientation (Horizontal (H)/Vertical (V)/Both (B))	B	B	B
(E & W) Cracks location (Ih/Fh/s(s1-s2)) (in) [a]	(0/55/1-3)W (0/45/3-4)E	(0/55/1-3)W (0/45/3-4)E	(0/55/1-3)W (0/45/3-4)E
(E & W) Average crack slope and location (Slope/L(%)/Hcs) [b]	(30/50/10-15)W (45/50/10)E	(30/50/10-15)W (45/50/10)E	(30/50/10-15)W (45/50/10)E
(E & W) Face crack propagation (Total-P(%)/Rel.-Length(r1-r2)) [c]	100/2	100/-	100/-
New flexural cracks (Yes/No)	No	No	No
New shear cracks only (L(%)/Length/Height location) [d]	-	-	-
(N & S) Crack width (in/mm)	-	-	-
(E & W) Crack width (in/mm)	0.14/3.50 (E)	0.24/6.00 (E)	0.39/10.00 (E)
Spalling of concrete cover (Location-Face/Damaged Height (in))	(Base-(N&S)/0-10) (Right-(E)/0-22)	(Base-(N&S)/0-15) (Center-(E)/0-22)	(Base-(N&S)/0-15) (Center-(E&W)/-)
Crushing of concrete (Location-Face/Damaged Depth(in))	Base-(N&S)/2.5	Base-(N&S)/-	Base-(N&S)/-
Exposure of reinforcement steel (Location-Face/Height (in))	Right-(E)/0-22 (cycle 3)	Center-(E)/0-22	Center-(E)/0-22
Buckling of longitudinal reinforcement (Location)	-	-	Base-(N&S)

[a] (Initial height from the column base (in) /Final height form the column base (in) / Average values of spacing between cracks (in))
[b] (Crack slope from vertical line / Location in east or west faces from tension face north or south, e.g., 50% as the middle of east or west faces / Height of the crack slope (in))
[c] (Maximum total crack propagation percentage in east or west faces from tension face north or south, e.g., 50% as half of east or west faces covered with cracks / Values of relative crack length propagation (in))
[d] (Location in east or west faces from tension face north or south, e.g., 50% as the middle of east or west faces / Shear only crack length (in) / Height at the middle of the crack in east or west planes (in))

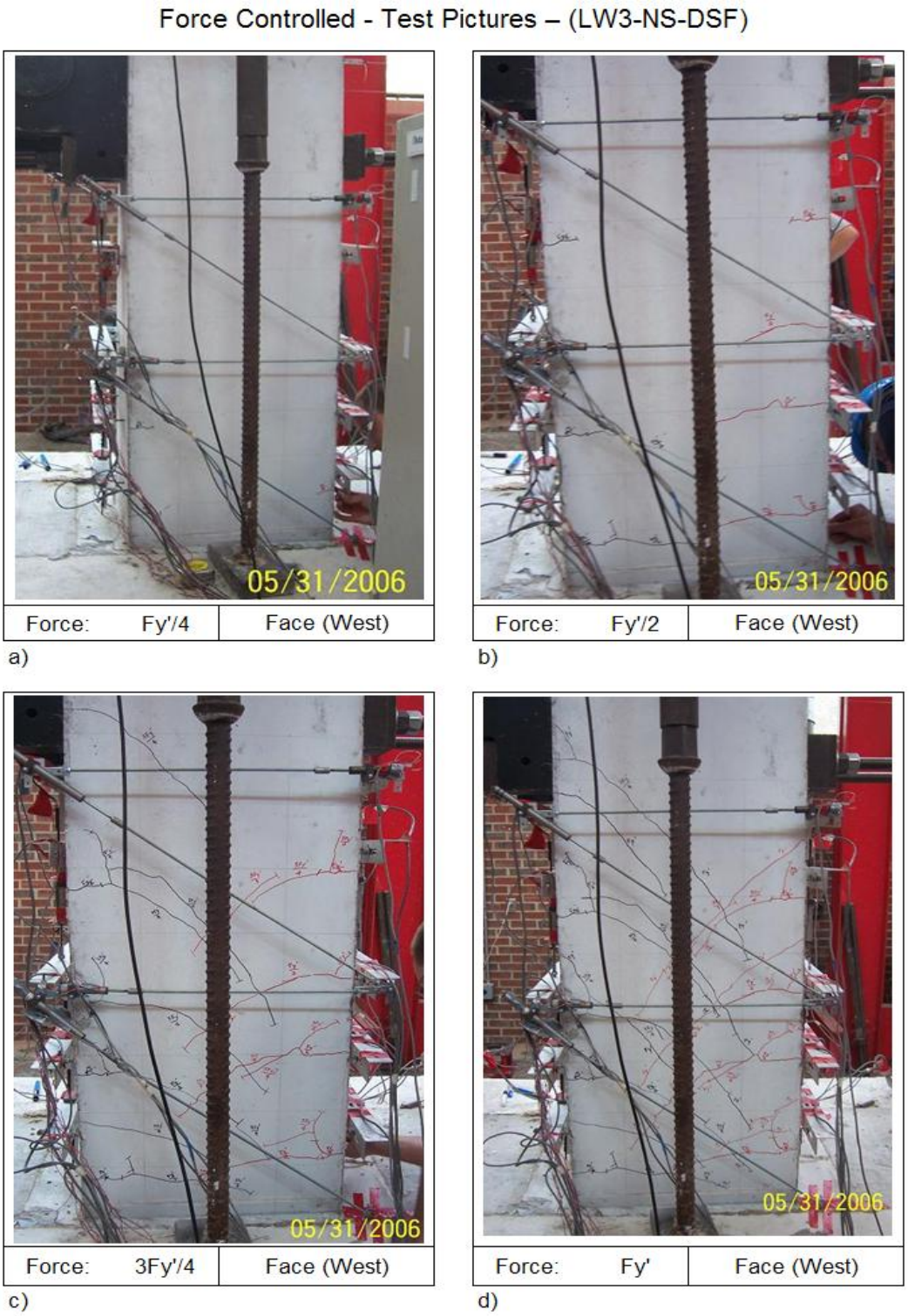

Figure 6.18. Force Controlled Loading – (LW3-NS-DSF)

Displacement Controlled - Test Pictures – (LW3-NS-DSF)

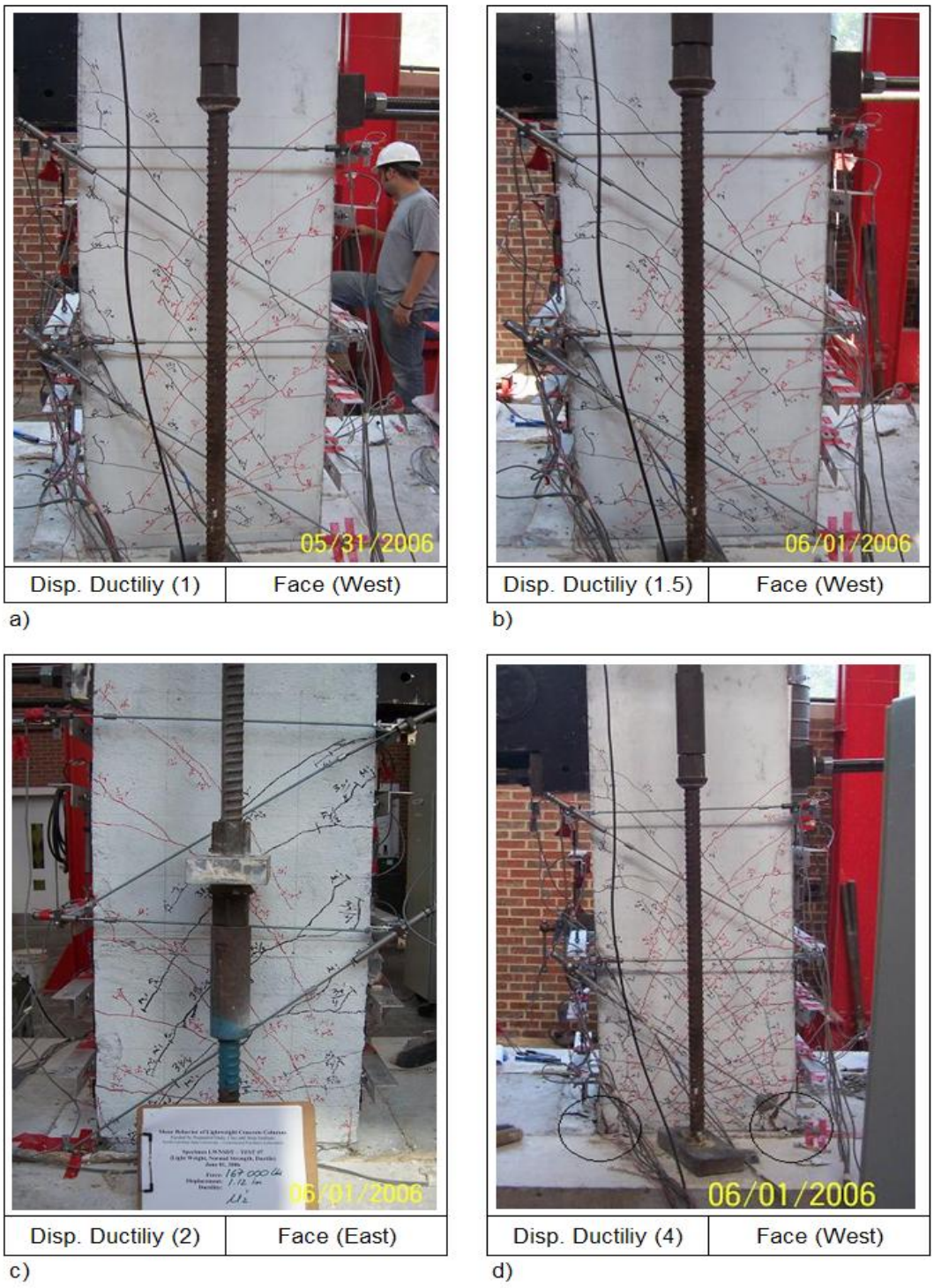

Figure 6.19. Displacement Controlled Loading – (LW3-NS-DSF) – Ductility One to Four

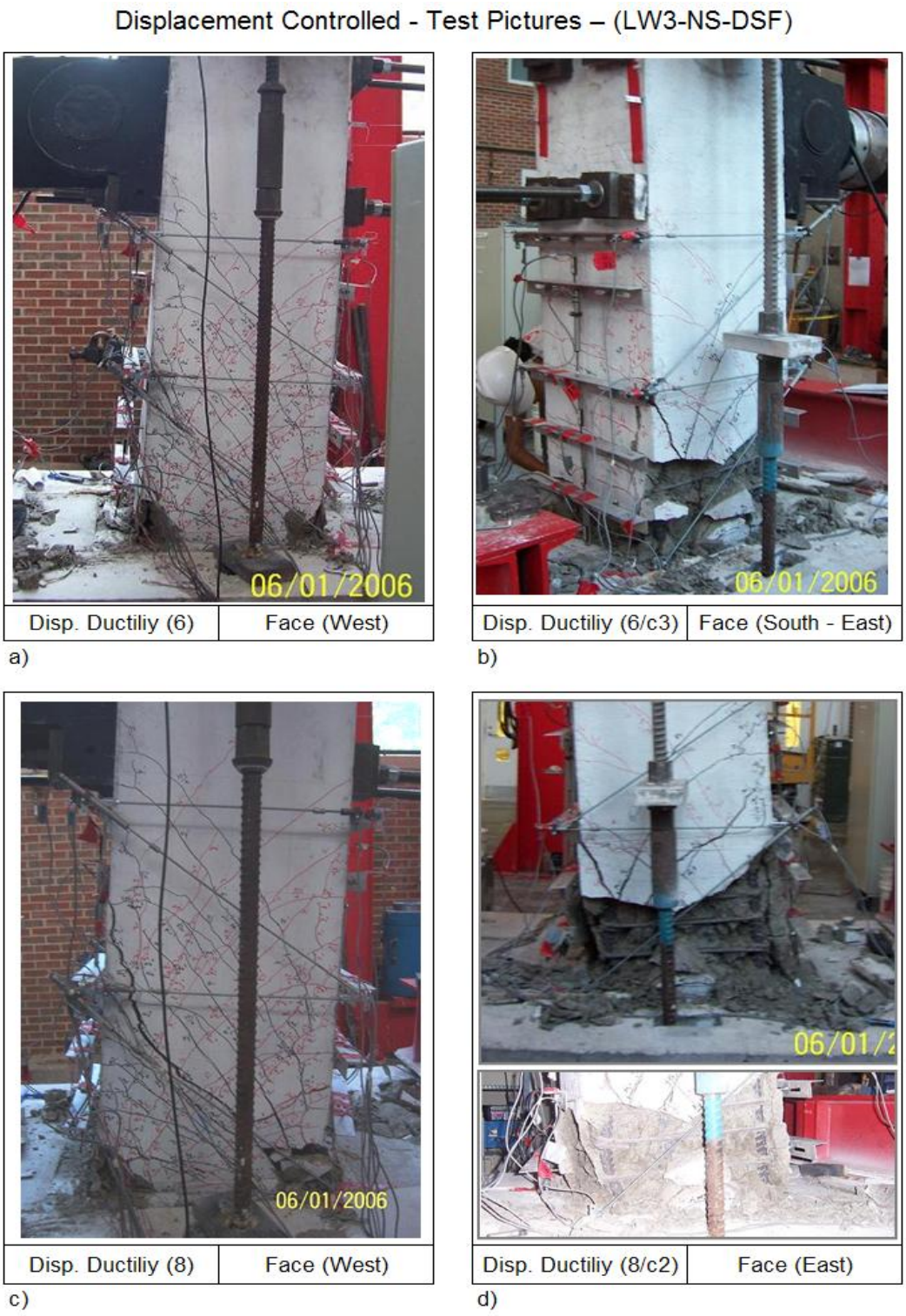

Figure 6.20. Displacement Controlled Loading – (LW3-NS-DSF) – Ductility Six to Failure

6.5 Tests Results

Results of all ductile shear failure tests are presented in this section. In addition, aspects about the shear performance of all the specimens are also discussed. However, it is important to mention that the profound analysis of the data is discussed in chapter seven.

6.5.1 Hysteretic Responses and Peak Cycle Envelopes

Force versus displacement responses are presented in Figure 6.21 (a, b, c, & d) corresponding to tests (NW-NS-DSF), (LW1-NS-DSF), (LW2-NS-DSF), and (LW3-NS-DSF). In all these tests, the hysteretic loops defined by the lateral force versus the lateral top displacement have a mild pinched shape compared to the well defined pinched shape of all brittle shear failure tests as discussed in section 5.5.1. The pinched shape of the loops is more evident in tests (LW2-NS-DSF) and (LW3-NS-DSF). It is important to mention that for tests (NW-NS-DSF) and (LW1-NS-DSF), the cycles did not reach the desired displacements in the pulling direction due to the limitation in the tension capacity of the actuator in that direction. For that reason, the shape of the hysteretic loops is less pinched in tests (NW-NS-DSF) and (LW1-NS-DSF). Finally, the pinched shape of the ductile shear failure specimens is milder than that of the brittle shear failure specimens due to the higher amount of transverse steel, better concrete confinement, less spacing between stirrups, and more ductility capacity.

The pinched shape of the hysteretic loops is associated with shear performance of reinforced concrete elements. In fact, that type of behavior was desired for the experimental tests in

order to study the shear performance of lightweight concrete. Furthermore, as shown in Figure 6.23 (a & d), the same pinched shape was observed in moment versus base curvature hysteretic responses of tests (NW-NS-DSF) and (LW3-NS-DSF). For some reason, moment versus curvature of tests (LW2-NS-DSF) does not present a clear pinched shape as shown in Figure 6.23 (c).

Strength degradation was more significant and evident in lightweight concrete specimens. In fact, the normal weight concrete specimen (NW-NS-DSF) continued providing additional strength up to displacement ductility ($\mu_\Delta 6$) as shown in Figure 6.21 and Figure 6.22. Lightweight concrete specimens started to lose strength at lower levels of deformation. Consequently, the normal weight concrete specimen performed with a slightly more ductile behavior than lightweight concrete specimen as it was also observed in chapter 5 for the brittle shear failure specimens. Despite that fact, similar shear strength was provided by all ductile shear failure specimens.

6.5.2 Average Curvature and Transverse Reinforcement Steel Strain Profiles

Average curvature profiles were used to calculate top displacements due to flexural deformation. As shown in Figure 6.25, average curvature profiles of ductile shear failure specimens are relatively similar and consistent with what was expected. Moreover, the maximum curvature is located at the base of the column and it was calculated considering a strain penetration length due to stresses in the longitudinal reinforcement steel inside the footing member. In the same manner, curvature profiles are relatively similar as shown in

Figure 6.25. Indeed, first yielding curvature was reached consistently when first yielding (Fy') of the column cross section was also reached for tests (NW-NS-DSF), (LW2-NS-DSF), and (LW3-NS-DSF).

In relation to the transverse reinforcement steel strain profiles shown in Figure 6.24, it was observed that, consistently for all the specimens, yielding of the stirrups started when the column reached a level of deformation equals to displacement ductility ($\mu_\Delta 4$). Similarly, the location of more activity in terms of deformation and strain in the stirrups was approximately between 10 to 15 inches from the base of the column. In fact, this data is consistent with visual observations for all ductile shear failure specimens about the location of most deformation activity and the intersection of principal cracks in faces (E & W) as stated in previous sections of this chapter. The actual strain of the stirrups represents valuable information for estimating the actual stress of the transverse steel at different levels of deformation. Finally, this information has been used in chapter 7 in order to obtain actual shear strength contribution by the transverse steel at different levels of deformation.

6.5.3 Displacement Components

Displacement components due to Flexural and shear deformation were calculated separately using the data obtained during the test by linear potentiometers. In fact, the displacement components were compared to total top displacements measured by string linear

potentiometers. As a result, Figure 7.2 shows the graphs that relate top column displacements versus displacement components for each ductile shear failure specimen.

In general, it can be observed that the rate of increment in the displacements due to flexural deformation tends to decrease as the total lateral displacement increases. On the contrary, the rate of increment in displacements due to shear deformation tends to increase as the total displacement increases. This was also observed for the brittle shear failure tests in chapter 5, section 5.5. The above mentioned behavior of the displacement components is confirmed by visual observations during the tests. In fact, as described in the tests observation matrices presented in this chapter, flexural cracks appeared mainly during force controlled loading while after reaching the yielding point, almost no new flexural cracks appeared. On the contrary, shear only cracks did not appear at low levels of lateral load, but most of them started to appear towards reaching the first yielding point and beyond that level of deformation.

Finally, it is important to mention that there is a significant difference between the total top displacement and the sum of displacement components in tests (NW-NS-DSF), (LW1-NS-DSF), and (LW2-NS-DSF) as shown in Figure 7.2 (a, b, & c). This difference could be explained considering the fact that the information presented does not take into account additional displacement components. For instance, displacement components due to rigid body rotation of the entire column-footing beam connection, additional displacement due to flexural and shear deformation in the column-footing beam connection below the column

base, displacement due to slippage of longitudinal reinforcement, and any other displacement component that was not measured. In fact, significant activity in the connection was observed in terms of deformation, but it was not measured, see Figure 6.15 (d). The above mentioned factors could explain the differences between the sum of displacement components and total top displacements.

6.5.4 Failure Mode

Observations during the tests as well as the data obtained revealed significant activity in terms of shear and flexural deformation of all ductile shear failure specimens. However the expected ductile shear failure mode did not occur in any of the ductile shear failure specimens. In all cases, evidence of the above mentioned fact were the mild buckling of the longitudinal reinforcement observed at the base of the column faces (N & S) and the lack of evidence of a ductile shear failure such as the rupture of a stirrup. However, a ductile shear failure was close to occur as discussed in chapter 7, and activity in terms of shear deformation was significant as spalling of the concrete cover in faces (E & W) and well defined shear cracks revealed during the tests.

The recorded force deformation responses did not exceed the predicted shear capacities at high levels of deformation, and the specimens developed a flexural or flexural-shear failure mode. The maximum recorded lateral force was approximately 15% less than the predicted shear capacity at failure for all ductile shear failure tests. However, due to the significant

shear deformation caused by high shear demand close to exceed the capacity, shear strength, shear deformation, and shear performance under reversed cyclic loading was measured and analyzed at various levels of deformation revealing valuable information about the impact of lightweight concrete on shear performance. Detailed aspects about the performance of the specimen are discussed in chapter 7.

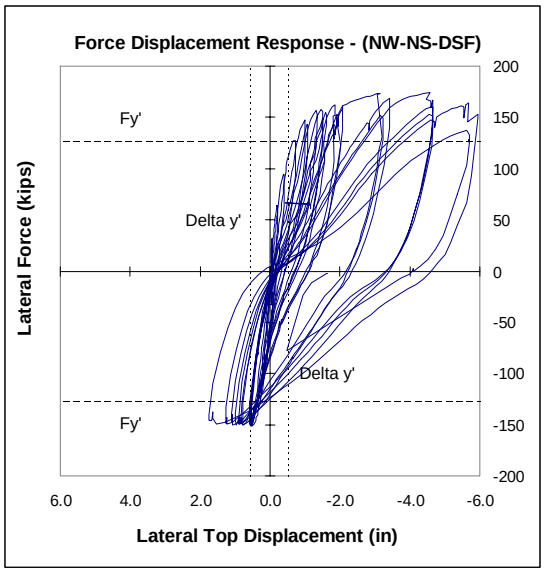

a) Specimen (NW-NS-DSF)

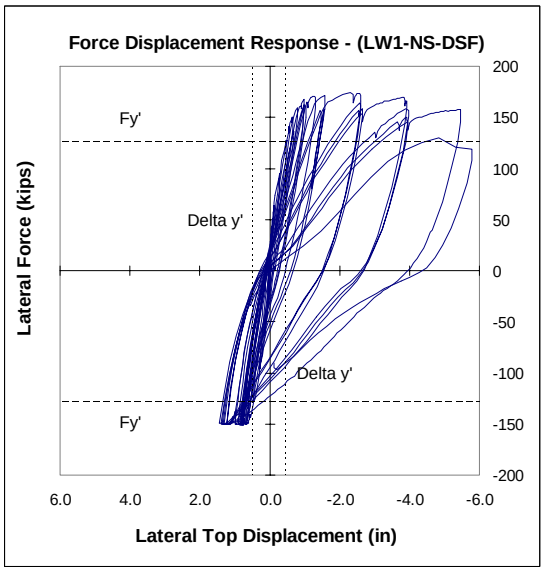

b) Specimen (LW1-NS-DSF)

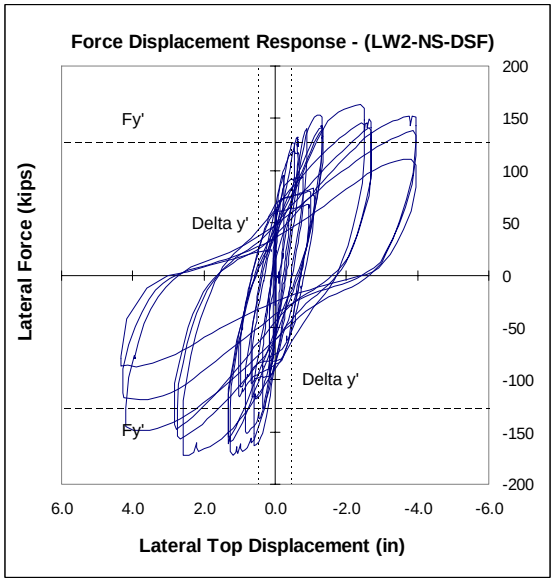

c) Specimen (LW2-NS-DSF)

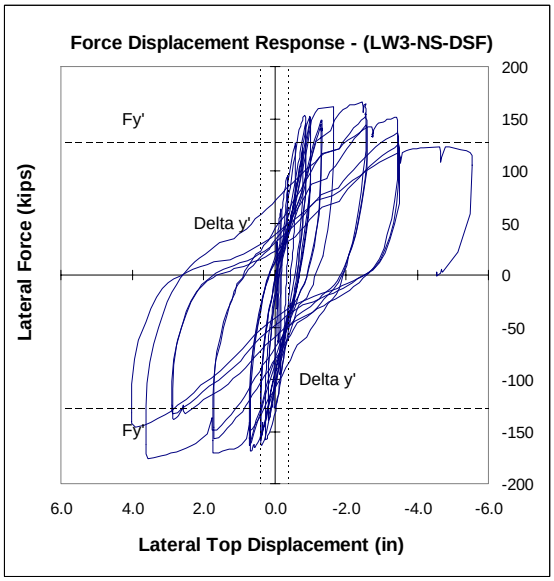

d) Specimen (LW3-NS-DSF)

Figure 6.21. Force versus Lateral Top Displacement Histories – Ductile Shear Failure Specimens

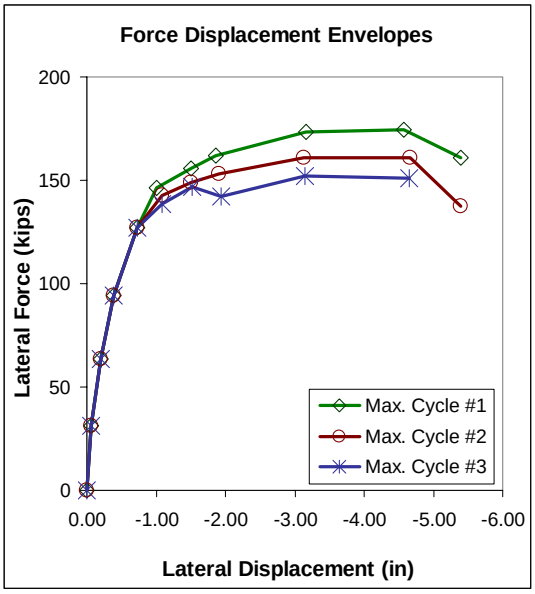

a) Specimen (NW-NS-DSF)

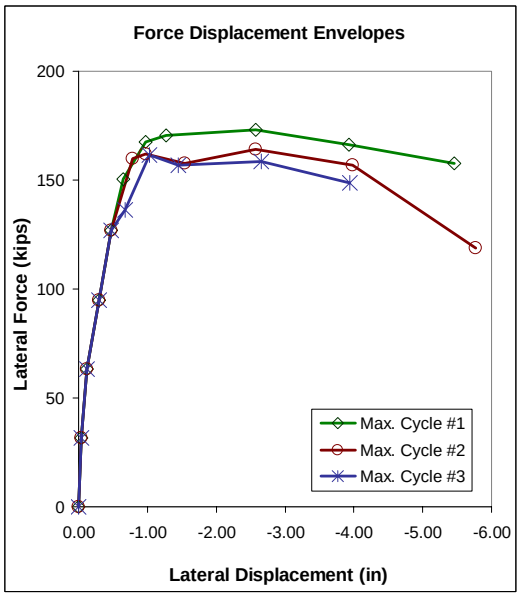

b) Specimen (LW1-NS-DSF)

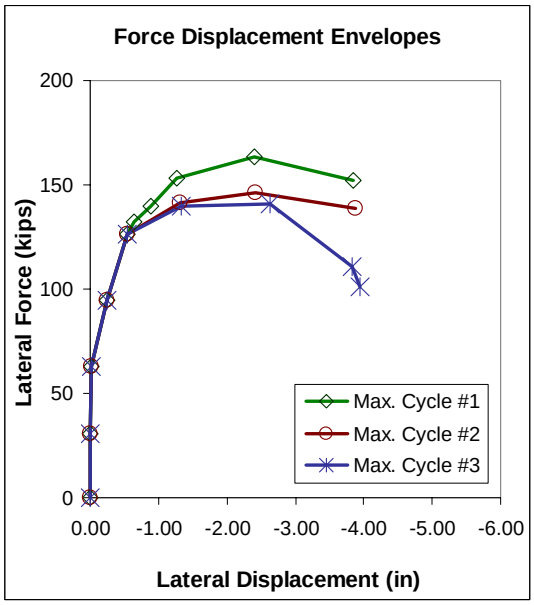

c) Specimen (LW2-NS-DSF)

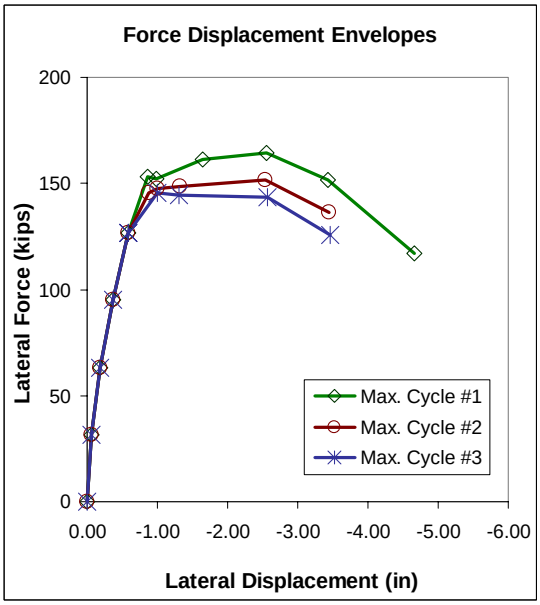

d) Specimen (LW3-NS-DSF)

Figure 6.22. Force Displacement Envelopes – Ductile Shear Failure Specimens

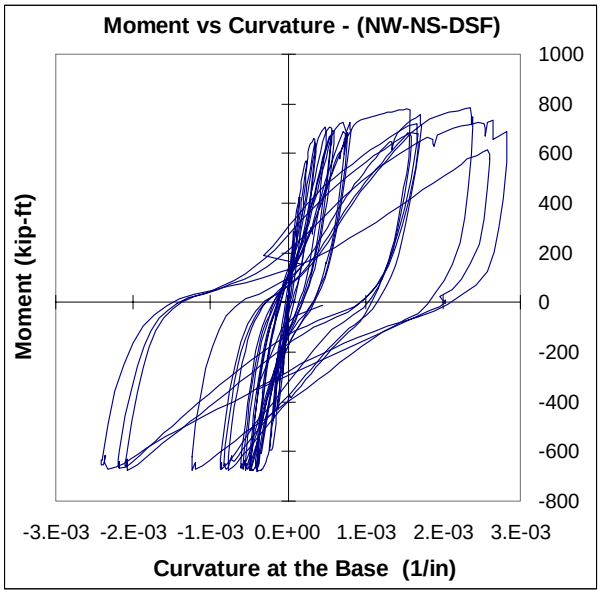

a) Specimen (NW-NS-DSF)

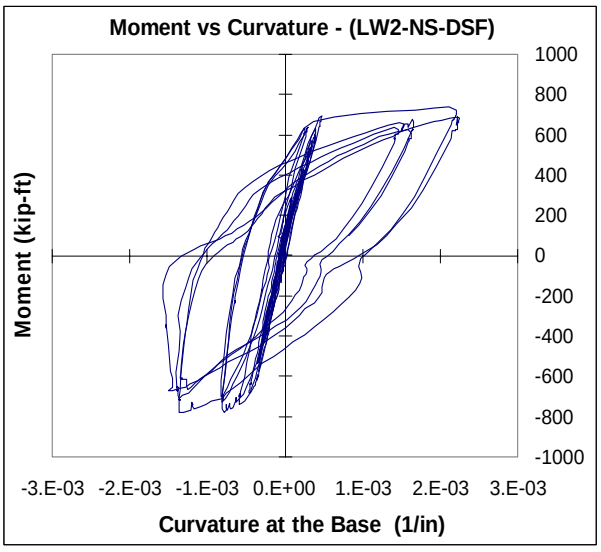

b) Specimen (LW2-NS-DSF)

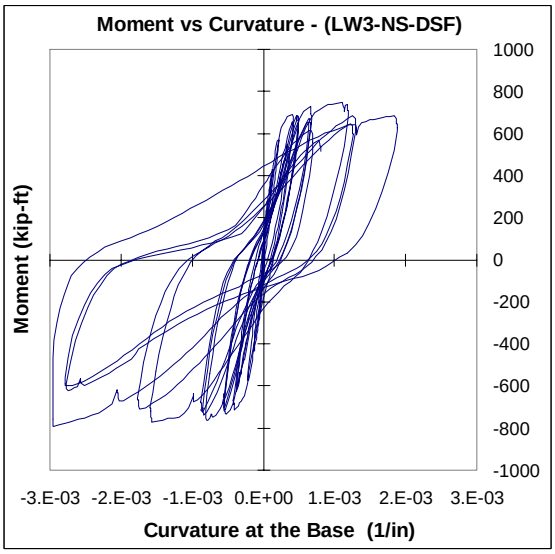

c) Specimen (LW3-NS-DSF)

Figure 6.23. Moment versus Curvature Histories – Ductile Shear Failure Specimens

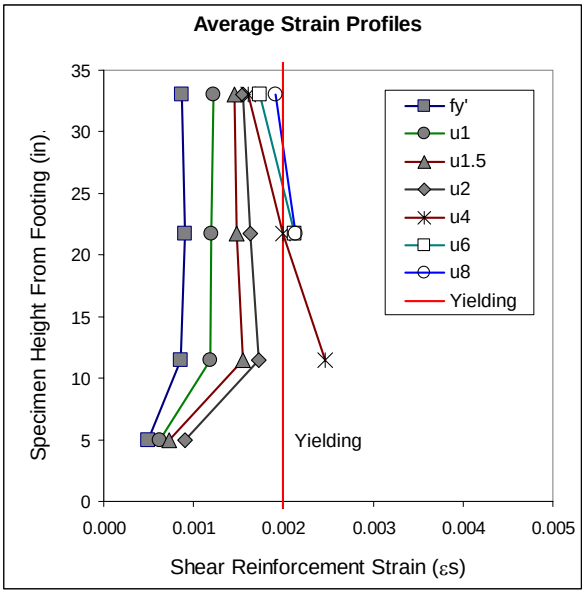

a) Specimen (NW-NS-DSF)

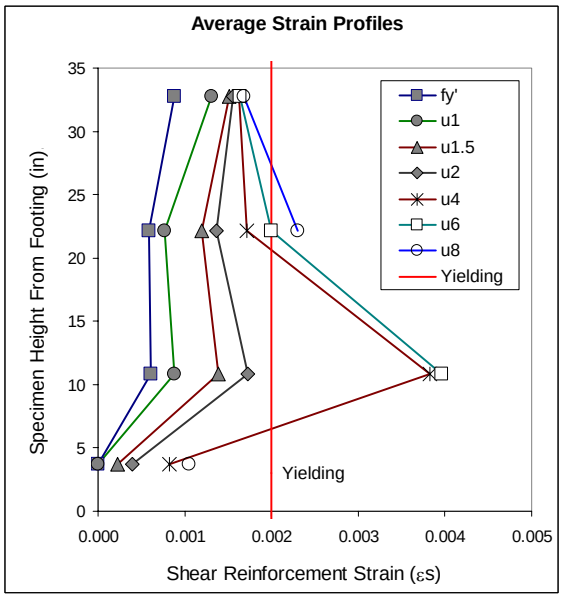

b) Specimen (LW1-NS-DSF)

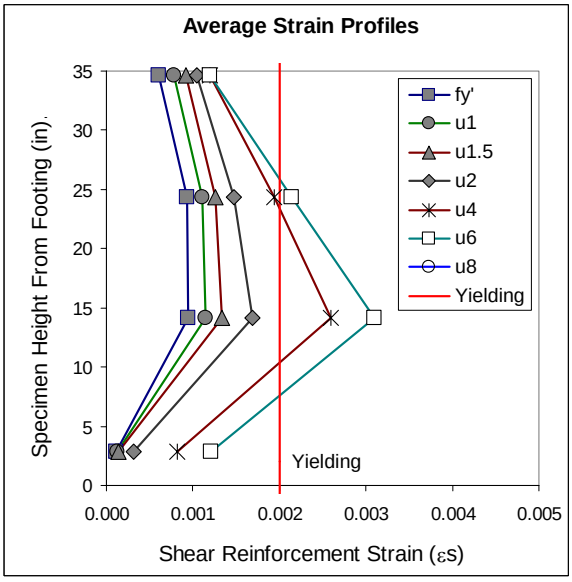

c) Specimen (LW2-NS-DSF)

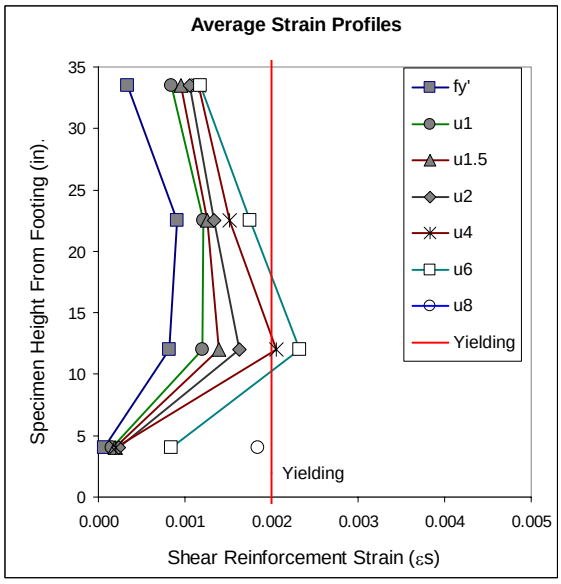

d) Specimen (LW3-NS-DSF)

Figure 6.24. Transverse Reinforcement Steel Strain Profiles – Ductile Shear Failure Specimens

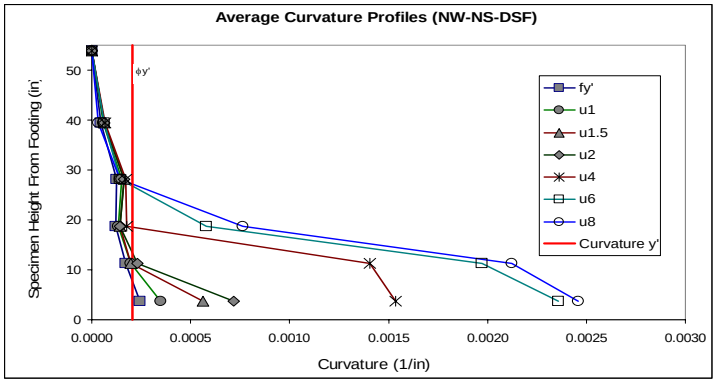

a) Specimen (NW-NS-DSF)

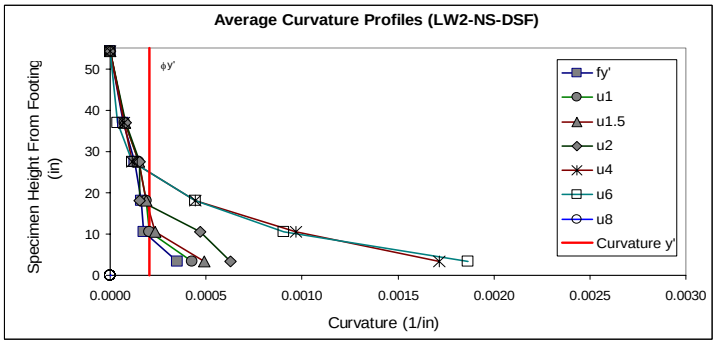

b) Specimen (LW2-NS-DSF)

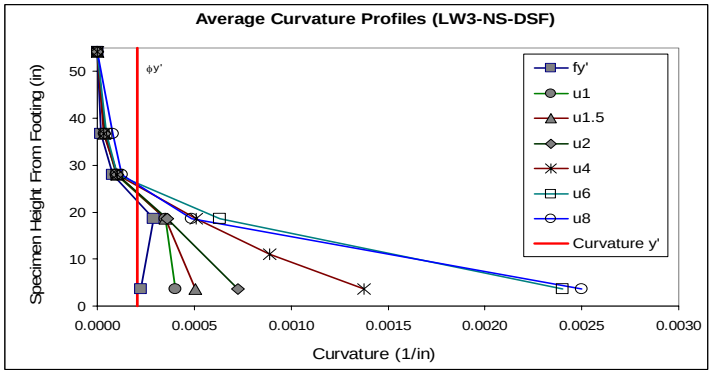

c) Specimen (LW3-NS-DSF)

Figure 6.25. Curvature Profile – Ductile Shear Failure Specimens

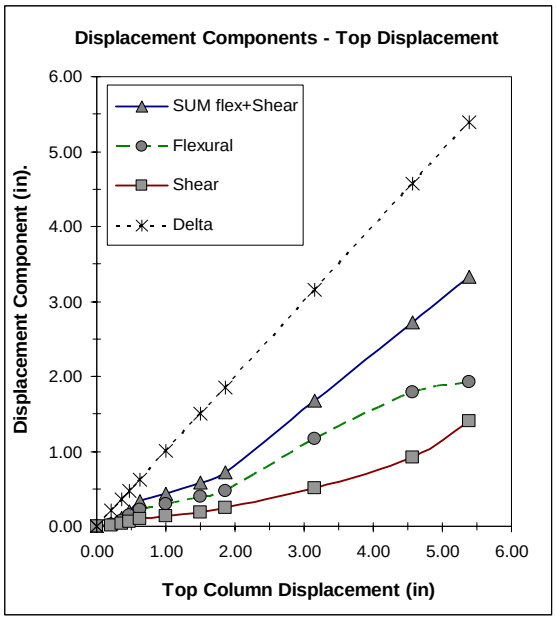

a) Specimen (NW-NS-DSF)

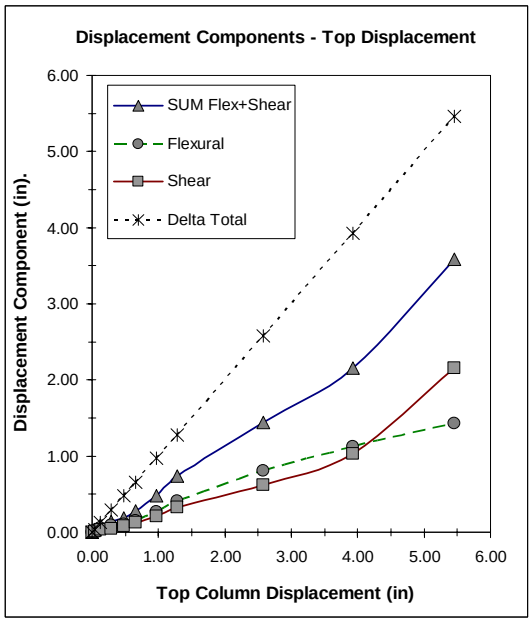

b) Specimen (LW1-NS-DSF)

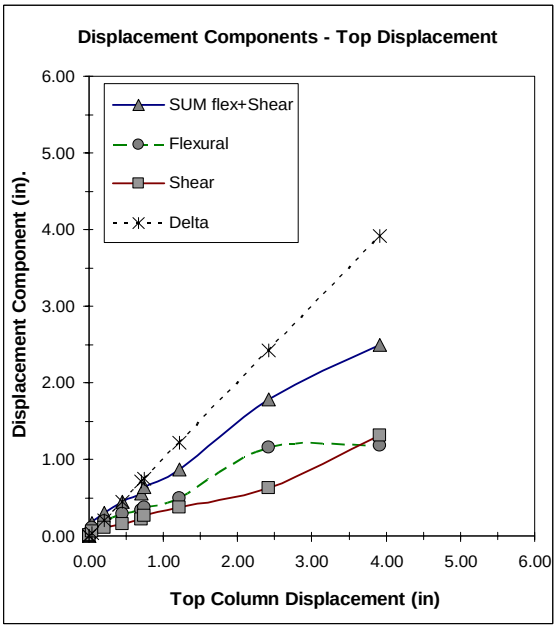

c) Specimen (LW2-NS-DSF)

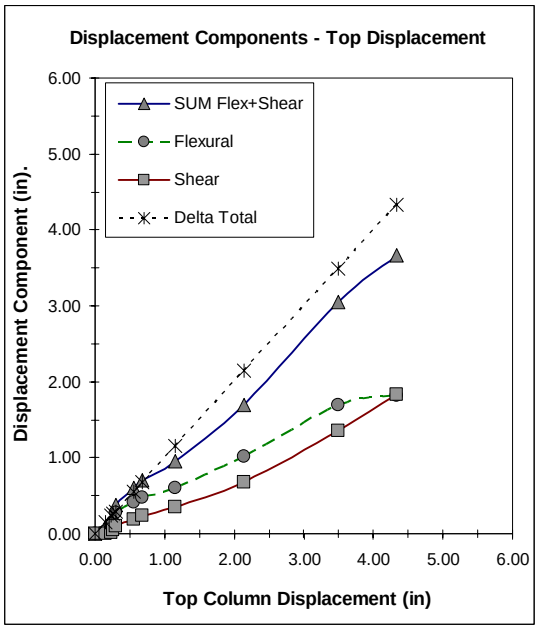

d) Specimen (LW3-NS-DSF)

Figure 6.26. Displacement Components – Ductile Shear Failure Specimens

Chapter 7: SHEAR PERFORMANCE OF LIGHTWEIGHT CONCRETE

Focusing on the objective of the research, which is to study the shear performance of reinforced lightweight concrete square columns under hysteretic shear demands, a comparative analysis is presented in this chapter. In fact, for all brittle and ductile shear failure specimens, aspects such as shear strength, deformation capacity, damping, and energy dissipation are discussed in order to asses the shear performance of lightweight concrete. Moreover, a three component shear model proposed by Priestley et al. (1994), modified for lightweight concrete (Kowalsky et al., 1999), then revised by Kowalsky and Priestley (2000 a) for circular reinforced concrete columns in seismic regions, and also revised for lightweight concrete (Kowalsky et al., 2000 b) is compared to the experimental results obtained in this research for normal and lightweight reinforced concrete square columns. The above mentioned model was developed to predict the nominal shear strength of columns based on actual strengths, obtained in various experiments, considering various levels of deformation and seismic demands.

7.1 Shear Strength

7.1.1 Brittle Shear Failure Specimens – Shear Strength

Regarding shear strength of all brittle shear failure specimens, the normal weight concrete specimen (NW-NS-BSF), reached the highest shear strength even considering that its

compressive strength was the lowest. In fact, even though the difference in the shear strength between normal and lightweight concrete specimens was not significant, it was consistent in all hysteretic cycles applied at the same level of deformation during displacement controlled loading. For all cycles, (NW-NS-BSF) specimen developed the highest shear strength as shown in the shear force versus lateral top displacement envelopes for all brittle shear failure specimens in Figure 7.2 (a, b, & c).

It is important to notice that (NW-NS-BSF) specimen sustained its shear strength for more cycles and at larger levels of deformation compared to the lightweight concrete specimens that developed shear strength degradation earlier. Moreover, strength degradation was also slightly more significant for lightweight concrete specimens, particularly, in the case of specimen (LW2-NS-BSF). Figure 7.2 (a, b, & c) reveals more displacement capacity of (NW-NS-BSF) specimen compared to lightweight concrete specimens. Finally, a negative stiffness after yielding is evident for specimens (LW1, 2 &3 –NS-BSF) while it occurred later in the case of specimen (NW-NS-BSF).

7.1.2 Ductile Shear Failure Specimens – Shear Strength

In the same manner, specimen (NW-NS-DSF) reached a slightly higher shear strength compared to lightweight concrete ductile shear failure specimens. However, that was not the case for cycles two and three where, at the same level of deformation, specimen (LW1-NS-DSF) reached a slightly higher strength. Nevertheless, concrete compressive strength at the day of tests was significantly higher for specimen (LW1-NS-DSF) than for specimen (NW-

NS-DSF). In addition, it is important to notice that the results are very consistent in all cases, and that differences in shear strength were not significant (approximately 10%) as shown in Figure 7.3 (a, b, &c). Finally, force versus lateral top displacement envelopes for all ductile shear failure specimens are shown in Figure 7.3.

Furthermore, in the same manner as in test (NW-NS-BSF), (NW-NS-DSF) specimen sustained its shear strength for more cycles and at larger levels of deformation compared to the lightweight concrete specimens that developed shear strength degradation earlier. In fact, while (NW-NS-DSF) specimen developed a positive stiffness after yielding, lightweight concrete specimens tended to lose strength at lower levels of deformation, and presenting slightly more strength degradation. Figure 7.3 shows the tendency of specimens (LW1, 2, & 3 –NS-DSF) to develop negative stiffness after yielding. This was more evident for specimens (LW2 & 3-NS-DSF).

Finally, it is important to mention that even though all ductile shear failure specimens were designed to develop a shear failure mechanism as predicted by the analytical model, the results indicated that the failure mechanism was more of a flexural or flexural-shear type. The ductile shear failure specimens started to develop a plastic hinge at the base of the column, and at the same time a well defined shear crack was observed. The maximum recorded shear force reached by the specimens was approximately 15% lower than the shear capacity predicted by the analytical model. With that difference in the shear strength, it was not possible to exceed the shear capacity of the specimen and to cause a shear failure as

predicted. There was no evidence of rupture of stirrups while a mild buckling of the column longitudinal reinforcement was observed at failure in all ductile shear failure tests.
The predicted and actual shear capacities were higher than the shear demand even in the lower plateau at high levels of deformation where shear strength degradation occurred as it can be observed in Figure 7.6 and Figure 7.4 (b). In addition, some additional strength, not considered in the analytical model, was provided by secondary transverse stirrups located in the opposite direction compared to the principal stirrups, and placed in the column to provide more confinement as shown in Figure 7.1. Indeed, for the analytical model, the above mentioned stirrups were assumed to have no significant effect in the shear strength of the column. However, Figure 7.6 shows the effect of considering the effect of the secondary stirrup as well as all actual parameters in the predicted shear capacity envelopes. Predicted shear capacity envelopes and force displacement responses in Figure 7.6 considered actual compressive strengths of each specimen, each concrete stress-strain relationships for normal and lightweight concrete as shown in Figure 9.50 and Figure 9.51 of the appendix (Kowalsky et al., 2000 b), and the additional contribution to the transverse steel shear strength component provided by the small leg of the secondary stirrup (see Figure 7.1).

The secondary stirrup placed in the transverse direction to the shear demands enhanced the shear performance of the element in terms of shear strength and ductility. Considering the additional shear strength provided by the secondary stirrup, a smaller shear span ratio would have been necessary to develop the desired ductile shear failure. It is important to notice that such contribution is not considered by many structural designers, and that it could represent a

subject of future studies to optimize predictions. Finally, any additional shear strength provided by the above mentioned secondary transverse stirrups could have reduced the probabilities of reaching a ductile shear failure dramatically due to the nature of the failure. Nonetheless, by careful consideration of the demands in the shear reinforcement it is possible to determine relative (Vc) components of shear strength to compare the difference in the shear strength provided by lightweight concrete compared to normal weight concrete at high levels of deformation.

Predicted calculations presented in this chapter take into account the effect of the small leg of the secondary stirrup on the shear strength of the columns considering a percentage of its transverse area to be added to the total shear reinforcement area as proposed by Priestley et al. (1996) in their book "Seismic Design and Retrofit of Bridges." The shear reinforcement area following this approach was 17% greater than the initially used for the ductile shear failure analytical model as shown in Figure 7.1 (4.67Ash compared to 4.00 Ash).

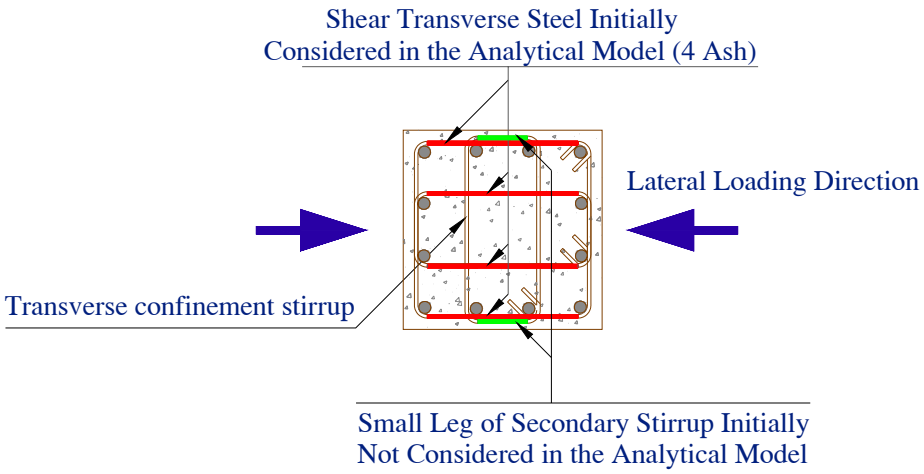

Figure 7.1. Transverse Steel Considered in Ductile Shear Failure Analytical Model

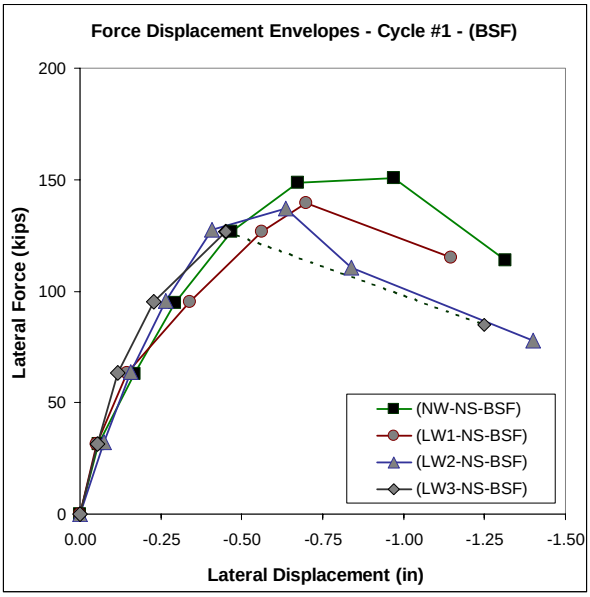

a) Cycle #1 Envelopes (BSF) Tests

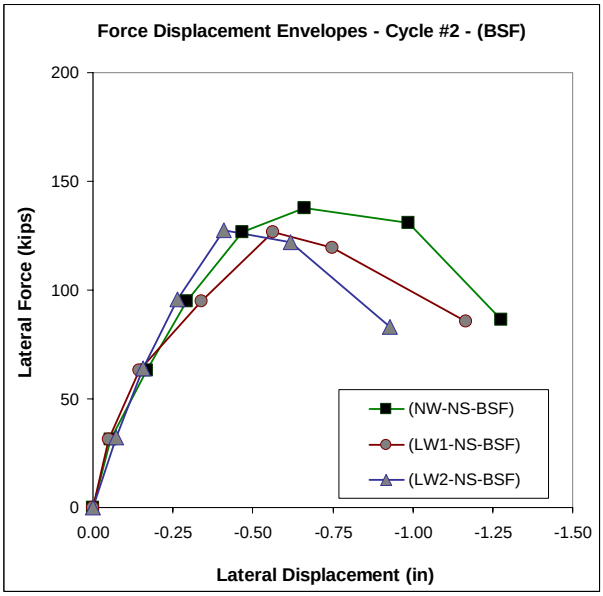

b) Cycle #2 Envelopes (BSF) Tests

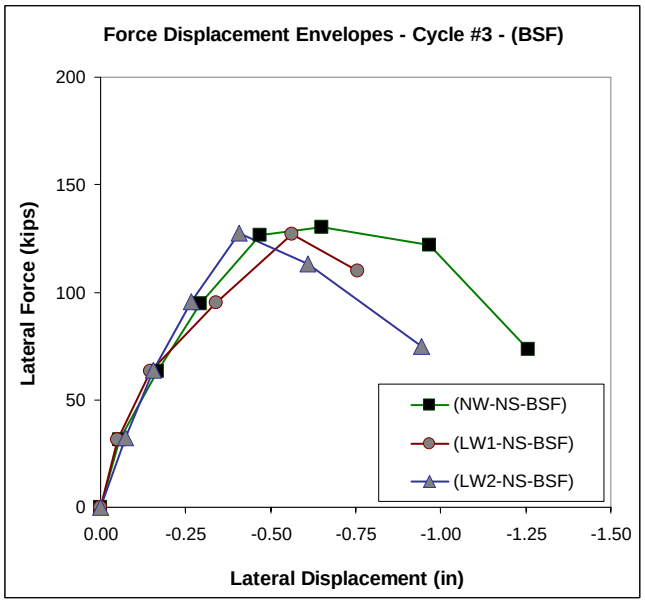

c) Cycle #3 Envelopes (BSF) Tests

Figure 7.2. Force Displacement Envelopes – Brittle Shear Failure Specimens

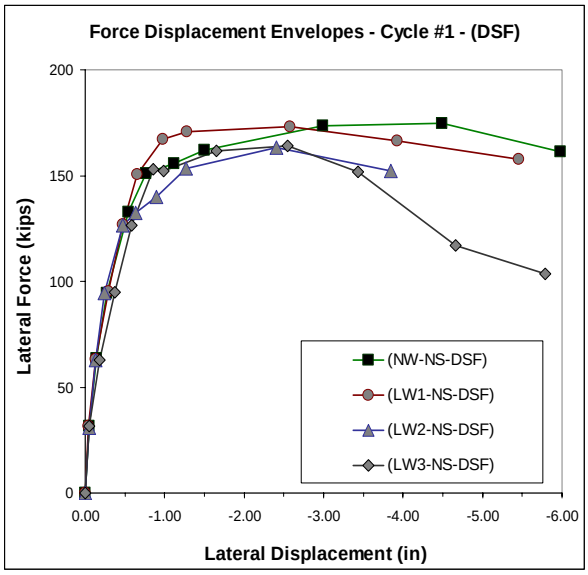

a) Cycle #1 Envelopes (DSF) Tests

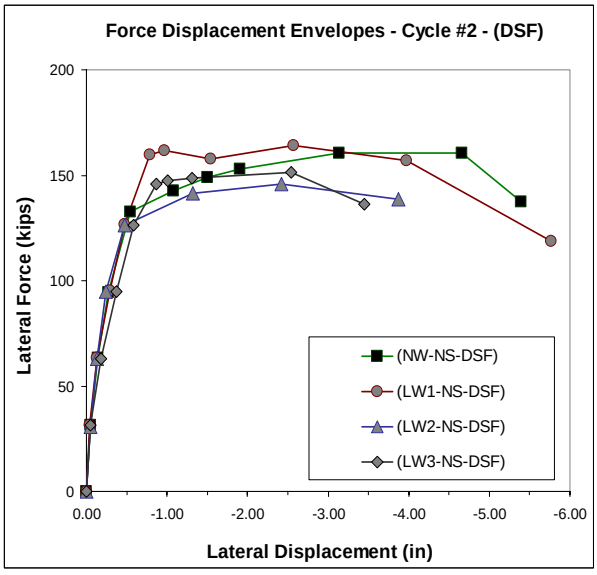

b) Cycle #2 Envelopes (DSF) Tests

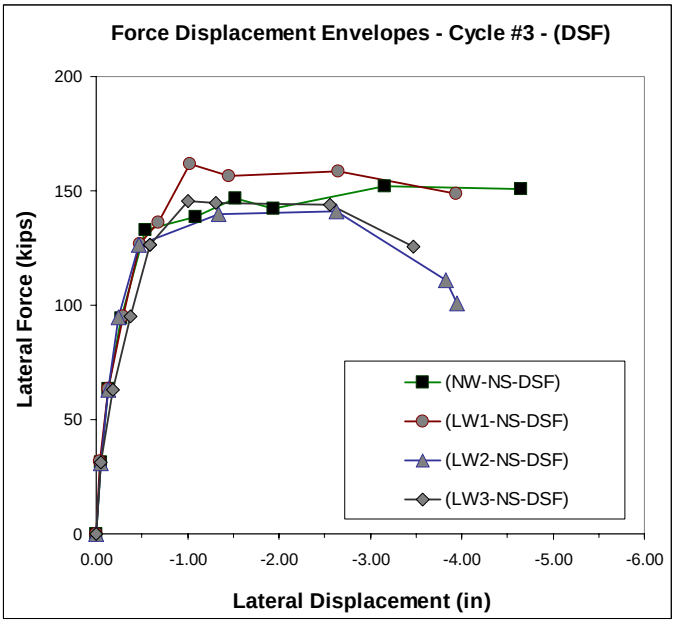

c) Cycle #3 Envelopes (DSF) Tests

Figure 7.3. Force Displacement Envelopes – Ductile Shear Failure Specimens

7.2 Recorded Data - Shear Transfer Mechanism

The three shear strength component model proposed by Priestley et al. (1994), modified for lightweight concrete (Kowalsky et al., 1999), and revised by Kowalsky et al. (2000 b) based on experimental tests of large scale lightweight concrete circular columns under reversed loading, was used to predict values compared to the actual results of all brittle and ductile shear failure tests of this research. This section presents the results of the comparative analysis, and discusses the effect of reinforced lightweight concrete in the shear performance of square columns. It is important to mention that the above mentioned model, developed to predict the nominal shear strength of circular columns, considered the lower bound of various experimental results to asses the shear capacity envelope. Consequently, the same criterion is considered when analyzing the results as well as to revise the shear capacity envelope model for reinforced lightweight concrete square columns.

Among the components, as described in (Eq. 2-6), the shear transfer mechanism model takes into account an axial load shear strength component contribution (Vp) as described in section 2.4. The shear strength contribution due to the axial load was calculated at different levels of deformation using actual data of each specimen. Changes in the neutral axis depth and axial load during the response of each specimen were considered.

The shear strength contribution provided by the transverse steel reinforcement as described in section 2.4 was estimated for each specimen using actual data obtained in each test at different levels of deformation. In fact, (*Vs*) was calculated taking into account the actual angle of the compression strut (θ) as measured during each test by visual inspection of the cracks, and the actual stress of the transverse reinforcement (*fsh*) at specific levels of deformation. The actual angle of the compression strut (θ) was measured from the vertical axis and it was defined by the average slope of the principal shear cracks on faces (E & W) as described in section 2.4. The stress of the transverse steel was estimated as a function of the strain profile of the transverse reinforcement obtained by internal instruments (strain gages) at different levels of deformation as shown in chapters 5 and 6 for each set of specimens. The location of maximum activity in terms of shear deformation that was the same where maximum tensile strains in the transverse steel occurred was considered to estimate the stress in the stirrups (*fsh*). Moreover, the spacing between stirrups (*s*), and the area of the transverse steel (*Ash*) was assigned for each specimen as they were built, and the transverse steel ratio was different for brittle and ductile shear failure specimens. The concrete cover (*cov*) was the same for all the specimens.

Finally, for each specimen, the actual shear strength component provided by the concrete (*Vc*) was obtained by subtracting the other two components, described in the above paragraphs, to the total shear demand applied by the actuator at the corresponding level of deformation and lateral force. Actual values of (*Vc*), obtained from equation (Eq. 7-1) were

compared to predicted values obtained by equation (Eq. 2-7) to determine the effect of lightweight concrete in shear performance. Predicted values of (*Vc*) were calculated using the material properties, shear span depth ratio, longitudinal steel ratio, and displacement ductility level of each test at different levels of deformation. Furthermore, in order to objectively compare all the specimens, actual values of the normalized coefficient (γ) that relates shear strength of the concrete (*Vc*) to displacement ductility levels were obtained using equation (Eq. 7-2). Finally, these values were compared to the predicted envelope proposed by the model for the coefficient (γ) versus displacement ductility levels as described by equation (Eq. 7-3). It is important to mention that coefficients (α) and (β) in equations (Eq. 2-12), (Eq. 2-13), and (Eq. 7-2) were constant values for all the specimens because they relate shear span depth ratio and longitudinal steel ratio respectively to the shear strength component of the concrete (*Vc*), and these values were the same for all the specimens. Finally, it is important to mention that equation (Eq. 7-3) for coefficient (γ) was modified for lightweight concrete (Kowalsky et al., 2000 b) based on large scale reversed loading tests of circular columns. It is the intention of this research to revise this equation to be applied for lightweight concrete square columns.

$$V_{c(Actual)} = V_{n(\mathrm{Re}corded)} - V_{s(\mathrm{Re}corded-Data)} - V_{p(\mathrm{Re}corded-Data)} \qquad \textbf{(Eq. 7-1)}$$

$$\gamma_{(Actual)} = \frac{V_{c(Actual)}}{\alpha\beta\sqrt{f'c}\left(0.8A_g\right)} \qquad \textbf{(Eq. 7-2)}$$

$$0.035 \le \gamma = 0.25 - 0.0358 \cdot (\mu_{\Delta} - 2) \le 0.25 \qquad \textbf{(Eq. 7-3)}$$

7.2.1 Lightweight Concrete Shear Strength

7.2.1.1 Shear Strength at Low Deformation Levels

For both sets of specimens, brittle and ductile shear failure specimens, coefficient (γ) is the variable that indicates the relationship between actual and predicted shear strengths of the concrete. For the case of the brittle shear failure specimens that failed at low levels of deformation, specifically for the normal weight concrete specimen (NW-NS-BSF), the model predicts the shear strength in the lower bound of the actual points, and with a good level of accuracy as shown in Figure 7.4 (a). On the other hand, for specimens (LW1, 2, & 3 –NS-BSF), the actual values of (γ) are consistently below the predicted shear capacity coefficient for low levels of deformation, and the difference is significant when considering the lower bound of (γ) values and the predicted envelope.

Moreover, based on the consistency of the pattern of the actual values of (γ) corresponding to all lightweight concrete and brittle shear failure specimens, it was observed that strength degradation occurred at lower levels of deformation for lightweight concrete if compared to the predicted envelope and to the actual values of (γ) of the normal weight concrete specimen. Specimen (NW-NS-BSF) was more consistent to the predicted envelope

regarding strength degradation. Finally, in order to accurately asses the shear strength component provided by lightweight concrete in square columns, the upper limit of the (γ) coefficient in equation (Eq. 7-3), equals to 0.29 for normal weight concrete (Kowalsky and Priestley, 2000 a) and equals to 0.25 for lightweight concrete (Kowalsky et al., 2000 b) should be revised and changed to a lower value of approximately (0.175) corresponding to the lower bound of the actual points obtained by the experimental tests of this research. In the same manner, the point in which shear strength degradation starts to occur in equation (Eq. 7-3), at a displacement ductility of two (Kowalsky et al., 2000 b), should also be revised and changed to a lower value of approximately (μ_{Δ}=1.5) for lightweight concrete square columns. An additional reduction of 30% in the (γ) coefficient (Kowalsky et al., 2000 b) as shown in (Eq. 7-3) is recommended for the lower limit at high levels of deformation based on the relative demand in the transverse reinforcement shear strength component (*Vs*) of all ductile shear failure tests. The model would remain the same except for equation (Eq. 7-3) instead of which a new equation (Eq. 7-4) should be considered for square lightweight concrete columns. However, further research is necessary to optimize and validated the recommendations of this research. It is also important to mention that this research has taken into account only normal strength lightweight concrete.

$$0.025 \le \gamma = 0.175 - 0.0358 \cdot (\mu_{\Delta} - 1.5) \le 0.175 \qquad \textbf{(Eq. 7-4)}$$

7.2.1.2 Shear Strength of Ductile Shear Failure Specimens

Regarding the actual concrete shear strength of all ductile shear failure specimens, it is important to mention that the failure mechanism was not of a shear type as expected. For that reason, the lower plateau corresponding to the concrete shear capacity envelope coefficient (γ) at high levels of deformation was revised considering relative demands in the transverse reinforcement shear strength component only. However, as shown in Figure 7.4 (b), the strength degradation of all lightweight ductile shear failure specimens is consistent with the predicted model when considering different levels of deformation, and it tends to decrease following the predicted curve. Significant shear strength degradation was observed but not enough to cause a shear failure. However, the results obtained represent valuable information about the shear performance of the specimens and can be used as a comparison of relative demands.

Consistent with the data obtained during the brittle shear failure tests, lightweight concrete specimens (LW1 & 2 –NS-DSF) have values of (γ) significantly below the values obtained by specimen (NW-NS-DSF). On the contrary, specimen (LW3–NS-DSF) showed values of (γ) slightly over the values obtained by specimen (NW-NS-DSF). In the same manner, there is a relative difference between actual (γ) values, considering the lower bound of points corresponding to normal and lightweight concrete specimens than ranged between (0.05 to 0.15), Figure 7.4 (b). This is consistent with the observations pertaining (γ) values for brittle shear failure specimens, Figure 7.4 (a). In the cases of specimen (LW1 & 2 –NS-DSF), the

shear capacity was lower than the predicted by the analytical model at various levels of deformation as shown in Figure 7.4 (b). Finally, the actual values of (γ) corresponding to all lightweight concrete ductile shear failure tests were consistent and followed the same pattern.

7.2.1.3 Actual versus Predicted Shear Strength

Figure 7.5 and Figure 7.6 show the recorded lateral force versus displacement response, the theoretical flexural response, and the predicted shear capacity and design envelopes for all brittle and ductile shear failure specimens. The predicted values were calculated using a program (CUMBIA) developed by Montejo and Kowalsky (2006).

Theoretical flexural response is obtained from section analysis using the Mander model for confined concrete (Mander et al., 1988). Calculations considered either normal or lightweight concrete stress-strain relationships as proposed by Mander et al. (1988) for normal weight concrete, and as modified for lightweight concrete by Kowalsky et al. (2000 b). CUMBIA program also takes into account flexural and shear deformation components for the force displacement response of the system. Top displacements due to flexural deformation are estimated by the plastic hinge method proposed by Priestley et al. (1996) that simplifies the curvature distribution along the member, considering plastic deformation, to estimate displacements by the application of the moment-area method. Top displacements due to shear deformation are calculated by the application of a simplified method suggested by Priestley et al. (2006) based on three shear deformation components. One component considers shear stiffness in the elastic range prior to cracking as a function of the flexural

stiffness, the second component after shear cracking takes into account an equivalent strut-and-tie model for shear flexibility up to nominal moment, and the third component beyond yield where shear deformation is recommended to be increased in proportion to the flexural deformation after yield. Finally, CUMBIA predicts shear strength capacity and calculates design values considering the shear transfer mechanism described in section 7.2.

Top displacements due to shear deformation were considered for this research taking into account the shear span depth ratio of the specimens (M/VD = 2.57 < 3) as recommended by Priestley et al. (2006) when assessing a force displacement response. However, details of the above mentioned calculations are beyond the scope of this research and are not going to be discussed in this document since the objective of the research is to asses the shear performance of lightweight under seismic demands. In any case, comments about the differences between predicted and actual test data are presented, so analytical models might be validated or improved in the future considering the information presented in this document.

In the case of specimen (NW-NS-BSF), the predicted flexural response was consistent with the actual response and the specimen failed when the shear demand was very close to the predicted shear capacity as shown in Figure 7.5 (a). The predicted flexural response was also consistent with the actual response of specimens (LW1, 2, & 3-NS-BSF), but all lightweight concrete specimens failed at a significant lower lateral load than the predicted shear demand as shown in Figure 7.5 (b, c, & d). Specimen (LW1-NS-BSF) developed slightly less

stiffness than the predicted. This information confirms the necessity of reducing the predicted concrete shear strength component (Vc) for lightweight concrete square columns as recommended in section 7.2.1.1.

Figure 7.6 illustrates what was observed and described in previous sections regarding the failure mode of all ductile shear failure specimens. A flexural failure mechanism is explained by the difference between the actual shear demand and the predicted shear capacity calculated with actual concrete strengths of each specimen. It is important to notice that for specimen (NW-NS-DSF) the predicted and actual flexural response is very consistent. Even though something similar occurs with specimens (LW1, 2, & 3 -NS-DSF), a negative post-yield stiffness tends to occur earlier in contrast to the predicted response. It also appears as if the prediction is overestimating the initial stiffness of the specimens, especially in the case of specimen (LW3 -NS-DSF) as shown in Figure 7.6 (d). However, this may be explained by additional displacement components not measured during the test such as additional displacement due to rigid body rotation of the column-footing beam connection, or due to flexural and shear deformation of the above mentioned connection.

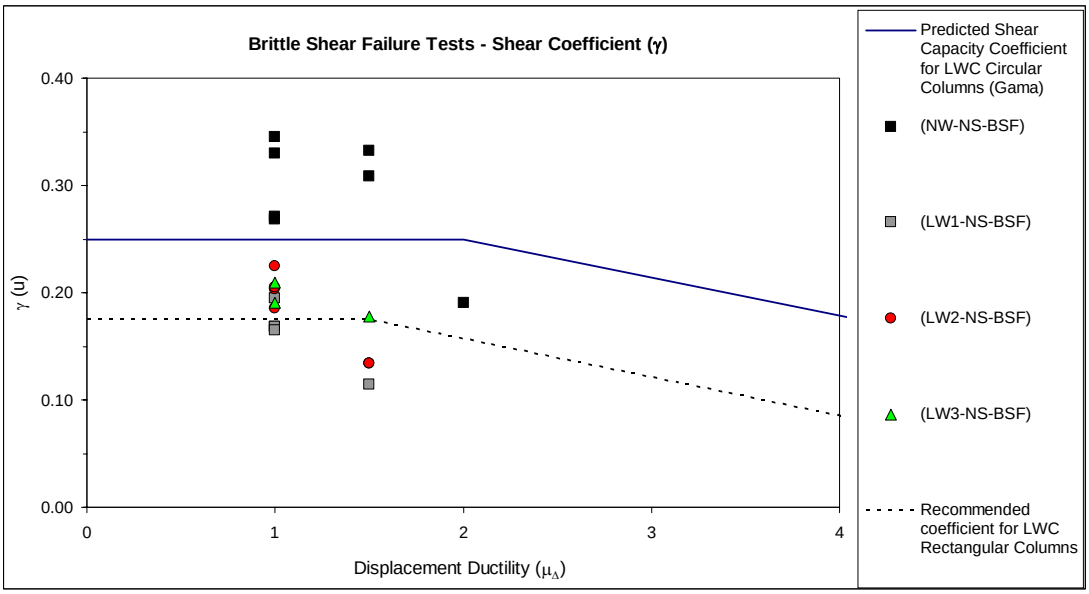

a) Actual Shear Capacity Coefficients – Brittle Shear Failure Tests

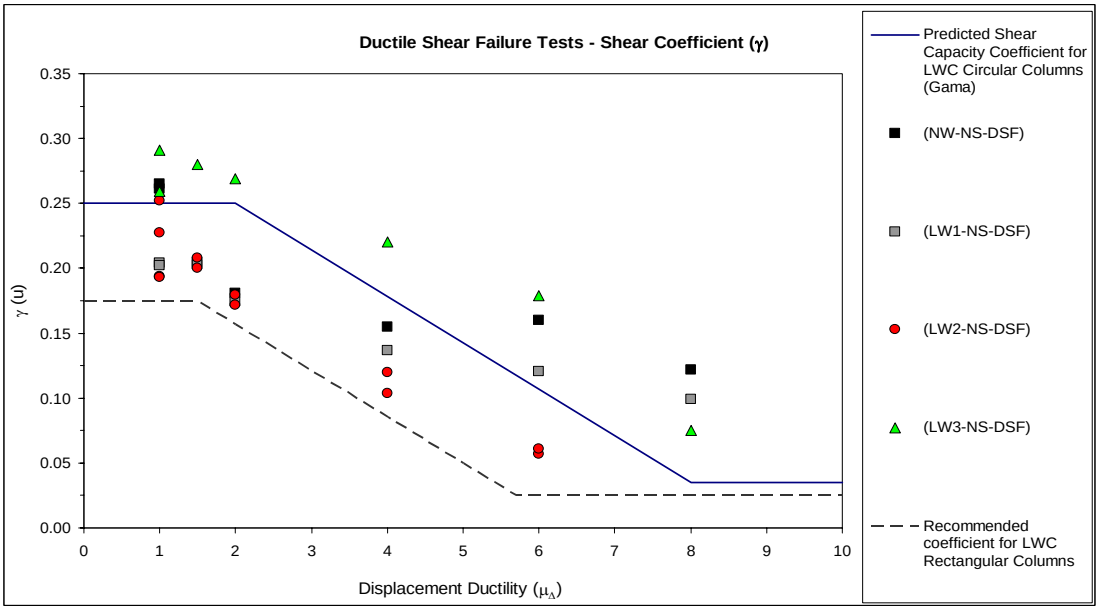

b) Actual Shear Capacity Coefficients – Ductile Shear Failure Tests

Figure 7.4. Actual Shear Capacity Coefficients

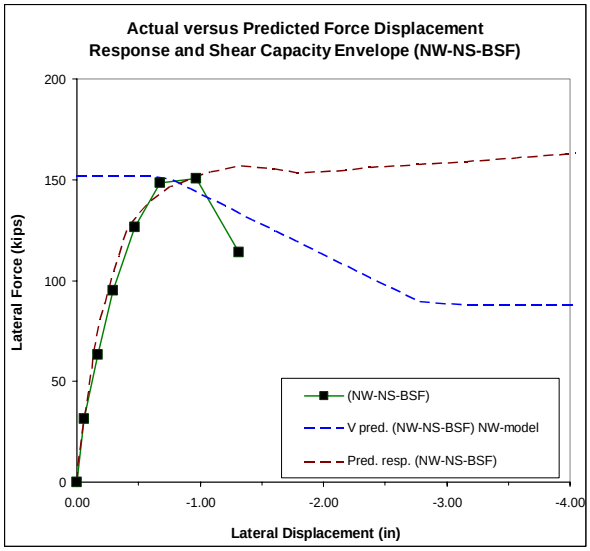

a) Specimen (NW-NS-BSF)

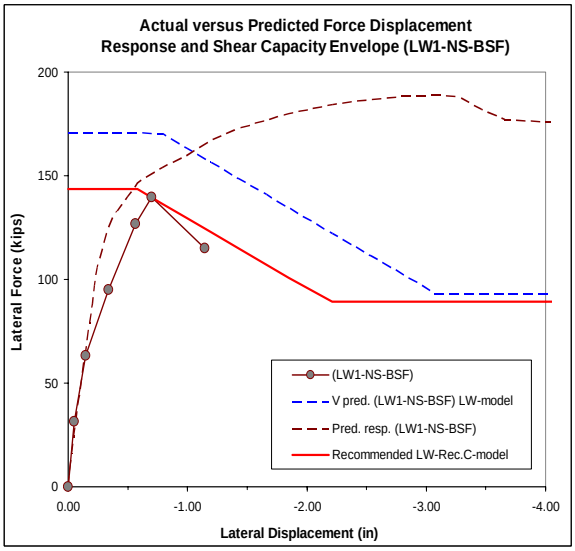

b) Specimen (LW1-NS-BSF)

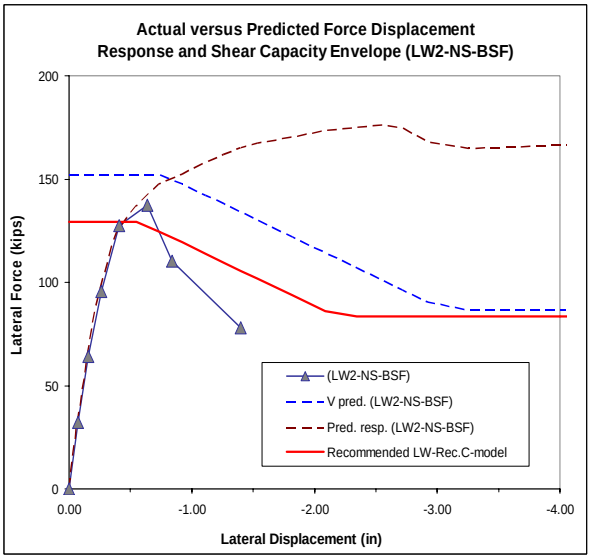

c) Specimen (LW2-NS-BSF)

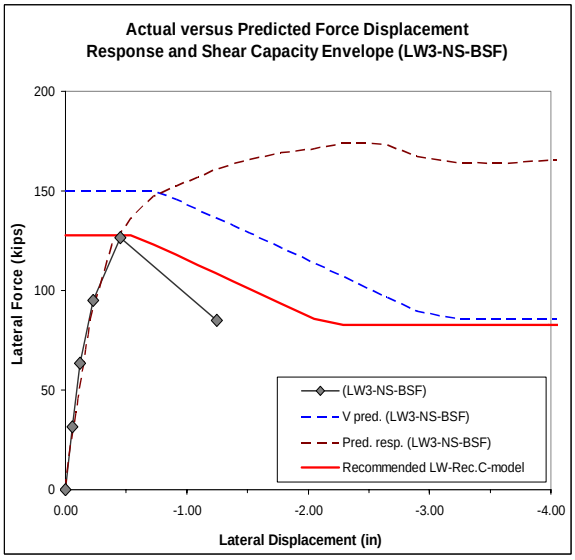

d) Specimen (LW3-NS-BSF)

Figure 7.5. Actual and Predicted Force Displacement Response – Brittle Shear Failure Specimens

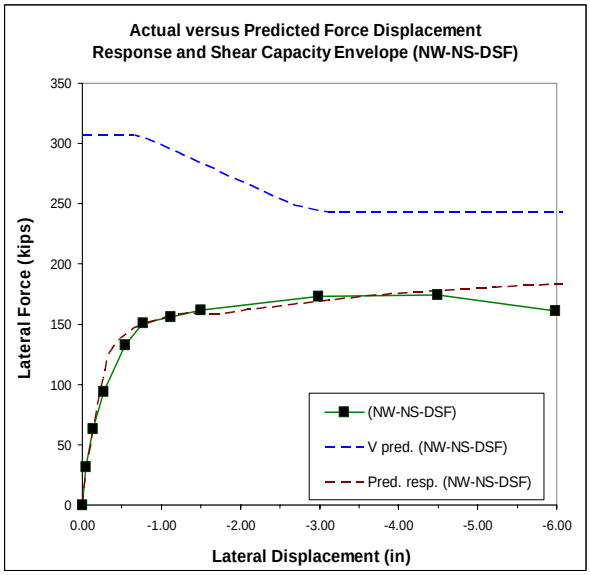

a) Specimen (NW-NS-DSF)

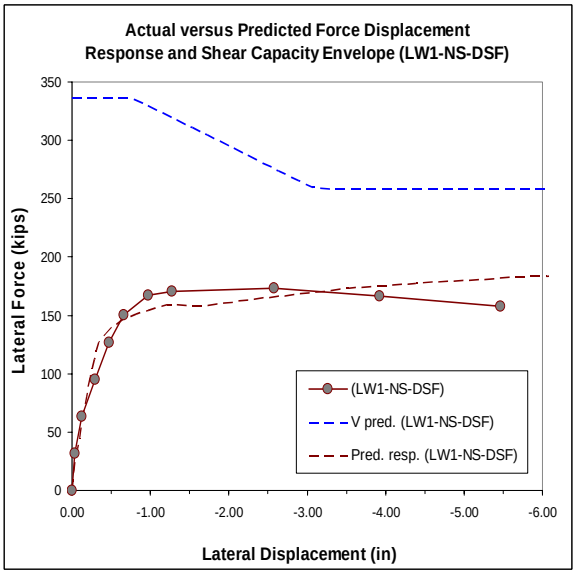

b) Specimen (LW1-NS-DSF)

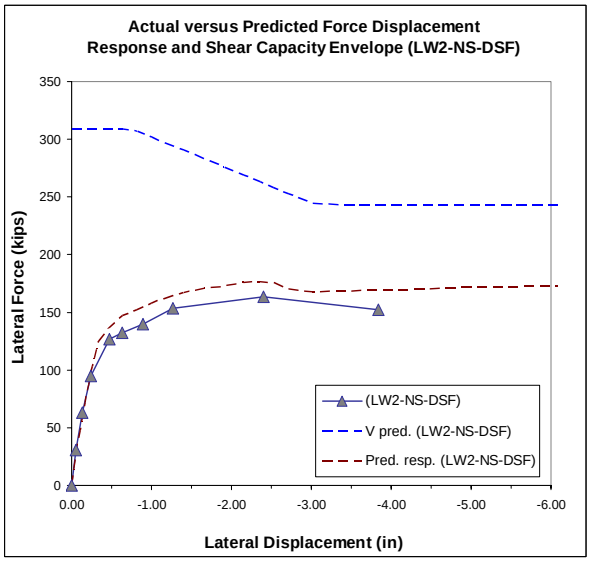

c) Specimen (LW2-NS-DSF)

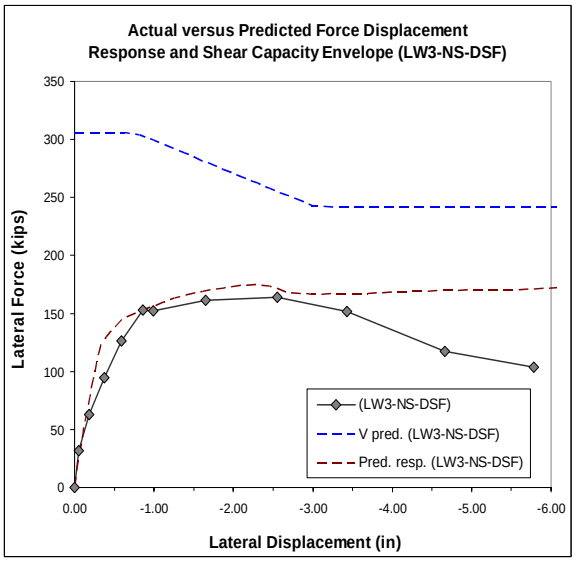

d) Specimen (LW3-NS-DSF)

Figure 7.6. Actual and Predicted Force Displacement Response – Ductile Shear Failure Specimens

7.3 Flexural and Shear Deformation

The two principal components of deformation are discussed in this section for all brittle and ductile shear failure specimens. All the calculations are based on actual data recorded during the tests as included in the appendix. Moreover, with the instrumentation (linear potentiometers) placed on the specimens, curvature and shear strain profiles were obtained at different levels of deformation, and top displacements due to shear and flexural deformation were calculated with that information. Furthermore, shear and flexural top displacement components were compared to total top displacements of each specimen in chapter 5 and 6. Finally, displacement components of all brittle and ductile shear failure specimens are compared in this section to determine the differences in shear performance.

7.3.1 Brittle Shear Failure Specimens – Deformation

In terms of flexural deformation, the behavior was very consistent for all brittle shear failure specimens. Figure 7.7 (a) shows top displacements due to flexural deformation versus total top column displacement graphs. In all cases, the rate of increment in the flexural displacement component tends to decrease as the total column displacement increases. Moreover, compared to the shear displacement component shown in Figure 7.7 (b), the maximum flexural displacement component is always lower than the shear one in all cases. In the same manner, all brittle shear failure specimens performed consistently in terms of shear deformation. Indeed, the shear displacement component was not significant at low

levels of deformation, but the rate of increment continued increasing as the top column displacement increased. In addition, for all the specimens there is a well defined kink in which the rate of increment changes significantly around the equivalent yielding point, and the rate of increment in the shear displacement component increases even more.

The shear displacement component of specimen (NW-NS-BSF) is clearly in the lower bound of all brittle shear failure points, Figure 7.7 (b). Being consistent, the same can be observed for specimen (NW-NS-DSF) as shown in Figure 7.12. As a result, lightweight concrete specimens developed slightly more shear deformation, and consequently a more brittle behavior as discussed in chapter five.

7.3.1.1 Actual and Predicted Force versus Displacement Component Response

Actual and predicted lateral force versus displacement component responses for all brittle shear failure tests are shown in Figure 7.8, Figure 7.9, Figure 7.10, and Figure 7.11. In the case of specimen (NW-NS-BSF) the actual and predicted values of shear demand are very consistent as shown in Figure 7.8 (b). However, in all lightweight concrete brittle shear failure specimens (LW1, 2, & 3-NS-BSF) the predicted response overestimates the shear strength as well as the stiffness and consequently the shear modulus. This observation is important to confirm the necessity of reducing the predicted shear strength of lightweight concrete square columns. In terms of deformation, it can also be deduced that lightweight concrete is more flexible than normal weight concrete. This is something that can be explained considering that the effect of aggregate interlock is reduced in lightweight concrete

where the fracture surface is smoother. Finally, regarding flexural displacement component responses of all brittle shear failure tests, it appears that the predicted values tend to slightly underestimate the flexural stiffness in the linear range.

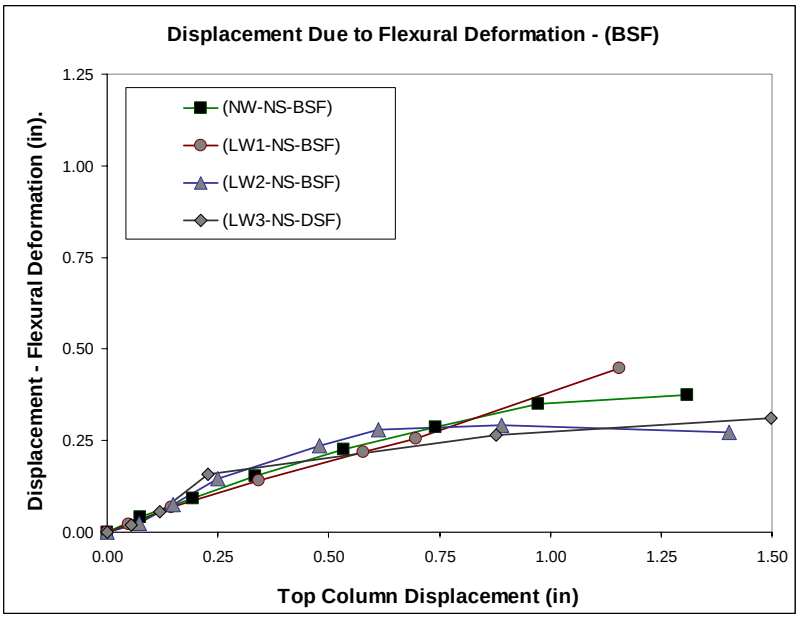

a) Flexural Displacement Component – Brittle Shear Failure Tests

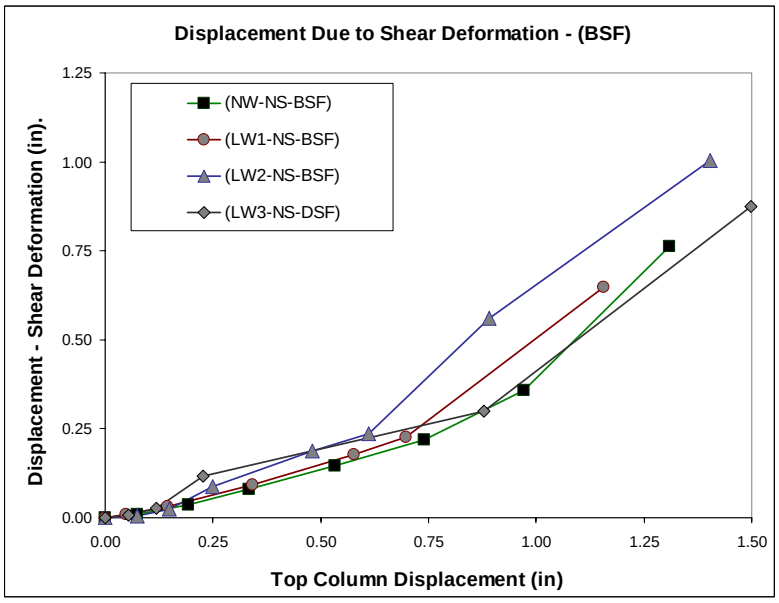

b) Shear Displacement Component – Brittle Shear Failure Tests

Figure 7.7. Displacement Components – Brittle Shear Failure Specimens

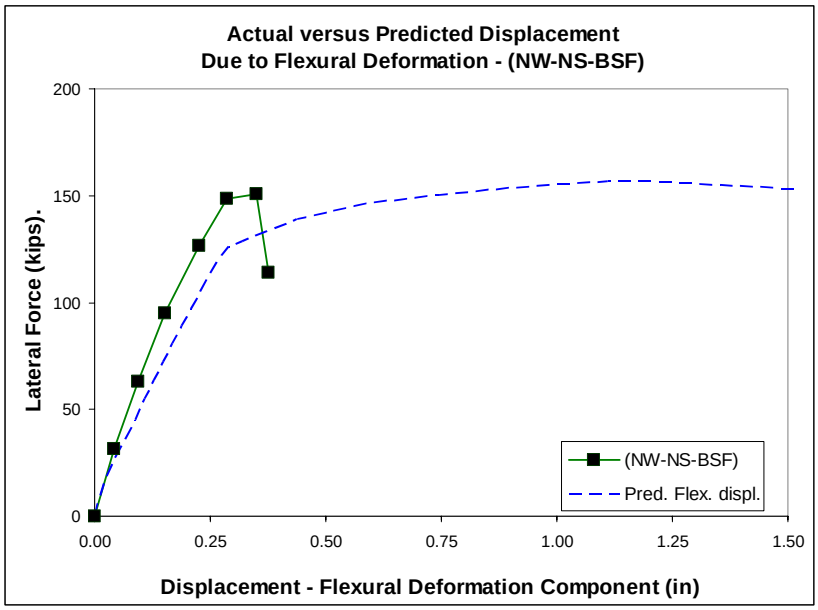

a) Actual and Predicted Flexural Displacement Component – (NW-NS-BSF)

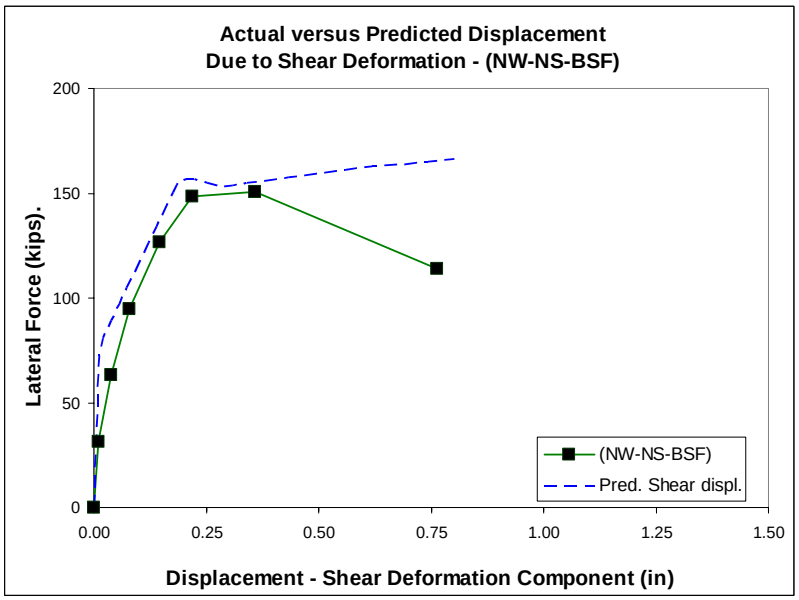

b) Actual and Predicted Shear Displacement Component – (NW-NS-BSF)

Figure 7.8. Actual and Predicted Displacement Components – (NW-NS-BSF)

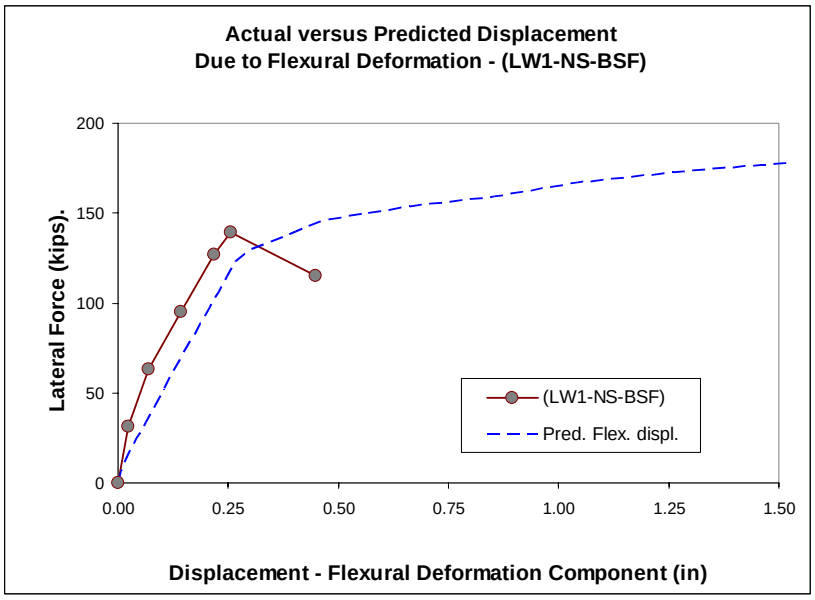

a) Actual and Predicted Flexural Displacement Component – (LW1-NS-BSF)

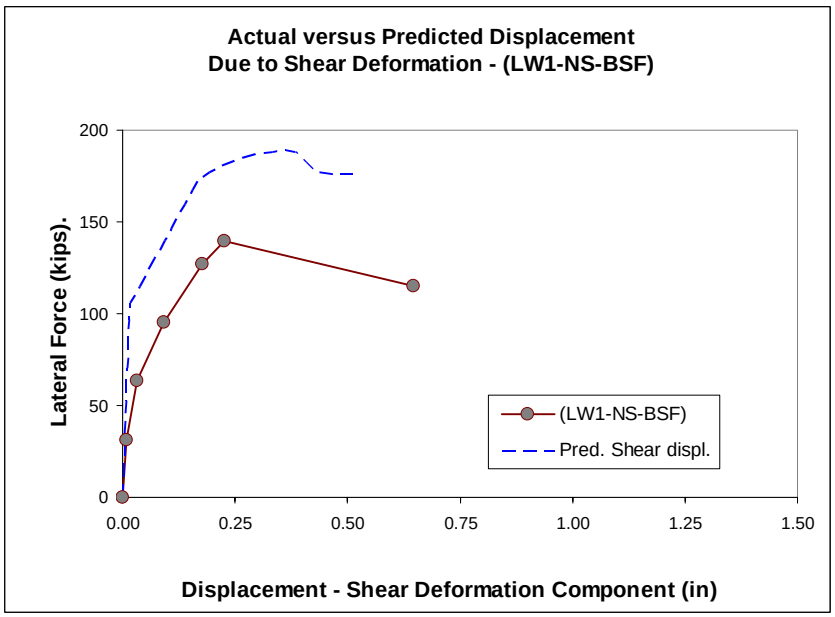

b) Actual and Predicted Shear Displacement Component – (LW1-NS-BSF)

Figure 7.9. Actual and Predicted Displacement Components – (LW1-NS-BSF)

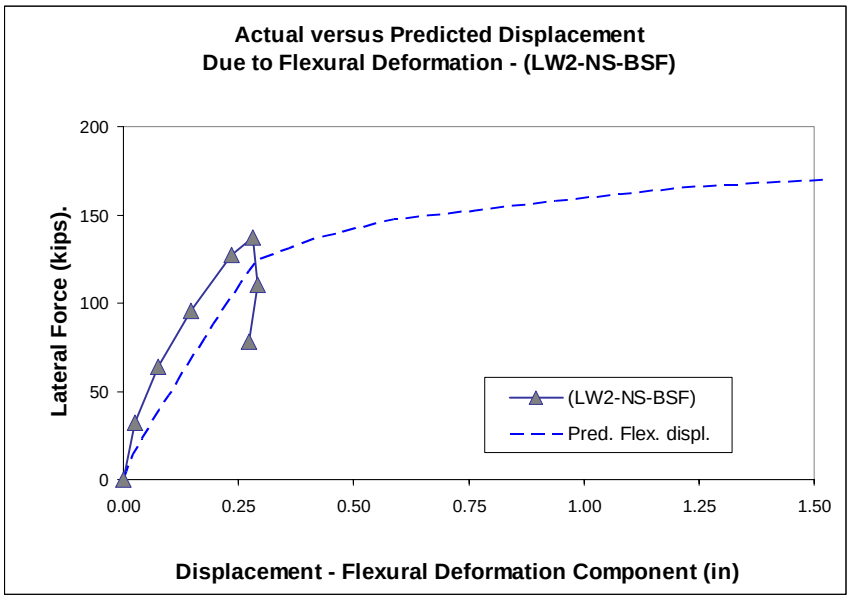

a) Actual and Predicted Flexural Displacement Component – (LW2-NS-BSF)

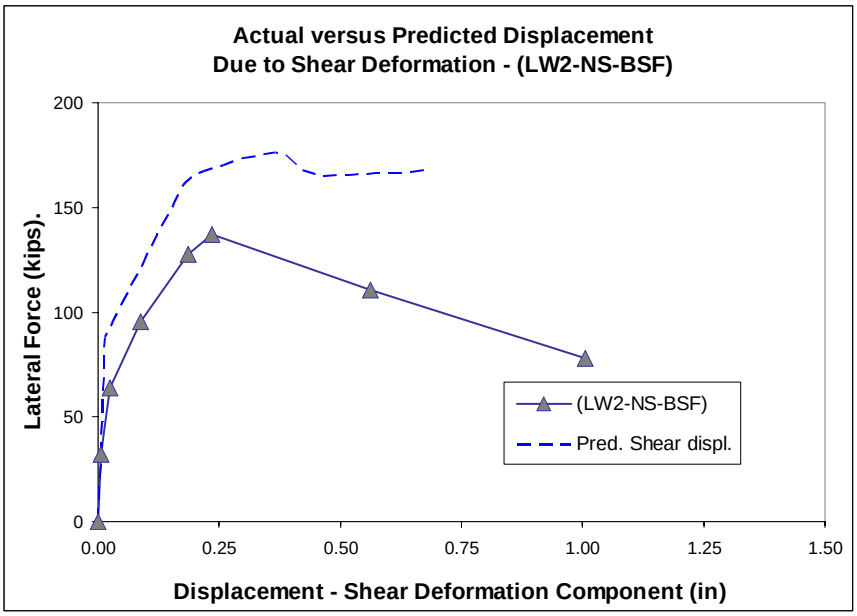

b) Actual and Predicted Shear Displacement Component – (LW2-NS-BSF)

Figure 7.10. Actual and Predicted Displacement Components – (LW2-NS-BSF)

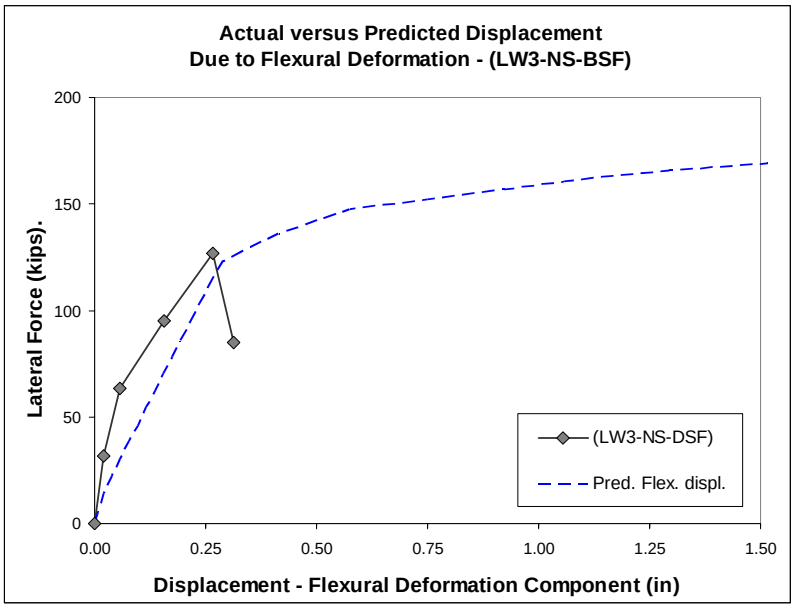

a) Actual and Predicted Flexural Displacement Component – (LW3-NS-BSF)

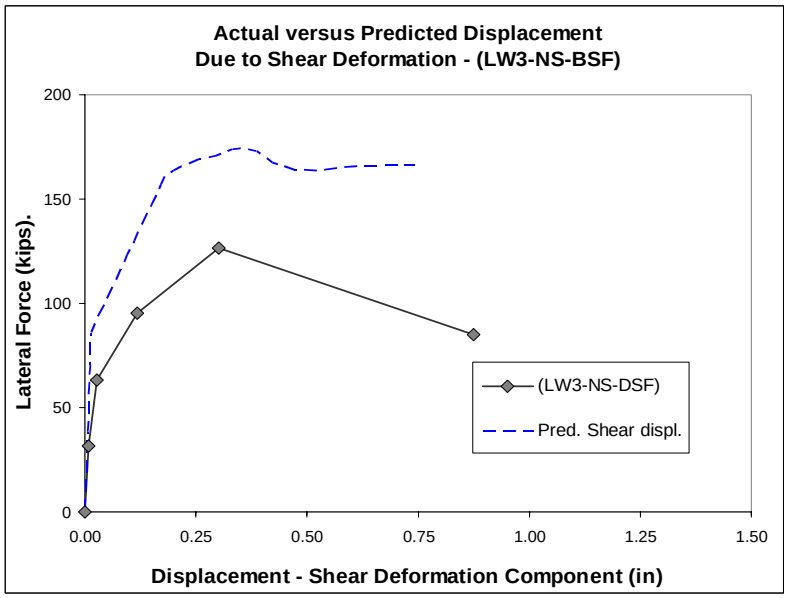

b) Actual and Predicted Shear Displacement Component – (LW3-NS-BSF)

Figure 7.11. Actual and Predicted Displacement Components – (LW3-NS-BSF)

7.3.2 Ductile Shear Failure Specimens - Deformation

Similarly to brittle, ductile shear failure specimens behaved consistently in terms of flexural and shear deformation as shown Figure 7.12 (a & b). Flexural displacement component also tended to decrease towards high levels of deformation, but this was not as evident as in all brittle shear failure tests. Regarding shear displacement components, shown in Figure 7.12 (b), they were not significant at low levels of deformation, but the rate of increment continued increasing as the top column displacement increased. Finally, as observed in the brittle shear failure specimens, the shear displacement component of specimen (NW-NS-DSF) is also in the lower bound of all ductile shear failure points as shown in Figure 7.12 (b). As a result, lightweight concrete specimens developed more shear deformation, and consequently a more brittle behavior was observed.

7.3.2.1 Actual and Predicted Force versus Displacement Component Response

Actual and predicted lateral force versus displacement component responses for all brittle shear failure tests are shown in Figure 7.13, Figure 7.14, Figure 7.15, and Figure 7.16. Regarding specimen (NW-NS-DSF), force versus shear and flexural displacement component responses are consistent with predicted values as shown in Figure 7.13. In the case of lightweight concrete ductile shear failure specimens, the predicted flexural displacement component response tends to develop a positive post-yield slope in contrast to recorded data that exhibits negative slopes as shown in figures Figure 7.14 (a) and Figure

7.16 (a). Consistent with observations about brittle shear failure specimens, predicted values tend to slightly underestimate the flexural displacement component stiffness in the linear range in all ductile shear failure tests. In terms of shear deformation of all ductile shear failure specimens, the predicted response overestimates the shear strength as well as the stiffness and consequently the shear modulus. This observation is consistent with predicted data for all brittle shear failure tests. In addition, shear deformation is underestimated in all cases as shown in Figure 7.13 (b), Figure 7.14 (b), Figure 7.15 (b), and Figure 7.16 (b).

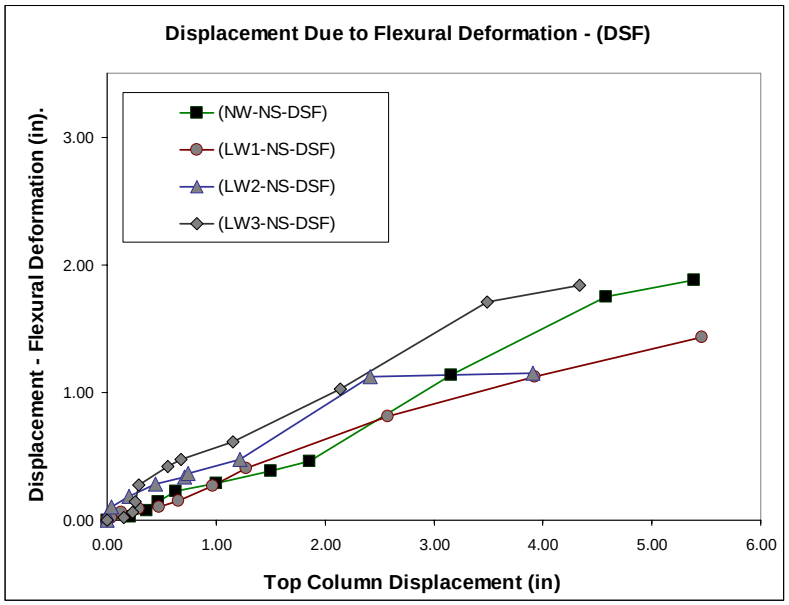

a) Flexural Displacement Component – Ductile Shear Failure Tests

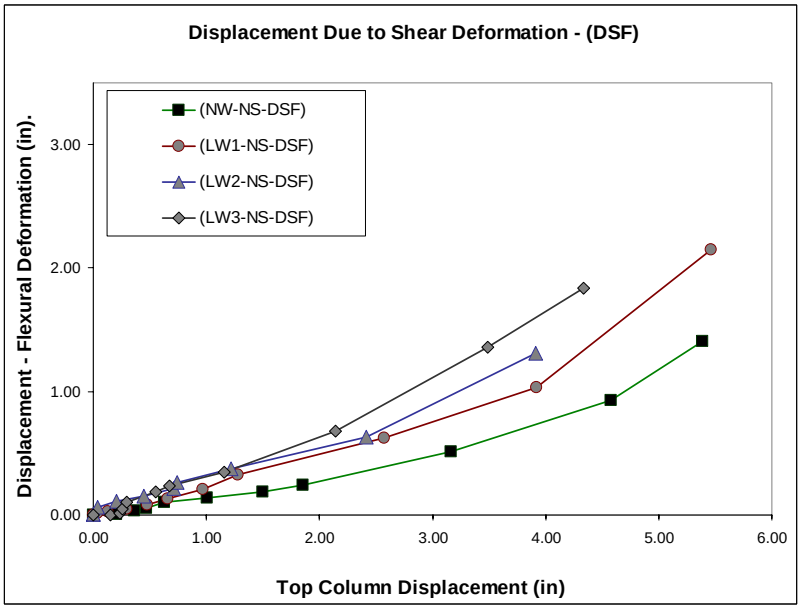

b) Shear Displacement Component – Ductile Shear Failure Tests

Figure 7.12. Displacement Components – Ductile Shear Failure Specimens

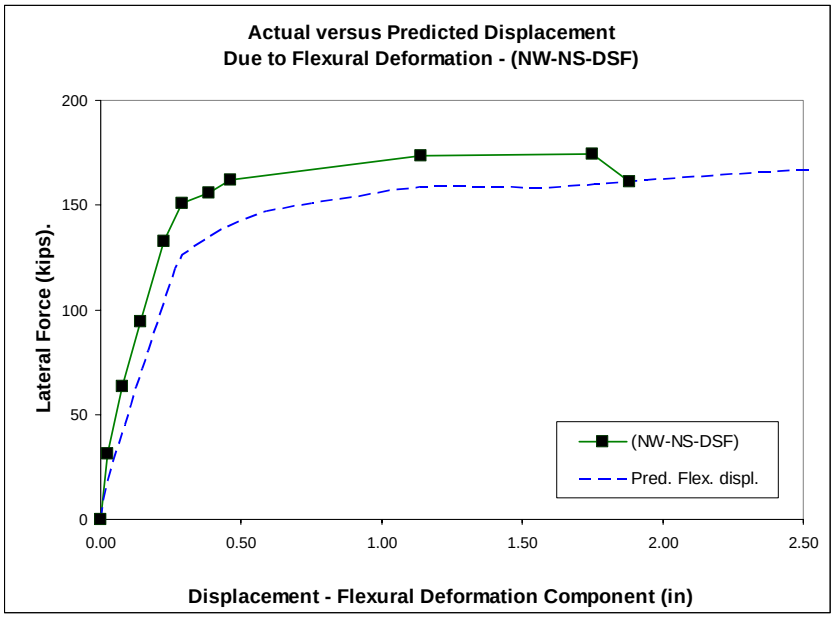

a) Actual and Predicted Flexural Displacement Component – (NW-NS-DSF)

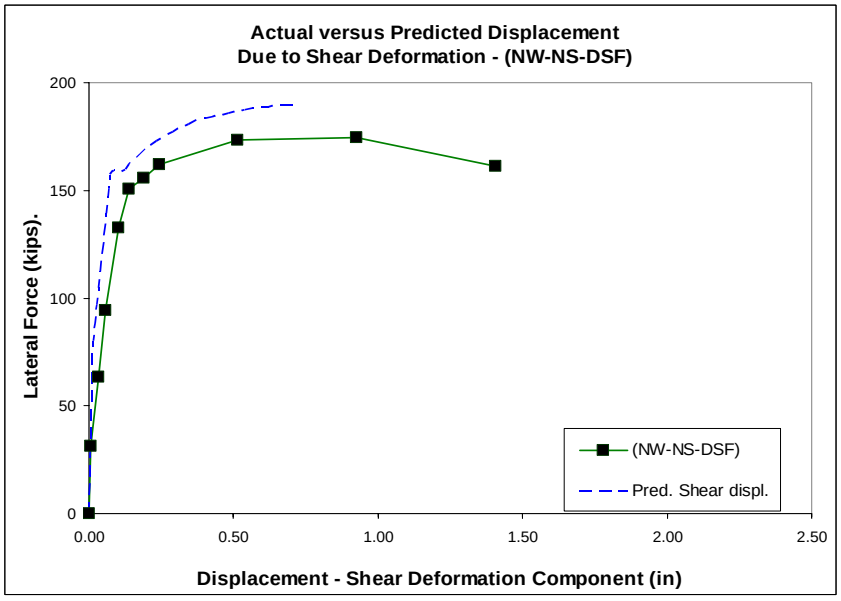

b) Actual and Predicted Shear Displacement Component – (NW-NS-DSF)

Figure 7.13. Actual and Predicted Displacement Components – (NW-NS-DSF)

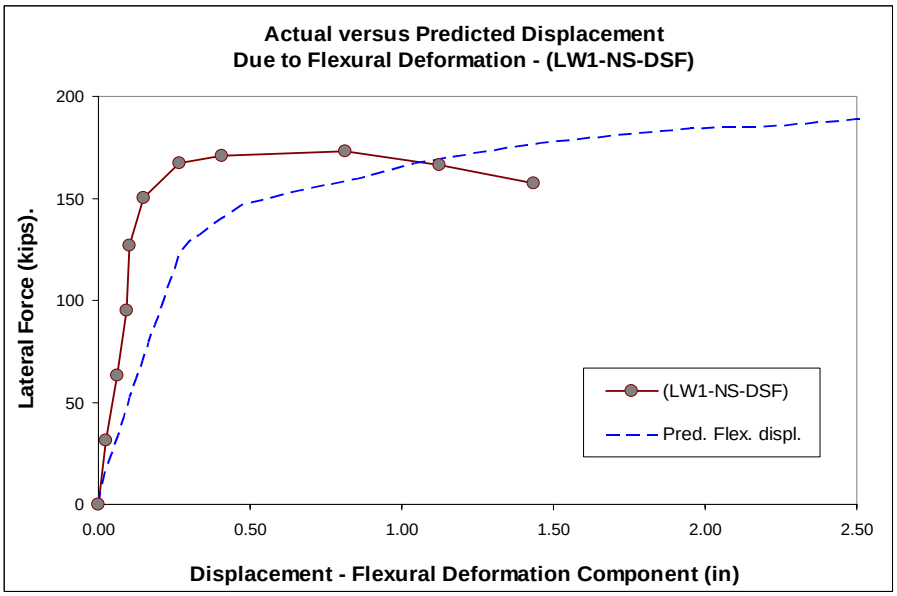

a) Actual and Predicted Flexural Displacement Component – (LW1-NS-DSF)

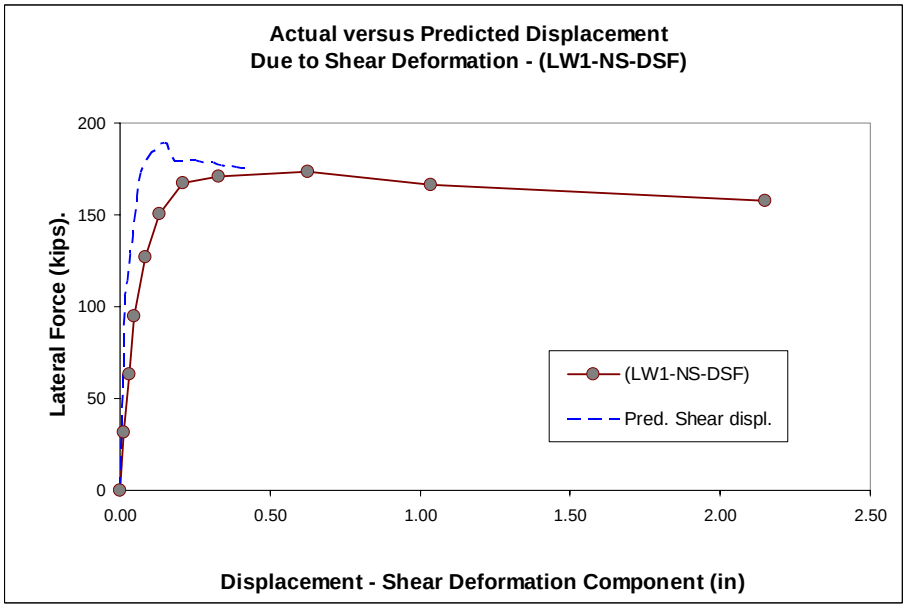

b) Actual and Predicted Shear Displacement Component – (LW1-NS-DSF)

Figure 7.14. Actual and Predicted Displacement Components – (LW1-NS-DSF)

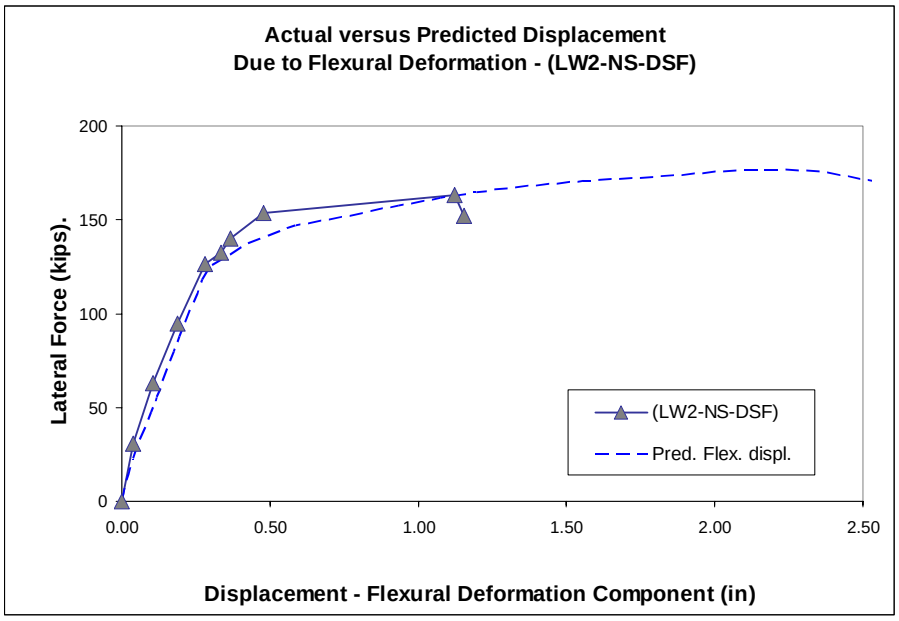

a) Actual and Predicted Flexural Displacement Component – (LW2-NS-DSF)

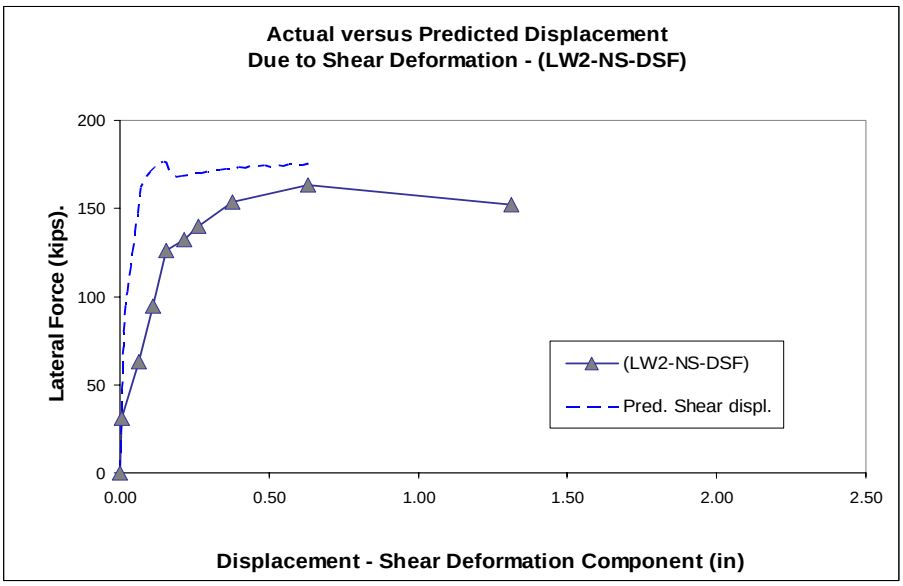

b) Actual and Predicted Shear Displacement Component – (LW2-NS-DSF)

Figure 7.15. Actual and Predicted Displacement Components – (LW2-NS-DSF)

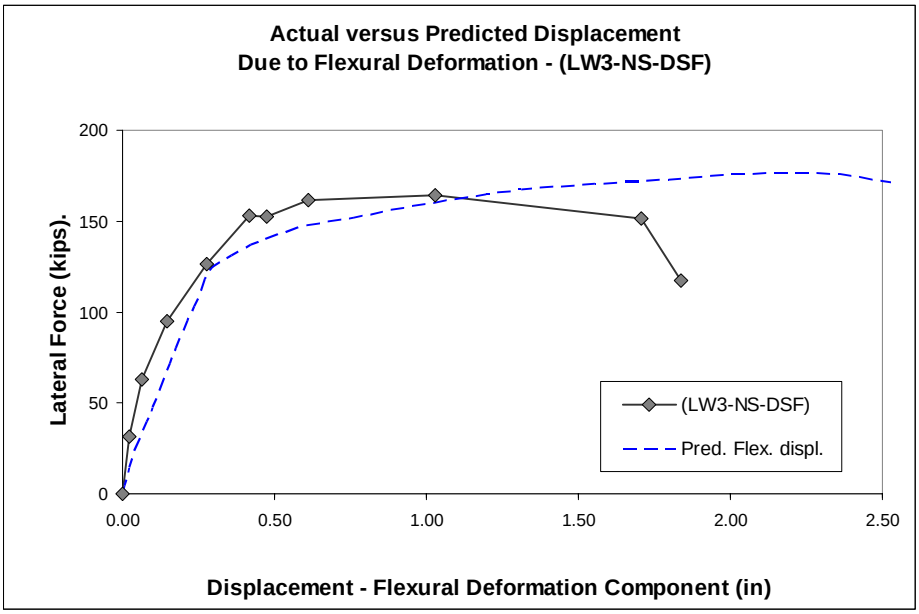

a) Actual and Predicted Flexural Displacement Component – (LW3-NS-DSF)

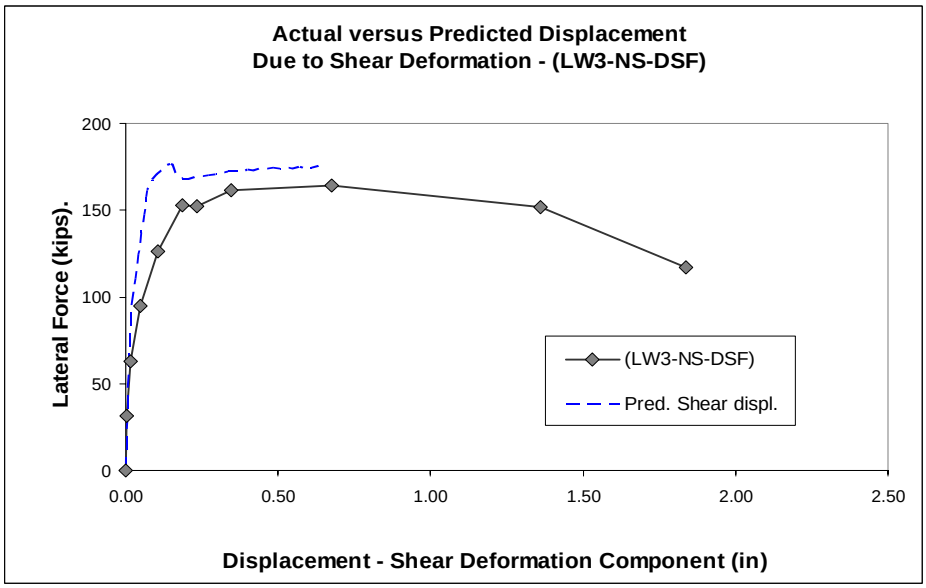

b) Actual and Predicted Shear Displacement Component – (LW3-NS-DSF)

Figure 7.16. Actual and Predicted Displacement Components – (LW3-NS-DSF)

7.4 Energy Dissipation and Damping

7.4.1 Brittle Shear Failure Specimens - Damping

In order to have a better understanding of the shear performance of reinforced lightweight concrete square columns, under cyclic lateral demands such as seismic events, indicators of the energy dissipation capacity represent valuable information to be analyzed and compared. In fact, when reinforced concrete elements are subjected to reversed cyclic hysteretic loading with significant displacements in the non-linear range, most of the energy dissipated comes from the behavior beyond yielding and due to plastic deformation of the reinforcement steel. The total amount of the above mentioned hysteretic energy is represented by the sum of subsequent areas defined by each hysteretic loop. As a result, considering also that the equivalent damping coefficient (Jacobsen, 1930) is proportional to the hysteretic energy dissipated by the specimen at each level of deformation, the damping coefficient is an indicator of the capacity of the element to dissipate energy under cyclic demands in non-linear range. In the case of this research, considering the same configuration and specifications of the specimens, expect for the aggregate type and the shear reinforcement, a relative comparative analysis can be done using the hysteretic damping coefficient as a good relative indicator of the energy absorption capacity of the elements.

Considering the criterion proposed by Jacobsen in which all cycles before reaching the maximum displacement are ignored, an approximate value of the hysteretic damping

coefficient was calculated for each specimen. This was considered a valid procedure taking into account the purpose of obtaining this information a relative measurement of the energy dissipation capacity and to be compared between specimens of the similar characteristics. Consequently, the capacity of reinforced lightweight concrete to dissipate energy was compared to the capacity of reinforced normal weight concrete for square columns.

In addition, hysteretic damping coefficients were estimated for brittle shear failure specimens (NW, LW1 & 2–NS-BSF) using equation (Eq. 7-6) as a function of the ratio between the areas of the hysteretic loop at the maximum level of deformation and the respective area of a rigid perfectly plastic loop that coincides with the maximum displacements as shown in Figure 7.17 (a, b, & c). The areas of the hysteretic loops at maximum deformation levels were calculated as the area of a polygon considering all the recorded points or coordinates. Furthermore, the equivalent damping coefficient can be estimated using equation (Eq. 7-5) where the viscous damping is added to the hysteretic damping coefficient. Finally, the viscous damping can be assumed to have a constant value, so the hysteretic damping is the variable used as a relative measurement of the energy dissipation capacity to be compared between the specimens.

$$\xi_{eq} = \xi_{v} + \xi_{hyst} \qquad \textbf{(Eq. 7-5)}$$

$$\xi_{hyst} = \frac{A_{loop}}{A_{RPP}} \cdot \frac{2}{\pi} \qquad \textbf{(Eq. 7-6)}$$

Consistent with the shear failure mechanism and with the low displacement capacity of the specimens, values of hysteretic damping coefficients obtained for brittle shear failure specimens (NW, LW1 & 2–NS-BSF) show a low energy absorption capacity in all cases. In fact if a 5.00% viscous damping is assumed, the equivalent damping coefficient of the specimens will have values between (ξ = 0.12 to 0.14). In any case, it is important to notice that the maximum damping coefficient corresponds to the normal weight concrete specimen (NW-NS-BSF) as shown in Figure 7.17 (a). Apparently, reinforced lightweight concrete square columns under cyclic shear demands tend to develop less energy dissipation capacity compared to those made of normal weight concrete. However the difference between the hysteretic damping coefficients of normal and lightweight concrete is not significant.

7.4.2 Ductile Shear Failure Specimens - Damping

Hysteretic damping coefficients were also estimated for ductile shear failure specimens (NW, LW1, 2, & 3–NS-DSF). In the same manner, equation (Eq. 7-6) was used to determine the value of the hysteretic damping coefficient as a function of the ratio between the areas of the hysteretic loop at the maximum level of deformation and the respective area of a rigid perfectly plastic loop that coincides with the maximum displacements as shown in Figure 7.18.

Also consistent with the failure mechanism and with the high displacement capacity, all ductile shear failure specimens developed hysteretic damping coefficients with significantly higher energy absorption capacity compared to brittle shear failure specimens. Moreover, if

a 5.00% viscous damping is assumed, the equivalent damping coefficient of the ductile shear failure specimens had values between (ξ = 0.20 – 0.25) compared to values between (ξ = 0.12 to 0.14) of the brittle shear failure specimens. As a result, ductile shear failure specimens developed approximately twice the energy absorption capacity developed by brittle shear failure specimens. The above mentioned fact is desirable for specimens under seismic demands either if the elements are made of normal or lightweight concrete. In fact, all the specimens had the same shear span depth ratio, longitudinal steel ratio, and were subjected to the same axial load and cyclic lateral loading demands. However, the difference in the amount of transverse steel ratio and the better concrete confinement provided to the ductile shear failure specimens by additional stirrups and less spacing between them, enhanced the performance of the specimens significantly, and increased the energy dissipation capacity as well as the displacement ductility capacity either for reinforced normal or lightweight concrete elements.

It is important to notice that the maximum damping coefficient corresponds to the normal weight concrete specimen (NW-NS-DSF) as it happened with specimen (NW-NS-BSF) and as shown in Figure 7.18 (a). Once again, reinforced lightweight concrete square columns under cyclic shear demands tend to develop less energy dissipation capacity compared to those made of normal weight concrete. However, it is important to mention that the difference was not significant, and that all specimens behaved consistently in terms of energy dissipation.

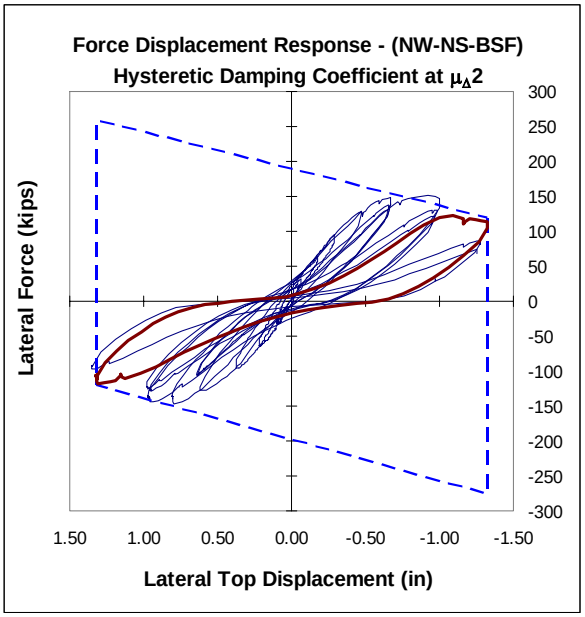

a) Damping: ξ_{hyst} = 8.32% (NW-NS-BSF)

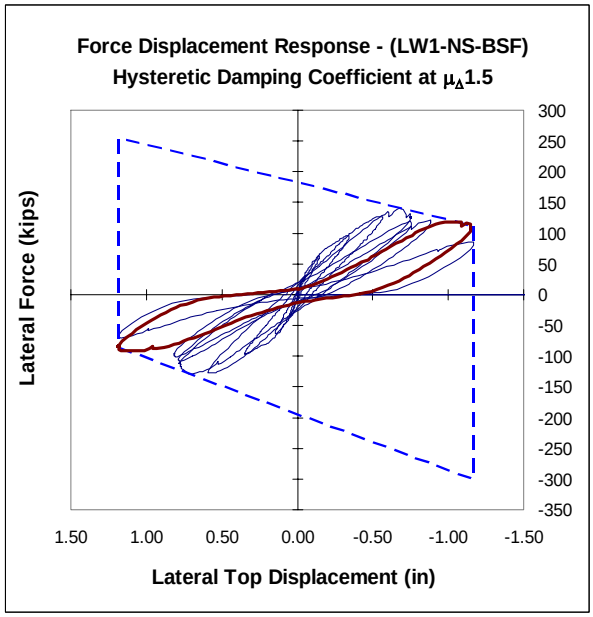

b) Damping: ξ_{hyst} = 7.35% (LW1-NS-BSF)

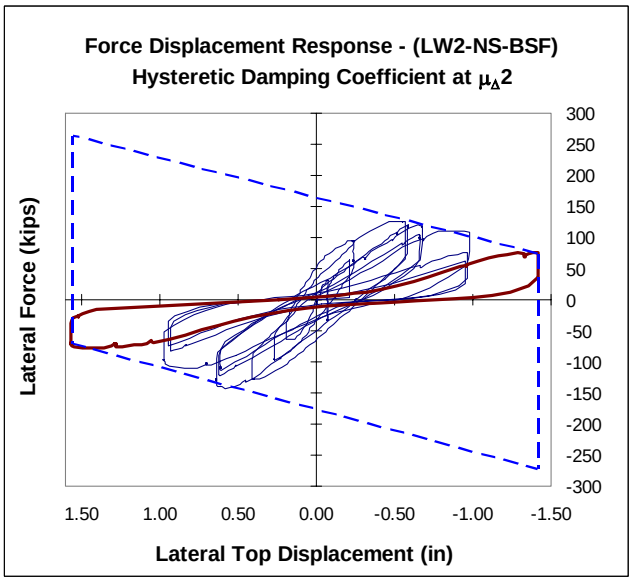

c) Damping: ξ_{hyst} = 7.51% (LW2-NS-BSF)

Figure 7.17. Hysteretic Damping Coefficients – Brittle Shear Failure Specimens

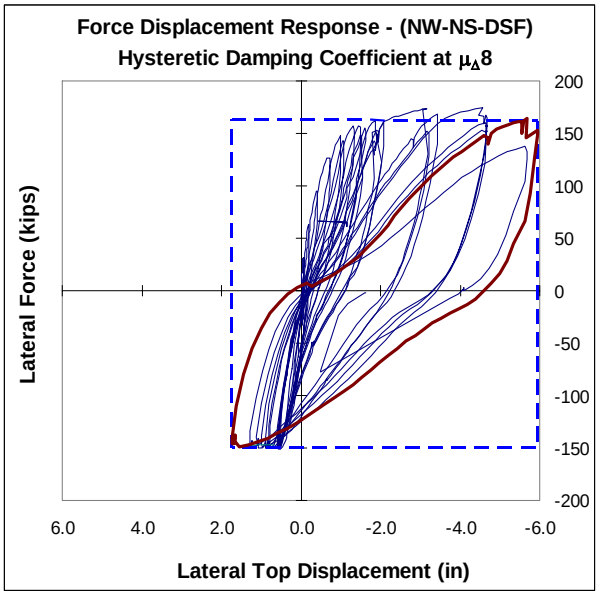

a) Damping: ξ_{hyst} = 24.41% (NW-NS-DSF)

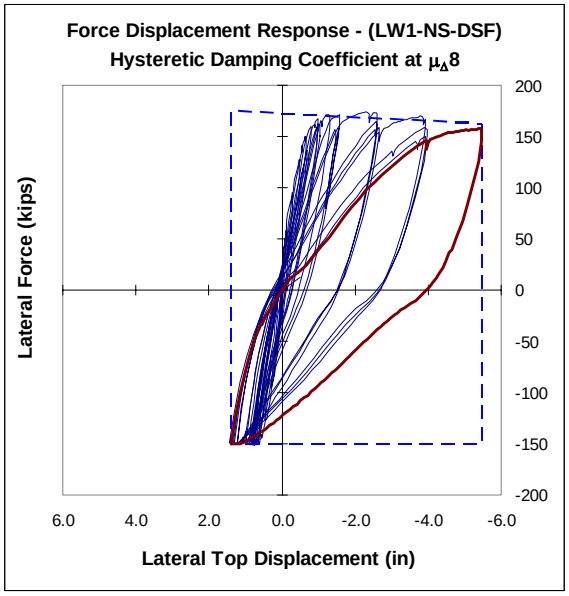

b) Damping: ξ_{hyst} = 24.03% (LW1-NS-DSF)

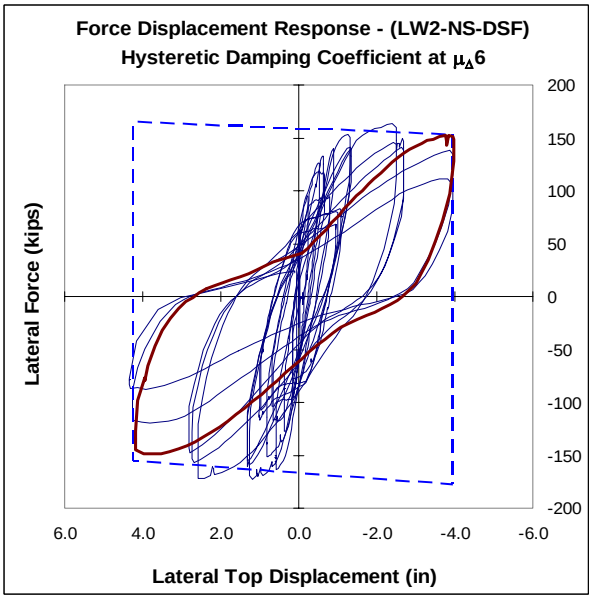

c) Damping: ξ_{hyst} = 22.26% (LW2-NS-DSF)

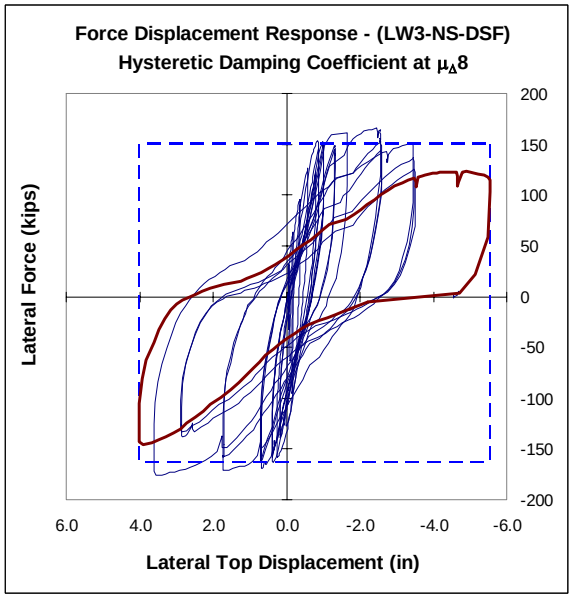

d) Damping: ξ_{hyst} = 20.55% (LW3-NS-DSF)

Figure 7.18. Hysteretic Damping Coefficients – Ductile Shear Failure Specimens

7.5 Failure Mechanism

It was observed that the failure mechanism corresponding to specimens (NW-NS-BSF), (LW1-NS-BSF), (LW2-NS-BSF), and (LW3-NS-BSF) was of a brittle shear failure type at low levels of deformation (μ_Δ = 1.5 & 2). In all cases, significant shear strength degradation was observed in the non-linear range. There was severe damage due to crushing of the concrete, spalling of the concrete cover, and exposure of the reinforcement at displacement ductility levels (μ_Δ = 1.5 & 2) as discussed in chapter 5. Furthermore, the angle of the compression strut was defined by large shear cracks with angles from the vertical axis between 30 to 40 degrees. Significant shear deformation was observed in the middle of faces (E & W), and shear cracks crossed the entire columns from north to south and from top to bottom demonstrating that the behavior of the specimens before failure was governed by shear deformation. In the same manner, it can be observed in Figure 7.7 how the top displacement component due to shear deformation is greater than the displacement component due to flexural deformation towards failure, and how it continued to increase with a significant positive rate while flexural deformation remained stable just before failure. Demonstrating the nature of the failure mechanism, an abrupt loss of the concrete shear strength component occurred after reaching the maximum capacity as it can be observed in Figure 7.7. In conclusion, all brittle shear failure specimens developed the expected failure mode.

The failure mechanism of specimens (NW-NS-DSF), (LW1-NS-DSF), (LW2-NS-DSF), and (LW3-NS-DSF) was not of a ductile shear failure type as expected. During all the tests, even though significant shear strength degradation was observed in the non-linear range, the shear demand did not exceed the capacity of the columns. There was severe damage caused by shear deformation as well as by flexural deformation. As discussed in chapter 6, in addition to crushing of the concrete, spalling of the concrete cover, and exposure of the reinforcement, a mild buckling of the reinforcement was observed at failure revealing a flexural or flexural-shear failure. Furthermore, failure of the specimens occurred at high displacement ductility levels (μ_Δ = 6 & 8) revealing considerable ductility capacity.

As discussed in chapter 6, displacement components due to shear and flexural deformation were both significant and had similar values before failure as shown in Figure 7.12. However, the shear displacement component had the tendency to increase while the flexural component had the tendency to decrease when reaching the failure point. Finally, even though significant shear deformation occurred during the tests of all ductile shear failure specimens, the shear demands did not exceed the actual shear capacity of the specimen causing a shear failure.

Chapter 8: SUMMARY AND CONCLUSIONS

The results of the experimental research on shear performance of reinforced lightweight concrete square columns in seismic regions are summarized in this section as well as conclusions and recommendations. The research considered eight large scale shear critical reversed cyclic tests of normal strength reinforced square lightweight and normal weight concrete columns.

The variables consisted of the structural aggregate and the shear reinforcement ratio. One normal and three lightweight concrete mixtures were used to build and test two sets of four specimens. One set was designed to develop a brittle shear failure at low levels of deformation, and the other to develop a ductile shear failure at high levels of deformation with the purpose of studying the shear performance of reinforced lightweight concrete at different levels of ductility. Lightweight concrete mixtures included expanded shale, clay, and slate structural lightweight aggregates produced in the Midwest and north, in the west coast, and in the southeast region of the United States. The shear span depth ratio of the specimens was (M/VD = 2.57). The compressive concrete strengths ranged from 3,900 to 7,300 psi. In addition, a constant axial load of 96 kips (5% of axial load capacity) was applied during the tests while a reversed cyclic lateral load simulated seismic demands.

8.1 Conclusions

1. In general, reinforced lightweight concrete developed lower shear strength compared to normal weight concrete and to predicted values calculated using the modified shear transfer mechanism for lightweight concrete (Kowalsky et al., 2000 b). This was observed in the brittle and ductile shear failure tests of this research. Consequently, it is appropriate to consider a reduction of the shear capacity assessment envelope.

2. For reinforced lightweight concrete square columns, a modification in the coefficient (γ) of the above mentioned shear transfer mechanism is recommended in order to reduce the concrete shear strength contribution in approximately 40% compared to the concrete shear strength provided by the revised model for lightweight concrete (Kowalsky et al., 2000 b) based on experimental tests of circular columns. The modification considers a shear strength reduction in the upper plateau at low levels of deformation as well as a reduction in the displacement ductility level at which strength degradation starts. Displacement ductility ($\mu\Delta=1.5$) instead of ($\mu\Delta=2$) as in the revised model for lightweight concrete (Kowalsky et al., 2000 b).

3. It was observed that reinforced lightweight concrete can be subjected to seismic shear demands since it can undergo large deformation in the non-linear range. Consequently, it can be used for structural elements in seismic regions when designed appropriately. Reinforced lightweight concrete can be designed to develop significant energy absorption and ductility

capacities. In fact, the difference between normal and lightweight concrete ductile shear failure tests in terms of energy dissipation and ductility was not very significant.

4. Increasing the shear reinforcement ratio and the level of confinement has a significant effect in terms of providing greater ductility and energy absorption capacity to lightweight concrete structural members.

5. Applicable to shear critical reinforced concrete members, it was observed in all brittle and ductile shear failure tests that the shear deformation component tended to increase after yield in the inelastic range while the flexural deformation component tended to get stable towards failure. A well defined kink or change in the rate of increment of shear deformation after yield was observed in brittle and ductile shear failure tests. The opposite occurred with flexural deformation that increased rapidly in the linear range and tended to reduce the rate of increment beyond yield.

6. Compared to normal weight concrete, strength degradation tended to occur earlier and a negative stiffness post-yield was observed in lightweight concrete specimens revealing more tendency of lightweight concrete to be governed by shear behavior. On the contrary, normal weight concrete specimens sustained shear strength for more cycles and at higher levels of deformation.

7. In general, crack spacing was smaller in the case of lightweight concrete specimens, and fracture surfaces passed through the aggregated in all cases reducing the effect of aggregate interlock in lightweight concrete shear performance compared to normal weight concrete.

8. Future research is necessary to validate the recommendations presented in this document. Moreover, future experiments should consider high strength concrete mixtures. Effective ductile shear failure modes should be considered in future tests to continue studying the behavior of lightweight concrete at high levels of deformation. Finally, with the information presented in this document as well as with additional new experimental data, analytical models for estimating the behavior of reinforced lightweight concrete should be revised and improved.

REFERENCES

Ahmad, S. H., Xie, Y., and Yu, T. (1995). Shear Ductility of Reinforced Lightweight Concrete Beams of Normal Strength and High Strength Concrete. Cement and Concrete Composites, 17, 147-159.

Berge, O. (1981). Reinforced Structures in Lightweight Aggregate Concrete. Thesis abstract, Chalmers University of Technology, Goteborg, 353-362.

Clarke, J.L. (1987). Shear Strength of Lightweight Aggregate Concrete Beams; Design to BS 8110. Magazine of Concrete Research. Vol. 39, No. 141, 205-213.

Hamadi, Y.D. and Regan, P.E. (1980). Behaviour of Normal and Lightweight Aggregate Beams with Shear Cracks. The Structural Engineer. Vol 58B, No. 4, 71-79.

Hanson, J.A. (1958). Shear Strength of Lightweight Reinforced Concrete Beams. Journal of the American Concrete Institute, Proceedings, Vol. 55, No. 3, 387-403.

Ivey, D.L. and Buth, E. (1967). Shear Capacity of Lightweight Concrete Beams. Journal of the American Concrete Institute, Proceedings, 64-54, 634-643.

Jacobsen, L.S. (1930). Steady Forced Vibrations as Influenced by Damping. ASME Transactione; 52(1): 169-181.

Kowalsky, M. J., and Dwairi, H. M. (2003). Review of Parameters Influencing the Seismic Design of Lightweight Concrete Structures. High-Performance Structural Lightweight Concrete, American Concrete Institute, SP 218-3, 29-49.

Kowalsky, M. J., and Priestley, M. J. N. (2000 a). Improved Analytical Model for Shear Strength of Circular Reinforced Concrete Columns in Seismic Regions. ACI Structural Journal, 97-S42, 388-396.

Kowalsky, M. J., Priestley, M. J. N., and Seible, F. (1999). Shear and Flexural Behavior of Lightweight Concrete Bridge Columns in Seismic Regions. ACI Structural Journal, 96-S16, 136-148.

Kowalsky, M. J., Priestley, M. J. N., and Seible, F. (2000 b). Dynamic Behavior of Lightweight Concrete Bridges. ACI Structural Journal, 97-S63, 602-618.

Mander, J.B., Priestley, M.J.N., and Park, R. (1988). Theoretical Stress-Strain Model for Confined Concrete. Journal of the Structural Division, ASCE 1988, Vol. 114, No. 8, 1804-1826.

Montejo, L. A., Kowalsky M. J. (2006). Set of Codes for the Analysis of Reinforced Concrete Members, Cumbia Program. Department of Civil, Construction and Environmental Engineering, North Carolina State University, 1-39

Priestley, M. J. N.; Verma, R.; and Xiao, Y. (1994). Seismic Shear Strength of Reinforced Concrete Columns. Journal of Structural Engineering, ASCE, Vol. 120, No. 8, 2310-2329.

Priestley, M.J.N., Seible, F., Calvi, G.M. (1996). Seismic Design and Retrofit of Bridge Structures. John Wiley and Sons, New York.

Ramirez, J.A. (2003). Shear Strength of Lightweight Concrete Beams with Stirrups Near Code Minimum. The Art and Science of Structural Concrete Design, American Concrete Institute, SP-213-7, 119-134.

Salandra, M.A., Ahmad, S.H. (1989). Shear Capacity of Reinforced Lightweight High-Strength Concrete Beams. ACI structural journal, 86-S69, 697-704.

American Concrete Institute (2005) Building Code and Comentary, (ACI 318-05)

Chapter 9: APPENDIX

9.1 Shear Critical Single Bending Columns – Conceptual Understanding

A conceptual analysis of the behavior of shear critical reinforced concrete columns under single bending is presented in this section. In order to visualize the behavior of columns under uni-axial single bending it is important to consider that, for reinforced concrete members, cracks appear when tension stresses have exceeded the tension strength of the concrete. Moreover, the orientation and location of cracks is a sourced of valuable information in terms of revealing flow of stresses, level of deformation and type, and also level of damage related to material strains. For instance, flexural cracks occur on the tension side of a member subjected to bending, and are perpendicular to tension stresses, see Figure 9.1 (b). Shear cracks are perpendicular to tension tresses and parallel to the compression stresses as shown in Figure 9.1 (c). Structural designers may intuitively infer the location and orientation of cracks when considering deformed shapes and maximum stresses caused by certain demands such as illustrated in Figure 9.1 and Figure 9.2.

In terms of deformation, flexural and shear deformation occur in a single bending column subjected to a lateral load applied on the free head of the column as shear and moment are transferred to the member as described in Figure 9.1 and Figure 9.2. Moreover, flexural and shear components of deformation as well as location and orientation of cracks can be visualized when considering the principle of superposition as in Figure 9.1. In fact, in terms

of shear, the effect caused by the lateral load applied on top of the single bending column is clear when considering only shear deformation as a separate component as shown in Figure 9.1 (c). In the same manner, the orientation of shear cracks in reinforced concrete columns is also illustrated as a result of analyzing the shear deformation component, and taking into account that cracks are perpendicular to tension stresses or to principal stretching axis. In general, the deformed shape and the distribution of cracks will be a combination of both flexural and shear deformation components as shown in Figure 9.1 (d).

In order to visualize and acquire a better understanding of shear performance of reinforced concrete columns in terms of stress flow and crack orientation, it is useful to analyze equilibrium of internal forces either considering moment or shear distribution diagrams as illustrated in Figure 9.2. In fact, the resultants of the orthogonal internal forces, at the corners of a square particle in equilibrium, define compressive and tensile flow of stresses. Moreover, the orientation of the tensile stress flow is perpendicular to the shear crack orientation while the orientation of the compressive stress flow is parallel to the shear crack.

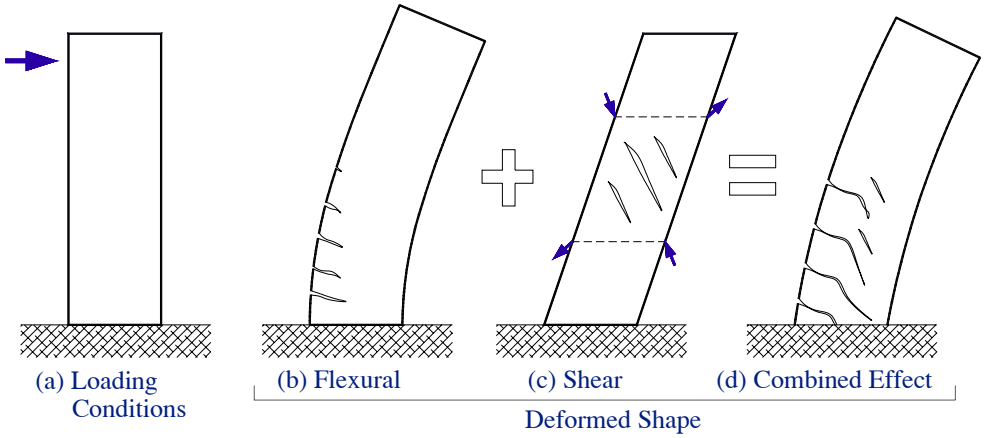

Figure 9.1. Deformation Components – Single Bending Reinforced Concrete Column

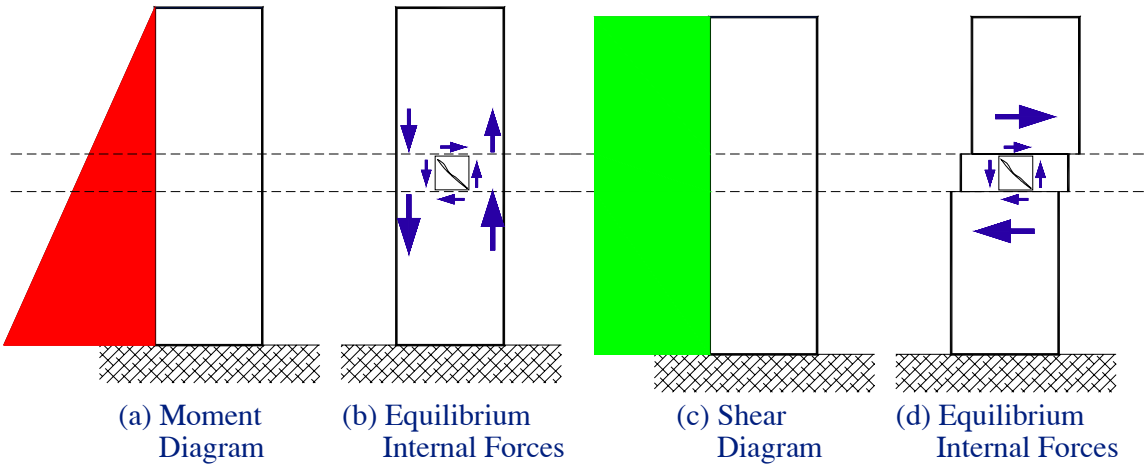

Figure 9.2. Illustration of Internal Forces in Equilibrium – Single Bending Column

9.2 Linear Potentiometer and Strain Gage Histories - Test (NW-NS-BSF)

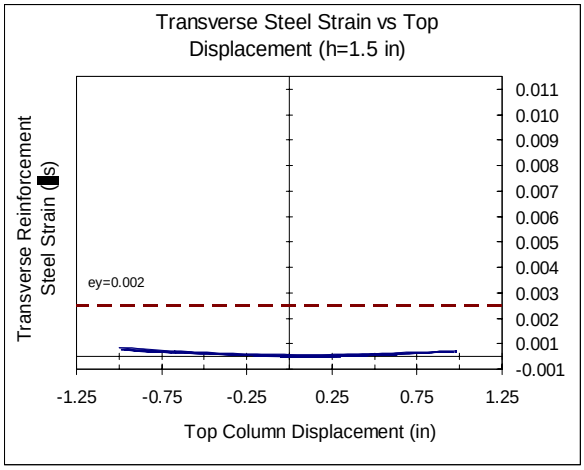

a) Height from the column base (h=1.5 in)

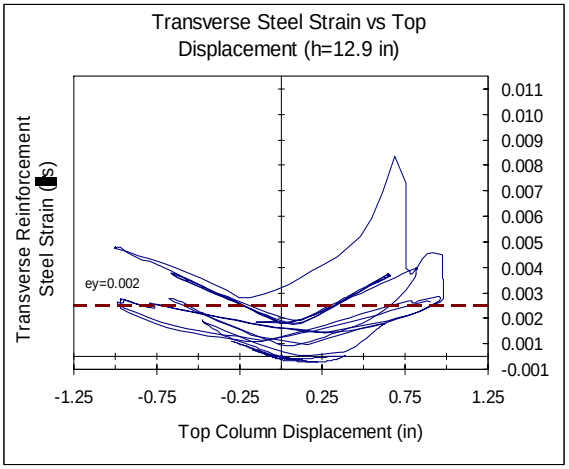

b) Height from the column base (h=12.9 in)

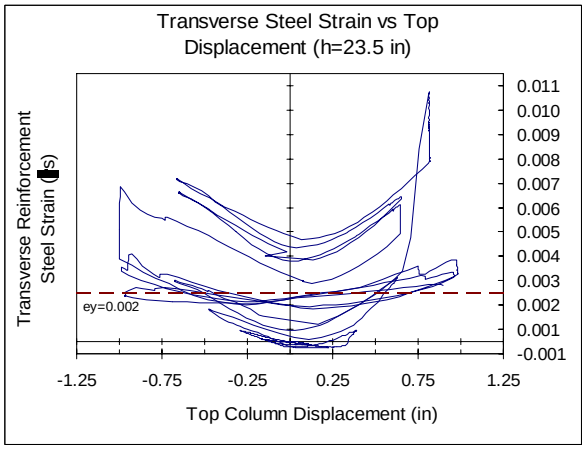

c) Height from the column base (h=23.5 in)

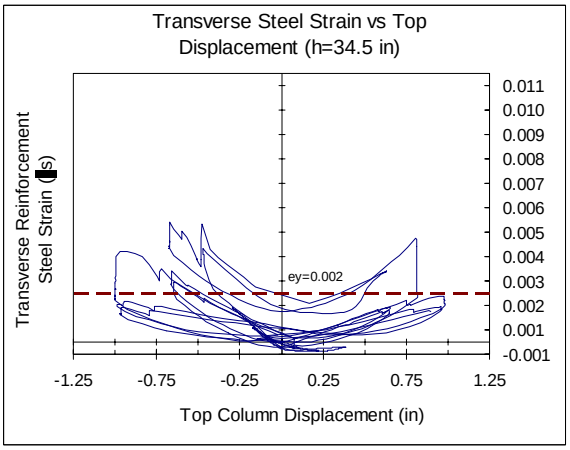

d) Height from the column base (h=34.5 in)

Figure 9.3. Average Transverse Steel Strain versus Top Column Displacement (NW-NS-BSF)

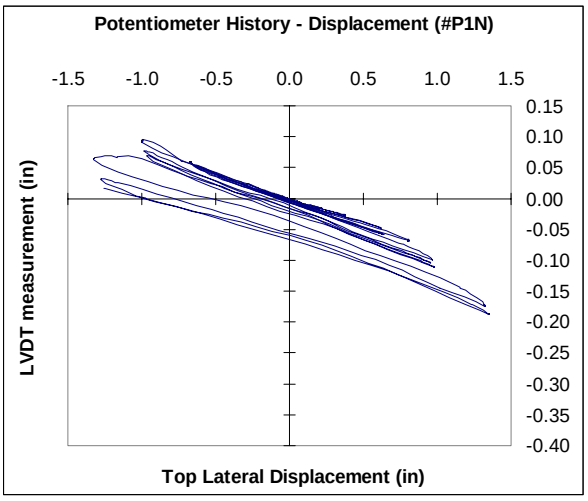

a) P. North. Gage at (h_1-h_2)=(0-7.5) in

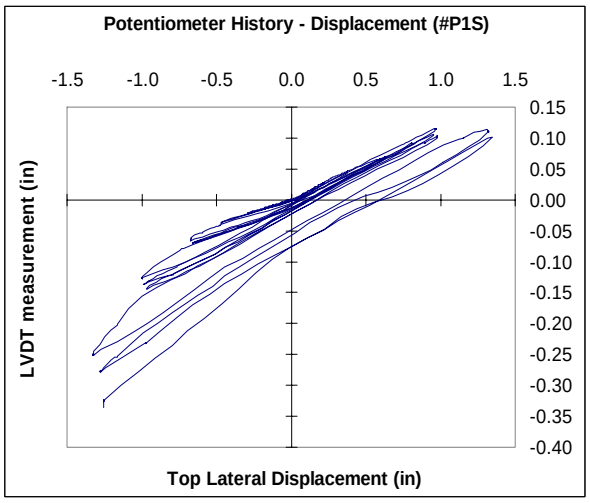

b) P. South. Gage at (h_1-h_2)=(0-7.5) in

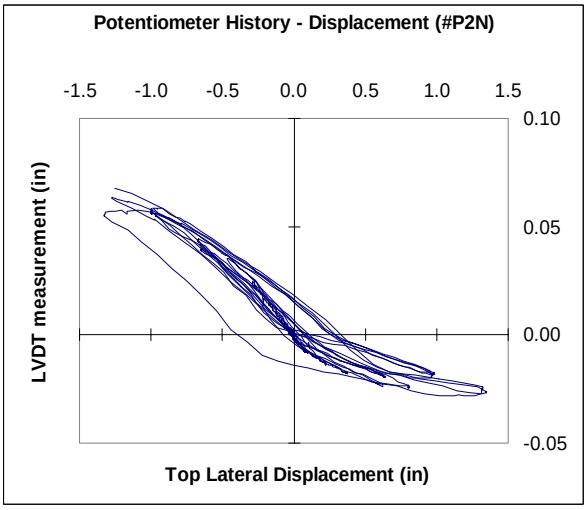

c) P. North. Gage at (h_1-h_2)=(7.5-15) in

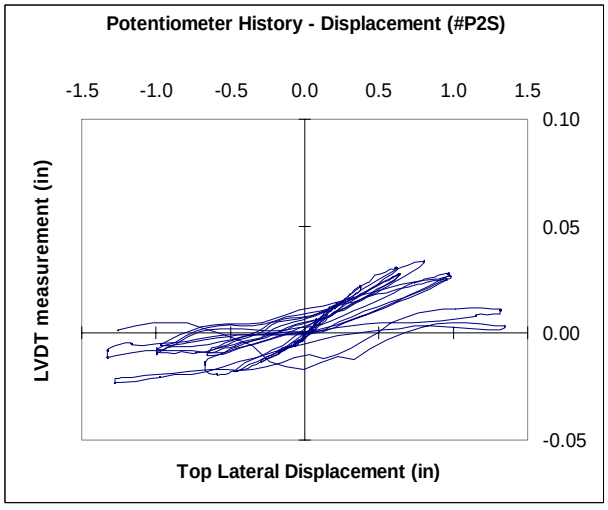

d) P. South. Gage at (h_1-h_2)=(7.5-15) in

Figure 9.4. Linear Potentiometer Histories at Gages 1 and 2 – North and South Faces (NW-NS-BSF)

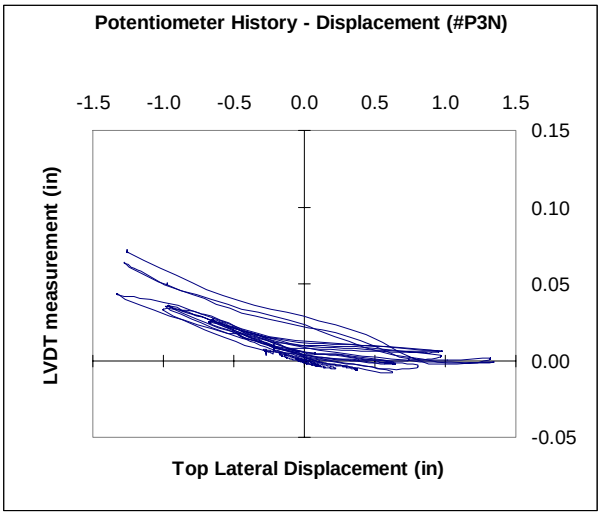

a) P. North. Gage at (h_1-h_2)=(15-22.5) in

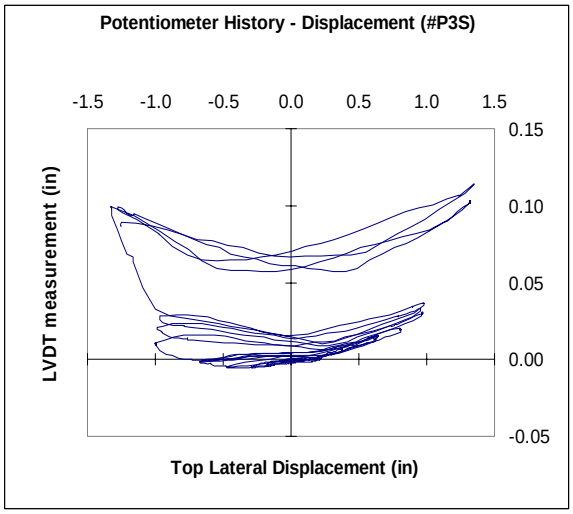

b) P. South. Gage at (h_1-h_2)=(15-22.5) in

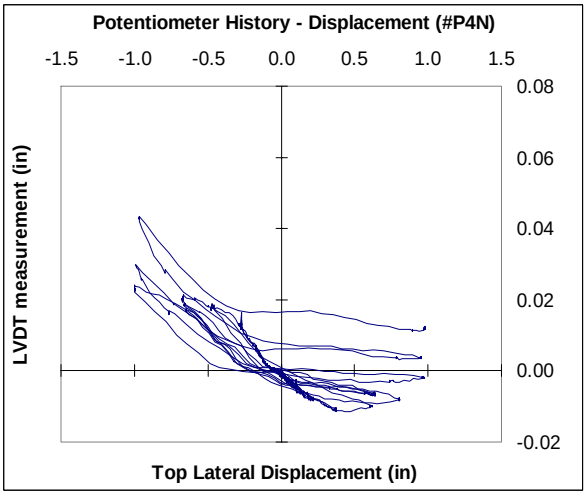

c) P. North. Gage at (h_1-h_2)=(22.5-33.75) in

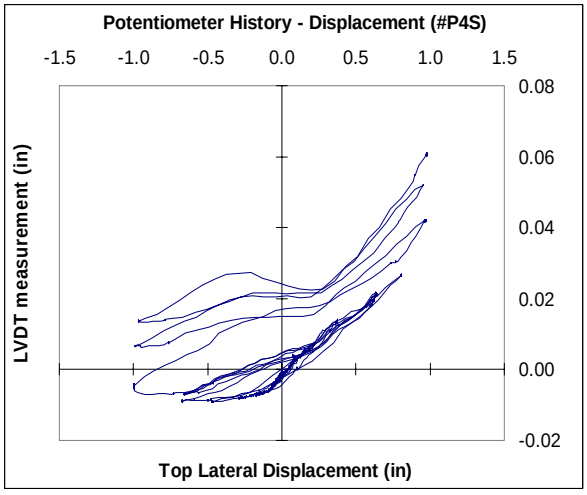

d) P. South. Gage at (h_1-h_2)=(22.5-33.75) in

Figure 9.5. Linear Potentiometer Histories at Gages 3 and 4 – North and South Faces (NW-NS-BSF)

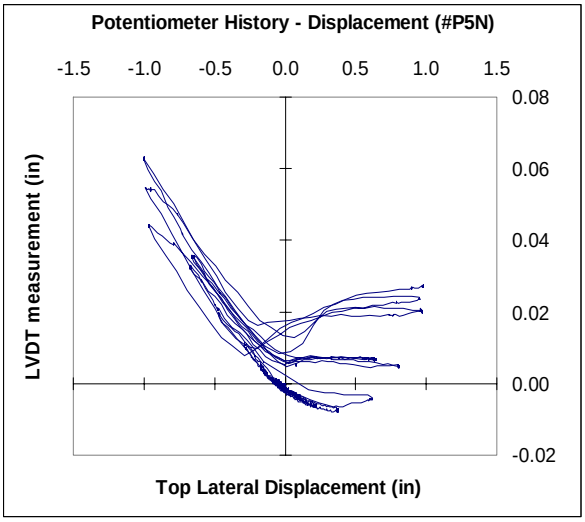

a) P. North. Gage at (h_1-h_2)=(33.75-45) in

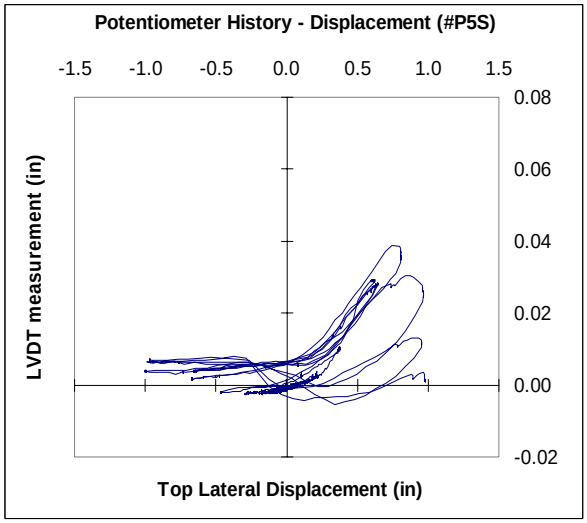

b) P. South. Gage at (h_1-h_2)=(33.75-45) in

Figure 9.6. Linear Potentiometer Histories at Gage 5 – North and South Faces (NW-NS-BSF)

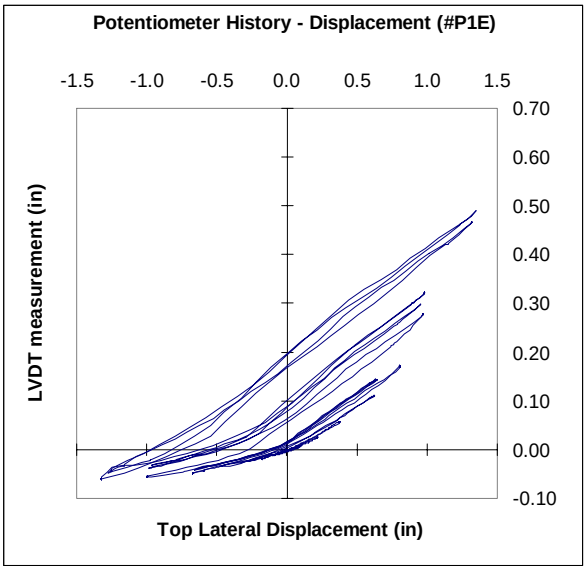

a) P. East. Diagonal at (h_1-h_2)=(0-22.5) in

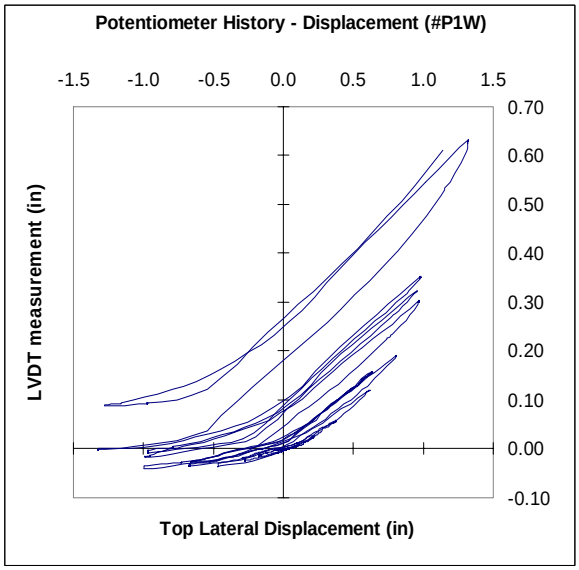

b) P. West. Diagonal at (h_1-h_2)=(0-22.5) in

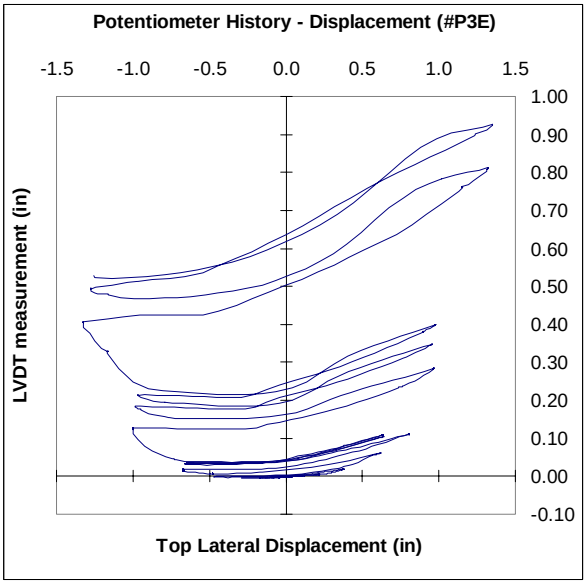

c) P. East. Diagonal at (h_1-h_2)=(22.5-45) in

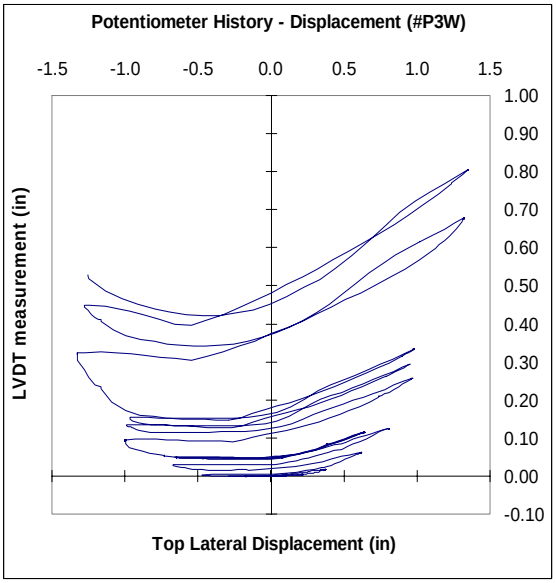

d) P. West. Diagonal at (h_1-h_2)=(22.5-45) in

Figure 9.7. Linear Potentiometer Histories – Diagonal Elements – East and West Faces (NW-NS-BSF)

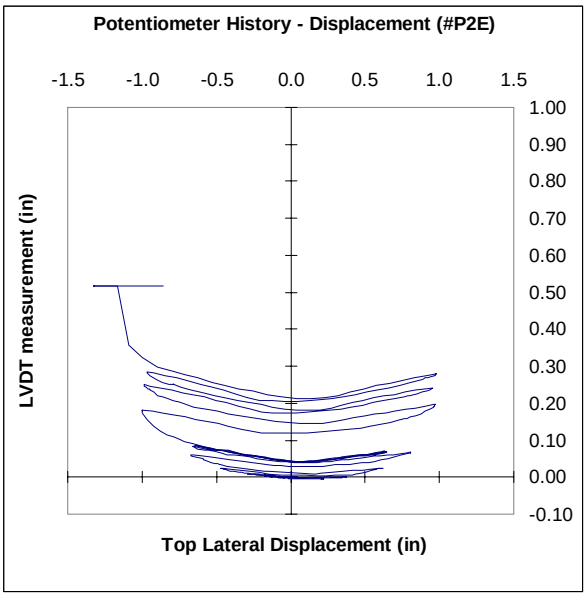

a) P. East. Horizontal at (h=22.5 in)

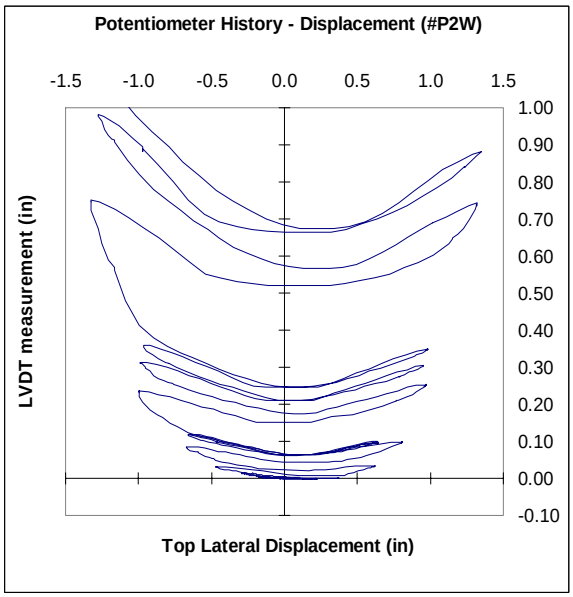

b) P. West. Horizontal at (h=22.5 in)

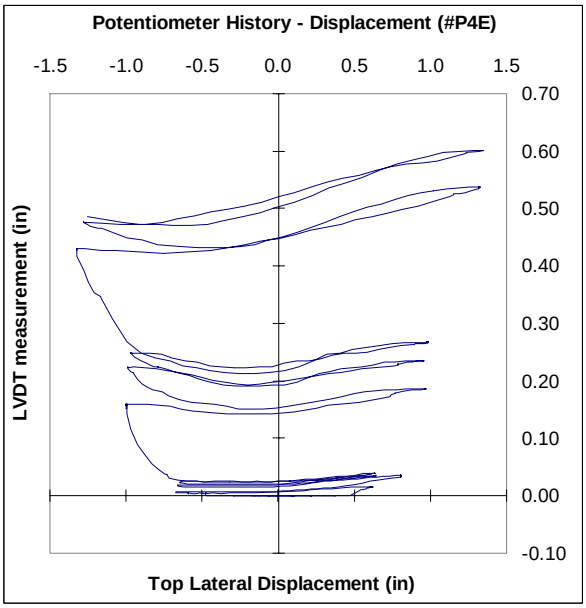

c) P. East. Horizontal at (h=45 in)

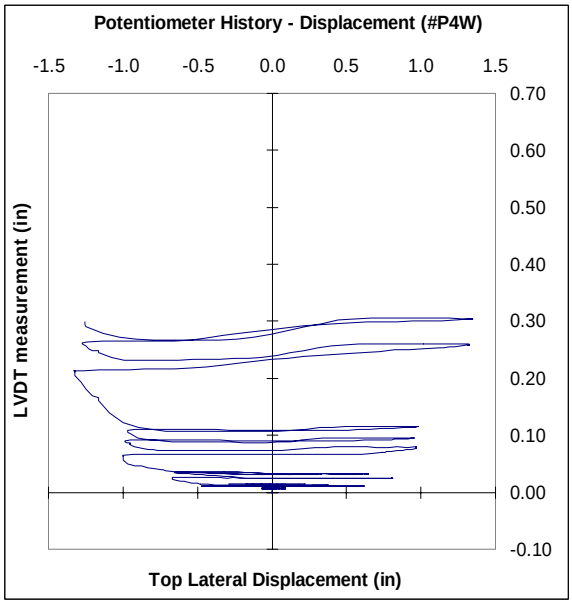

d) P. West. Horizontal at (h=45 in)

Figure 9.8. Linear Potentiometer Histories – Horizontal Elements – East and West Faces (NW-NS-BSF)

9.3 Linear Potentiometer and Strain Gage Histories - Test (LW1-NS-BSF)

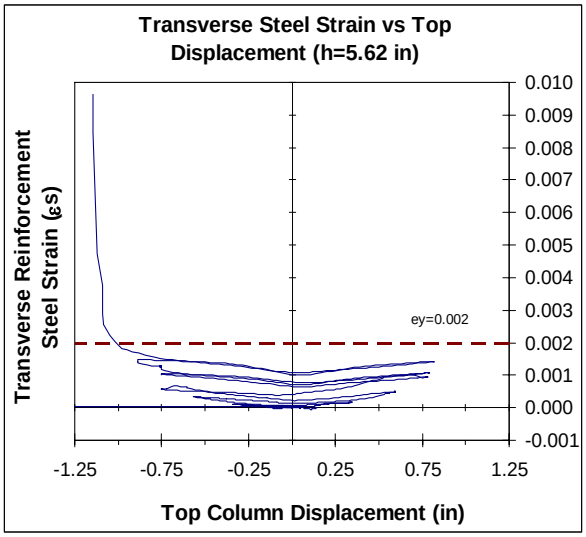

a) Height from the column base (h=5.62 in)

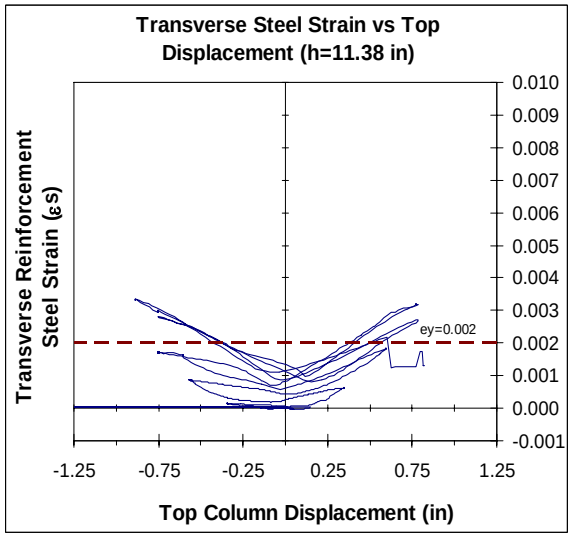

b) Height from the column base (h=11.38 in)

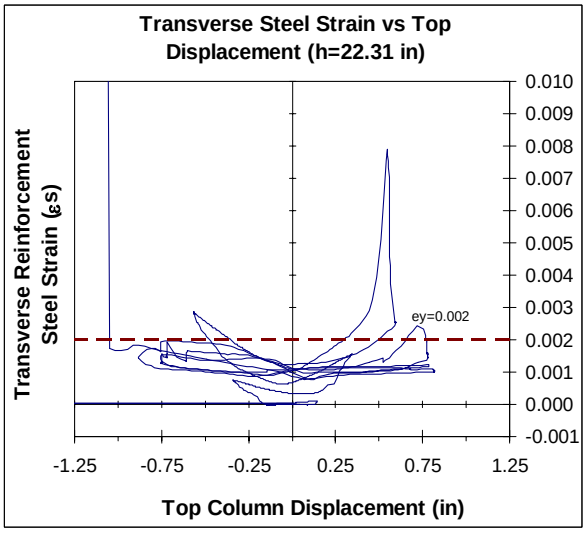

c) Height from the column base (h=22.31 in)

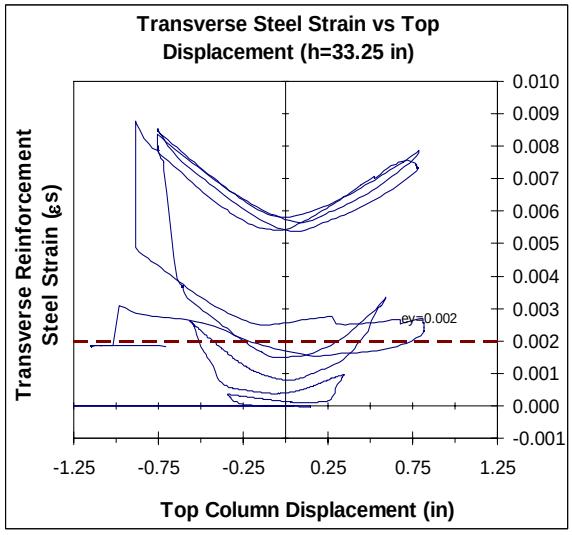

d) Height from the column base (h=33.25 in)

Figure 9.9. Average Transverse Steel Strain versus Top Column Displacement (LW1-NS-BSF)

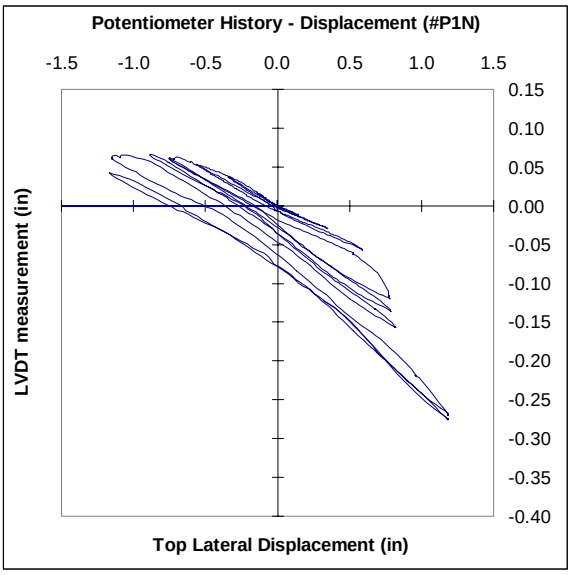

a) P. North. Gage at (h_1-h_2)=(0-7.5) in

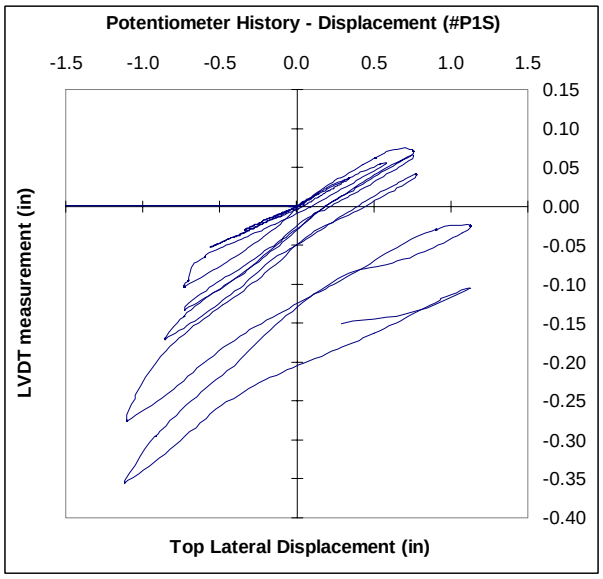

b) P. South. Gage at (h_1-h_2)=(0-7.5) in

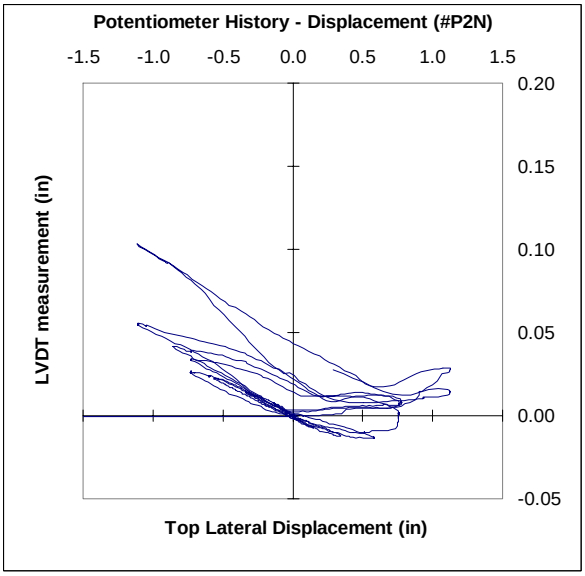

c) P. North. Gage at (h_1-h_2)=(7.5-15) in

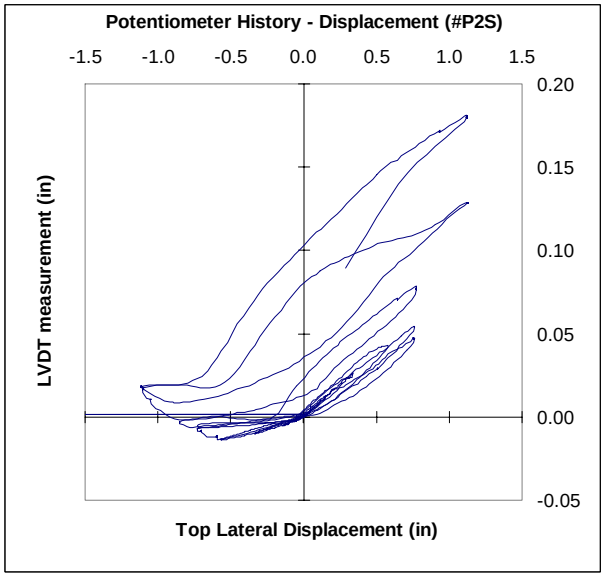

d) P. South. Gage at (h_1-h_2)=(7.5-15) in

Figure 9.10. Linear Potentiometer Histories at Gages 1 and 2 – North and South Faces (LW1-NS-BSF)

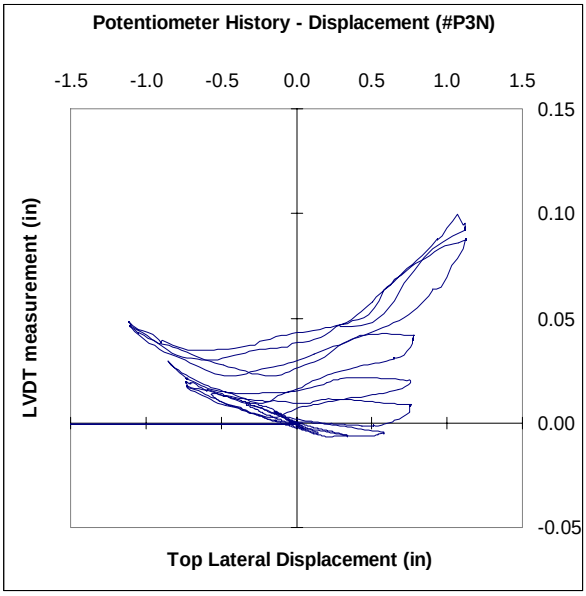

a) P. North. Gage at (h_1-h_2)=(15-22.5) in

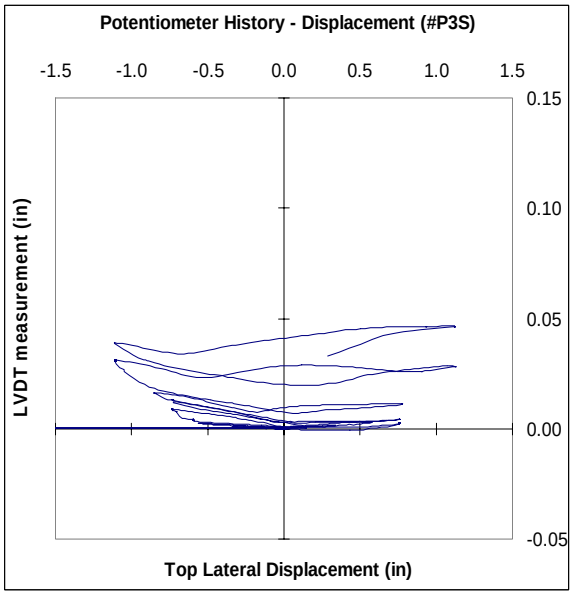

b) P. South. Gage at (h_1-h_2)=(15-22.5) in

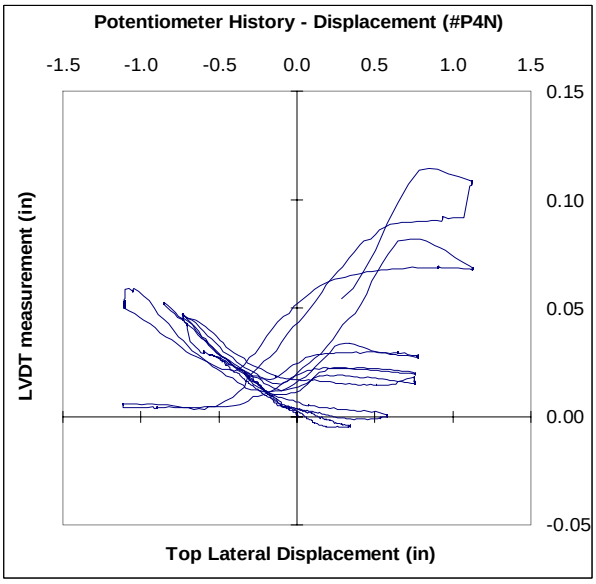

c) P. North. Gage at (h_1-h_2)=(22.5-33.75) in

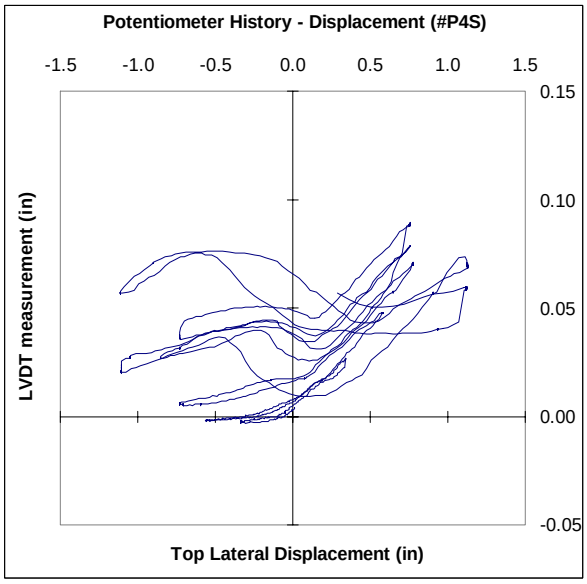

d) P. South. Gage at (h_1-h_2)=(22.5-33.75) in

Figure 9.11. Linear Potentiometer Histories at Gages 3 and 4 – North and South Faces (LW1-NS-BSF)

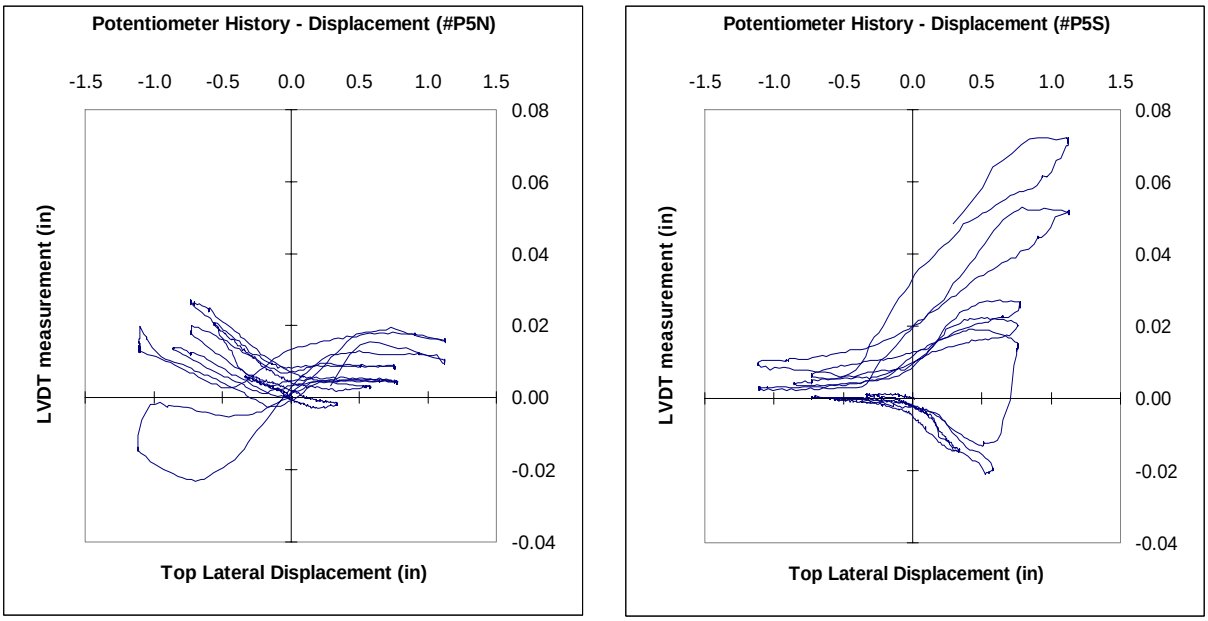

a) P. North. Gage at (h_1-h_2)=(33.75-45) in

b) P. South. Gage at (h_1-h_2)=(33.75-45) in

Figure 9.12. Linear Potentiometer Histories at Gage 5 – North and South Faces (LW1-NS-BSF)

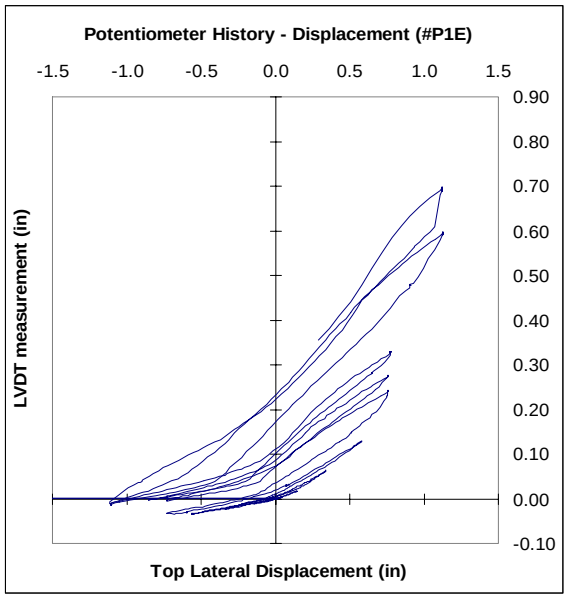

a) P. East. Diagonal at (h_1-h_2)=(0-22.5) in

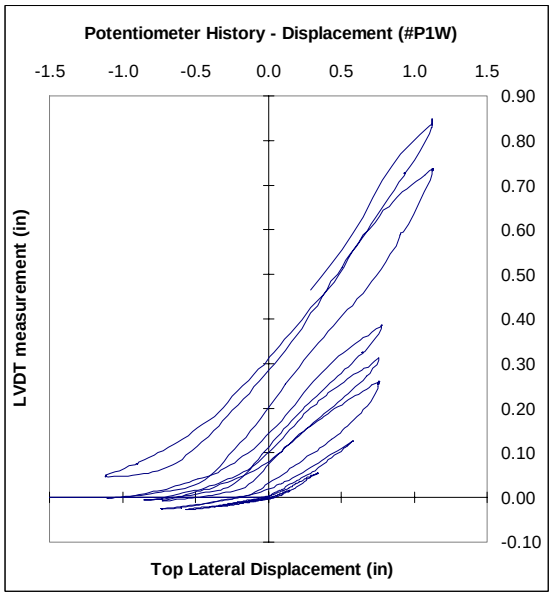

b) P. West. Diagonal at (h_1-h_2)=(0-22.5) in

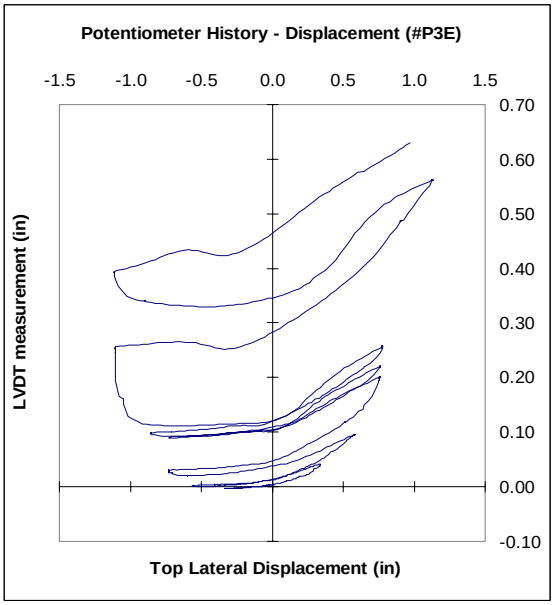

c) P. East. Diagonal at (h_1-h_2)=(22.5-45) in

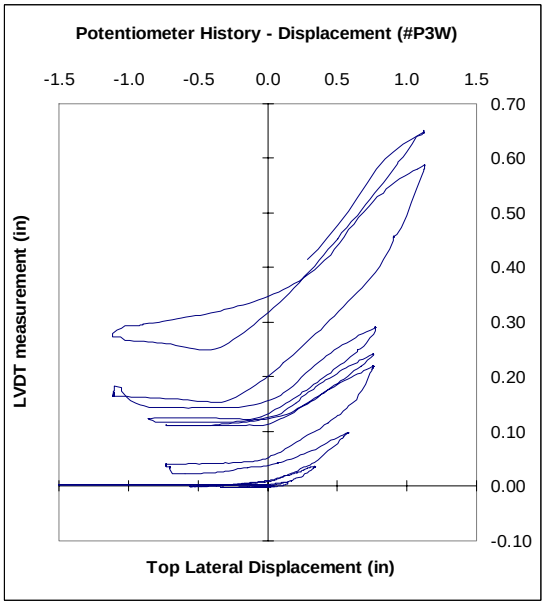

d) P. West. Diagonal at (h_1-h_2)=(22.5-45) in

Figure 9.13. Linear Potentiometer Histories – Diagonal Elements – East and West Faces (LW1-NS-BSF)

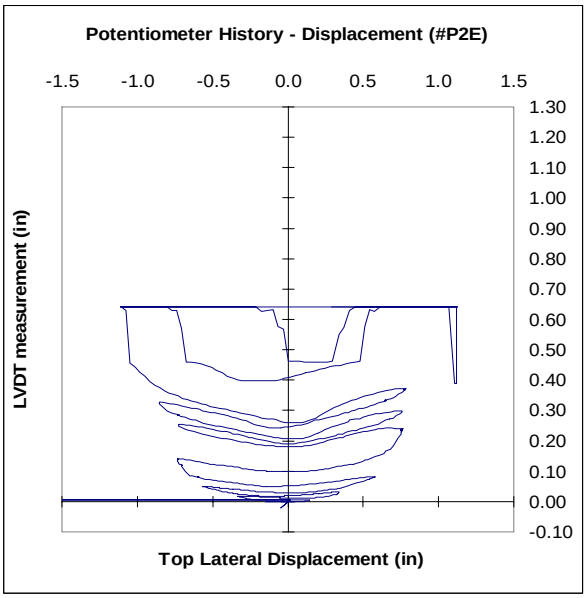

a) P. East. Horizontal at (h=22.5 in)

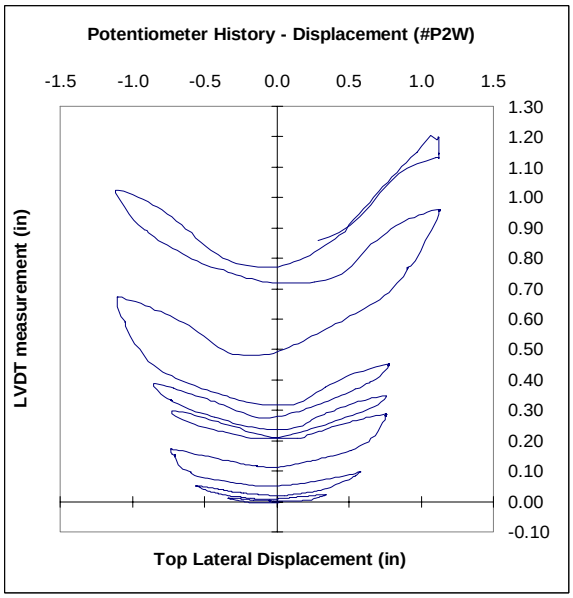

b) P. West. Horizontal at (h=22.5 in)

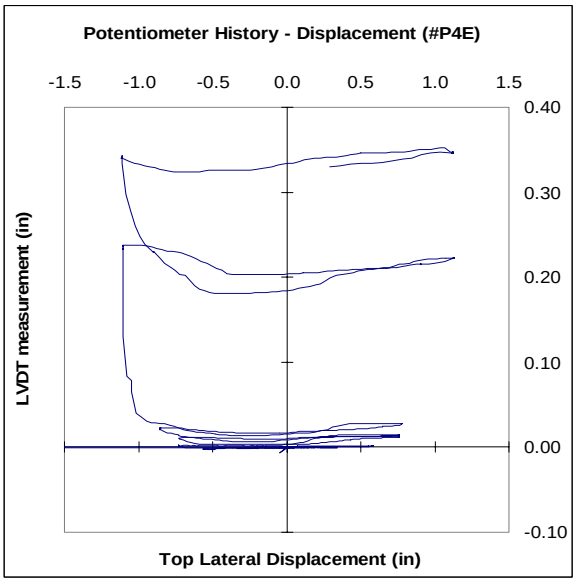

c) P. East. Horizontal at (h=45 in)

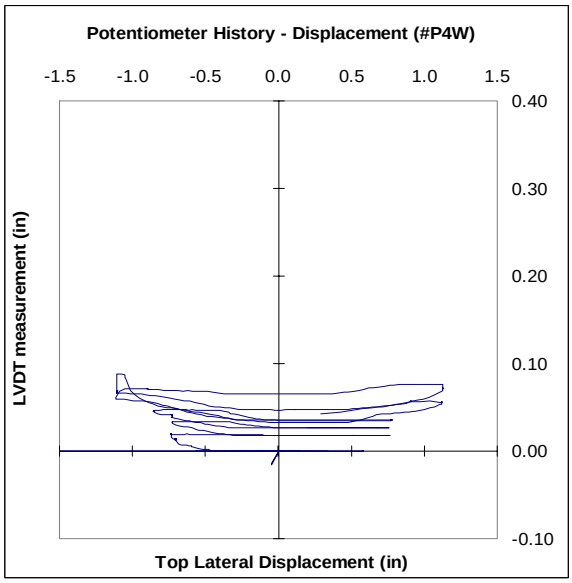

d) P. West. Horizontal at (h=45 in)

Figure 9.14. Linear Potentiometer Histories – Horizontal Elements–East and West Faces (LW1-NS-BSF)

9.4 Linear Potentiometer and Strain Gage Histories - Test (LW2-NS-BSF)

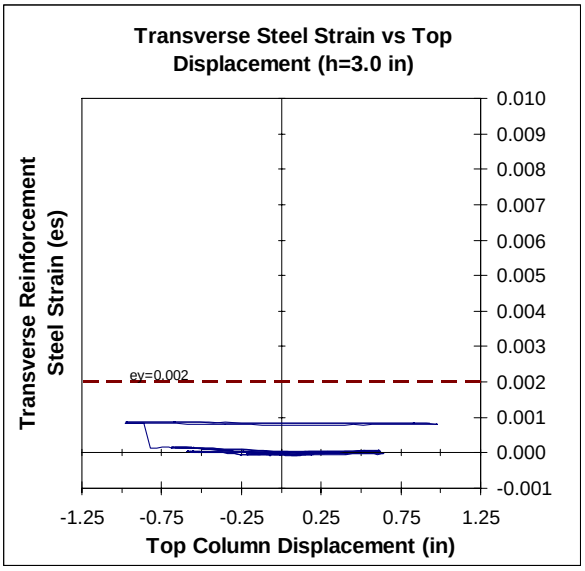

a) Height from the column base (h=5.62 in)

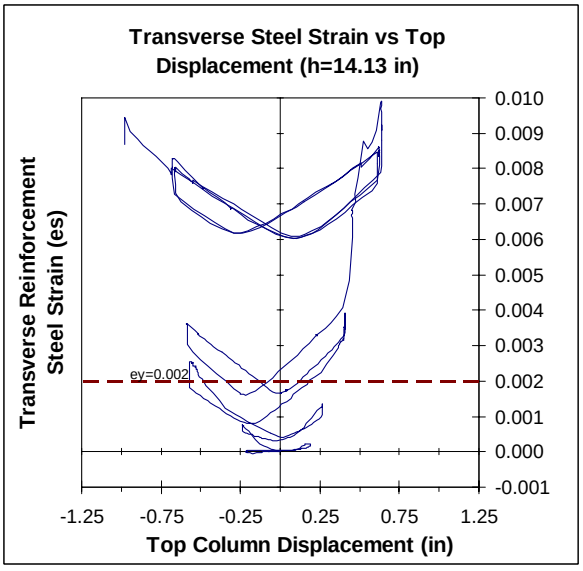

b) Height from the column base (h=11.38 in)

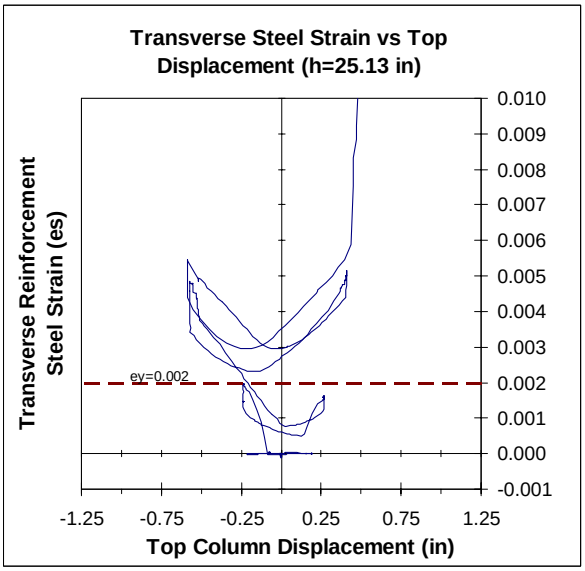

c) Height from the column base (h=22.31 in)

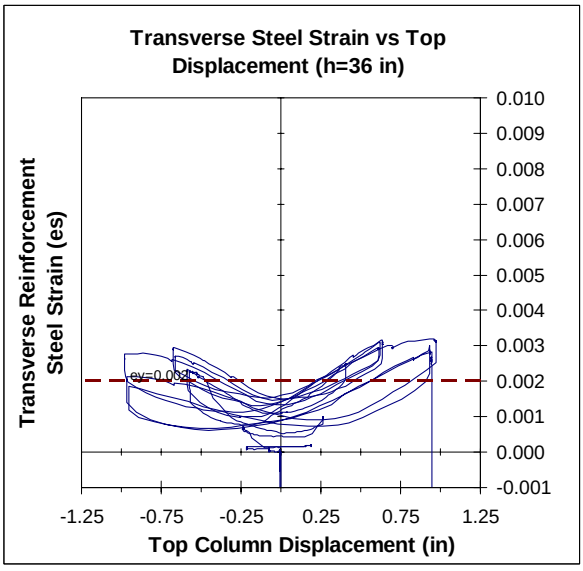

d) Height from the column base (h=33.25 in)

Figure 9.15. Average Transverse Steel Strain versus Top Column Displacement (LW2-NS-BSF)

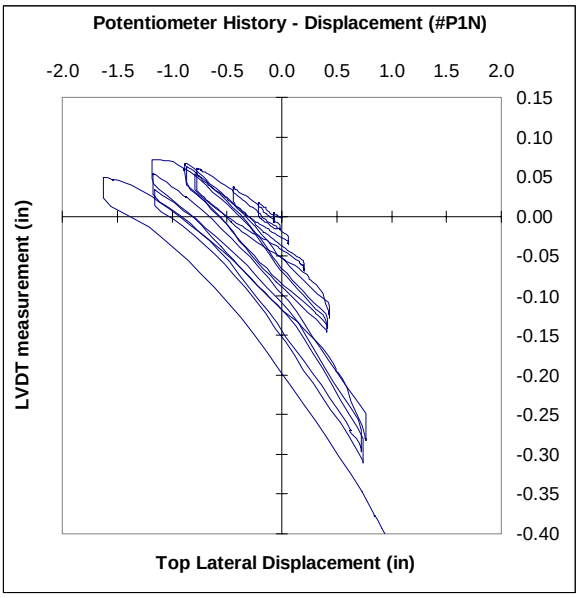

a) P. North. Gage at (h_1-h_2)=(0-7.5) in

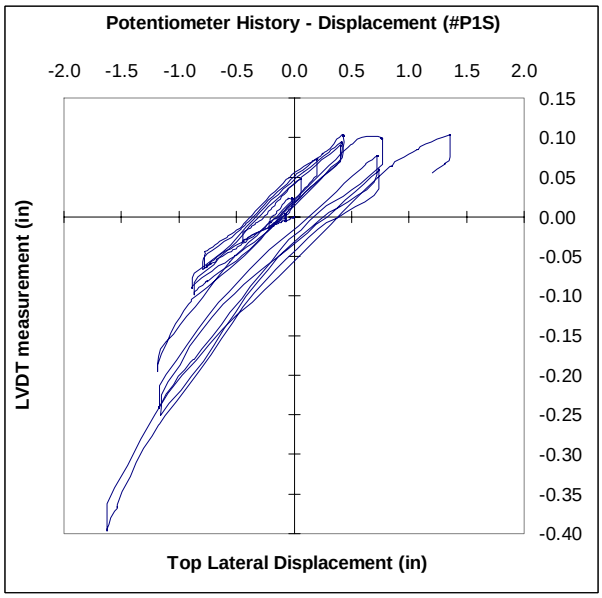

b) P. South. Gage at (h_1-h_2)=(0-7.5) in

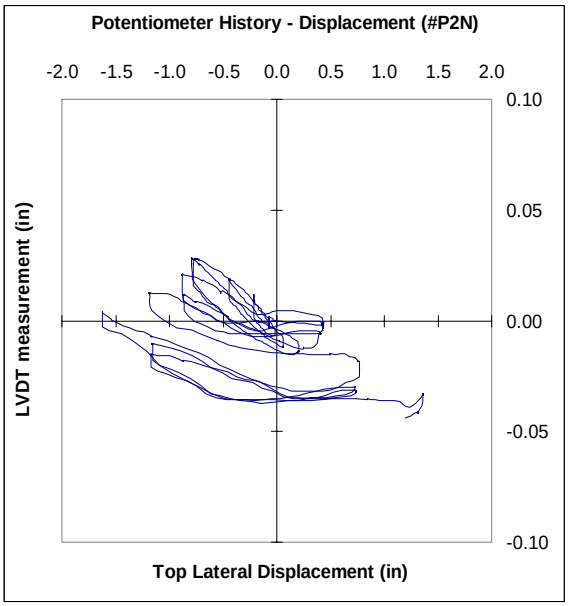

c) P. North. Gage at (h_1-h_2)=(7.5-15) in

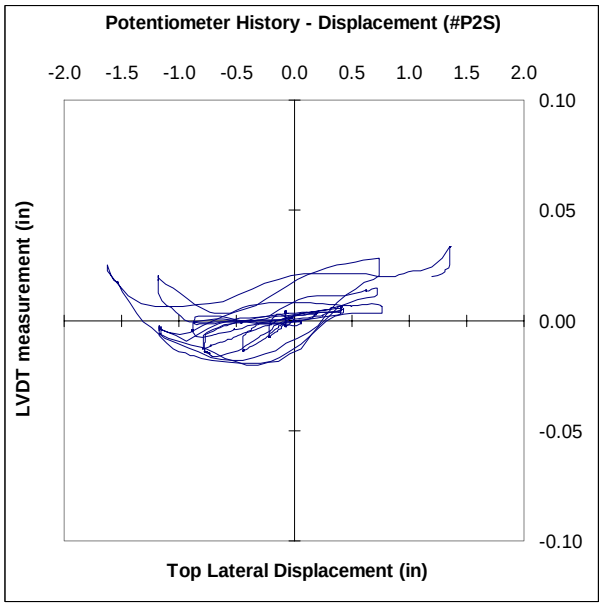

d) P. South. Gage at (h_1-h_2)=(7.5-15) in

Figure 9.16. Linear Potentiometer Histories at Gages 1 and 2 – North and South Faces (LW2-NS-BSF)

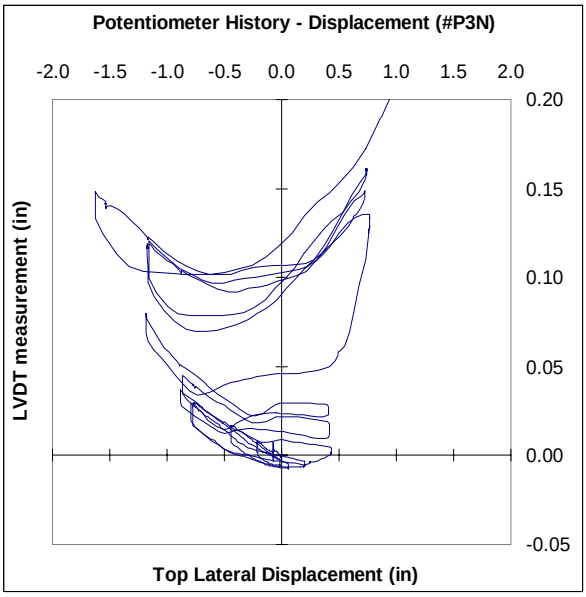

a) P. North. Gage at (h_1-h_2)=(15-22.5) in

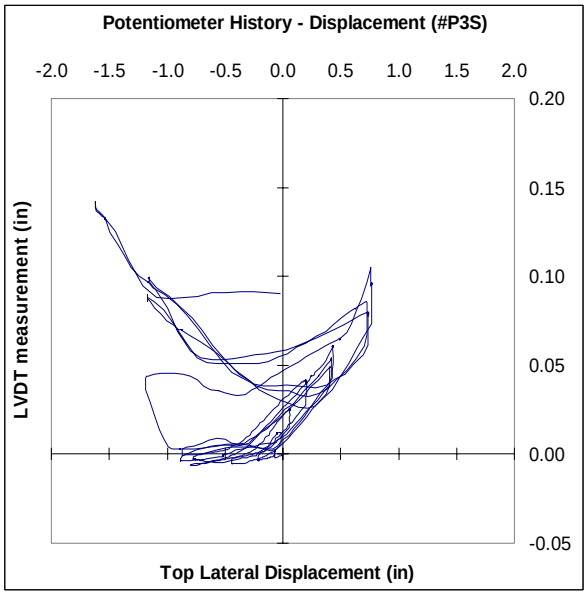

b) P. South. Gage at (h_1-h_2)=(15-22.5) in

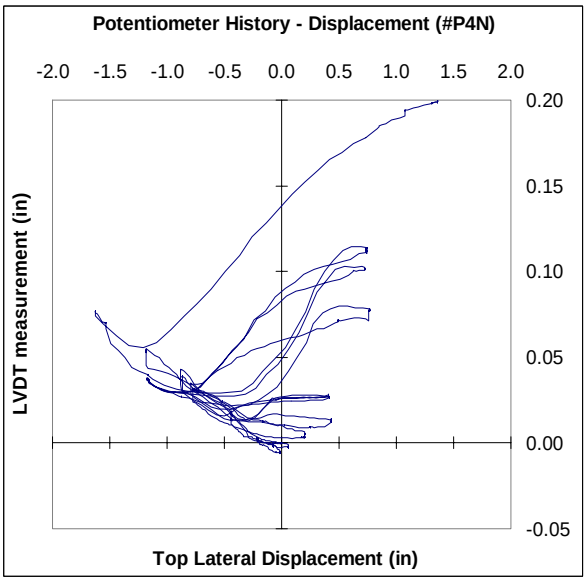

c) P. North. Gage at (h_1-h_2)=(22.5-33.75) in

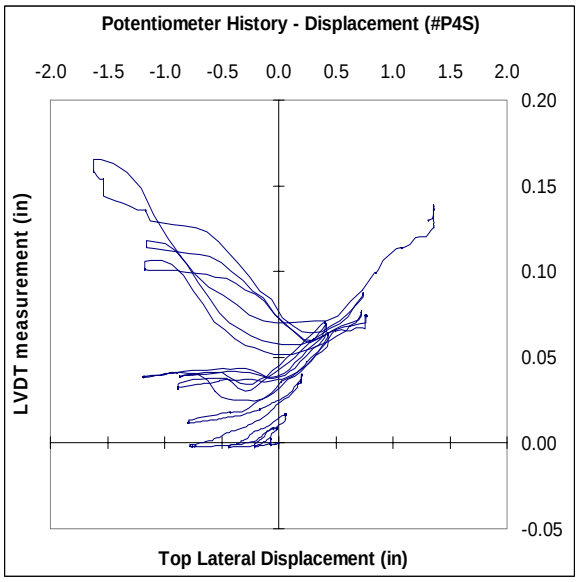

d) P. South. Gage at (h_1-h_2)=(22.5-33.75) in

Figure 9.17. Linear Potentiometer Histories at Gages 3 and 4 – North and South Faces (LW2-NS-BSF)

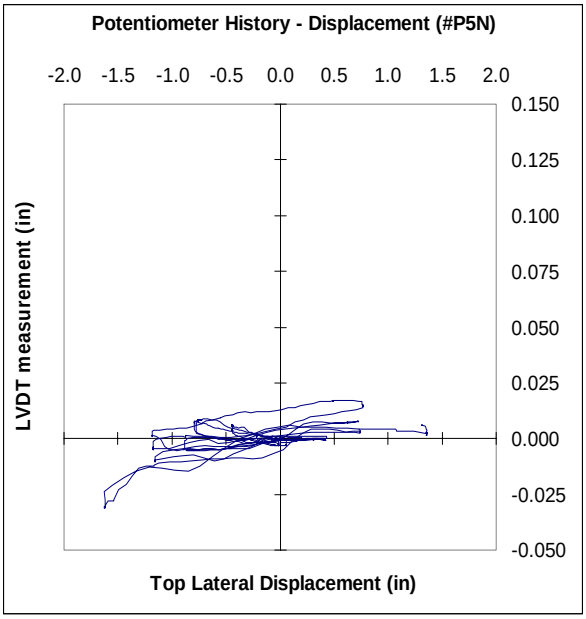

a) P. North. Gage at (h_1-h_2)=(33.75-41.25) in

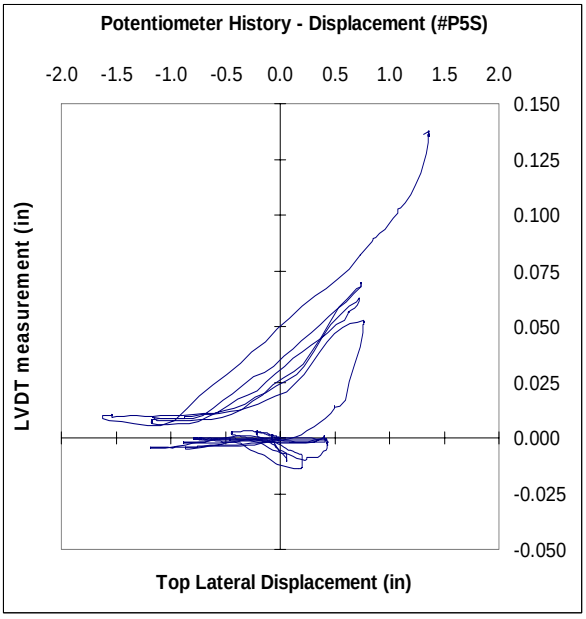

b) P. South. Gage at (h_1-h_2)=(33.75-41.25) in

Figure 9.18. Linear Potentiometer Histories at Gage 5 – North and South Faces (LW2-NS-BSF)

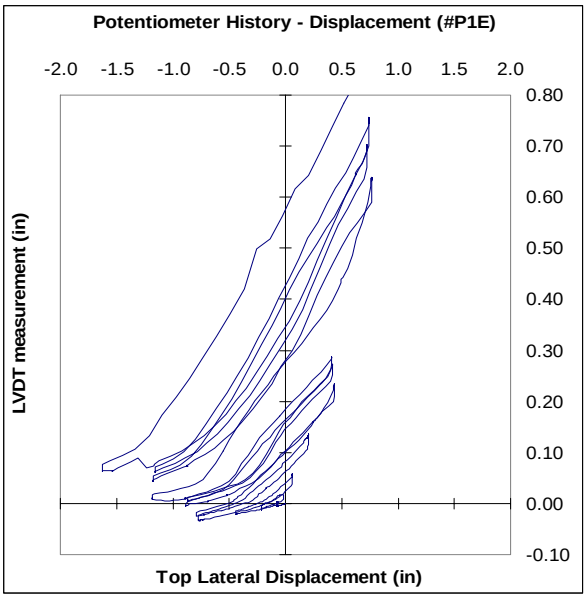

a) P. East. Diagonal at (h_1-h_2)=(0-22.5) in

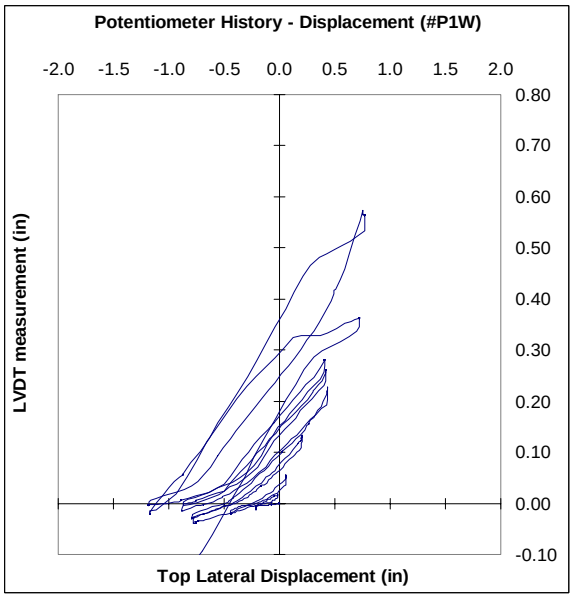

b) P. West. Diagonal at (h_1-h_2)=(0-22.5) in

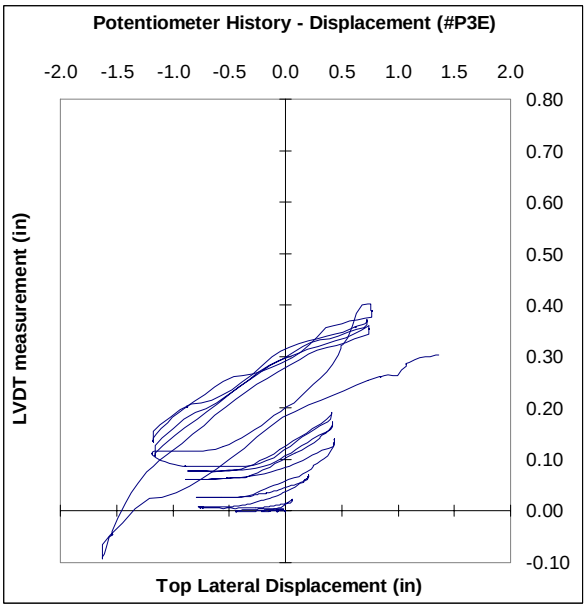

c) P. East. Diagonal at (h_1-h_2)=(22.5-41.25) in

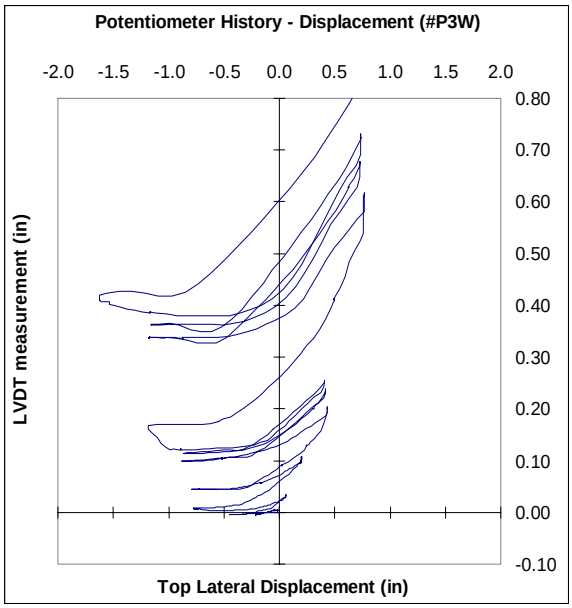

d) P. West. Diag. at (h_1-h_2)=(22.5-41.25) in

Figure 9.19. Linear Potentiometer Histories – Diagonal Elements – East and West Faces (LW2-NS-BSF)

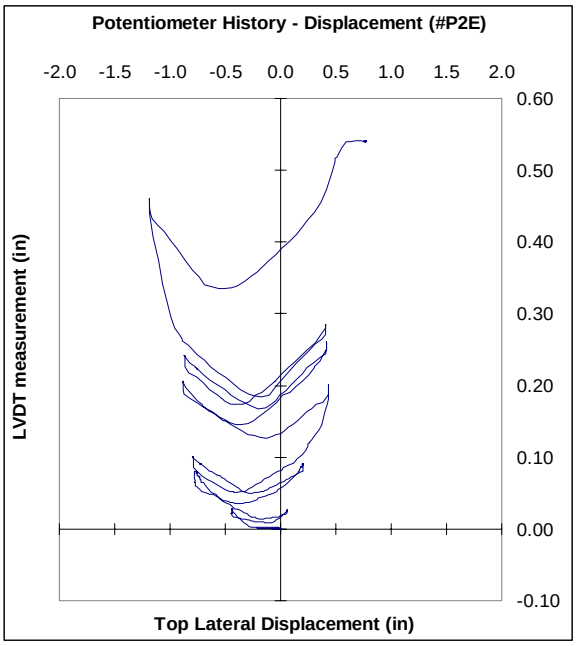

a) P. East. Horizontal at (h=22.5 in)

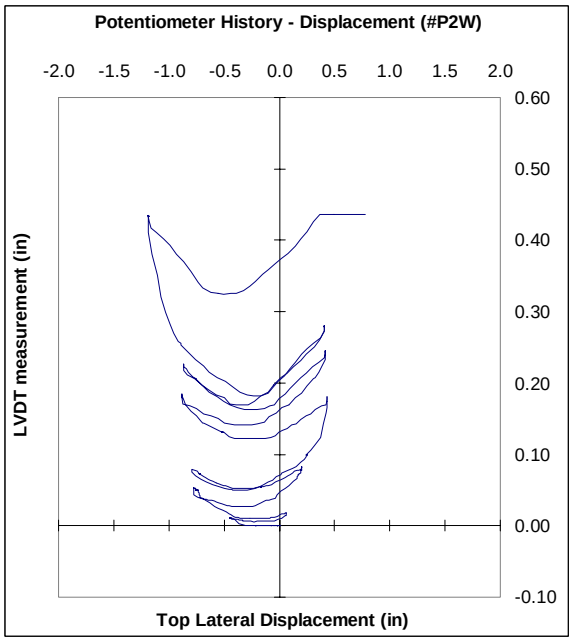

b) P. West. Horizontal at (h=22.5 in)

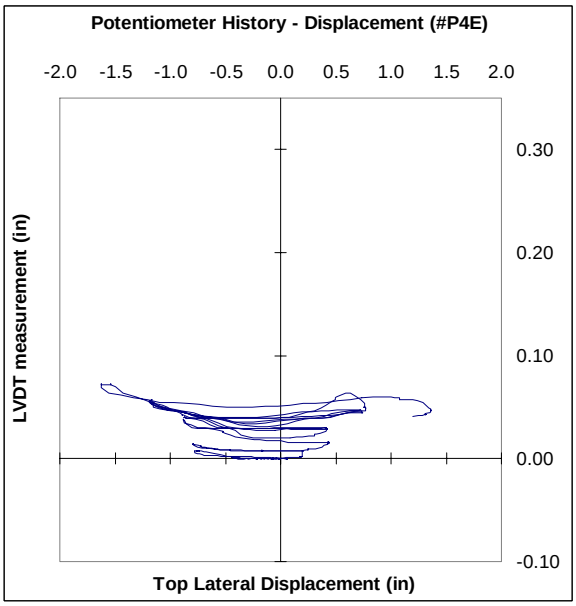

c) P. East. Horizontal at (h=41.25 in)

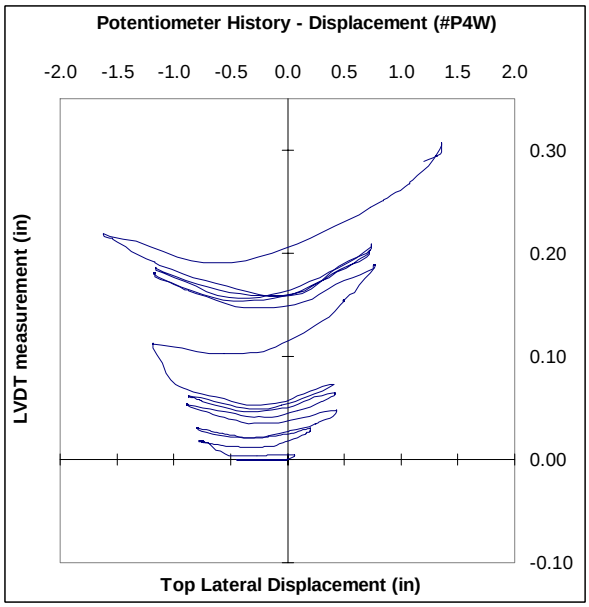

d) P. West. Horizontal at (h=41.25 in)

Figure 9.20. Linear Potentiometer Histories – Horizontal Elements–East and West Faces (LW2-NS-BSF)

9.5 Linear Potentiometer and Strain Gage Histories - Test (LW3-NS-BSF)

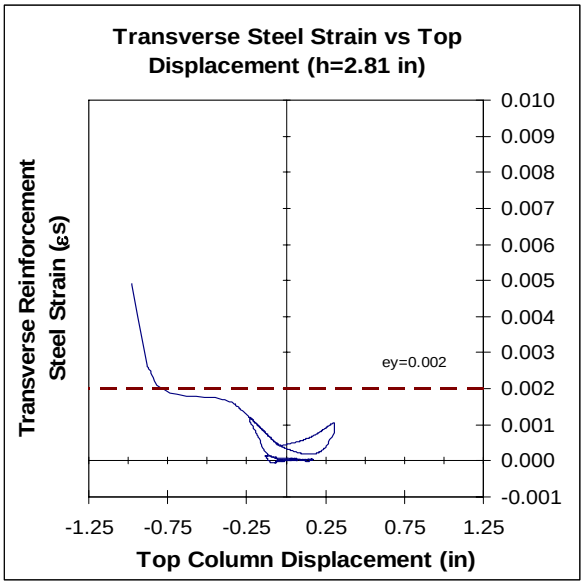

a) Height from the column base (h=2.81 in)

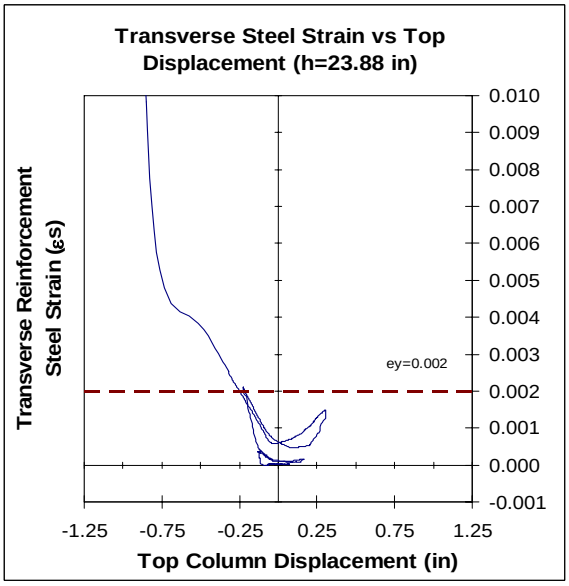

b) Height from the column base (h=23.88 in)

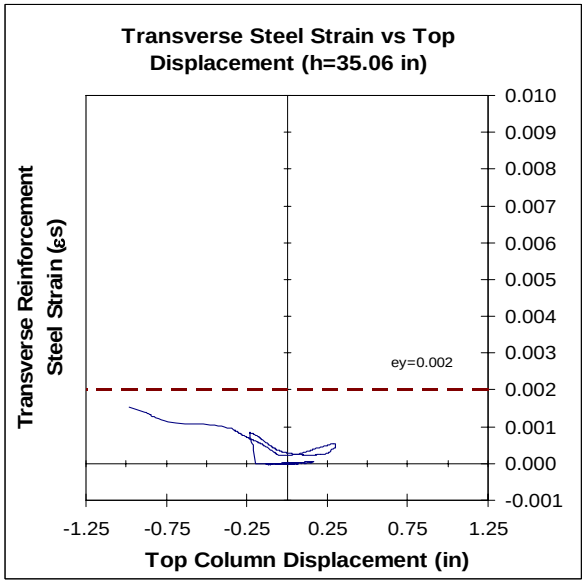

c) Height from the column base (h=35.06 in)

Figure 9.21. Average Transverse Steel Strain versus Top Column Displacement (LW3-NS-BSF)

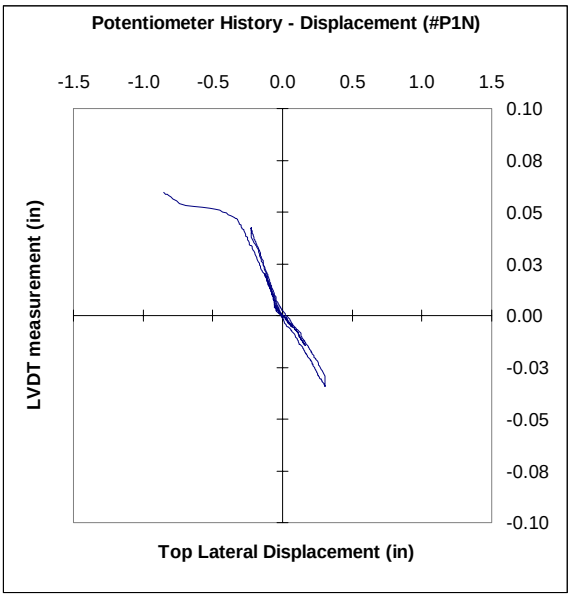

a) P. North. Gage at (h_1-h_2)=(0-7.5) in

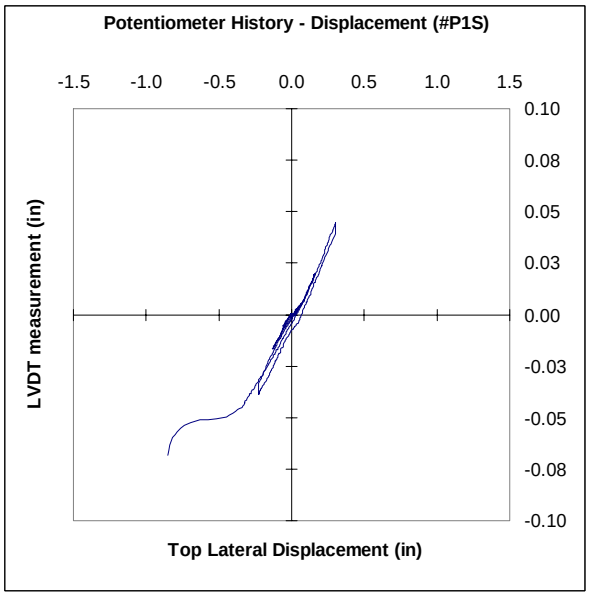

b) P. South. Gage at (h_1-h_2)=(0-7.5) in

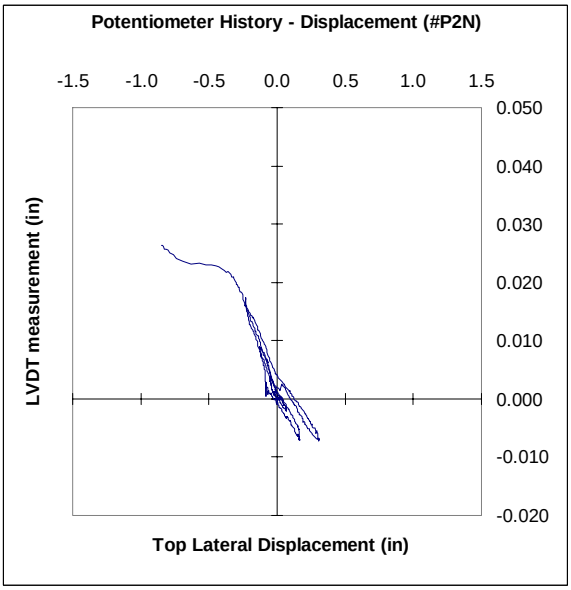

c) P. North. Gage at (h_1-h_2)=(7.5-15) in

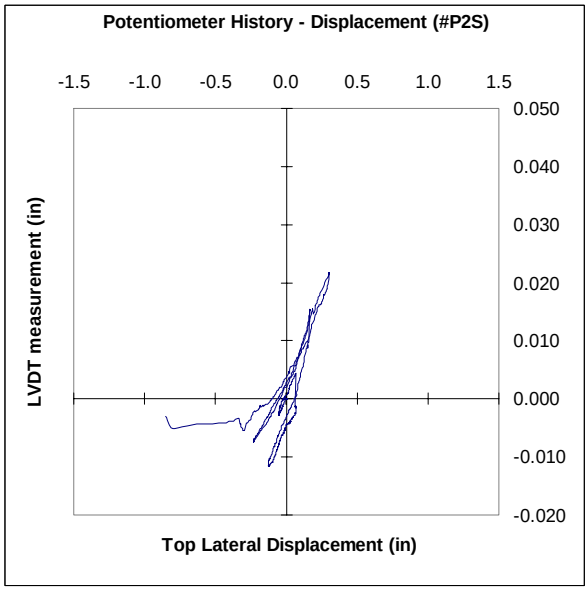

d) P. South. Gage at (h_1-h_2)=(7.5-15) in

Figure 9.22. Linear Potentiometer Histories at Gages 1 and 2 – North and South Faces (LW3-NS-BSF)

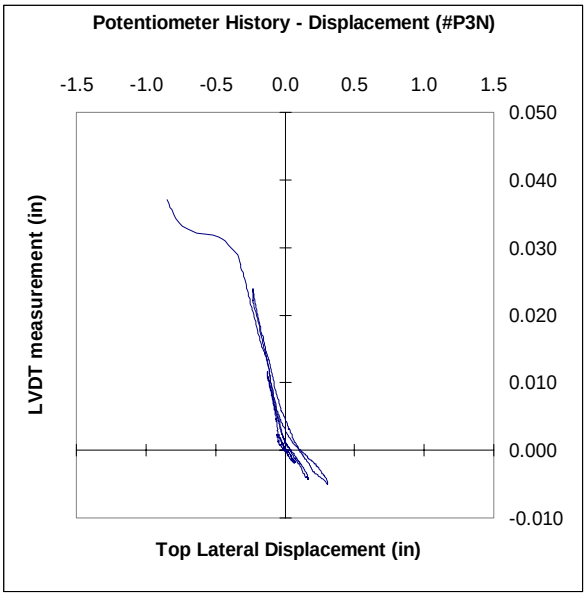

a) P. North. Gage at (h_1-h_2)=(15-22.5) in

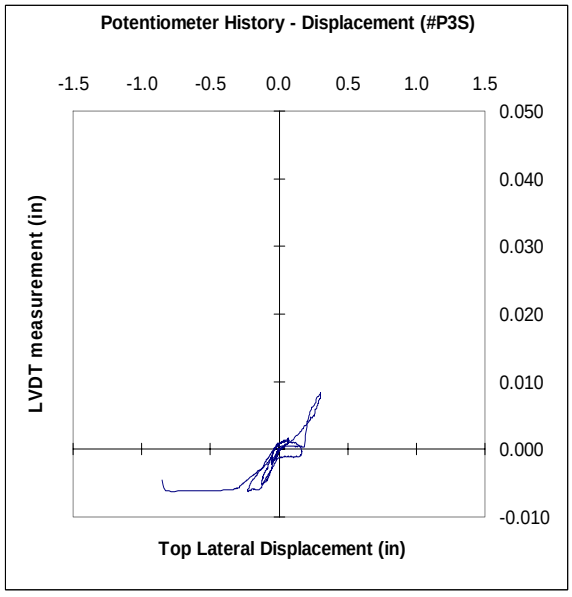

b) P. South. Gage at (h_1-h_2)=(15-22.5) in

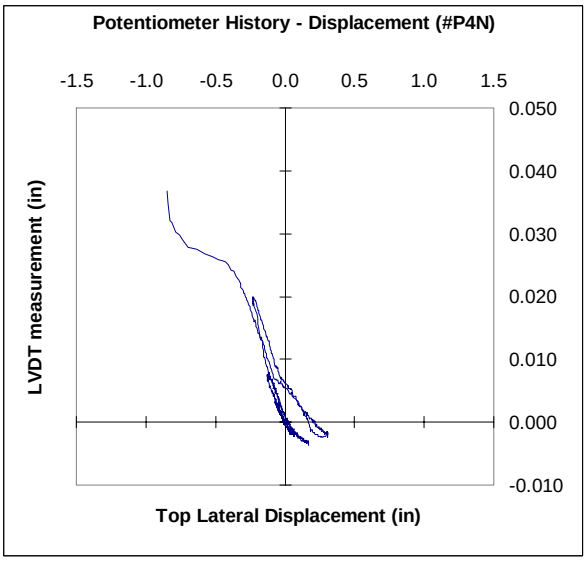

c) P. North. Gage at (h_1-h_2)=(22.5-33.75) in

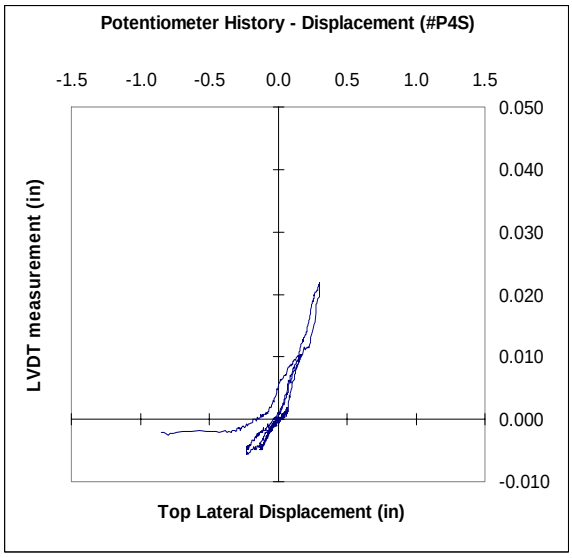

d) P. South. Gage at (h_1-h_2)=(22.5-33.75) in

Figure 9.23. Linear Potentiometer Histories at Gages 3 and 4 – North and South Faces (LW3-NS-BSF)

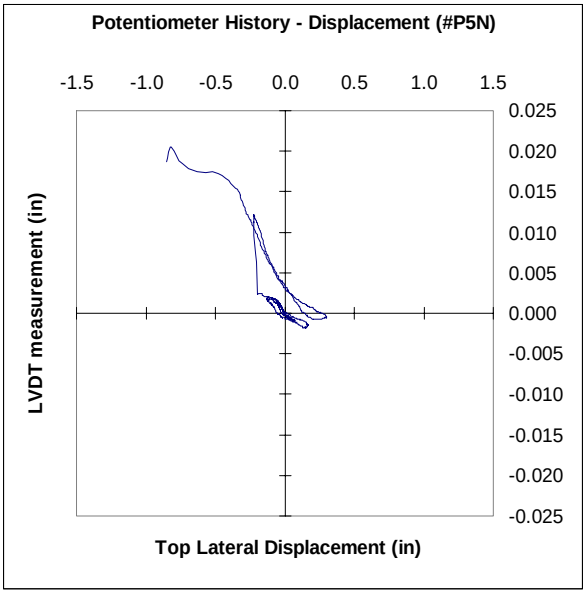

a) P. North. Gage at (h_1-h_2)=(33.75-40.38) in

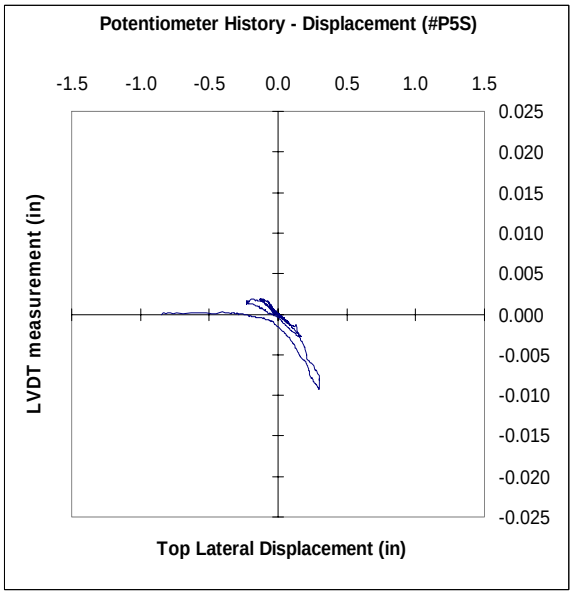

b) P. South. Gage at (h_1-h_2)=(33.75-40.38) in

Figure 9.24. Linear Potentiometer Histories at Gage 5 – North and South Faces (LW3-NS-BSF)

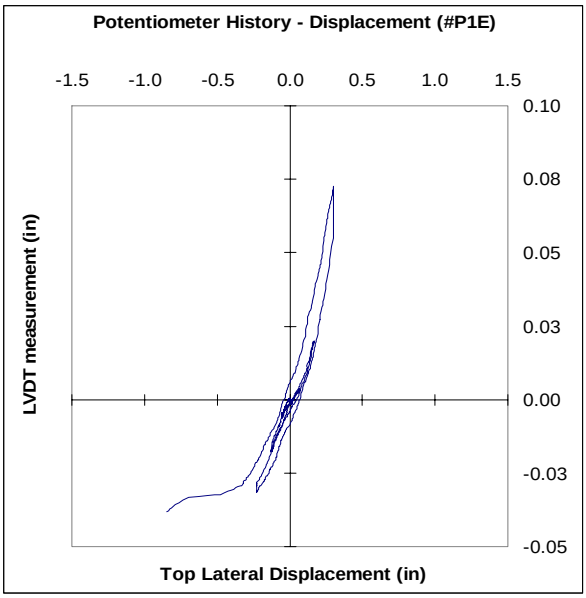

a) P. East. Diagonal at (h_1-h_2)=(0-22.5) in

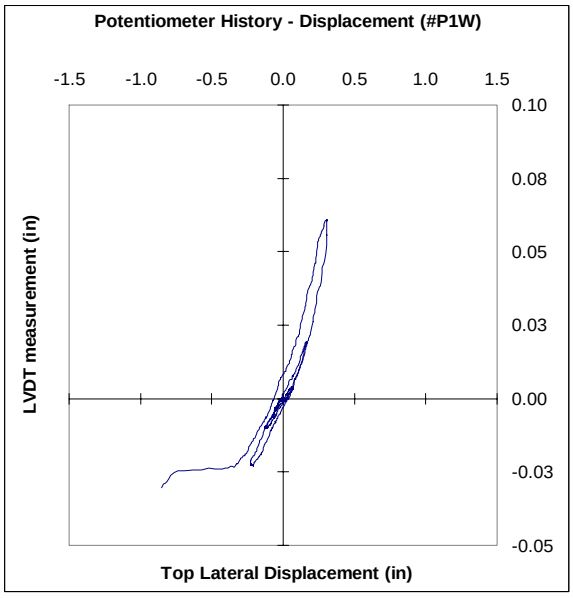

b) P. West. Diagonal at (h_1-h_2)=(0-22.5) in

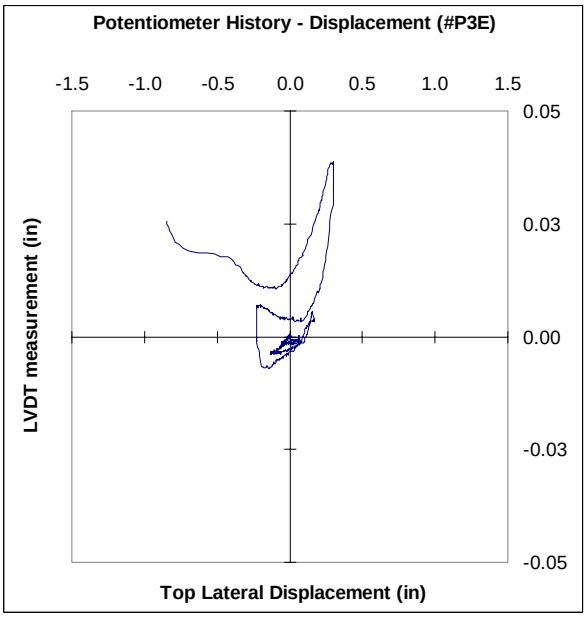

c) P. East. Diagonal at (h_1-h_2)=(22.5-40.38) in

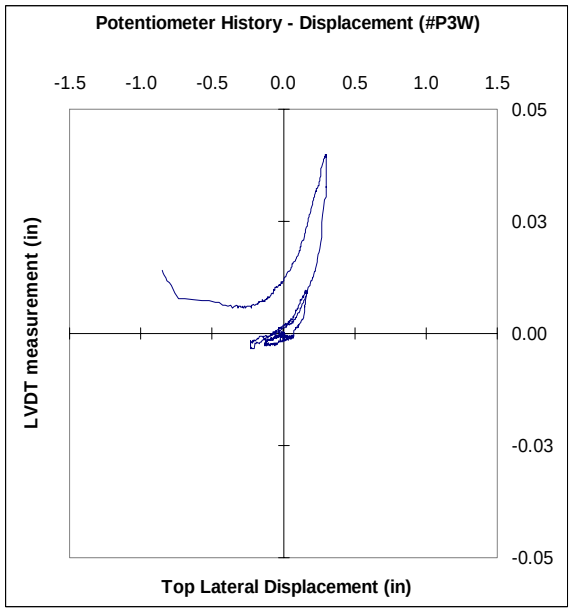

d) P. West. Diag. at (h_1-h_2)=(22.5-40.38) in

Figure 9.25. Linear Potentiometer Histories – Diagonal Elements – East and West Faces (LW3-NS-BSF)

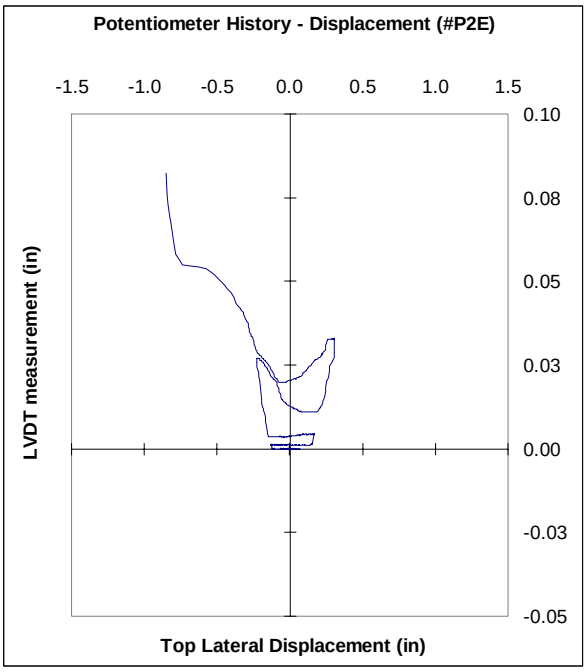

a) P. East. Horizontal at (h=22.5 in)

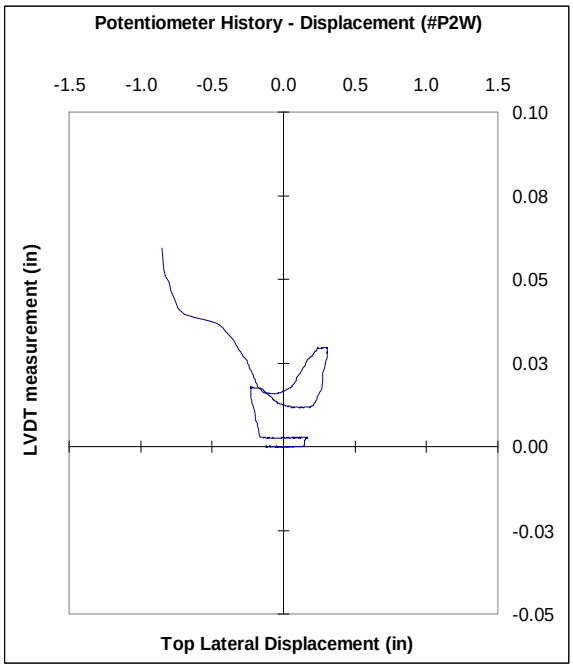

b) P. West. Horizontal at (h=22.5 in)

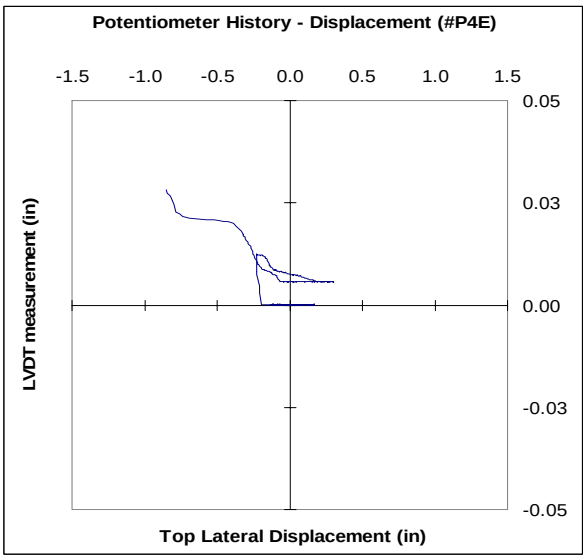

c) P. East. Horizontal at (h=40.38 in)

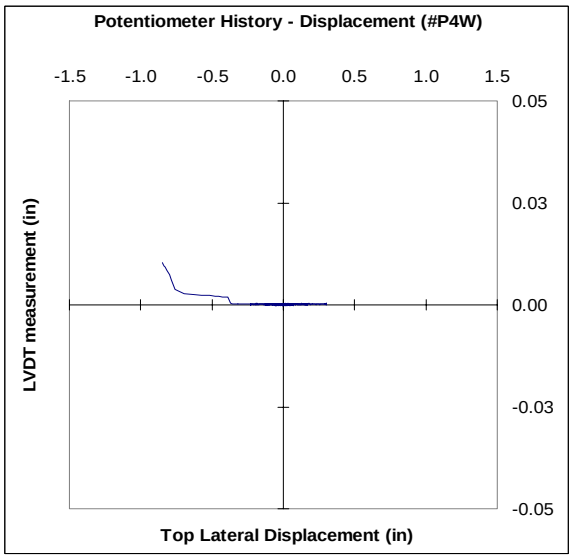

d) P. West. Horizontal at (h=40.38 in)

Figure 9.26. Linear Potentiometer Histories – Horizontal Elements–East and West Faces (LW3-NS-BSF)

9.6 Linear Potentiometer and Strain Gage Histories - Test (NW-NS-DSF)

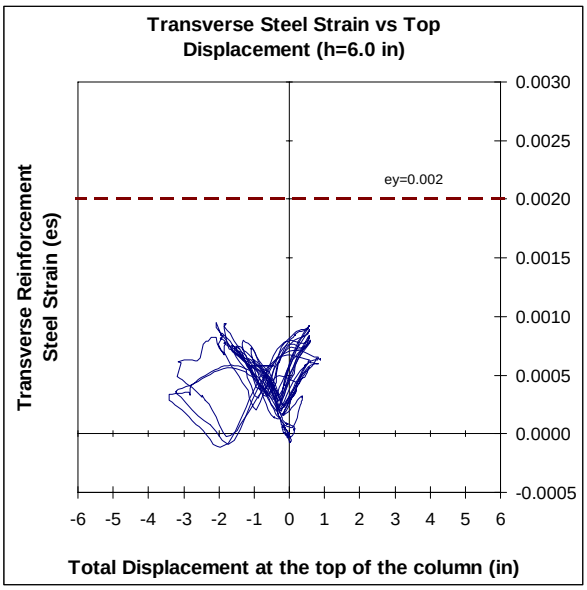

a) Height from the column base (h=6.00 in)

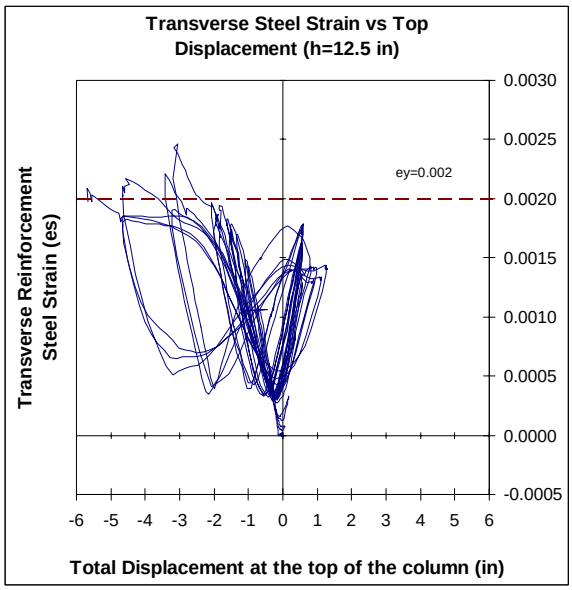

b) Height from the column base (h=12.50 in)

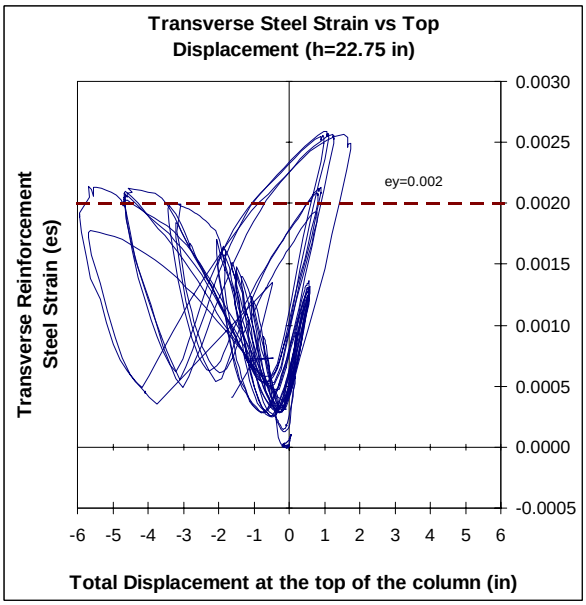

c) Height from the column base (h=22.75 in)

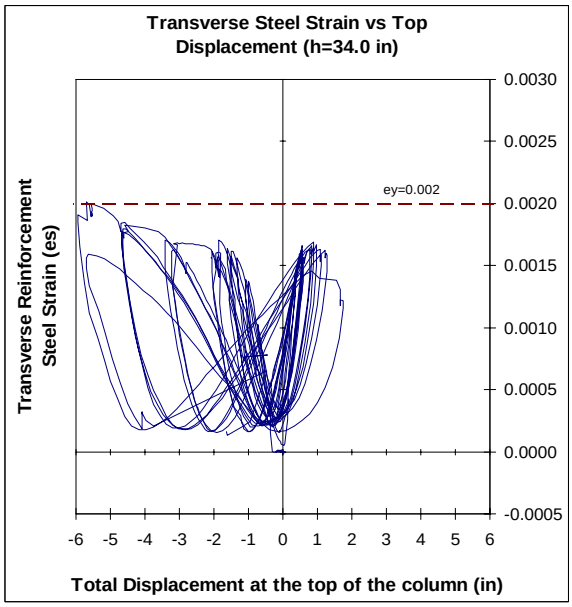

d) Height from the column base (h=34.00 in)

Figure 9.27. Average Transverse Steel Strain versus Top Column Displacement (NW-NS-DSF)

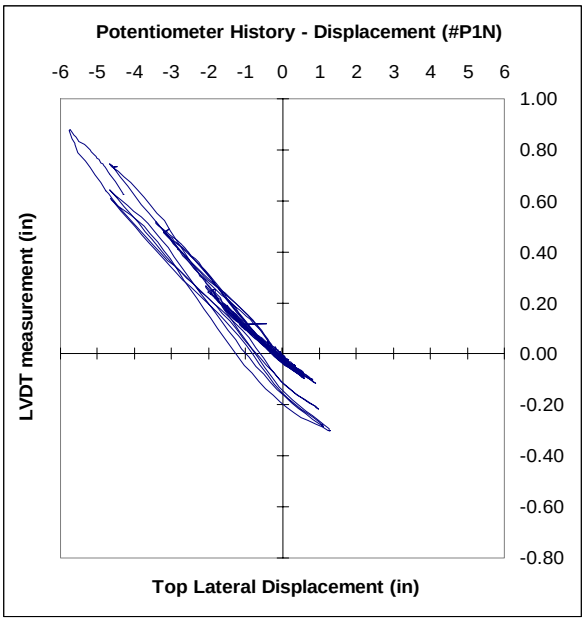

a) P. North. Gage at (h_1-h_2)=(0-7.5) in

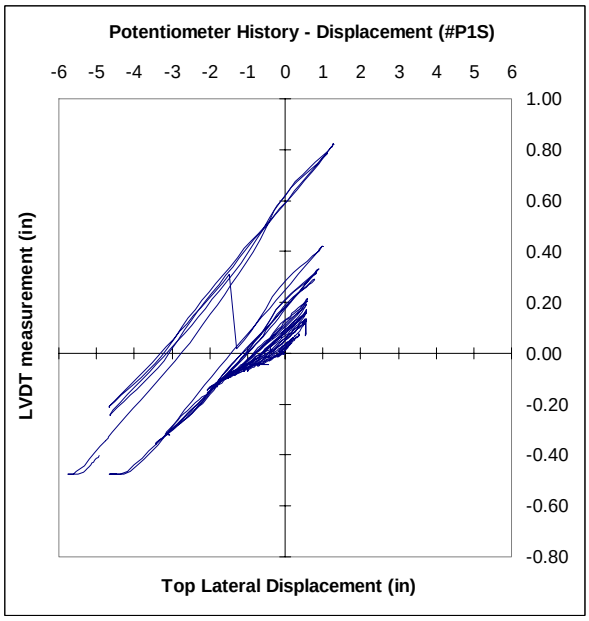

b) P. South. Gage at (h_1-h_2)=(0-7.5) in

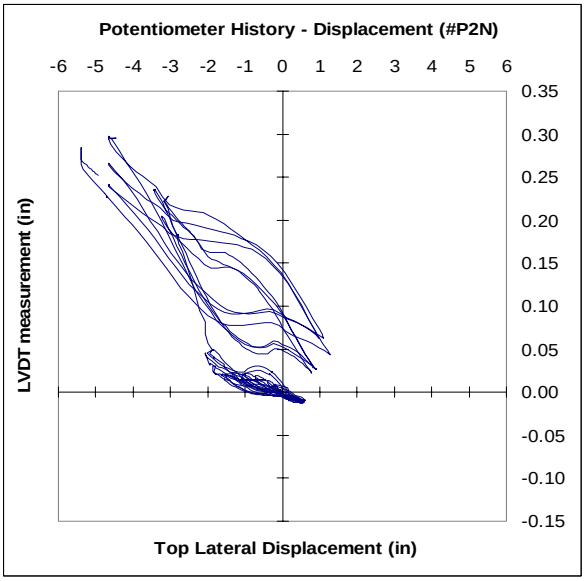

c) P. North. Gage at (h_1-h_2)=(7.5-15) in

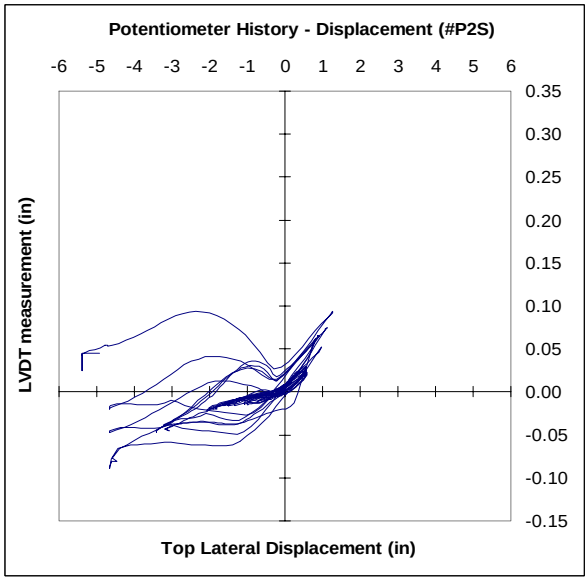

d) P. South. Gage at (h_1-h_2)=(7.5-15) in

Figure 9.28. Linear Potentiometer Histories at Gages 1 and 2 – North and South Faces (NW-NS-DSF)

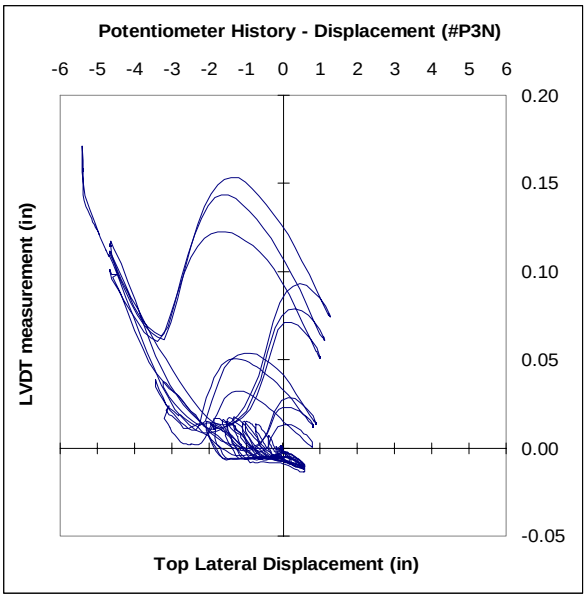

a) P. North. Gage at (h_1-h_2)=(15-22.5) in

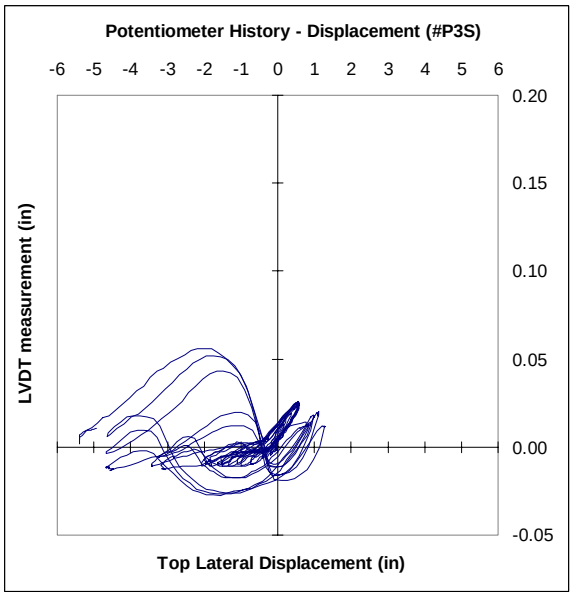

b) P. South. Gage at (h_1-h_2)=(15-22.5) in

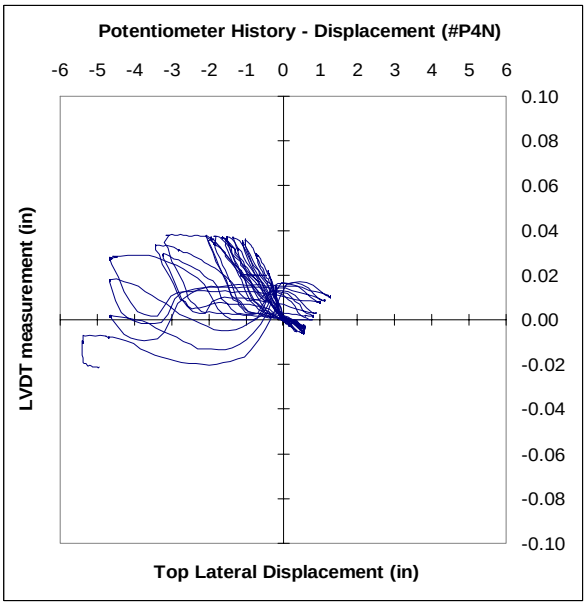

c) P. North. Gage at (h_1-h_2)=(22.5-33.75) in

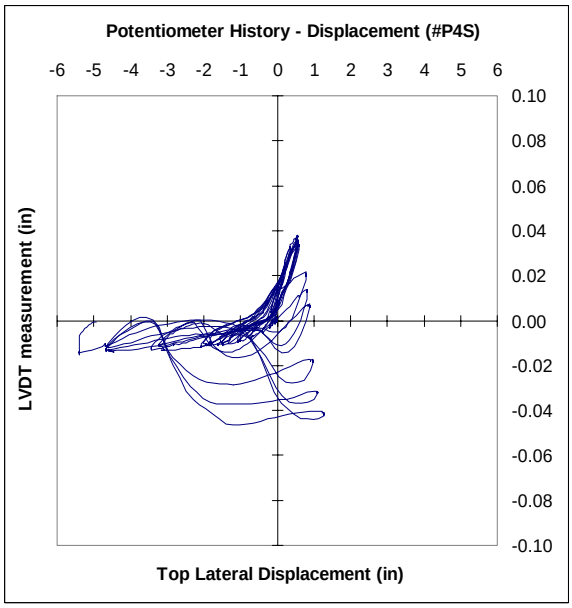

d) P. South. Gage at (h_1-h_2)=(22.5-33.75) in

Figure 9.29. Linear Potentiometer Histories at Gages 3 and 4 – North and South Faces (NW-NS-DSF)

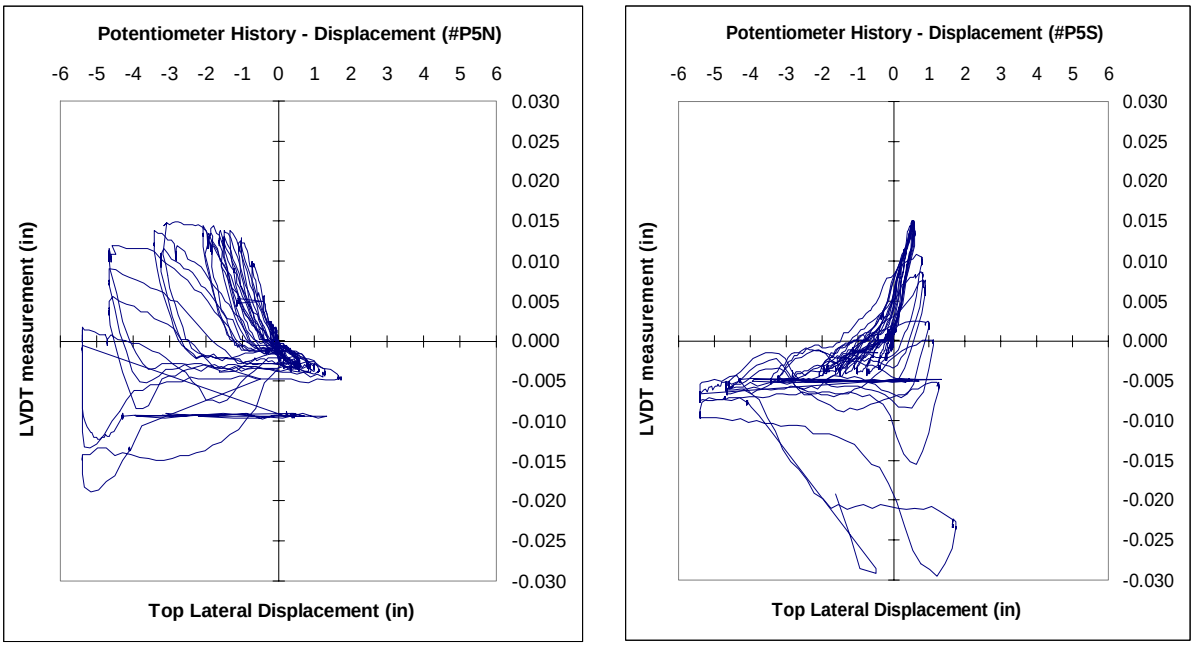

a) P. North. Gage at (h_1-h_2)=(33.75-45) in

b) P. South. Gage at (h_1-h_2)=(33.75-45) in

Figure 9.30. Linear Potentiometer Histories at Gage 5 – North and South Faces (NW-NS-DSF)

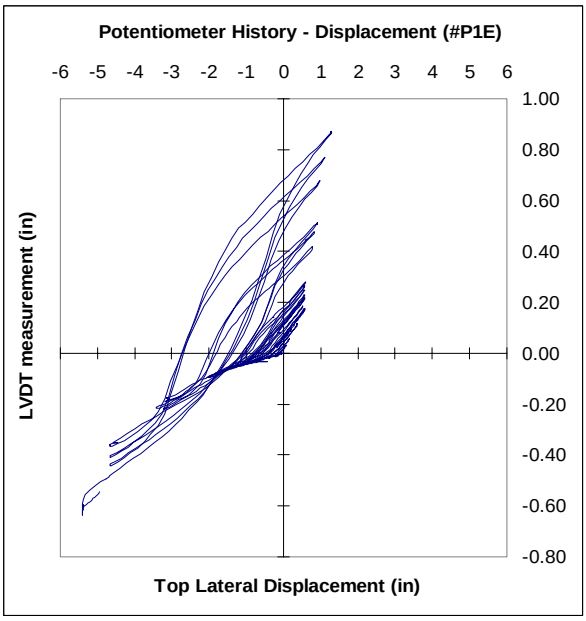

a) P. East. Diagonal at (h_1-h_2)=(0-22.5) in

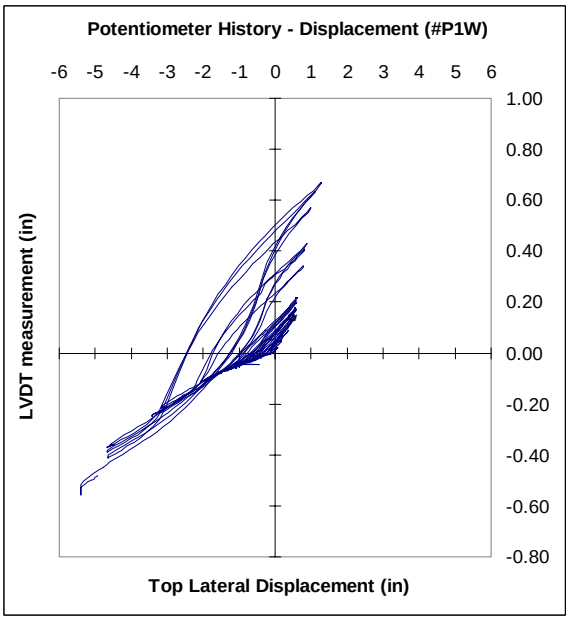

b) P. West. Diagonal at (h_1-h_2)=(0-22.5) in

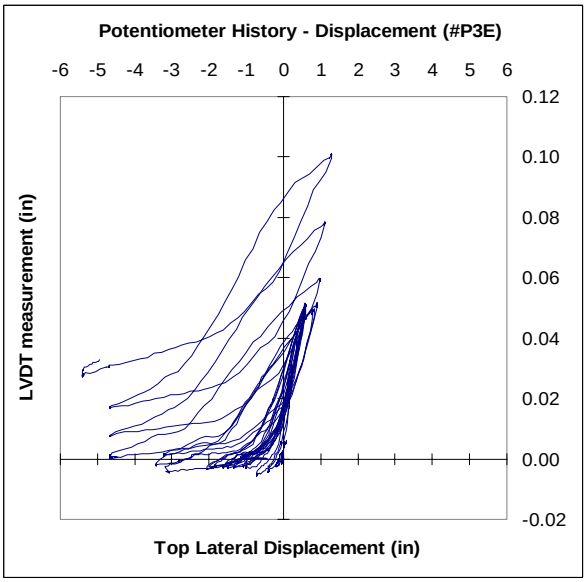

c) P. East. Diagonal at (h_1-h_2)=(22.5-45) in

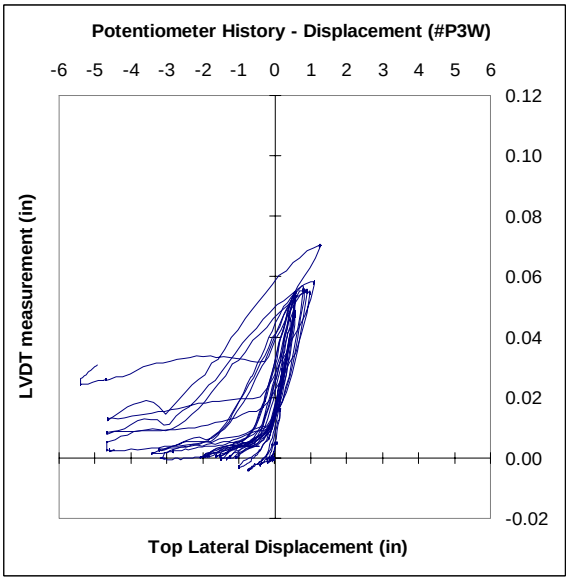

d) P. West. Diagonal at (h_1-h_2)=(22.5-45) in

Figure 9.31. Linear Potentiometer Histories – Diagonal Elements – East and West Faces (NW-NS-DSF)

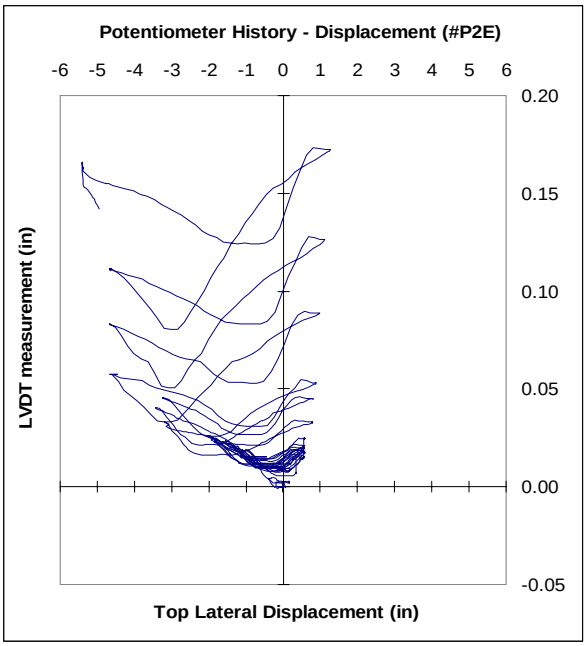

a) P. East. Horizontal at (h=22.5 in)

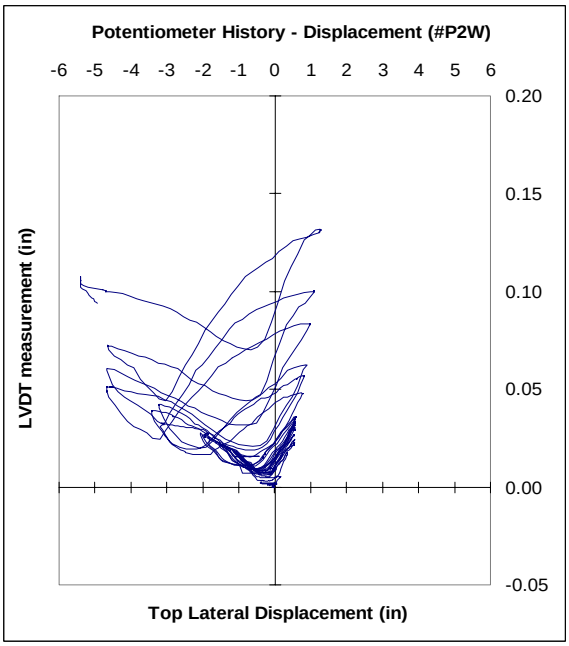

b) P. West. Horizontal at (h=22.5 in)

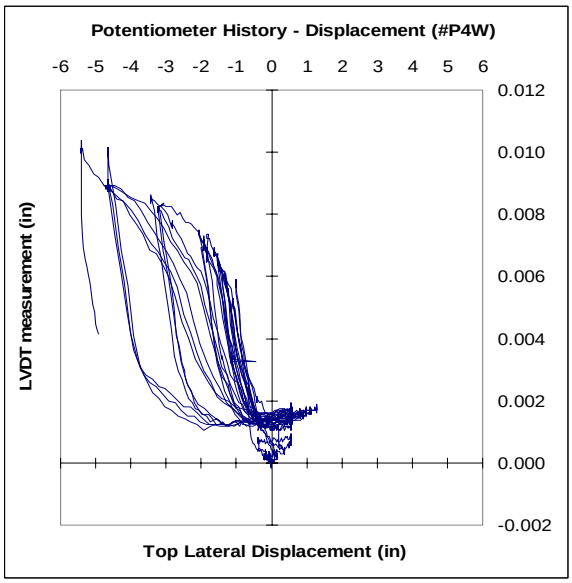

d) P. West. Horizontal at (h=45 in)

Figure 9.32. Linear Potentiometer Histories – Horizontal Elements – East and West Faces (NW-NS-DSF)

9.7 Linear Potentiometer and Strain Gage Histories - Test (LW1-NS-DSF)

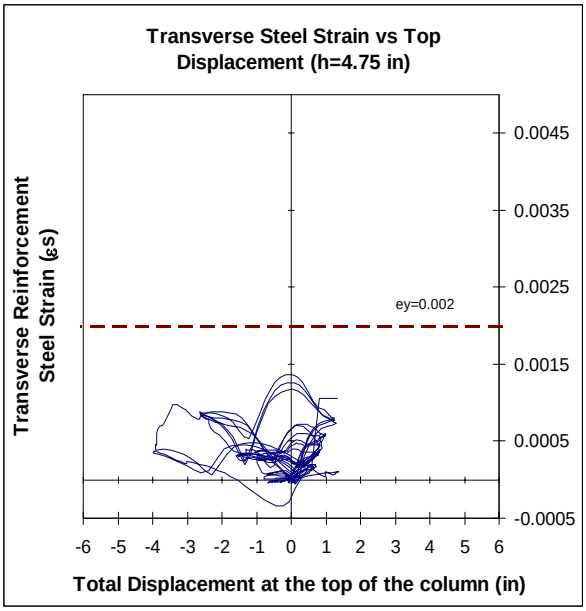

a) Height from the column base (h=4.75 in)

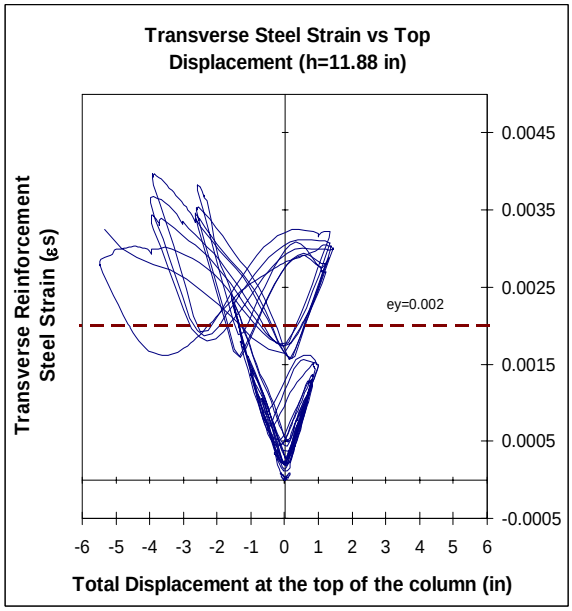

b) Height from the column base (h=11.88 in)

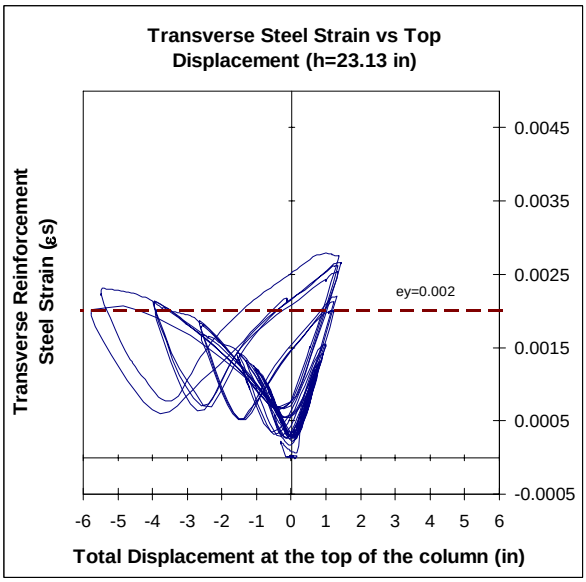

c) Height from the column base (h=23.13 in)

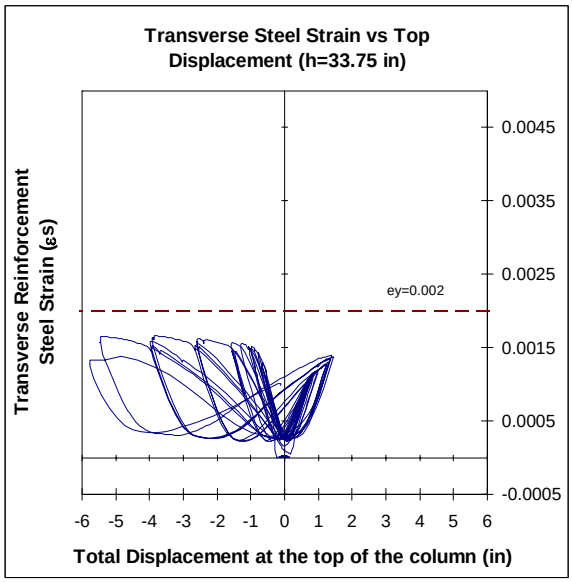

d) Height from the column base (h=33.75 in)

Figure 9.33. Average Transverse Steel Strain versus Top Column Displacement (LW1-NS-DSF)

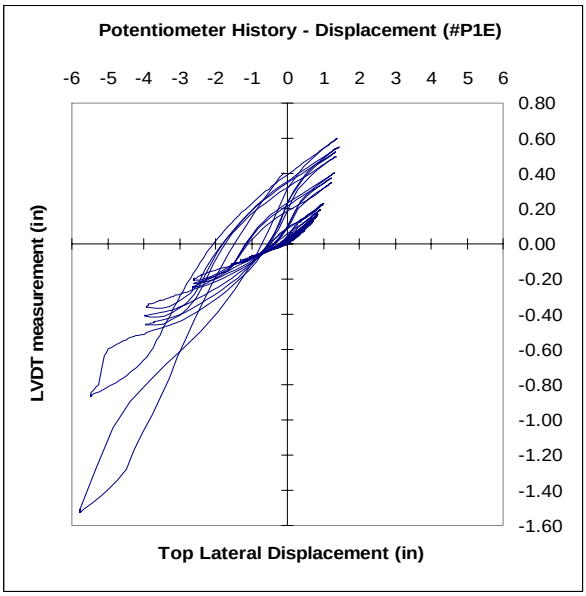

a) P. East. Diagonal at (h_1-h_2)=(0-22.5) in

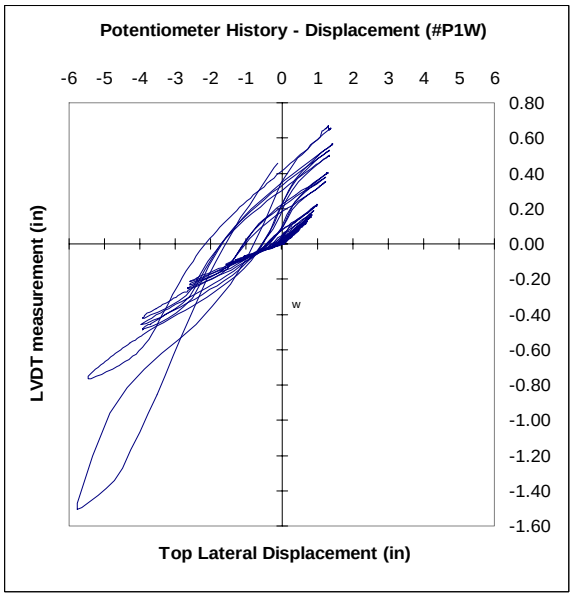

b) P. West. Diagonal at (h_1-h_2)=(0-22.5) in

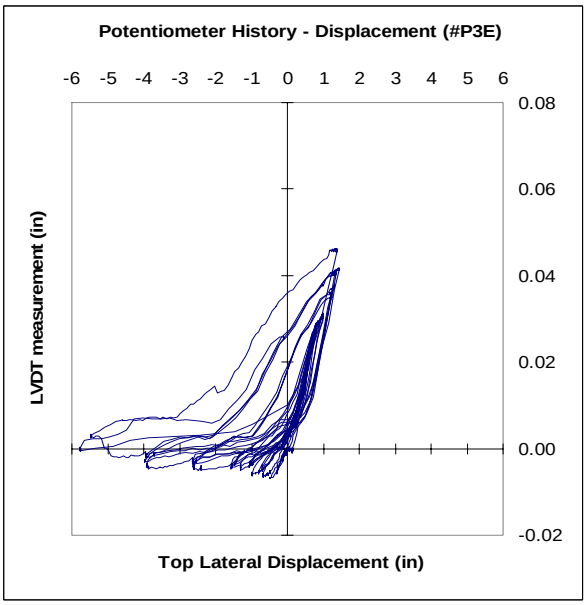

c) P. East. Diagonal at (h_1-h_2)=(22.5-45) in

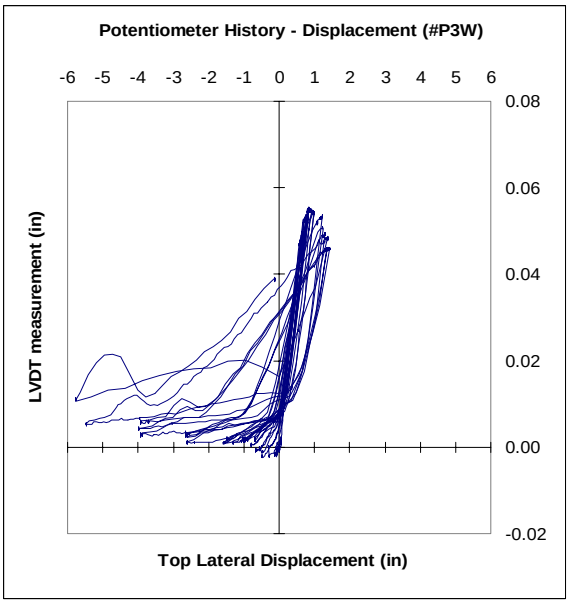

d) P. West. Diagonal at (h_1-h_2)=(22.5-45) in

Figure 9.34. Linear Potentiometer Histories – Diagonal Elements – East and West Faces (LW1-NS-DSF)

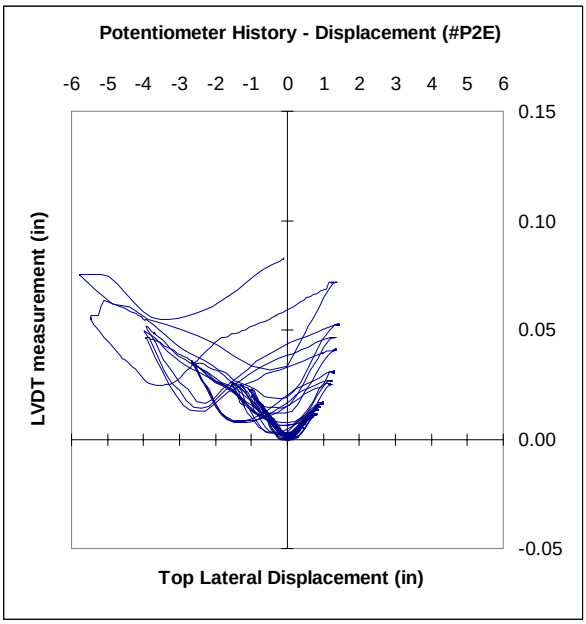

a) P. East. Horizontal at (h=22.5 in)

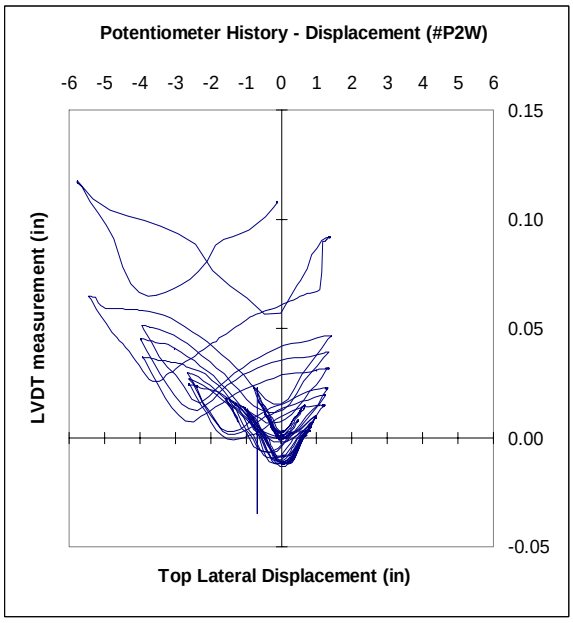

b) P. West. Horizontal at (h=22.5 in)

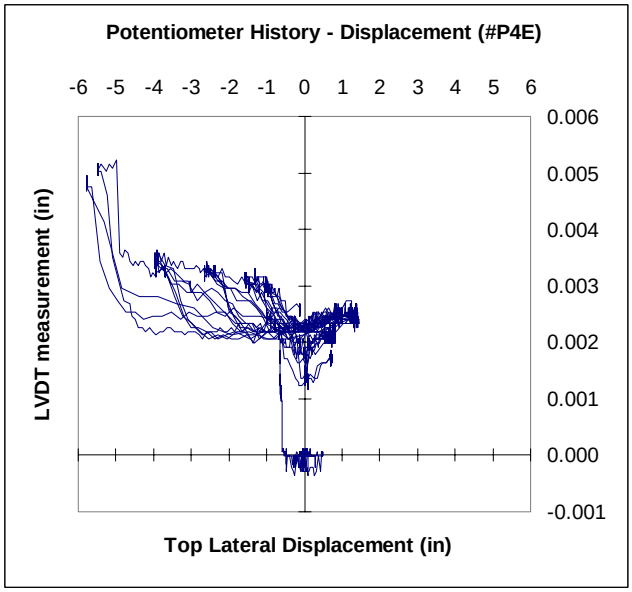

d) P. East. Horizontal at (h=45 in)

Figure 9.35. Linear Potentiometer Histories–Horizontal Elements – East and West Faces (LW1-NS-DSF)

9.8 Linear Potentiometer and Strain Gage Histories - Test (LW2-NS-DSF)

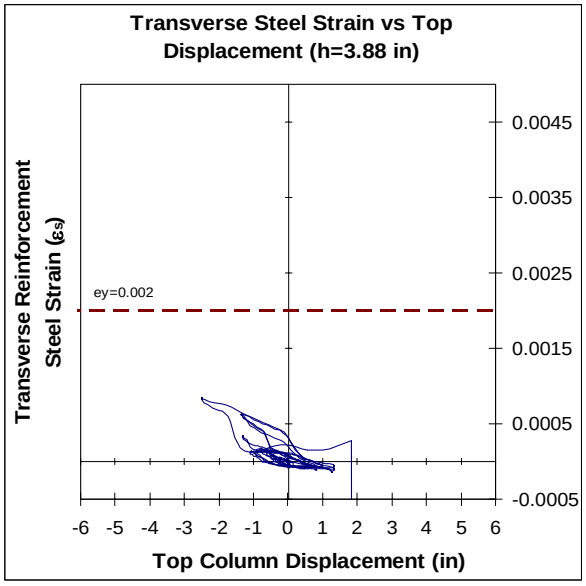

a) Height from the column base (h=3.88 in)

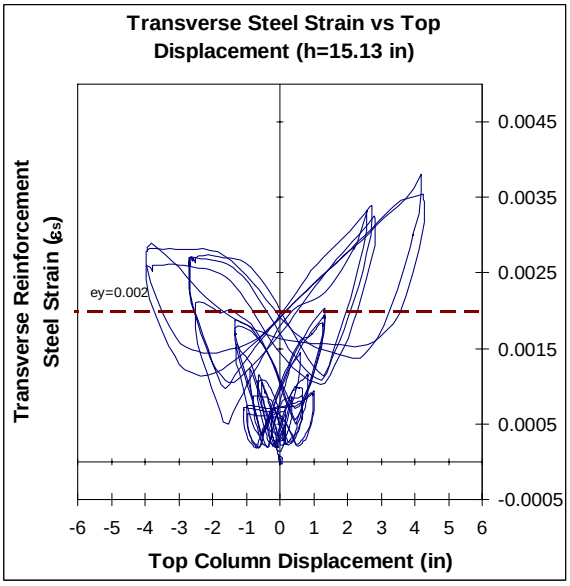

b) Height from the column base (h=15.13 in)

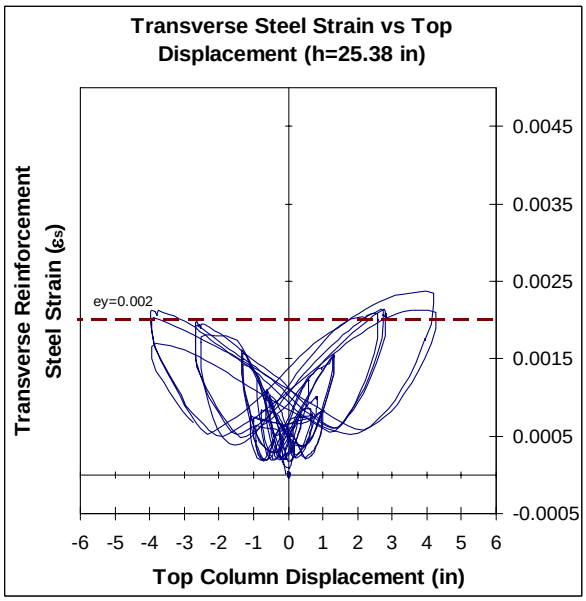

c) Height from the column base (h=25.38 in)

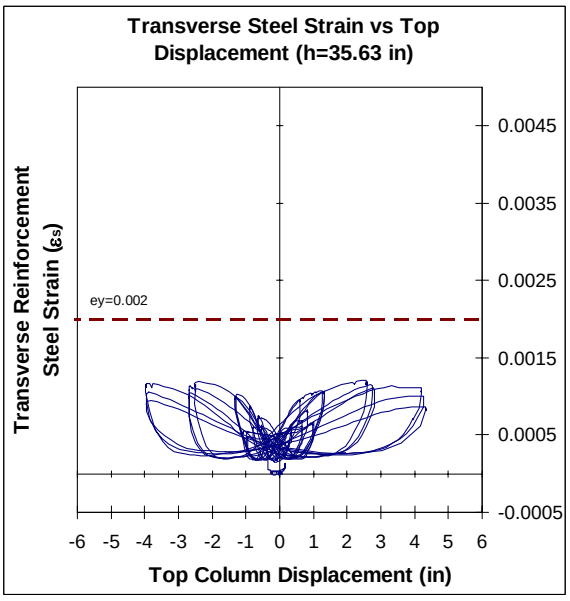

d) Height from the column base (h=35.63 in)

Figure 9.36. Average Transverse Steel Strain versus Top Column Displacement (LW2-NS-DSF)

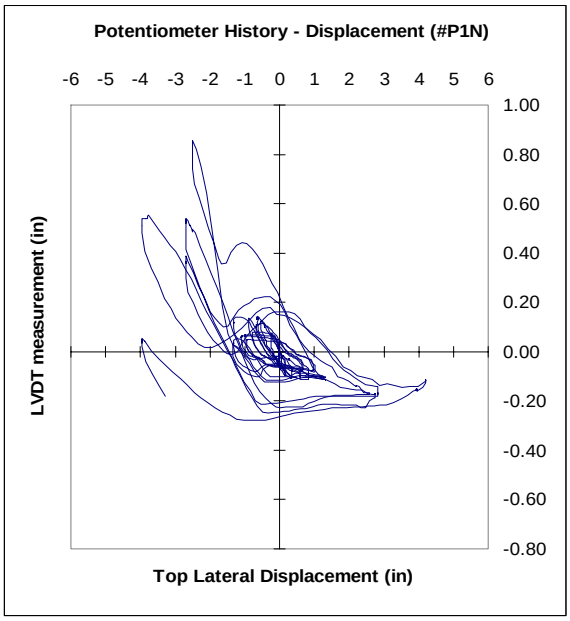

a) P. North. Gage at (h_1-h_2)=(0-7.5) in

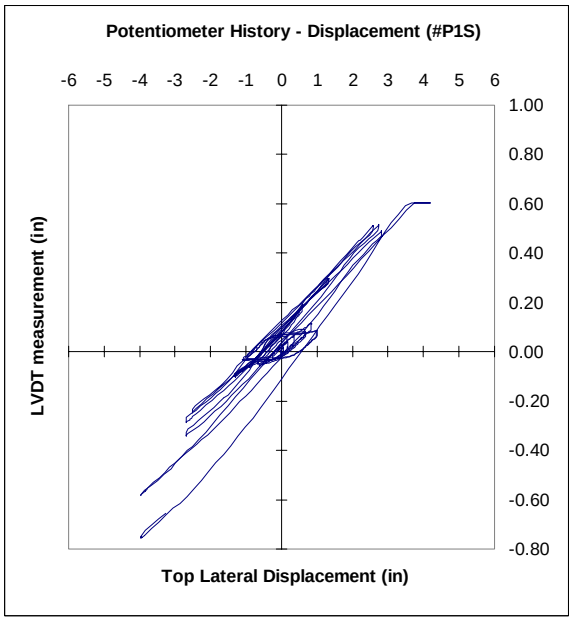

b) P. South. Gage at (h_1-h_2)=(0-7.5) in

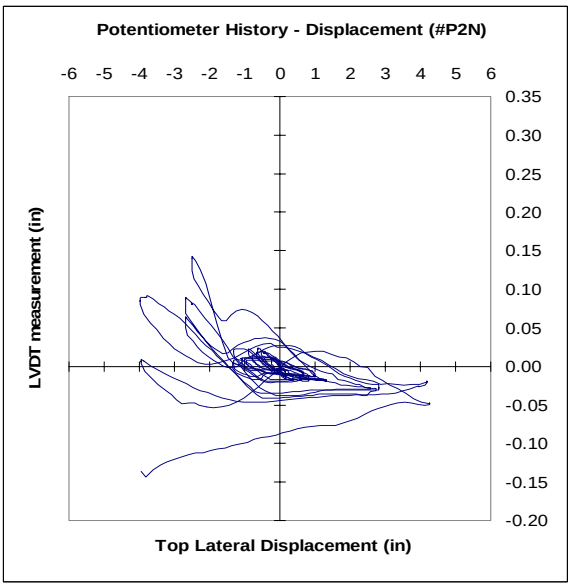

c) P. North. Gage at (h_1-h_2)=(7.5-15) in

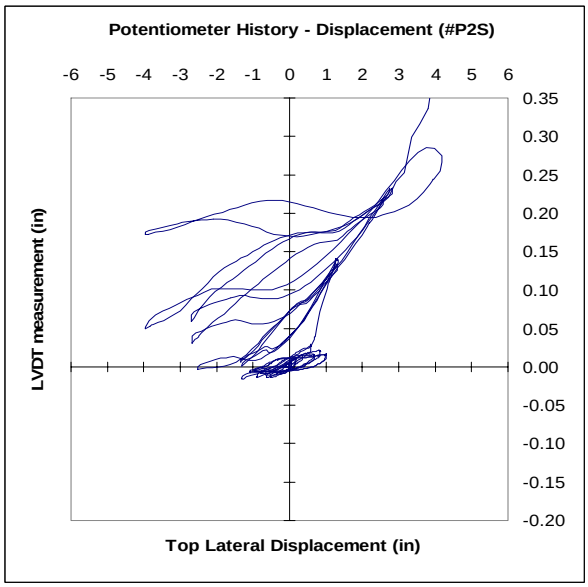

d) P. South. Gage at (h_1-h_2)=(7.5-15) in

Figure 9.37. Linear Potentiometer Histories at Gages 1 and 2 – North and South Faces (LW2-NS-DSF)

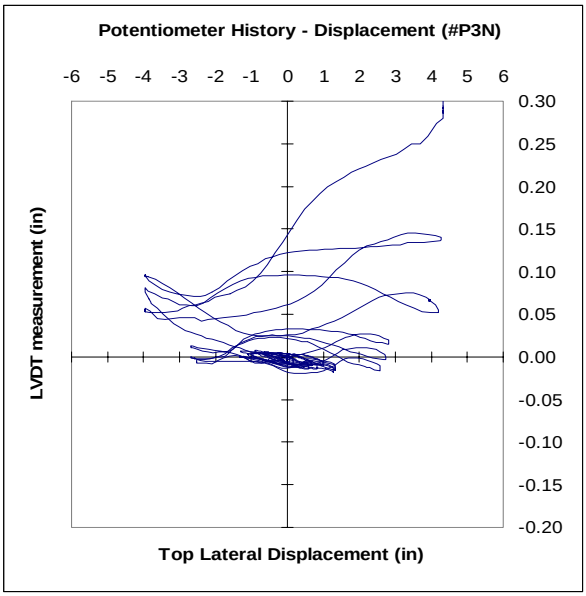

a) P. North. Gage at (h_1-h_2)=(15-22.5) in

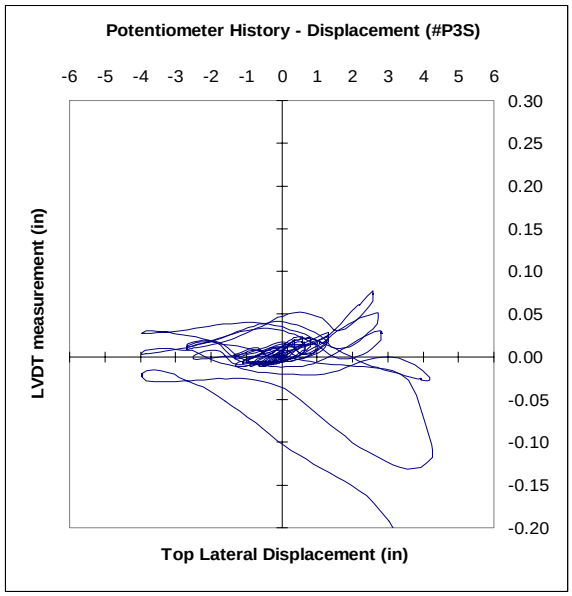

b) P. South. Gage at (h_1-h_2)=(15-22.5) in

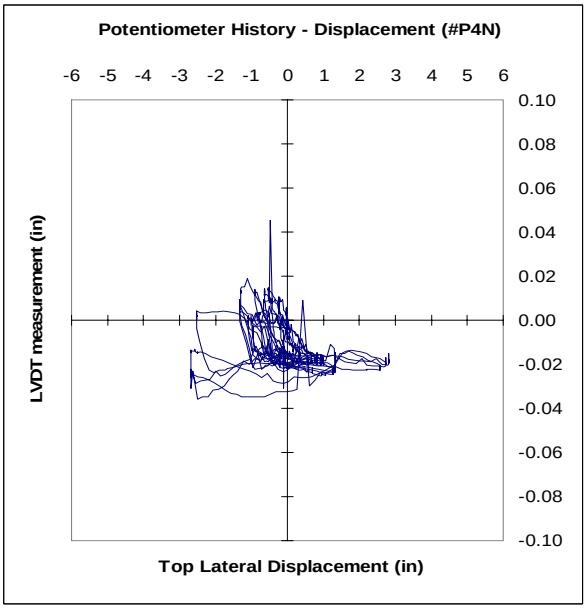

c) P. North. Gage at (h_1-h_2)=(22.5-33.75) in

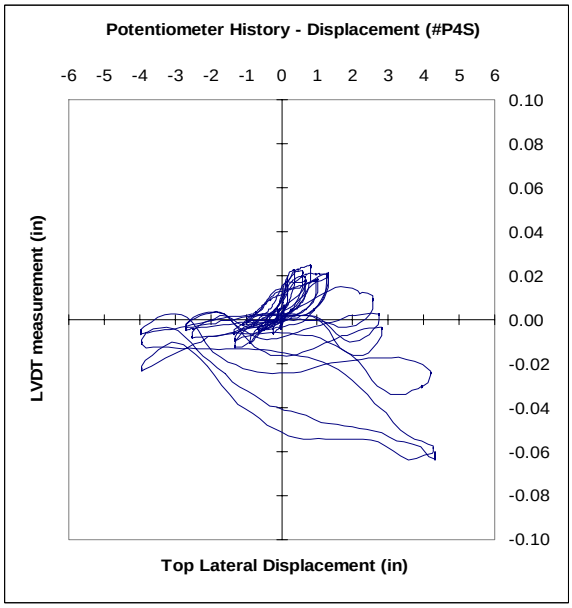

d) P. South. Gage at (h_1-h_2)=(22.5-33.75) in

Figure 9.38. Linear Potentiometer Histories at Gages 3 and 4 – North and South Faces (LW2-NS-DSF)

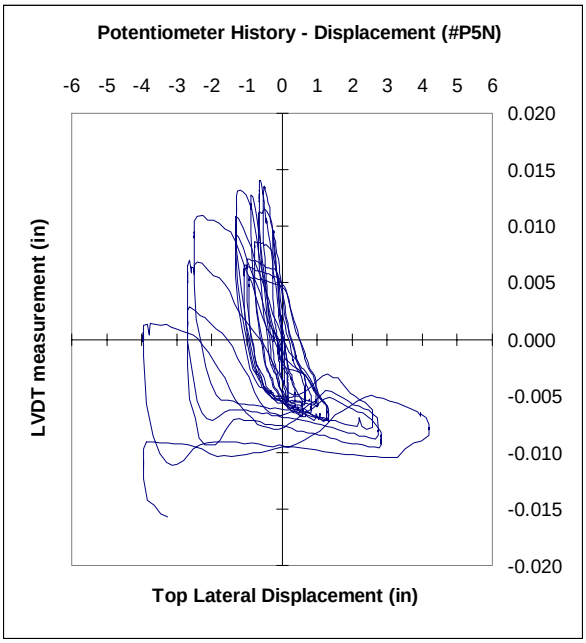

a) P. North. Gage at (h_1-h_2)=(33.75-41.25) in

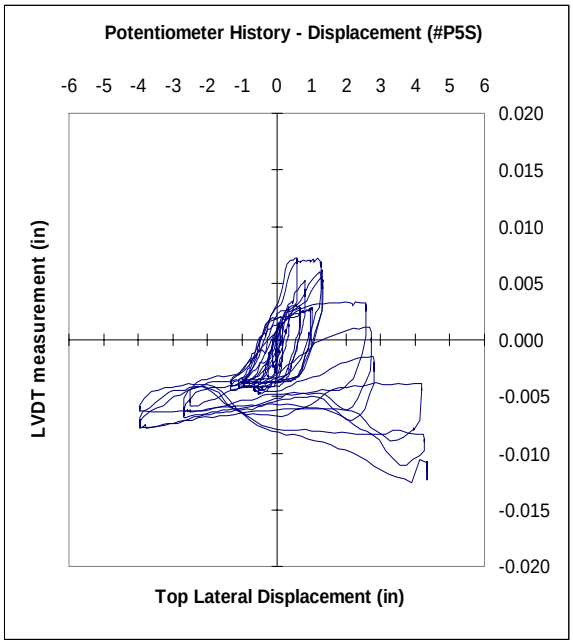

b) P. South. Gage at (h_1-h_2)=(33.75-41.25) in

Figure 9.39. Linear Potentiometer Histories at Gage 5 – North and South Faces (LW2-NS-DSF)

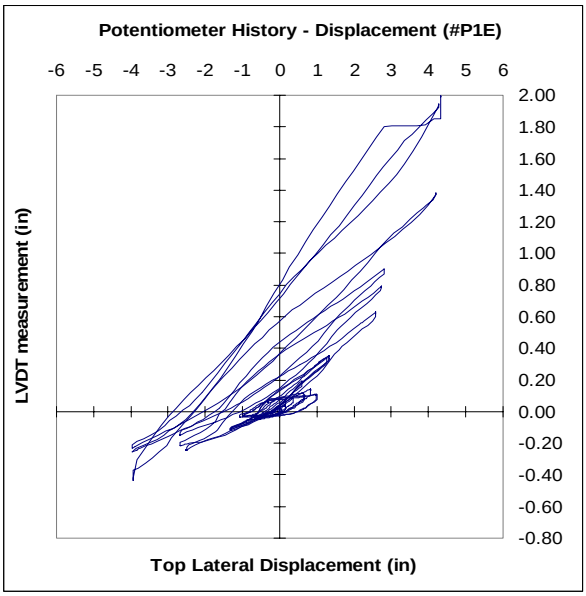

a) P. East. Diagonal at (h_1-h_2)=(0-22.5) in

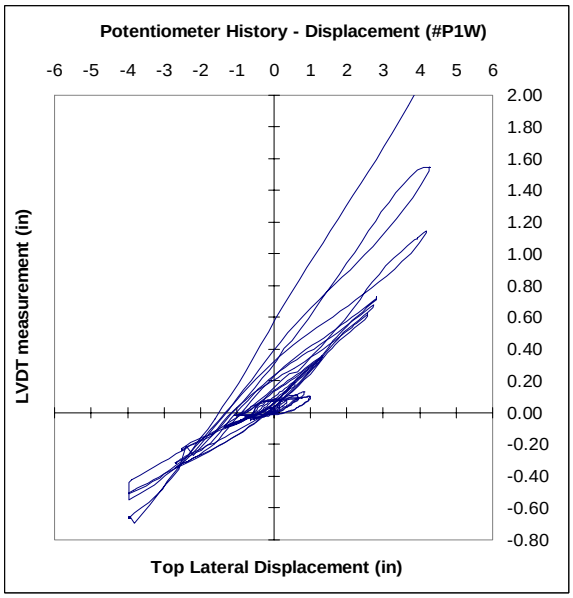

b) P. West. Diagonal at (h_1-h_2)=(0-22.5) in

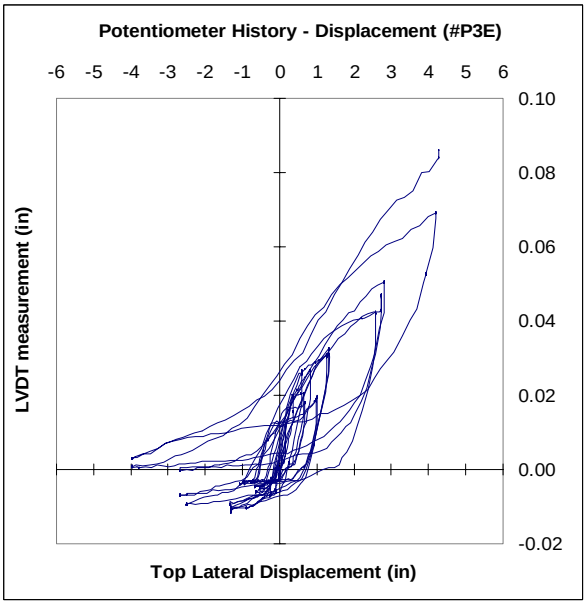

c) P. East. Diagonal at (h_1-h_2)=(22.5-41.25) in

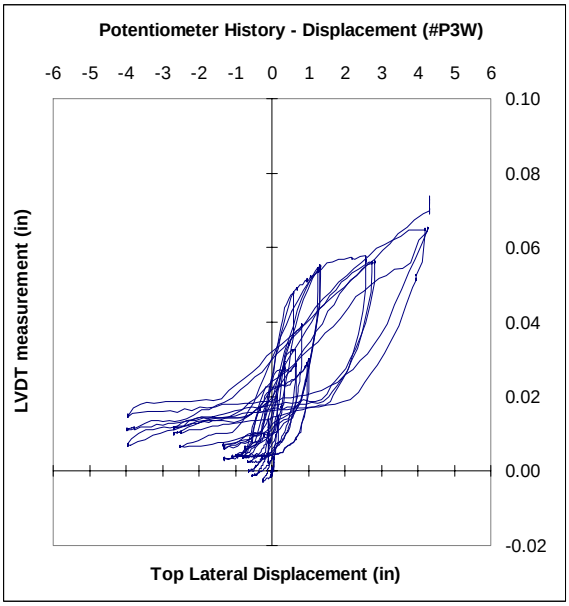

d) P. West. Diag. at (h_1-h_2)=(22.5-41.25) in

Figure 9.40. Linear Potentiometer Histories – Diagonal Elements – East and West Faces (LW2-NS-DSF)

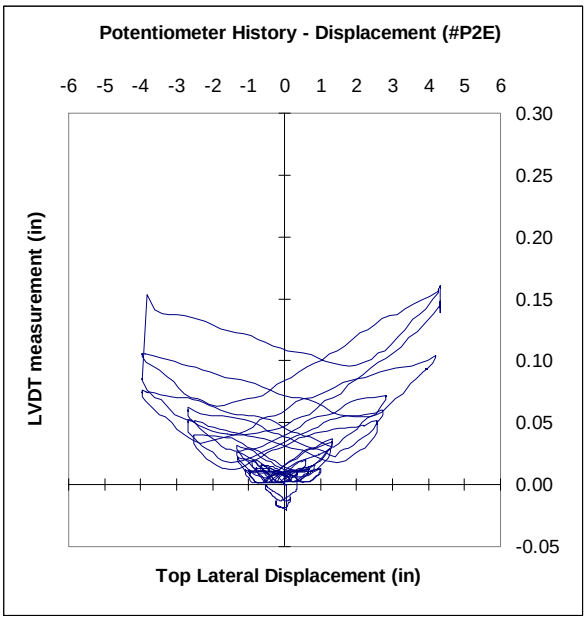

a) P. East. Horizontal at (h=22.5 in)

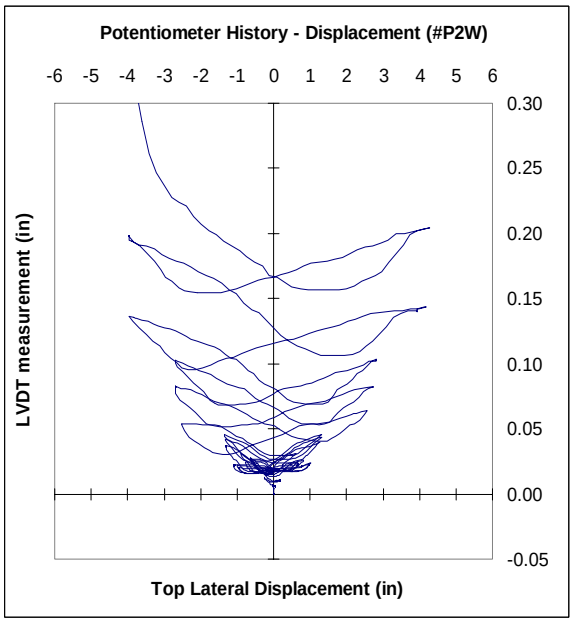

b) P. West. Horizontal at (h=22.5 in)

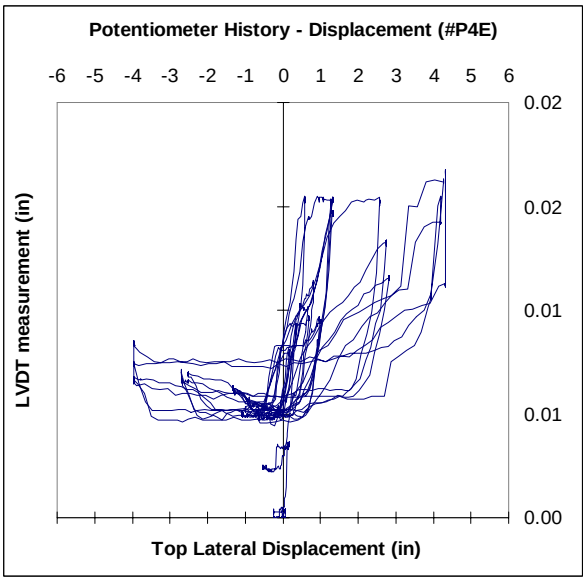

c) P. East. Horizontal at (h=41.25 in)

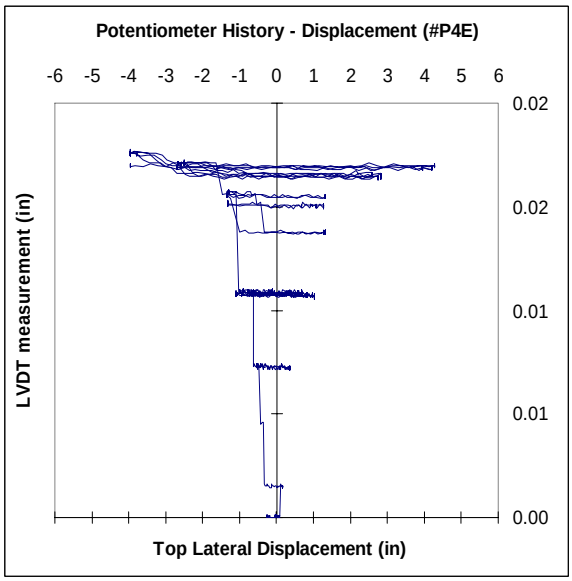

d) P. West. Horizontal at (h=41.25 in)

Figure 9.41. Linear Potentiometer Histories–Horizontal Elements–East and West Faces (LW2-NS-DSF)

9.9 Linear Potentiometer and Strain Gage Histories - Test (LW3-NS-DSF)

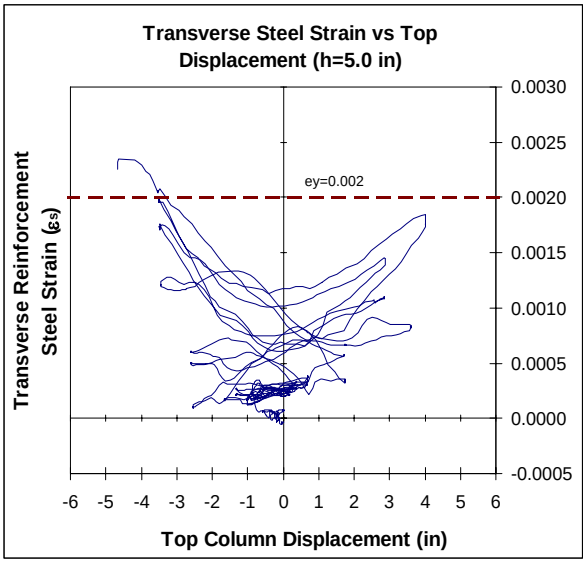

a) Height from the column base (h=5.00 in)

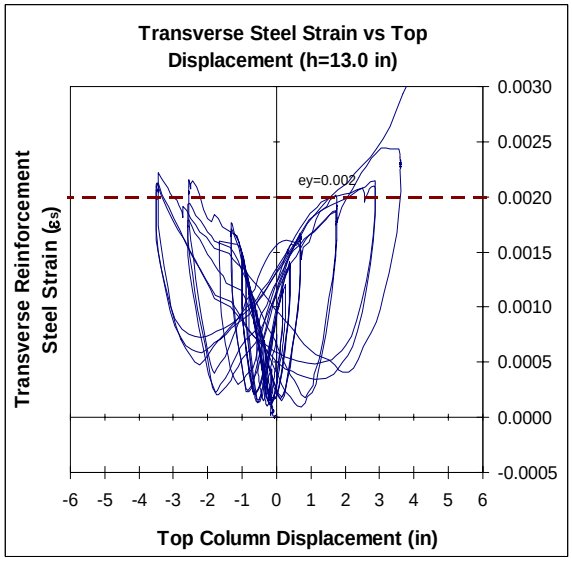

b) Height from the column base (h=13.00 in)

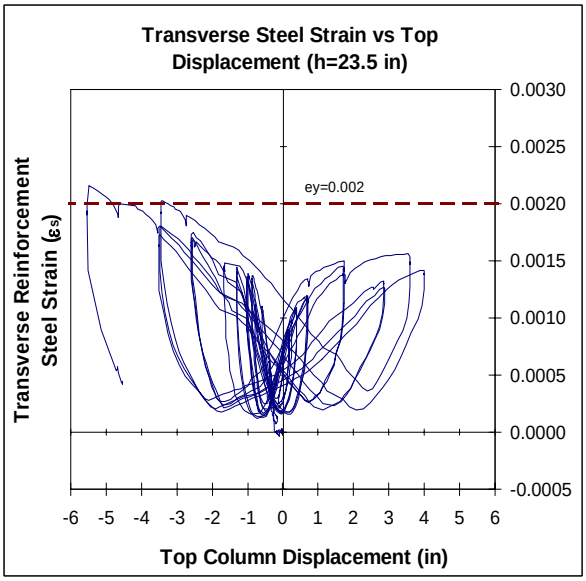

c) Height from the column base (h=23.50 in)

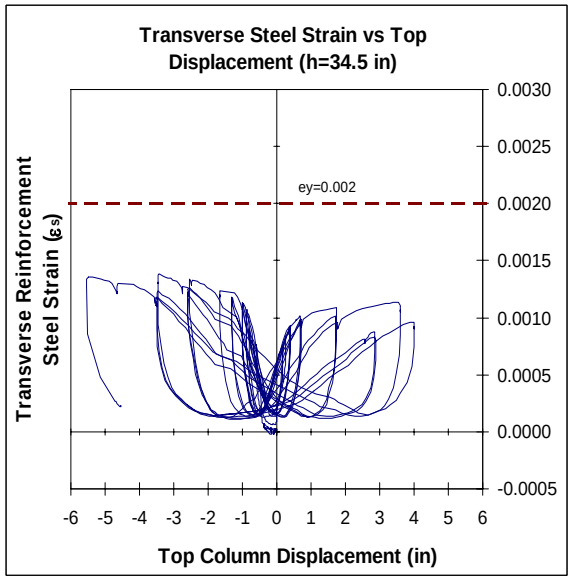

d) Height from the column base (h=34.50 in)

Figure 9.42. Average Transverse Steel Strain versus Top Column Displacement (LW3-NS-DSF)

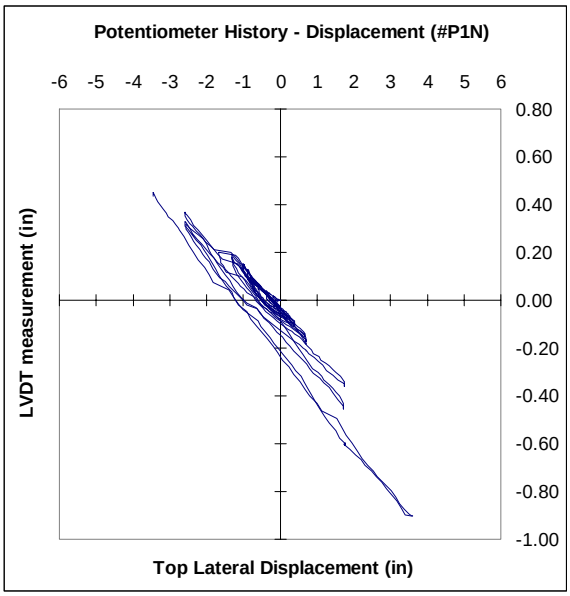

a) P. North. Gage at (h_1-h_2)=(0-7.5) in

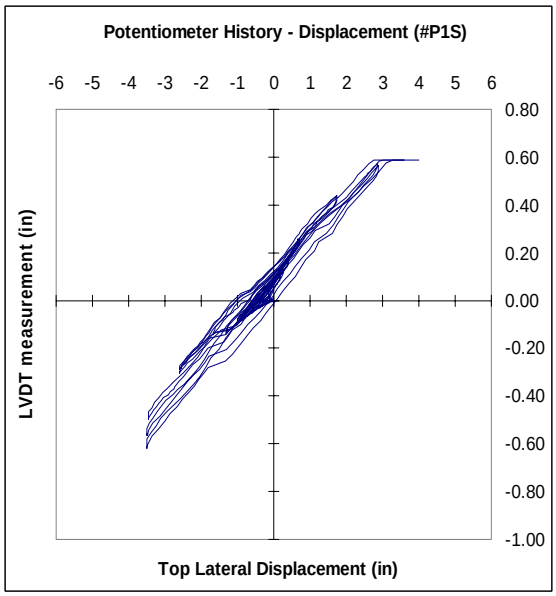

b) P. South. Gage at (h_1-h_2)=(0-7.5) in

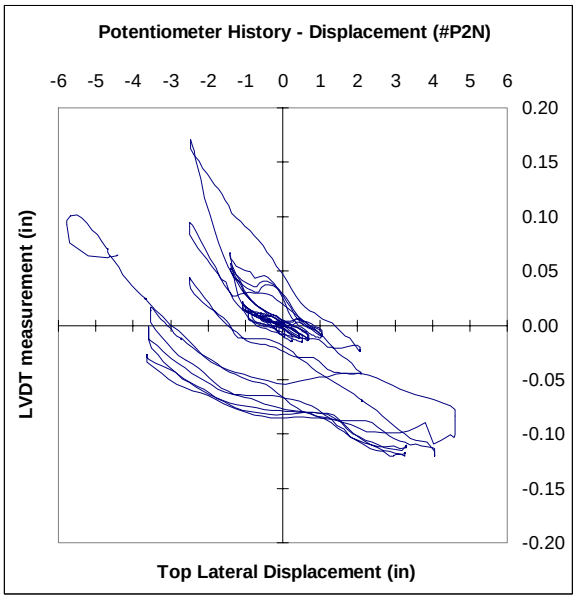

c) P. North. Gage at (h_1-h_2)=(7.5-15) in

Figure 9.43. Linear Potentiometer Histories at Gages 1 and 2 – North and South Faces (LW3-NS-DSF)

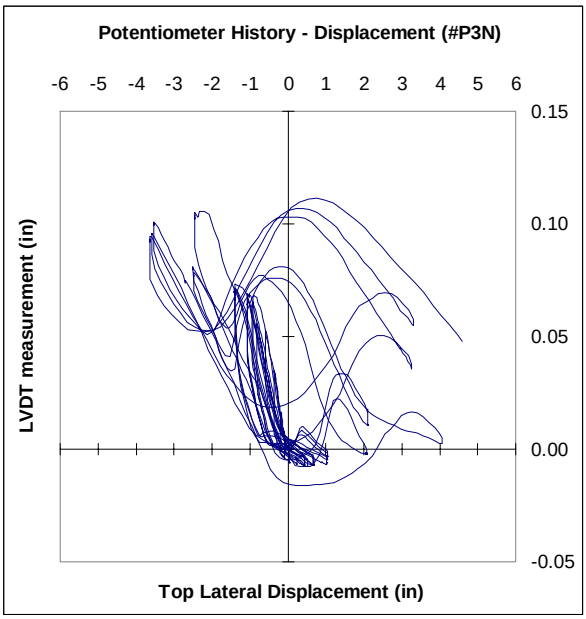

a) P. North. Gage at (h_1-h_2)=(15-22.5) in

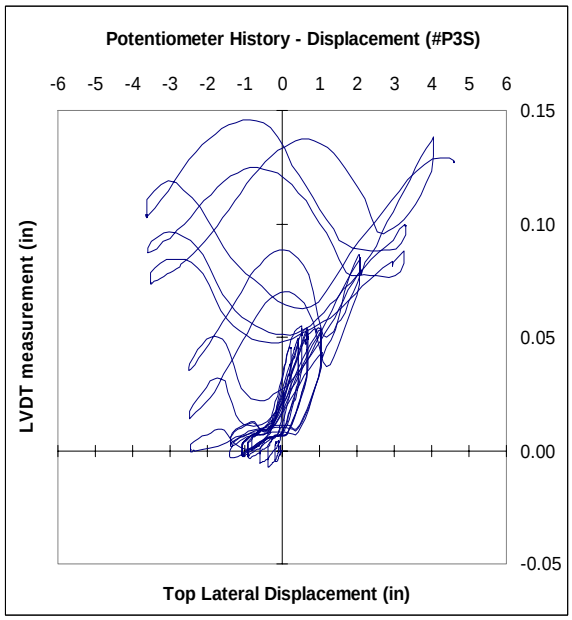

b) P. South. Gage at (h_1-h_2)=(15-22.5) in

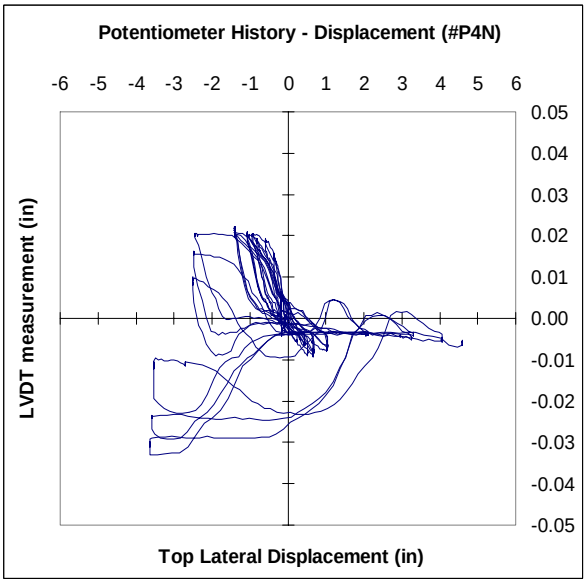

c) P. North. Gage at (h_1-h_2)=(22.5-33.75) in

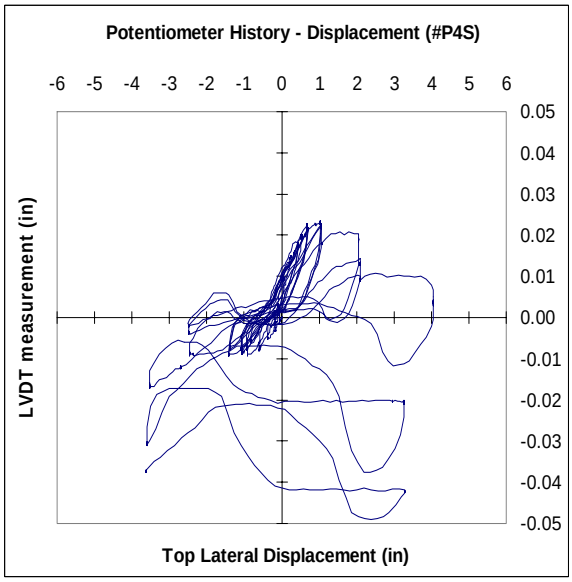

d) P. South. Gage at (h_1-h_2)=(22.5-33.75) in

Figure 9.44. Linear Potentiometer Histories at Gages 3 and 4 – North and South Faces (LW3-NS-DSF)

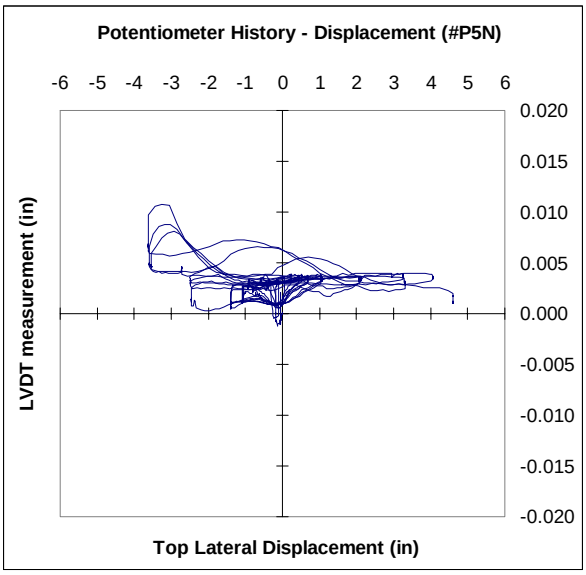

a) P. North. Gage at (h_1-h_2)=(33.75-40.08) in

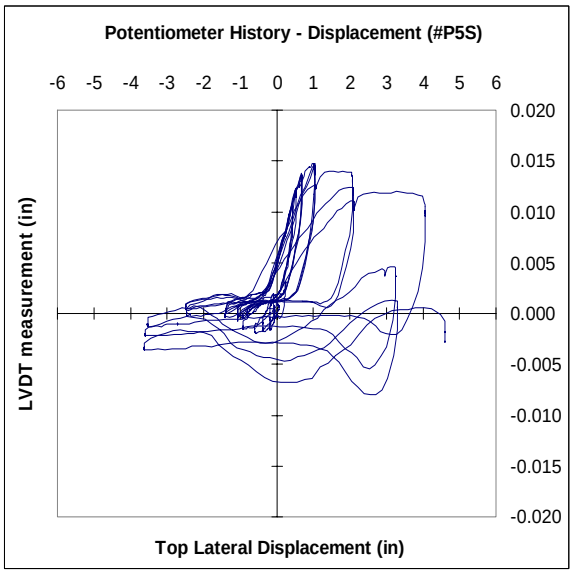

b) P. South. Gage at (h_1-h_2)=(33.75-40.08) in

Figure 9.45. Linear Potentiometer Histories at Gage 5 – North and South Faces (LW3-NS-DSF)

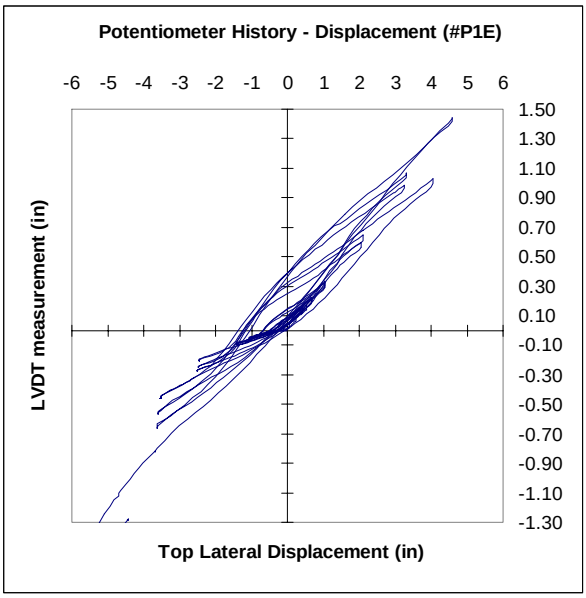

a) P. East. Diagonal at (h_1-h_2)=(0-22.5) in

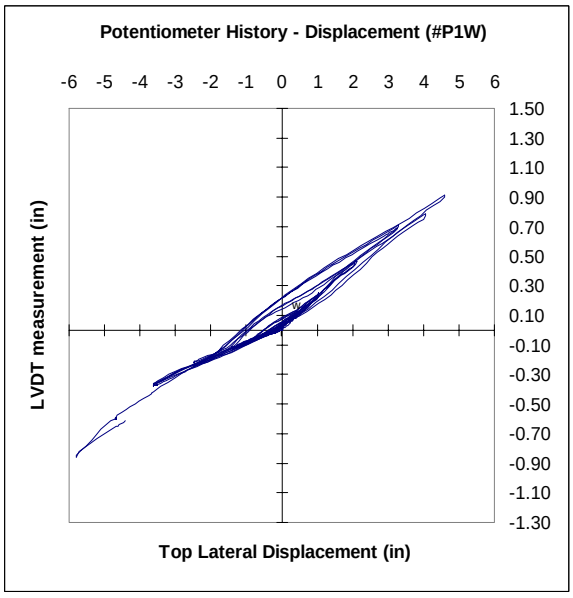

b) P. West. Diagonal at (h_1-h_2)=(0-22.5) in

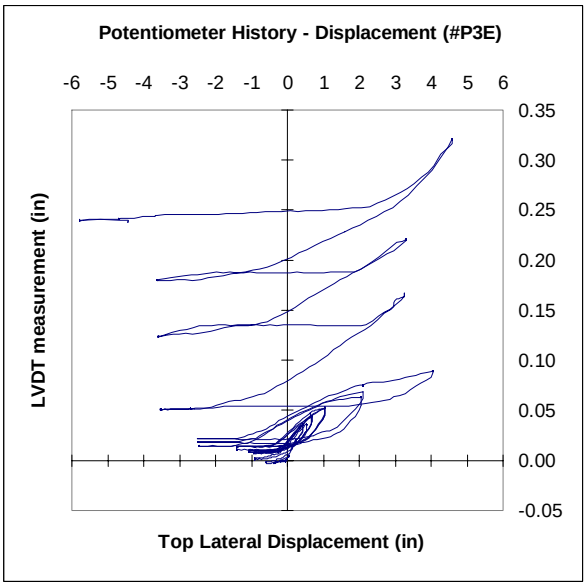

c) P. East. Diagonal at (h_1-h_2)=(22.5-40.08) in

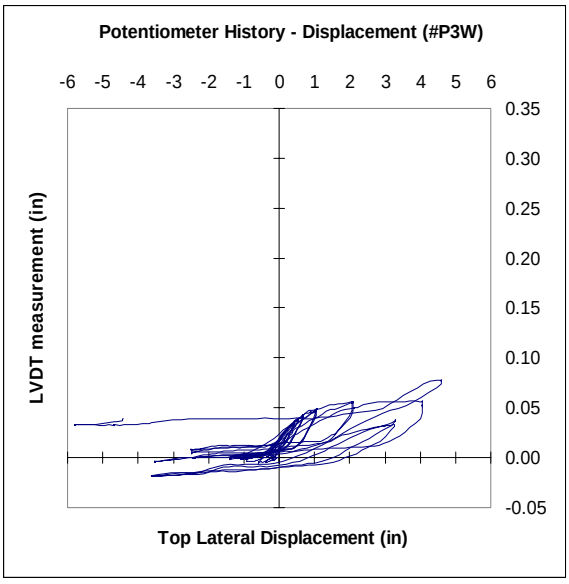

d) P. West. Diag. at (h_1-h_2)=(22.5-40.08) in

Figure 9.46. Linear Potentiometer Histories – Diagonal Elements – East and West Faces (LW3-NS-DSF)

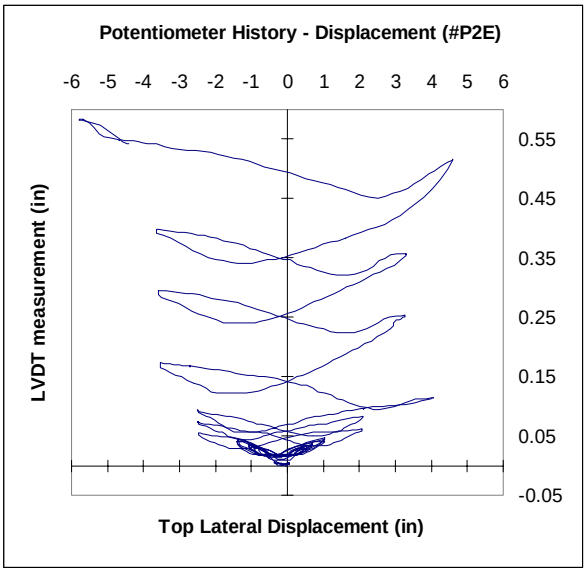

a) P. East. Horizontal at (h=22.5 in)

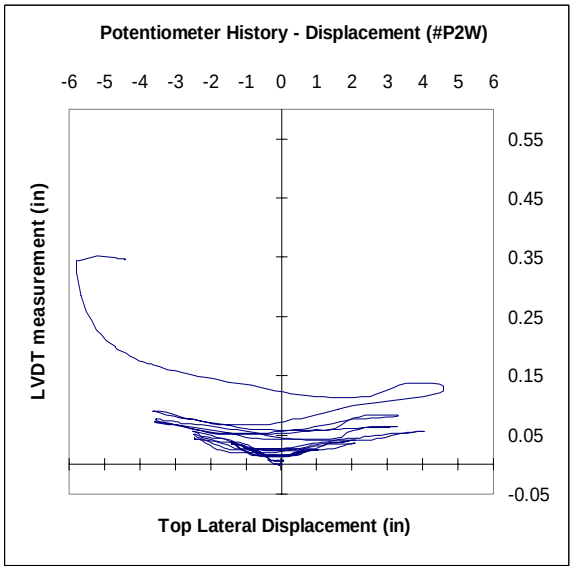

b) P. West. Horizontal at (h=22.5 in)

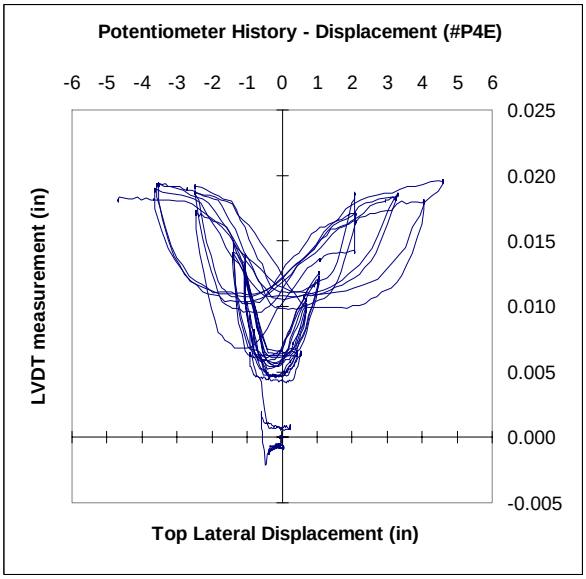

c) P. East. Horizontal at (h=40.08 in)

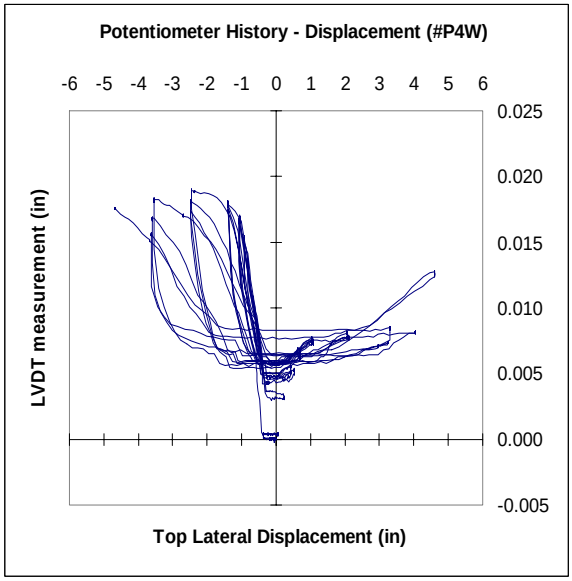

d) P. West. Horizontal at (h=40.08 in)

Figure 9.47. Linear Potentiometer Histories – Horizontal Elements–East and West Faces (LW3-NS-DSF)

9.10 Axial Load Histories – Brittle Shear Failure Tests

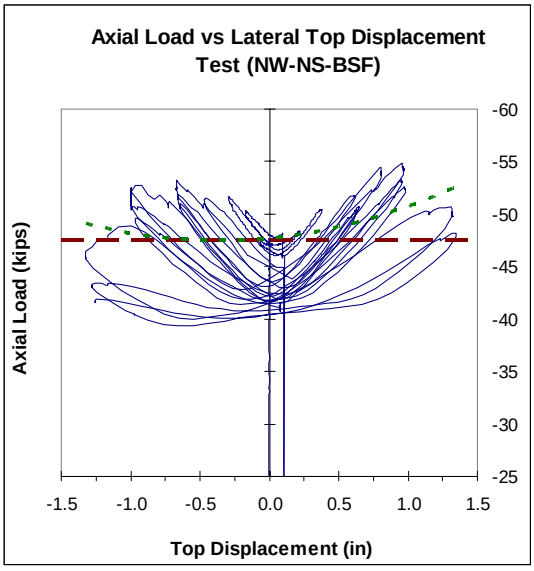

a) Specimen (NW-NS-BSF)

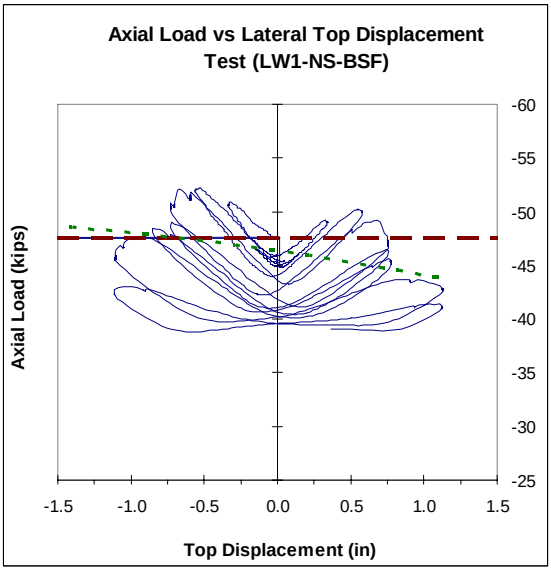

b) Specimen (LW1-NS-BSF)

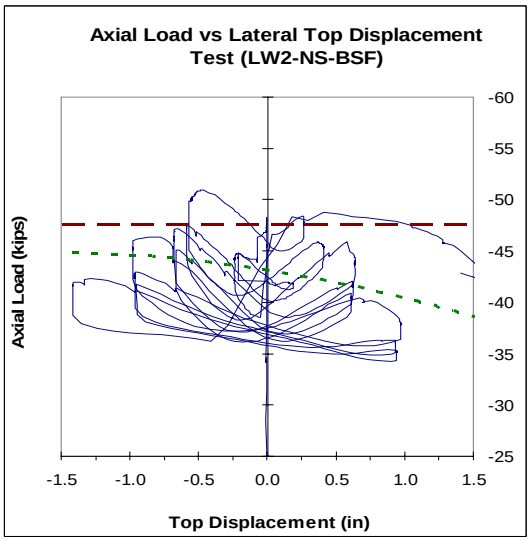

c) Specimen (LW2-NS-BSF)

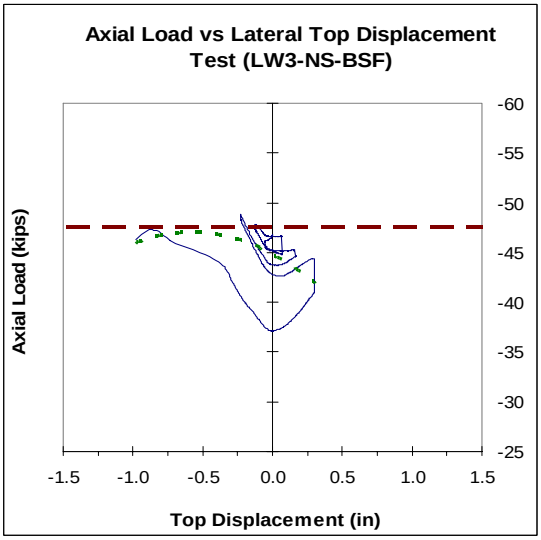

d) Specimen (LW3-NS-BSF)

Figure 9.48. Axial Load versus Lateral Top Displacement Histories – Brittle Shear Failure Specimens

9.11 Axial Load Histories – Ductile Shear Failure Tests

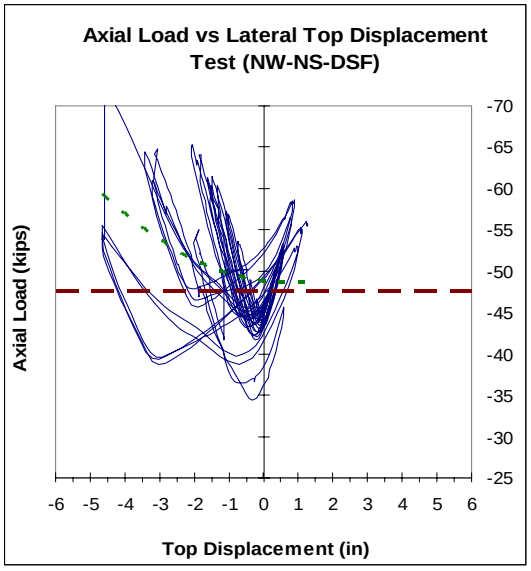

a) Specimen (NW-NS-DSF)

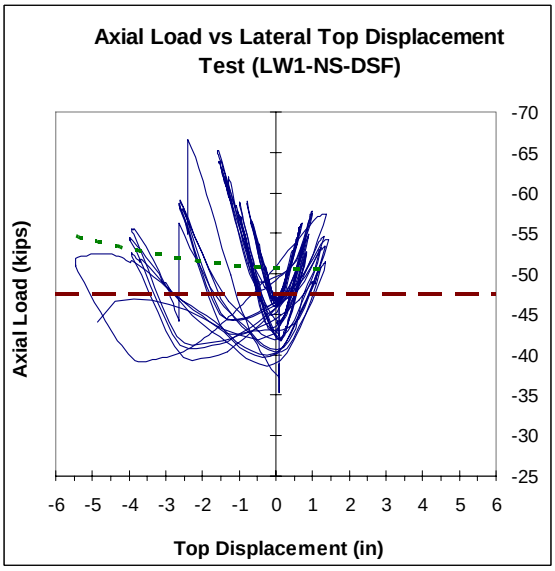

b) Specimen (LW1-NS-DSF)

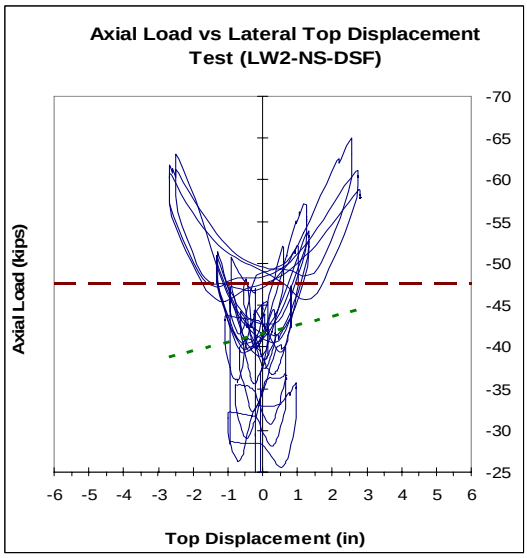

c) Specimen (LW2-NS-DSF)

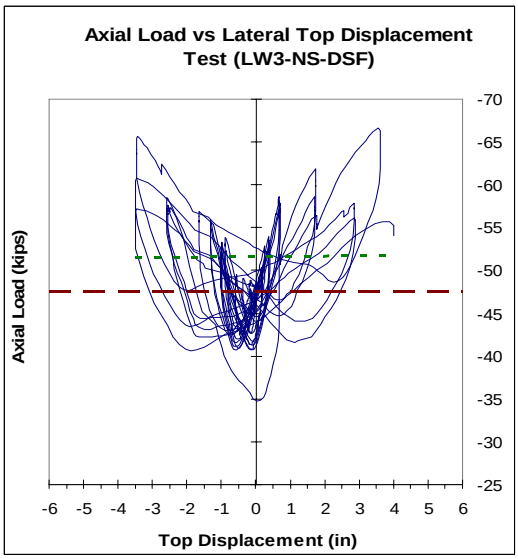

d) Specimen (LW3-NS-DSF)

Figure 9.49. Axial Load versus Lateral Top Displacement Histories – Ductile Shear Failure Specimens

9.12 Predicted Concrete Stress-Strain Relationship–Brittle Shear Failure Specimens

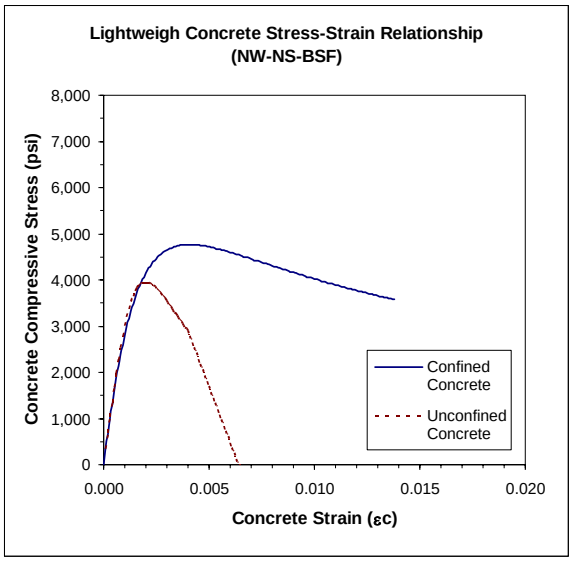

a) Specimen (NW-NS-BSF)

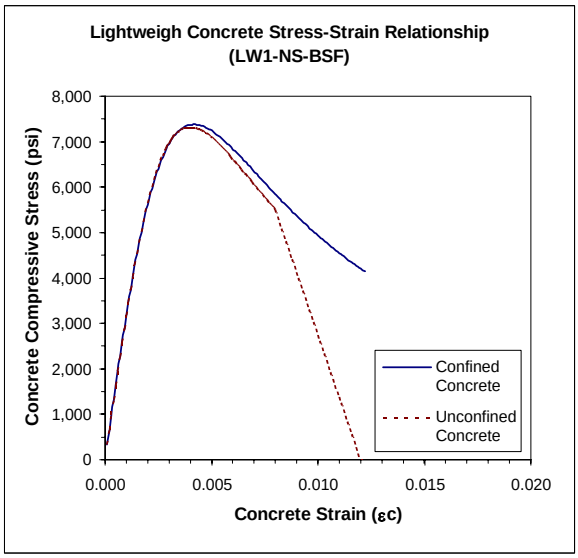

b) Specimen (LW1-NS-BSF)

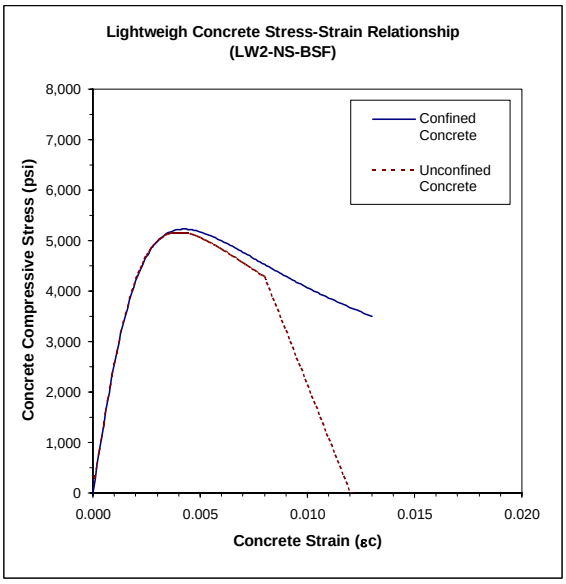

c) Specimen (LW2-NS-BSF)

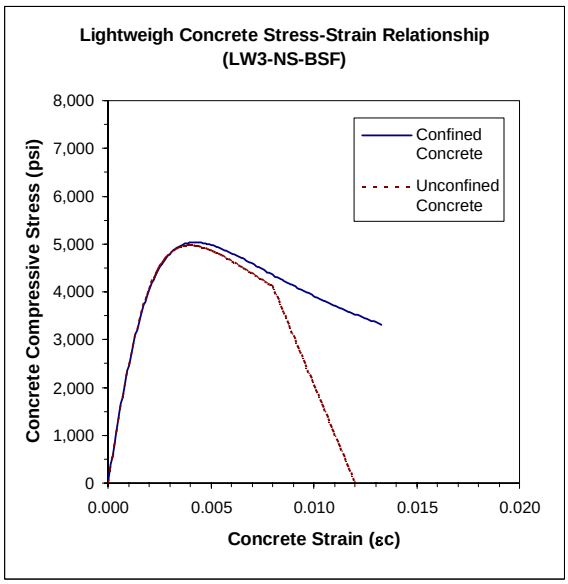

d) Specimen (LW3-NS-BSF)

Figure 9.50. Concrete Shear Stress-Strain Relationships – Brittle Shear Failure Specimens

9.13 Predicted Concrete Stress-Strain Relationship–Ductile Shear Failure Specimens

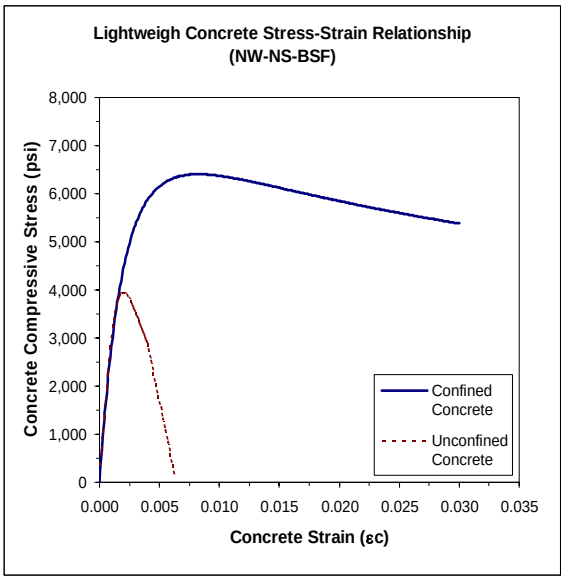

a) Specimen (NW-NS-DSF)

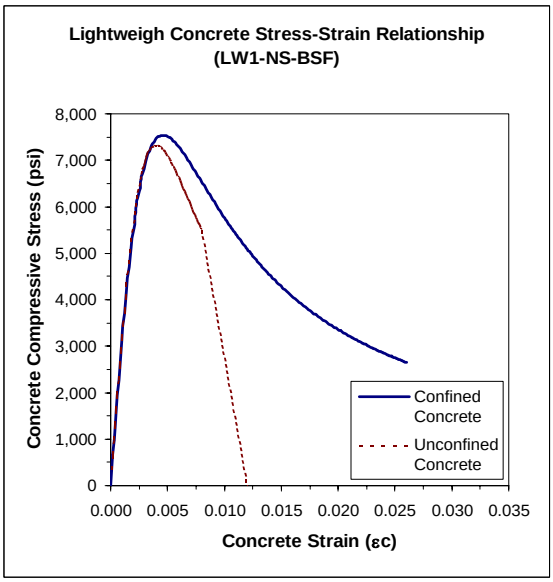

b) Specimen (LW1-NS-DSF)

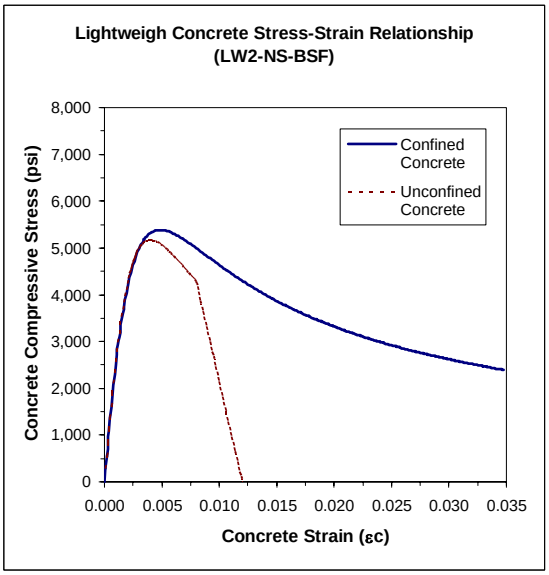

c) Specimen (LW2-NS-DSF)

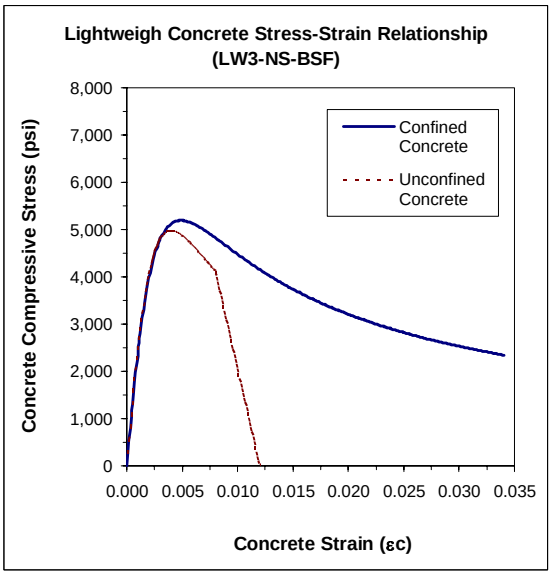

d) Specimen (LW3-NS-DSF)

Figure 9.51. Concrete Shear Stress-Strain Relationships – Ductile Shear Failure Specimens

9.14 NOTATION

A_g = *Gross section area of the column*

A_s = *Longitudinal reinforcement area*

A_{sh} = *Area of cross section of transverse reinforcement (hoop – stirrup)*

A_{sp} = *Area of cross section of transverse reinforcement (spiral)*

bw = *Section width*

c = *Neutral axis depth*

cov = *Concrete cover*

D = *Depth of the rectangular column section or diameter of the column*

Dhi = *Horizontal distance between linear potentiometers to measure flexural deformation on faces (N & S) - cell #i*

$\Delta'y$ = *First yield displacement of the column*

Δy = *Top yield displacement of the column*

Δ_{flex} = *Top displacement due to flexural deformation*

Δ_{shear} = *Top displacement due to shear deformation*

dbl = *Diameter of longitudinal reinforcement*

ε_c = *Concrete strain*

εsi = *Shear strain of the specimen measured on faces (E & W) #i*

Ec = *Concrete young's modulus*

Es = *Steel elastic modulus*

f'_c	=	*Compressive strength of the concrete*
$\phi'y$	=	*First yield curvature of the section*
ϕ	=	*Curvature of the section*
ϕy	=	*Equivalent yield curvature of the section*
ϕi	=	*Average curvature in cell #i*
f'_{sp}	=	*Splitting tensile strength of the concrete*
f'_{sh}	=	*Stress in the transverse steel (hoop – stirrup)*
Fi	=	*Lateral force at nominal flexural capacity*
Fy'	=	*Lateral force corresponding to first yield of longitudinal reinforcement*
fy	=	*Yield stress of reinforcement steel*
Gi	=	*Length of gauge for cell #i (flexural deformation)*
γ	=	*Coefficient relating ductility to strength of concrete shear strength contribution*
L	=	*Height of the column*
L_{clear}	=	*Clear length of the column*
Leff	=	*Effective column length*
Lp	=	*Plastic hinge length*
lsp	=	*Strain penetration length*
$\mu\Delta$	=	*Displacement ductility*
M	=	*Moment*
Mn	=	*Nominal moment capacity*

My	=	*Section first yield moment*
P	=	*Axial load*
PNi	=	*Linear potentiometer on face north - cell #i*
PSi	=	*Linear potentiometer on face south - cell #i*
s	=	*Spacing of transverse reinforcement*
SHi	=	*Vertical distance for shear deformation measurements - faces (E & W) #i*
SBi	=	*Horizontal distance for shear deformation measurements - faces (E & W) #i*
SDi	=	*Diagonal distance for shear deformation measurements - faces (E & W) #i*
$S\theta i$	=	*Angle between diagonal and horizontal lines defined by linear potentiometers for shear deformation on faces (E & W) #i*
θ	=	*Angle of compression strut from column longitudinal axis to shear crack*
θi	=	*Average rotation in cell #i - Flexural deformation*
ρ_l	=	*Longitudinal steel ratio*
ρ_s	=	*Transverse volumetric steel ratio*
V_c	=	*Strength of concrete - Shear transfer mechanism*
V_n	=	*Nominal shear strength*
V_p	=	*Shear strength component provided by a compressive axial load*
V_s	=	*Steel truss component of shear strength*